UNIVERSIDAD COMPLUTENSE DE MADRID

FACULTAD DE CIENCIAS FÍSICAS

Departamento de Física Aplicada I (Termología)

TESIS DOCTORAL

Membrane technologies for brine treatment and membrane reuse

Tecnologías de membranas para el tratamiento de salmueras y reutilización de membranas /

MEMORIA PARA OPTAR AL GRADO DE DOCTOR

PRESENTADA POR

Julio Antonio Sanmartino Rodríguez

Directores

Mohamed Khayet Souhaimi
María del Carmen García Payo

Madrid, 2018

UNIVERSIDAD COMPLUTENSE DE MADRID

Facultad de Ciencias Físicas Departamento de Física Aplicada I
(Termología)

TESIS DOCTORAL

Membrane technologies for brine treatment and membrane reuse

Tecnologías de membranas para el tratamiento de salmueras y reutilización de membranas

Memoria para optar al grado de Doctor en Física

Julio Antonio Sanmartino Rodríguez

Directores

Mohamed Khayet Souhaimi

María del Carmen García Payo

UNIVERSIDAD COMPLUTENSE DE MADRID

DEPARTMENT OF APPLIED PHYSICS I FACULTY OF PHYSICS

Membrane technologies for brine treatment and membrane reuse

JULIO ANTONIO SANMARTINO RODRIGUEZ

Doctoral Thesis 2017

Supervisors

MOHAMED KHAYET SOUHAIMI
MARÍA DEL CARMEN GARCÍA PAYO

Department of Applied Physics I
Faculty of Physics
University Complutense of Madrid-UCM
Avda. Complutense s/n, 28040
Madrid (Spain)

To all those who have made it possible:

family, directors, friends

List of publications, patents, conferences, congress contributions and contracts with companies

Publications derived from the PhD Thesis

1. *Desalination and concentration of saline aqueous solutions up to supersaturation by air gap membrane distillation and crystallization fouling*
   Authors: J.A. Sanmartino, M. Khayet, M.C. García-Payo, H. El Bakouri, A. Riaza
   Journal: Desalination
   Volume: 393
   Pages: 39-51
   Date: 2016

2. *Modeling and optimization of a solar forward osmosis pilot plant by response surface methodology*
   Authors: M. Khayet, J.A. Sanmartino, M. Essalhi, M.C. García-Payo, N. Hilal
   Journal: Solar Energy
   Volume: 137
   Pages: 290-302
   Date: 2016

Publications in process

3. *Treatment of reverse osmosis brines: chemical pretreatments and direct contact membrane distillation*
   Authors: J.A. Sanmartino, M. Khayet, M.C. García-Payo, H. El Bakouri, A. Riaza
   Journal: Desalination
   State: To be submitted

4. *Reuse of discarded membrane distillation membranes in wastewater treatment by microfiltration*
   Authors: J. A. Sanmartino, M. Khayet, M. C. García-Payo
   Journal: Journal of Membrane Science
   State: Under revision

Chapters in books

5. *Desalination by membrane distillation*
   Authors: J. A. Sanmartino, M. Khayet, M. C. García-Payo
   Book title: Emerging membrane technology for sustainable water treatment
   Editors: Nicholas P. Hankins and Rajindar Singh
   Editorial: Elsevier
   Chapter: 4
   ISBN: 978-0-444-63312-5
   Date: 2016

Other publications

6. *Fouling in Membrane Distillation, Osmotic Distillation and Osmotic Membrane Distillation*
   Authors: Mourad Laqbaqbi, Julio Antonio Sanmartino, Mohamed Khayet, Carmen García-Payo and Mehdi Chaouch
   Journal: Applied Science
   Volume: 7
   Pages: 334-373
   Date: 2017

Patents

1. *Conjunto de membranas de fibra hueca y sus aplicaciones*
   Authors: Mohamed Khayet, Carmen García-Payo, Julio Antonio Sanmartino, Juan Pablo Pocostales, Rocío Rodríguez, Abel Riaza and Francisco Javier Bernaola
   Nº patent: P201630188
   International request number: PCT/ES2017/070039
   State: pending acceptance
   Date: 2017

Conferences and congress contributions

1. *Desalación de disoluciones salinas de altas concentraciones por destilación en membranas con cámara de aire*
   Authors: J.A. Sanmartino, M. Khayet, M.C. García-Payo, H. El Bakouri, A. Riaza
   Congress: XXXIV Reunión Bienal de la Real Sociedad Española de Física
   Place: Valencia (Spain)
   Type of contribution: oral
   Date: 15-19 Julio 2013

2. *Destilación en membrana con cámara de aire de disoluciones salinas saturadas*
   Authors: J.A. Sanmartino, M. Khayet, M.C. García-Payo
   Congress: XXXV Reunión Bienal de la Real Sociedad Española de Física
   Place: Gijón (Spain)
   Type of contribution: oral
   Date: 13-17 Julio 2015

3. *Concentration of hypersaline solutions up to supersaturation by different membrane distillation configurations*
   Authors: Julio Sanmartino, Alia Baroudi, Mohamed Khayet, Carmen García-Payo
   Congress: 12th International Meeting on Thermodiffusion (IMT-12)
   Place: Madrid (Spain)
   Type of contribution: poster
   Date: 30 Mayo-3 Junio 2016

Contracts with companies

1. **Project title:** *Application of hybrid membrane systems for the treatment of brines from desalination plants (MEMsa)*
   Participants: University Complutense of Madrid and Abengoa Water SLU
   Duration: October 2011 to December 2012

2. **Project title:** *Design, construction and operation of a hollow fiber membrane distillation pilot plant (HOFI-MED-PLANT)*
   Participants: University Complutense of Madrid and Abengoa Water SLU
   Duration: January 2013 to December 2016

3. **Project title:** *Design and construction of hollow fiber membrane distillation modules (HOFI-Modules)*
   Participants: University Complutense of Madrid and Abengoa Water SLU
   Duration: October 2014 to March 2015

Index of contents

Abstract

The exponential growth of the world population during last decades, the increment in the industrial use of water, the contamination and the improper use of water resources, are the current responsible of water scarcity problem. This situation has forced to adopt different mechanisms to obtain fresh water, like desalination and wastewater recovery. In this field, desalination of seawater has become the main considered option to alleviate the problem of lack of water in coastal regions. Among the different desalination processes, membrane technologies are the most used worldwide. Among them, reverse osmosis (RO) is the most used and industrially implemented technology because of its economic competitiveness compared with other processes. However, the problem related to the concentrated brine discharge to the environment is not solved yet. During last years, membrane science and technology have been incessantly improving trying to find solutions to this environmental issue. As a result, other membrane-based processes have appeared as suitable solutions. Among them, the thermally-driven membrane process, membrane distillation (MD) has been proposed to treat this high concentrated brine for water production and reduction of its volume.

Chapter 2 is dedicated to explore the possibilities of MD technology in the field of desalination. A comprehensive study of MD process is presented including its configurations, mechanisms of transport, membranes, modules, effects of different operating conditions on the MD performance, possibilities to be coupled with other technologies to form integrated/hybrid processes, use of renewable energy systems, etc.

Chapter 3 is focused on the application of MD technology to concentrate brines discharged from RO plants to practically zero discharge to environment. This chapter is divided into two sections: i)- the treatment of a synthetic brine (65 g/L of sodium chloride, NaCl) and ii)- the treatment of an RO brine. For this purpose, polytetrafluorethylene (PTFE) membranes of different pore sizes have been used. In the first part, synthetic brines were concentrated above the saturation concentration of NaCl using the air gap MD (AGMD) configuration until the membrane pores were blocked or wetted. In general, a

good quality distillate was produced with salt rejection factors greater than 99.9%. Once the saturation limit of NaCl was overpassed, the crystallization fouling phenomenon was studied. This phenomenon was found to be the responsible of the pore blocking/wetting of the membrane pores resulting in a decrease of both the water production rate and the thermal efficiency of the MD process. As consequence, the pore blocked or wetted membranes have been discarded for use in MD.

A more complex strategy has been considered for the concentration of RO brine due to the presence of carbonates and sulfates, the less soluble salts and responsible of membrane pore wetting due to their precipitation. To avoid this phenomenon, different chemical pretreatments (CPTs) followed by the direct contact MD (DCMD) process have been adopted. It was found that the CPTs that managed to eliminate the sulfate ions from the RO brine were the most efficient, improving the DCMD performance owing to the highest obtained permeate flux, lowest permeate flux decline and best permeate quality.

It is known that one of the main MD drawbacks is the irreversible membrane pore wetting. Once the pores are blocked or wetted the efficiency of the MD process is reduced and the membrane is finally discarded. Therefore, the reuse of these discarded membranes is a possible solution to prevent their disposal and save costs. In chapter 4, the possibility to reuse these MD membranes in microfiltration (MF) process has been proposed for the first time and explored. These discarded membranes have been applied in MF for the treatment of aqueous solutions of humic acid (HA) as an example but not limited to it. The permeate flux, separation factor or performance index depended on the membrane characteristics and the initial state of the MD membranes. It was found that the reused membranes exhibited similar MF performance to new membranes.

Finally, another possibility of a great interest in membrane science and technology is to reuse RO brines as a draw solution in forward osmosis (FO), which is a water treatment/separation technology of emerging interest due to its low energy consumption. In chapter 5, a solar thermal and photovoltaic-powered FO pilot plant has been optimized by means of a statistical experimental design and response surface methodology (RSM). The main objective was to figure out the optimum operating parameters in order to maximize the water permeate flux, the reverse solute flux selectivity, the specific water permeate flux and the specific FO performance index while both the reverse solute diffusion and the total energy consumption were minimized. Monte Carlo simulation method has been conducted to determine the optimum operating conditions of the FO pilot plant. The determined optimum operating parameters have been confirmed experimentally. To maintain the concentration of the draw solution high or which is the same, its driving force high, a solar powered RO pilot plant has been proposed. In this PhD Thesis, one of the future objectives that can offer better regeneration efficiency of the draw solution, especially when using saline solutions such as brines, is MD instead of RO forming a hybrid FO/MD system.

Resumen

El crecimiento exponencial de la población mundial durante las últimas décadas, unido al incremento en el uso industrial del agua, la contaminación y el uso indebido de los recursos hídricos son los responsables actuales del problema de la escasez de agua. Esta situación ha obligado a adoptar diferentes mecanismos para la obtención de agua dulce, como la desalación y la recuperación de aguas residuales. En este campo, la desalación del agua del mar se ha convertido en la principal opción utilizada para aliviar el problema de la falta de agua en las regiones costeras. Entre los diferentes procesos de desalación, las tecnologías de membranas son las más utilizadas en todo el mundo. Entre ellas, el proceso de ósmosis inversa (OI) es el método más estudiado e implementado industrialmente debido a su competitividad económica en comparación con otros procesos. Sin embargo, los problemas relacionados con la descarga de salmueras concentradas al medio ambiente no han sido resueltos todavía. Durante los últimos años, la ciencia y tecnología de membranas ha mejorado incesantemente tratando de encontrar soluciones a estos problemas ambientales. Como resultado, otros procesos basados en membranas han aparecido como soluciones adecuadas. Entre ellos, la destilación en membrana (DM) se ha propuesto como un proceso de membrana no isotérmico para tratar soluciones acuosas de alta concentración salina derivadas de otros procesos de desalación para la producción de agua y la reducción del volumen de desecho.

El capítulo 2 está dedicado a explorar las posibilidades de la tecnología DM en el campo de la desalación. Se presenta un amplio estudio del proceso de DM, incluyendo sus configuraciones, mecanismos de transporte, membranas, módulos, efectos de las diferentes condiciones de operación en DM, sus posibilidades de ser acoplado con otras tecnologías para formar procesos integrados/híbridos y también el uso de sistemas de energía renovable, etc.

El capítulo 3 está enfocado en la aplicación de la tecnología de DM para concentrar

las salmueras procedentes de plantas de OI hasta conseguir una descarga prácticamente nula al medio ambiente. Este capítulo está dividido en dos secciones: i) el tratamiento de salmueras sintéticas (65 g/L de cloruro sódico, NaCl), y ii) el tratamiento de salmueras procedentes de las plantas de desalación por OI. Para ello, se utilizaron membranas de poli tetrafluoretileno (PTFE) con dos diferentes tamaños de poro. En la primera parte, las salmueras sintéticas se concentraron por encima de la concentración de saturación del NaCl usando la configuración de DM con cámara de aire (DMCA) hasta que los poros de la membrana se bloquearon o mojaron. En general, se produjo un destilado de buena calidad con un factor de rechazo de sal mayor al 99,9%. Una vez superado el límite de saturación del NaCl, se estudió el fenómeno de ensuciamiento debido a la cristalización de las sales. Este fenómeno es el responsable del bloqueo o mojado de los poros, disminuyendo la producción de agua y la eficiencia térmica del proceso de DM. Como consecuencia, las membranas bloqueadas o mojadas deben desecharse para su uso en DM.

Más complejo es concentrar salmueras procedentes de OI debido a la presencia de carbonatos y sulfatos, las sales menos solubles y responsables del mojado de los poros de la membrana debido a su precipitación. Para evitar este fenómeno, se adoptaron diferentes pretratamientos químicos (PTQs) seguidos por el proceso de DM por contacto directo (DMCD). Los PTQs que lograron eliminar los iones sulfato de la salmuera de OI resultaron ser los más eficientes, mejorando el rendimiento del proceso de DMCD a través de un mayor flujo de permeado, una menor caída de éste con el tiempo y una mejor calidad de permeado.

Es ampliamente conocido que uno de los mayores inconvenientes de la DM es el mojado irreversible de los poros de la membrana. Una vez que los poros se bloquean o mojan, la eficacia del procedimiento de DM se reduce y la membrana se termina desechando. Por lo tanto, su reutilización es una posible solución para evitar su eliminación y ahorrar costes. En el capítulo 4, se estudia por primera vez la posibilidad de reutilizar estas membranas de DM desechadas en el proceso de microfiltración (MF). Estas membranas se emplearon en MF para tratar disoluciones acuosas de ácido húmico (AH) como un ejemplo, pero no limitado a él. Los resultados del flujo de permeado, factor de separación o índice de rendimiento dependieron de las características de la membrana y del estado de éstas una vez desechadas en DM. A pesar de esto, las membranas reutilizadas de DM presentaron un rendimiento similar al de membranas nuevas.

Por último, otra posibilidad de gran interés en la ciencia y tecnología de membranas es reutilizar las salmueras procedentes de OI como disolución osmótica en el proceso de ósmosis directa (OD), una tecnología de tratamiento/separación de aguas de creciente interés debido a su bajo consumo energético. En el capítulo 5 se ha optimizado una planta piloto de OD, acoplada a tecnologías solar térmica y fotovoltaica, mediante un diseño experimental estadístico y una metodología de superficie de respuesta (RSM). El objetivo principal fue determinar los parámetros óptimos de operación con el fin de maximizar el

flujo de permeado de agua, la selectividad del retroflujo de soluto, el flujo específico de permeado de agua y el índice de rendimiento específico de OD, mientras que la difusión inversa del soluto y el consumo total de energía se minimizaron. Utilizando el método de simulación de Monte Carlo se han determinado las condiciones óptimas de operación de la planta piloto de OD, y éstas se han confirmado experimentalmente. En este estudio, se propuso la regeneración de la disolución osmótica, con el fin de mantener su concentración alta, es decir su fuerza motriz elevada, utilizando una planta piloto de OI alimentada por energía solar. En esta Tesis doctoral, se propone como uno de los objetivos futuros que pueden ofrecer una mejor eficiencia en la regeneración de la disolución osmótica, especialmente cuando se utilizan disoluciones salinas como salmueras, la utilización de DM en lugar de OI formando un sistema híbrido OD/DM.

Chapter 1

Introduction

1.1. Motivation and objectives

Among 70% of the planet surface area covered by water, about 97.5% corresponds to saline water and only the remaining 2.5% represents fresh water being 80% of this fresh water in form of ice caps or combined as soil moisture [1]. In fact, both forms are vulnerable to climate change effect and are not easily accessible for all.

In the last century, water use and consumption has been growing at more than twice the increase of population rate. The three worldwide largest consuming sectors are agriculture (70%), industry (19%) and domestic use (11%) [1]. Unfortunately, water is not distributed evenly throughout the planet and it is not available in sufficient quantities either when or where it is needed. About a 70% of available fresh water is located in rivers, lakes and underground aquifers. Furthermore, rainfall is irregularly distributed around the globe. According to the United Nations [2], 1,8 billion people will be living in countries or regions with absolute water scarcity in 2025, and two thirds of the world population could be under water stress conditions. Industrial development together with population growth have greatly increased the demand for potable water, causing an estimated increase in water withdrawals of about 50% by 2025 in developing countries and about 18% in developed countries [2].

It is known that water is an increasingly critical factor in decisions regarding the location of industrial activities. However, severe ecosystem damages (i.e. depletion or salinization of water, land desertification, etc.) may be caused if water extraction rates

exceed natural renewal rates [3]. This situation has forced many countries to adopt active and efficient programs for desalination and recovery of wastewater. In this context, over the past three decades, numerous desalination and wastewater treatment plants have been installed worldwide.

Desalination of seawater or brackish water has become an attractive solution to systematic water scarcity being one of the most sustainable alternative solutions to provide fresh water for many communities and industrial sectors [4]. Thermal processes, especially in warms countries of the Middle East, and membrane technologies are currently the two major considered technologies in the desalination field [1, 5-7]. The success of membrane methods during last years is based on their operational simplicity, high salt separation and permeability, and the possibility for their integration to other technologies forming hybrid systems [8]. Among the considered membrane processes (i.e. electrodialysis (ED) and pressure-driven membrane processes such as microfiltration (MF), ultrafiltration (UF), nanofiltration (NF), reverse osmosis (RO) represents 2/3 of the contracted capacity [9]. However, the problems related to the concentrated brine discharges to the environment and to the energy costs are not solved yet [10, 11]. During last decade, a great attention has been devoted to other membrane separation processes of emerging interest such as the osmotic separation processes forward osmosis (FO) and pressure retarded osmosis (PRO) as well as to membrane distillation (MD) due to their considerable advantages in desalination and wastewater treatment. Moreover, the use of renewable energies and the possibility to reuse wastes such as brines produced by RO plants and to recycle disposed membranes together with the optimization of hybrid desalination plants to increase water recovery factor, appear as promising possibilities leading to increase the water production rate, reduce the specific energy consumption and protect the environment. Some of these possibilities have been proposed in the present PhD Thesis.

A state of the art review of desalination by MD is presented in the second chapter of this PhD Thesis and the third chapter ting deals with the possibility to manage the brine discharge from RO desalination plants through the use of two different MD systems (i.e. air gap MD, AGMD, and direct contact MD, DCMD). A study of the optimum operation conditions together with a deep analysis of the brine influence on MD membranes were carried out. Moreover, chemical pretreatments were applied to the RO brine to improve the MD performance.

As it is well known, the main drawback of MD technology is the irreversible wetting of the membrane pore resulting in a considerable decline of the MD performance and to the subsequent discard of the membrane from its use in MD. A possible option is to reuse these discarded membranes to prevent their disposal and save costs. Attempts are made in the fourth chapter of the present PhD Thesis to reuse MD membranes in MF for water treatment. To better understand the MF process, membrane requirements, fouling phenomenon and their industrial application are presented in section 1.2.

Another possibility that might be of a great interest in membrane science in general and RO field in particular is to reuse RO brines as draw solution in FO technology. This draw solution can be regenerated by means of different water treatment processes including the membrane processes RO and MD forming hybrid systems FO/RO and FO/MD, respectively for the treatment of wastewaters. In fact, MD proved to be an attractive process for the treatment of supersaturated saline solutions with high performance. The fifth chapter is focused on the optimization of a solar FO pilot plant and the subsequent regeneration of the draw solution in order to maintain its concentration high or which is the same its driving force high.

The main objective is to figure out the optimum operating parameters of a photovoltaic-powered FO pilot plant in order to maximize the water permeate flux, the reverse solute flux selectivity, the specific water permeate flux and the specific FO performance index while both the reverse solute diffusion and the total energy consumption were minimized. A statistical experimental design and response surface methodology (RSM) have been used. For a better understanding of the fifth chapter, a brief description of the characteristics of FO process, its advantages and challenges are indicated in section 1.3.

1.2. Microfiltration (MF) process and fouling phenomenon

Microfiltration (MF) is a pressure-driven separation process. It is widely used in the food industry, wastewater treatment, medicine and biotechnology [12, 13] for concentrating or purifying/separating macromolecules, microorganisms, colloids and suspended particles from aqueous solutions depending on the membrane pore size [14]. The feed solution to be treated is forced to pass through a microporous membrane by means of a transmembrane pressure (*TMP*), producing from one membrane side a permeate water and from another side a concentrate retentate. *TMP* together with the membrane characteristics are the two fundamental factors for the MF process, determining both the permeate production and the foulant separation ratio.

1.2.1. Transmembrane pressure (TMP)

Compared to the other pressure-driven membrane processes (i.e. RO, NF and UF), MF is usually operated at relatively low *TMP*, < 0.4 MPa [13, 14]. The *TMP*, defined as the difference between the pressure at the membrane feed side and that at the permeate side of membrane, represents the driving force of the MF process. In the cross-flow mode, the most commonly design in MF devices, the solution to be treated usually flows tangentially

to the membrane surface [15]. The pressure applied on the feed membrane side can be calculated as the mean of the pressures at the inlet and outlet of the device [13]:

$$TMP = \frac{(P_{in} + P_{out})}{2} - P_p \tag{1.1}$$

where P_{in} and P_{out} are the pressure of the feed solution at the inlet and outlet of the MF device, respectively. It must be pointed out that the pressure at the permeate side, P_p, is usually negligible.

The permeate flux (J) is governed by the general filtration equation (Darcy's law) [14, 16, 17]:

$$J = \frac{TMP}{\eta R} \tag{1.2}$$

were η is the fluid viscosity and R is the mass transfer resistance. Therefore, by increasing *TMP*, the permeate flux through the membrane also increases.

1.2.2. MF Membrane requirements

The MF performance is also directly associated with the overall membrane properties. To obtain a high-water production rate, the membranes should be highly porous, with great pore sizes (i.e. the maximum allowable pore size is limited by the size of the particle(s) to be separated from the feed solution, usually in a range of 0.1-1.0 μm [13]), should exhibit low pore tortuosity (i.e. the pores go straight across the membrane thickness) and as thin as possible. Thus, the relationship between the applied *TMP* and the permeate flux is given by the hydraulic permeability of the membrane (L_p) as follows [13]:

$$J = L_p \times TMP \tag{1.3}$$

L_p is defined as a function of the membrane parameters as follows [13, 14]:

$$L_p = \frac{\varepsilon r^2}{8\eta\tau\delta} \tag{1.4}$$

where ε is the membrane porosity, r is the pore radius, τ is the pore tortuosity and δ is the membrane thickness.

Regardless of the membrane form (i.e. flat sheet or hollow fiber membranes), and depending on the MF application, a large range of polymers and inorganic materials with wide pH and temperature ranges are employed in membrane preparation. This includes cellulose, cellulose diacetate (CA) and triacetate (CTA), polyvinylidene fluoride (PVDF), polyamide (PA), polysulfone (PS), polyethersulfone (PES), polycarbonate (PC) and polyvinylchloride (PVC), among others.

1.2.3. Fouling phenomenon

One of the important drawbacks of MF technology is fouling phenomenon [14, 16, 18]. During MF water treatment, solutes present in the feed solution are deposited on the membrane surface forming a cake layer (i.e. external fouling). This results in an increase of both the membrane resistance (R_m) and the resistance caused by fouling (R_f). Therefore, according to Eq. (1.2), the permeation rate is reduced affecting the economic viability of the process as a consequence [15]. This decline of the permeation rate occurs first at a rapid initial drop, followed by a long term gradual decrease and finally ended with a steady state permeate flux [13, 15]. In addition, small particles or macromolecules can also be adsorbed or deposited inside the pore structure of the membrane [15, 18, 19]. This is known as internal irreversible fouling.

In general, fouling phenomenon is related with the liquid characteristics such as the particle/membrane interactions, the particle size and the pH; with the membrane characteristics such as the pore size, the porosity and the hydrophilic character as well as with the hydrodynamic conditions such as the TMP, the flow velocity and the temperature [15, 20].

The control of fouling requires the implementation of technological solutions to compensate the decline of the permeation rate. The developed research studies have been focused in the optimization of the MF modules, the operating conditions and the development of fouling resistant membranes with novel and advanced materials to improve the separation efficiency and the chemical resistance [14, 16, 18, 19, 21-23]. For instance, in MF devices, the circulated feed solution tangentially to the membrane surface sweeps the deposited particles on the membrane surface reducing the thickness of the formed cake layer.

It must be pointed out that membrane materials show different fouling behaviors due to their free surface energy associated to their hydrophilic character. In general, hydrophobic membranes are more prone to fouling than the hydrophilic ones because of the attractive hydrophobic interaction between foulants and membranes [15]. As a result, much attention has been devoted to reduce fouling by modifying hydrophobic membranes to be more hydrophilic [24-26]. The interactions between molecules and between molecules and membrane surface depend not only on the membrane charge, but also on the

pH and on the physico-chemical properties of macromolecules of the solutions to be treated. These facts affect the repulsive forces and the water production rate [15].

In the chapter 4 of the present PhD Thesis, hydrophobic polytetrafluoroethylene (PTFE) membranes with two different mean pore sizes (i.e. 0.2 and 0.45 μm), discarded from the MD process due to the wetting/blocking effects after the treatment of both synthetic and RO brines, have been reused in MF for water treatment.

1.3. Forward osmosis (FO) process: applications and challenges

FO is a membrane separation process that utilizes the physical phenomenon of osmosis to transport water across a semipermeable asymmetric membrane, consisting of a dense active layer and a porous support layer [27]. The membrane must be placed between two solutions of different concentrations (i.e. a concentrated draw solution and a more dilute feed solution). The osmotic pressure difference or which is the same the concentration difference induces a water chemical potential difference, which is the driving force causing a spontaneous water flux across the membrane from the high water chemical potential aqueous solution (i.e. the feed solution that is brought into contact with the active layer of the membrane) to low water chemical potential aqueous solution (i.e. draw solution placed in contact with the permeate side of the membrane) [27-29]. Therefore, the FO process results in the concentration of the feed solution and dilution of the draw solution until an equilibrium of transmembrane hydrostatic pressure occurs [1, 27]. In RO process, a hydraulic pressure is applied in the opposite direction of the osmotic pressure gradient allowing to drive the water flux and permitting the production of potable water [1, 27, 30]. PRO appears as an intermediate process between FO and RO being the applied hydraulic pressure also in the opposite direction of the osmotic pressure gradient like RO but this pressure is below the osmotic pressure of the draw solution and therefore the net water permeate flux is still in the same direction as that of FO [27, 30]. PRO is applied for energy production. Generation of electricity by means of turbine(s) that depressurize(s) the draw solution due to the increase of the volume in the permeate side of the membrane modules and the subsequent enhancement of the pressure [30, 31].

The equation used to describe the water transport takes into account both the difference of the osmotic pressure between both sides of the membrane ($\Delta\pi$) and the applied pressure (ΔP), as follows [29, 32]:

$$J_w = A(\Delta\pi - \Delta P) \quad (1.5)$$

were J_w is the water flux and A is the water permeability constant of the membrane. In FO $\Delta P = 0$, $\Delta P > \Delta\pi$ in RO and $\Delta P < \Delta\pi$ in PRO, as shown in Fig. 1.1.

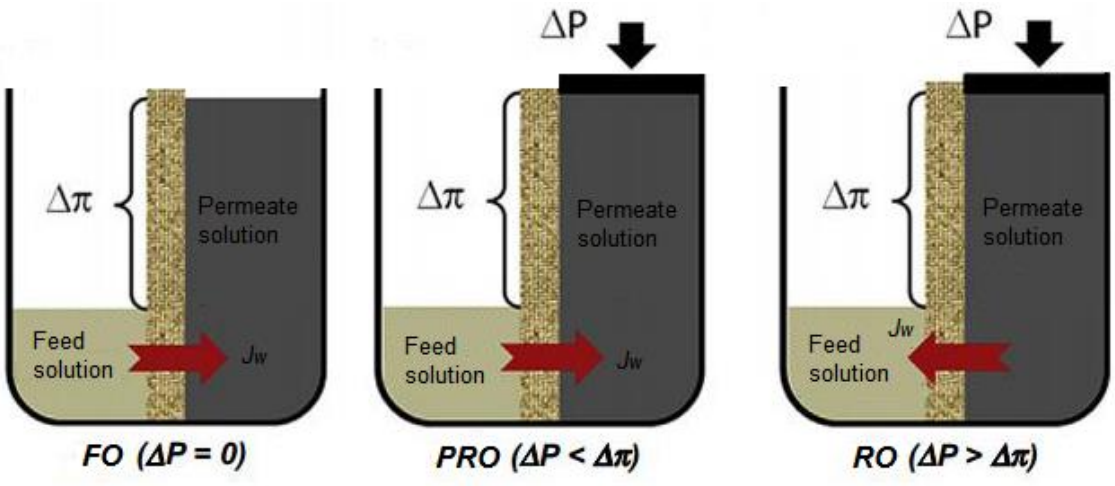

Figure 1.1. Schematic representation of different osmotic processes showing the water permeate flux (J_w) as a function of the transmembrane hydrostatic pressure applied. (Adapted with permission from Ref. [33]).

1.3.1. FO applications

The growing interest of FO during the last years in both academic research and industrial development [28, 29, 34, 35] is attributed mainly to their lower energy consumption compared to the pressure-driven processes like RO, NF, UF and MF [27, 29]. Moreover, FO also presents other potential advantages compared to other membrane processes such as its lower fouling tendency and easier fouling removal [36, 37]. Additionally, a great variety of contaminants can be effectively rejected by FO process permitting to achieve high water recovery rates [38-40]. Consequently, FO is applied in different fields, such as wastewater treatment [41, 42], desalination, osmotic dilution process [38] and coupled with other separation processes to form hybrid systems for different treatments, including FO-MD [43, 44], FO-PRO [45], FO- NF [41, 46] and FO-RO [42, 47, 48].

Despite these facts, FO technology is still in continuous improvements trying to overcome the many-faced challenges and barriers, as reductions of energy consumption and enhancement of water production cost, in order to extend its fields of industrial application.

1.3.2. FO challenges

Although FO is a process of emerging interest widely studied and applied in different fields, it is still suffering from the lack of membranes designed specifically for FO and more adequate draw solution, the issue of concentration polarization, membrane fouling and reverse solute diffusion that reduce the FO performance. Therefore, recent studies are focused on the design and development of novel FO membranes [49-52] and

into the research of new draw solutions [32, 53] that contribute to reduce the fouling effect, the concentration polarization and the reverse solute diffusion while increasing the FO performance. A brief description of the main challenges of FO is outlined as follows:

1.3.2.1. Concentration polarization

Concentration polarization is a common and unavoidable phenomenon in the FO process. It is caused by the transmembrane concentration difference, type of membrane and modules used as well as the hydrodynamics of both the feed and draw solution [27, 29]. The phenomenon induces a decrease in the osmotic pressure between both sides of the membrane (i.e. reducing the driving force) due to an increase in the osmotic pressure at the membrane active layer interface on the feed side of the membrane, or due to a decrease in the osmotic pressure at the membrane surface facing the draw solution. The concentration polarization phenomenon in FO process is attributed to the external (*ECP*) and internal (*ICP*) concentration polarization. *ECP* takes place at both surfaces of the membrane, while *ICP* occurs within the support layer of the membrane. As water permeates the active layer, the draw solution within the porous substructure becomes diluted [27, 54].

While the adverse effect of *ECP* can be mitigated by increasing the flow turbulence or velocity of the feed and/or permeate solution [27, 50], *ICP* is considered the most harmful, affecting considerably the FO performance (i.e. decline of the permeate flux) and increasing the reverse solute diffusion [54-56]. It is essential to develop specific FO membranes that contribute to minimize the *ICP*.

1.3.2.2. Membrane fouling

Like any other membrane process, membrane fouling is also an important and unavoidable phenomenon in FO applications especially when wastewaters are considered [36, 57-59]. Regardless of their organic, inorganic or biological nature, it contributes to reduce the permeate flux, especially when it is subjected to long-term operations. In addition, membrane fouling may influence the solute rejection of the FO membrane due to the modification of the membrane charge and its hydrophilicity [60, 61]. However, due to the lower hydraulic pressure employed in the FO process, fouling is almost fully reversible by water rinsing [36, 37]. It can be assumed, in general, that lower membrane fouling implies more water production, less cleaning and longer membrane life, thereby reducing operational and capital costs. Therefore, high fouling resistant membranes and new draw solutions should be investigated to minimize this phenomenon.

1.3.2.3. Reverse solute diffusion

In FO process, a reverse solute diffusion or reverse permeate flux from the draw solution through the membrane to the feed solution (J_s), is an unavoidable fact due to from one side to the type of the membrane and from the other side to the types of solutes of the draw solution [27, 32, 62]. Its value can be calculated as follows taking into account the variation of volume of the feed solution (V_f) and its concentration (C_f) in a predetermined time (Δ_t) taking into account the effective membrane area (A), by using the following equation [30, 63]:

$$J_s = \frac{\Delta\left(C_f V_f\right)}{A\Delta t} \tag{1.6}$$

The reverse solute diffusion reduces the driving force and may contaminate the feed solution [32]. This effect is also correlated with the membrane fouling effect [57, 64]. This issue should be minimized by means of the design and the development of both FO membranes with a high selectivity and an adequate draw solutions for a given membrane in order to improve the FO efficiency [29].

1.3.2.4. FO membrane engineering

It has become clear that the design and development of improved semi-permeable membranes for FO, by using novel materials and manufacturing techniques to get adequate morphological structures, is critical for the advance in the field of FO. Regardless of their morphology (i.e. flat-sheet or hollow fiber membrane) the membranes used in FO can be classified according to their fabrication methods into phase inversion-formed membranes, thin film composite (TFC) membranes and chemically modified membranes [29]. Practically all used membranes in FO are supported with a backing or embedded porous material. This support layer must be designed to minimize the structural parameter (S) calculated as follows [54, 65-67]:

$$S = \frac{t_s \tau}{\varepsilon} \tag{1.7}$$

were t_s is the support layer thickness, τ is the pore tortuosity and ε is the membrane porosity. S factor is a direct indicator of the *ICP* and a higher value of S results in a more severe *ICP* problem [67]. Therefore, membranes with high porosity, low tortuosity and very thin

thickness like interconnected nanofiber pore structure membranes are the most suitable to overcome the *ICP* issue [67].

Other desired characteristics for an adequate FO membrane are based in a high selectivity of the active layer to increase the feed solute rejection and prevent reverse solute diffusion, good hydrophilicity character to enhance the permeate flux and reduce membrane fouling and high mechanical strength to sustain hydraulic pressure [27, 29].

1.3.2.5. Investigation in draw solutions

As it is mentioned previously, the draw solution is the working fluid responsible for providing the necessary driving force for the FO process. Therefore, one of the main challenges of FO is to find a suitable draw solution exhibiting low water chemical potential (i.e. high osmotic pressure and high driving force) with minimum solute concentration and resulting in low reverse solute diffusion flux and low *ICP* effect, and easy to regenerate after its dilution in the FO process [27, 32, 53]. For example, the draw solution can have a high molecular size of the solute to limit the reverse solute diffusion and mitigate *ICP* as consequence [32, 53]. Other considerations for selection of suitable draw solutions are that the solute must be water-soluble, solid at ambient temperature and pressure, safely handled, and cheap enough to ensure economic viability of the process [32].

It is worth quoting that different types of draw solutions have been used in FO. These can be classified according to the solute type: inorganic solute, volatile solute, organic solute and polymer-based solute draw solutions. Among them, inorganic solutes are mostly used to prepare draw solutions because they are abundantly available in nature, inexpensive and exhibit high osmotic pressure that can induce high water flux [68]. Within the existing wide variety of inorganic solutes, sodium chloride (NaCl) is the most commonly used one as it is highly soluble, non-toxic at low concentrations, but above all, it is relatively easy to reconcentrate using conventional desalination processes like RO and MD technologies [32, 68]. MD is advisable in this case when high saline concentrations are considered as draw solutions for FO because as it is shown in this PhD Thesis can be used for the treatment of supersaturated saline aqueous solutions (chapter 3).

1.4. References

[1] H.T. El-Desouky, H.M. Ettouney, Fundamentals of salt water desalination, Elsevier, 2002.

[2] UN-Water Topics: Water Scarcity factsheet in: www.unwater.org, The United Nations Inter-Agency Mechanism on all Freshwater, 2013.

[3] S. Lattemann, T. Höpner, Environmental impact and impact assessment of seawater desalination, Desalination, 220 (2008) 1.

[4] M. Shatat, M. Worall, S. Riffat, Opportunities for solar water desalination worldwide: Review, Sustainable Cities and Society, 9 (2013) 67.

[5] M. Sarai Atab, A.J. Smallbone, A.P. Roskilly, An operational and economic study of a reverse osmosis desalination system for potable water and land irrigation, Desalination, 397 (2016) 174.

[6] M. Monnot, H.T.K. Nguyên, S. Laborie, C. Cabassud, Seawater reverse osmosis desalination plant at community-scale: Role of an innovative pretreatment on process performances and intensification, Chemical Engineering and Processing: Process Intensification, 113 (2017) 42.

[7] S.M. Shalaby, Reverse osmosis desalination powered by photovoltaic and solar Rankine cycle power systems: A review, Renewable and Sustainable Energy Reviews, 73 (2017) 789.

[8] F. Macedonio, E. Curcio, E. Drioli, Integrated membrane systems for seawater desalination: energetic and exergetic analysis, economic evaluation, experimental study, Desalination, 203 (2007) 260.

[9] J.P. Ducrotoy, M. Elliott, The science and management of the North Sea and the Baltic Sea: natural history, present threats and future challenges, Marine Pollution Bulletin, 57 (2008) 8.

[10] M.C. Mickley, Membrane concentrate disposal: Practices and regulation in Desalination and Water Purification Research and Development Program Report No. 123 (Second Edition). 2006.

[11] D.A. Roberts, E.L. Johnston, N.A. Knott, Impacts of desalination plant discharges on the marine environment: A critical review of published studies, Water Research, 44 (2010) 5117.

[12] G. Daufin, J.P. Escudier, H. Carrère, S. Bérot, L. Fillaudeau, M. Decloux, Recent and Emerging Applications of Membrane Processes in the Food and Dairy Industry, Food and Bioproducts Processing, 79 (2001) 89.

[13] C. Charcosset, Membrane Processes in Biotechnologies and Pharmaceutics, Elsevier, 2012.

[14] N.P. Hankins, R. Singh, Emerging membrane technology for sustainable water treatment, Elsevier, 2016.

[15] Y. El Rayess, C. Albasi, P. Bacchin, P. Taillandier, J. Raynal, M. Mietton-Peuchot, A. Devatine, Cross-flow microfiltration applied to oenology: A review, Journal of Membrane Science, 382 (2011) 1.

[16] H. Ju, B.D. McCloskey, A.C. Sagle, Y.-H. Wu, V.A. Kusuma, B.D. Freeman, Crosslinked poly(ethylene oxide) fouling resistant coating materials for oil/water separation, Journal of Membrane Science, 307 (2008) 260.

[17] Z. He, D.J. Miller, S. Kasemset, D.R. Paul, B.D. Freeman, The effect of permeate flux on membrane fouling during microfiltration of oily water, Journal of Membrane Science, 525 (2017) 25.

[18] Y. Huang, H. Li, L. Wang, Y. Qiao, C. Tang, C. Jung, Y. Yoon, S. Li, M. Yu, Ultrafiltration Membranes with Structure-Optimized Graphene-Oxide Coatings for Antifouling Oil/Water Separation, Advanced Materials Interfaces, 2 (2015).

[19] B.D. Freeman, I. Pinnau, Gas and Liquid Separations Using Membranes: An Overview, 876 (2004) 1.

[20] C. Güell, P. Czekaj, R.H. Davis, Microfiltration of protein mixtures and the effects of yeast on membrane fouling, Journal of Membrane Science, 155 (1999) 113.

[21] A.W. Mohammad, Y.H. Teow, W.L. Ang, Y.T. Chung, D.L. Oatley-Radcliffe, N. Hilal, Nanofiltration membranes review: Recent advances and future prospects, Desalination, 356 (2015) 226.

[22] X. Wang, D. Fang, B.S. Hsiao, B. Chu, Nanofiltration membranes based on thin-film nanofibrous composites, Journal of Membrane Science, 469 (2014) 188.

[23] Z. Wang, C. Crandall, R. Sahadevan, T.J. Menkhaus, H. Fong, Microfiltration performance of electrospun nanofiber membranes with varied fiber diameters and different membrane porosities and thicknesses, Polymer, 114 (2017) 64.

[24] P. Arribas, M. Khayet, M.C. García-Payo, L. Gil, Self-sustained electro-spun polysulfone nano-fibrous membranes and their surface modification by interfacial polymerization for micro- and ultra-filtration, Separation and Purification Technology, 138 (2014) 118.

[25] A. Mehrparvar, A. Rahimpour, M. Jahanshahi, Modified ultrafiltration membranes for humic acid removal, Journal of the Taiwan Institute of Chemical Engineers, 45 (2014) 275.

[26] B. Van der Bruggen, Chemical modification of polyethersulfone nanofiltration membranes: A review, Journal of Applied Polymer Science, 114 (2009) 630.

[27] T. Cath, A. Childress, M. Elimelech, Forward osmosis: Principles, applications, and recent developments, Journal of Membrane Science, 281 (2006) 70.

[28] D.L. Shaffer, J.R. Werber, H. Jaramillo, S. Lin, M. Elimelech, Forward osmosis: Where are we now?, Desalination, 356 (2015) 271.

[29] S. Zhao, L. Zou, C.Y. Tang, D. Mulcahy, Recent developments in forward osmosis: Opportunities and challenges, Journal of Membrane Science, 396 (2012) 1.

[30] M. Khayet, J.A. Sanmartino, M. Essalhi, M.C. García-Payo, N. Hilal, Modeling and optimization of a solar forward osmosis pilot plant by response surface methodology, Solar Energy, 137 (2016) 290.

[31] E. Nagy, J. Dudás, I. Hegedüs, Improvement of the energy generation by pressure retarded osmosis, Energy, 116 (2016) 1323.

[32] A. Achilli, T.Y. Cath, A.E. Childress, Selection of inorganic-based draw solutions for forward osmosis applications, Journal of Membrane Science, 364 (2010) 233.

[33] P. Arribas, M. Khayet, M.C. García-Payo, L. Gil, Novel and emerging membranes for water treatment by electric potential and concentration gradient membrane processes, (2015) 287.

[34] L. Chekli, S. Phuntsho, J.E. Kim, J. Kim, J.Y. Choi, J.S. Choi, S. Kim, J.H. Kim, S. Hong, J. Sohn, H.K. Shon, A comprehensive review of hybrid forward osmosis systems: Performance, applications and future prospects, Journal of Membrane Science, 497 (2016) 430.

[35] M. Taherian, S.M. Mousavi, Modeling and simulation of forward osmosis process using agent-based model system, Computers & Chemical Engineering, 100 (2017) 104.

[36] B. Mi, M. Elimelech, Chemical and physical aspects of organic fouling of forward osmosis membranes, Journal of Membrane Science, 320 (2008) 292.

[37] B. Mi, M. Elimelech, Organic fouling of forward osmosis membranes: Fouling reversibility and cleaning without chemical reagents, Journal of Membrane Science, 348 (2010) 337.

[38] T.Y. Cath, N.T. Hancock, C.D. Lundin, C. Hoppe-Jones, J.E. Drewes, A multi-barrier osmotic dilution process for simultaneous desalination and purification of impaired water, Journal of Membrane Science, 362 (2010) 417.

[39] C.R. Martinetti, A.E. Childress, T.Y. Cath, High recovery of concentrated RO brines using forward osmosis and membrane distillation, Journal of Membrane Science, 331 (2009) 31.

[40] S. Zhao, L. Zou, Effects of working temperature on separation performance, membrane scaling and cleaning in forward osmosis desalination, Desalination, 278 (2011) 157.

[41] S. Zhao, L. Zou, D. Mulcahy, Brackish water desalination by a hybrid forward osmosis–nanofiltration system using divalent draw solute, Desalination, 284 (2012) 175.

[42] O.A. Bamaga, A. Yokochi, B. Zabara, A.S. Babaqi, Hybrid FO/RO desalination system: Preliminary assessment of osmotic energy recovery and designs of new FO membrane module configurations, Desalination, 268 (2011) 163.

[43] Q. Liu, C. Liu, L. Zhao, W. Ma, H. Liu, J. Ma, Integrated forward osmosis-membrane distillation process for human urine treatment, Water Research, 91 (2016) 45.

[44] K.Y. Wang, M.M. Teoh, A. Nugroho, T.-S. Chung, Integrated forward osmosis–membrane distillation (FO–MD) hybrid system for the concentration of protein solutions, Chemical Engineering Science, 66 (2011) 2421.

[45] J.L. Prante, J.A. Ruskowitz, A.E. Childress, A. Achilli, RO-PRO desalination: An integrated low-energy approach to seawater desalination, Applied Energy, 120 (2014) 104.

[46] C.H. Tan, H.Y. Ng, A novel hybrid forward osmosis - nanofiltration (FO-NF) process for seawater desalination: Draw solution selection and system configuration, Desalination and Water Treatment, 13 (2010) 356.

[47] F. Zaviska, Y. Chun, M. Heran, L. Zou, Using FO as pre-treatment of RO for high scaling potential brackish water: Energy and performance optimisation, Journal of Membrane Science, 492 (2015) 430.

[48] D.L. Shaffer, N.Y. Yip, J. Gilron, M. Elimelech, Seawater desalination for agriculture by integrated forward and reverse osmosis: Improved product water quality for potentially less energy, Journal of Membrane Science, 415-416 (2012) 1.

[49] A. Tiraferri, N.Y. Yip, W.A. Phillip, J.D. Schiffman, M. Elimelech, Relating performance of thin-film composite forward osmosis membranes to support layer formation and structure, Journal of Membrane Science, 367 (2011) 340.

[50] J. Wei, C. Qiu, C.Y. Tang, R. Wang, A.G. Fane, Synthesis and characterization of flat-sheet thin film composite forward osmosis membranes, Journal of Membrane Science, 372 (2011) 292.

[51] A. Tiraferri, N.Y. Yip, A.P. Straub, S. Romero-Vargas Castrillon, M. Elimelech, A method for the simultaneous determination of transport and structural parameters of forward osmosis membranes, Journal of Membrane Science, 444 (2013) 523.

[52] T.Y. Cath, M. Elimelech, J.R. McCutcheon, R.L. McGinnis, A. Achilli, D. Anastasio, A.R. Brady, A.E. Childress, I.V. Farr, N.T. Hancock, J. Lampi, L.D. Nghiem, M. Xie, N.Y. Yip, Standard Methodology for Evaluating Membrane Performance in Osmotically Driven Membrane Processes, Desalination, 312 (2013) 31.

[53] Q. Ge, M. Ling, T.S. Chung, Draw solutions for forward osmosis processes: Developments, challenges, and prospects for the future, Journal of Membrane Science, 442 (2013) 225.

[54] G.T. Gray, J.R. McCutcheon, M. Elimelech, Internal concentration polarization in forward osmosis: role of membrane orientation, Desalination, 197 (2006) 1.

[55] K. Lutchmiah, A.R. Verliefde, K. Roest, L.C. Rietveld, E.R. Cornelissen, Forward osmosis for application in wastewater treatment: a review, Water Research, 58 (2014) 179.

[56] J.R. McCutcheon, R.L. McGinnis, M. Elimelech, A novel ammonia-carbon dioxide forward (direct) osmosis desalination process Desalination, 174 (2005) 1-11.

[57] S. Lee, C. Boo, M. Elimelech, S. Hong, Comparison of fouling behavior in forward osmosis (FO) and reverse osmosis (RO), Journal of Membrane Science, 365 (2010) 34.

[58] S. Zou, Y.N. Wang, F. Wicaksana, T. Aung, P.C.Y. Wong, A.G. Fane, C.Y. Tang, Direct microscopic observation of forward osmosis membrane fouling by microalgae: Critical flux and the role of operational conditions, Journal of Membrane Science, 436 (2013) 174.

[59] G. Blandin, H. Vervoort, P. Le-Clech, A.R.D. Verliefde, Fouling and cleaning of high permeability forward osmosis membranes, Journal of Water Process Engineering, 9 (2016) 161.

[60] R. Valladares Linares, V. Yangali-Quintanilla, Z. Li, G. Amy, Rejection of micropollutants by clean and fouled forward osmosis membrane, Water Research, 45 (2011) 6737.

[61] X. Jin, Q. She, X. Ang, C.Y. Tang, Removal of boron and arsenic by forward osmosis membrane: Influence of membrane orientation and organic fouling, Journal of Membrane Science, 389 (2012) 182.

[62] W.A. Phillip, J.S. Yong, M. Elimelech, Reverse Draw Solute Permeation in Forward Osmosis: Modeling and Experiments, Environmental Science & Technology, 44 (2010) 5170.

[63] S. Zhang, K.Y. Wang, T.S. Chung, H. Chen, Y.C. Jean, G. Amy, Well-constructed cellulose acetate membranes for forward osmosis: Minimized internal concentration polarization with an ultra-thin selective layer, Journal of Membrane Science, 360 (2010) 522.

[64] W.C. Lay, T.H. Chong, C.Y. Tang, A.G. Fane, J. Zhang, Y. Liu, Fouling propensity of forward osmosis: investigation of the slower flux decline phenomenon, Water Science & Technology, 61 (2010) 927.

[65] N.N. Bui, J.R. McCutcheon, Hydrophilic nanofibers as new supports for thin film composite membranes for engineered osmosis, Environmental Science & Technology, 47 (2013) 1761.

[66] M. Park, J.J. Lee, S. Lee, J.H. Kim, Determination of a constant membrane structure parameter in forward osmosis processes, Journal of Membrane Science, 375 (2011) 241.

[67] X. Song, Z. Liu, D.D. Sun, Nano gives the answer: breaking the bottleneck of internal concentration polarization with a nanofiber composite forward osmosis membrane for a high water production rate, Advanced Materials, 23 (2011) 3256.

[68] C. Klaysom, T.Y. Cath, T. Depuydt, I.F. Vankelecom, Forward and pressure retarded osmosis: potential solutions for global challenges in energy and water supply, Chemical Society Reviews, 42 (2013) 6959.

Chapter 2

Desalination by membrane distillation

Desalination of seawater is the technology predominantly used to alleviate the problem of water scarcity in coastal region. The sustainability of all desalination processes depends mainly on the reduction of energy costs, increase of water recovery factor and enhancement in recovery and reuse of the generated waste. Integrated/hybrid membrane processes have attracted much interest in desalination field. A membrane process that can be used in a combination with other processes is membrane distillation (MD).

The purpose of this chapter is to review the capability of MD to treat high concentrated aqueous solutions derived from other desalination processes. This possibility is attracting increasing interest due to the problem of brine discharges to the environment. Various benefits can be achieved with the utilization of MD in integrated/hybrid membrane processes, e.g. enhanced quality of the water produced, brine concentration until zero discharge and energy savings.

2.1. Introduction

Desalination of seawater or brackish water is one of the most sustainable alternative solutions to provide fresh water for many communities and industrial sectors [1]. However, two key economic and environmental issues need to be addressed: discharge of brine concentrates to the environment and energy cost constraints [2, 3].

Thermal and reverse osmosis (RO) processes are currently the two major desalination processes in use, accounting for 34.2% and 63.7% of the total capacity produced, respectively. The thermal separation processes include two main groups: (1) evaporation followed by condensation of the produced water vapor, i.e. multi-stage flash distillation process, which represents nearly one-third of the installed capacity, followed by multi-effect distillation, mechanical vapor compression and humidification and dehumidification processes among others [4] and (2) freezing, followed by melting of the formed water ice crystals (indirect and direct freezing processes [5]).

Membrane based processes include RO, nanofiltration (NF), membrane distillation (MD) and electrodialysis (ED). As shown in Fig. 2.1, RO is the most widely used membrane process, accounting for two-thirds of the contracted desalination capacity up to June of 2013.

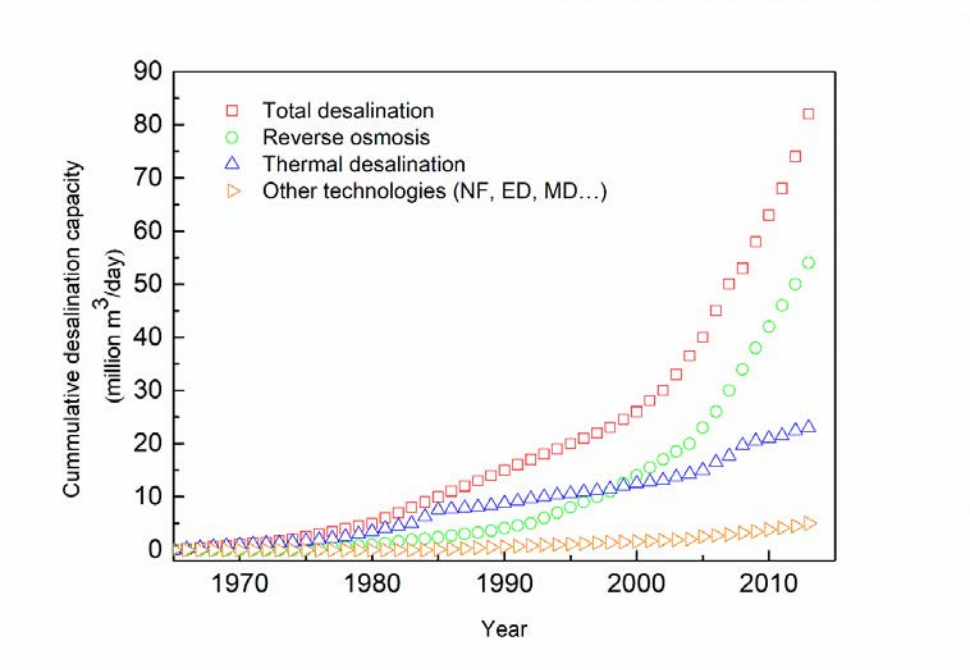

Figure 2.1. Growth of desalination capacity based on different used technologies. (Adapted with permission from Ref. [6]).

All desalination processes generate a residue with a high salt concentration, called brine. The brine characteristics depend on the source of the feedwater used, the pretreatment(s) deployed and the membrane process itself. Today, due to the environmental restrictions on discharged brines, brine treatment needs to be integrated into the desalination cycle, making the process environmentally sustainable. In the last 10 years, several process engineering strategies have been implemented in order to accomplish the conceptual goal of "zero discharge" of liquid (ZLD) [7, 8] as well as recovery of valuable by-products. These strategies are often called integrated or hybrid systems combining different individual technologies. In this context, MD exhibits a great

potential for the treatment of high-salinity aqueous solutions and it is, therefore, a suitable candidate for achieving ZLD.

2.2. Membrane distillation

2.2.1. Historical background

MD is a thermally driven process that is mainly suitable for treating water-based dilute feed solutions [9]. Although this technology has been known for more than 50 years, it still needs further development work at laboratory scale to facilitate its industrial implementation. An early form of MD was patented by Bodell in 1963, describing an apparatus and method to convert non-potable aqueous fluids to potable water [10-13]. Interest in the process, however, faded after the last sixties, due in part to the lower water production rates observed in comparison with RO technology. In the early 1980s, with the development of new membrane manufacturing techniques and novel membranes and modules with better characteristics, the MD process again drew interest, especially within academic communities [11, 13, 14].

The terminology for MD was first discussed and standardized during the Workshop on Membrane Distillation held in 1986 [15]. Since then, numerous studies have been carried out mainly in the academia. Fig. 2.2 shows this growing interest on MD technology based on the number of published studies in referred journals, especially in the last decade.

There are four main MD configurations: direct contact MD (DCMD), air gap MD (AGMD), vacuum MD (VMD), sweeping gas MD (SGMD). In addition, there are two MD hybrid variants: (AGMD+DCMD) termed liquid gap MD (LGMD) and (SGMD+AGMD) termed thermostatic SGMD (TSGMD). It is worth noting that the most used MD variant is DCMD, with 57.6% of the MD published studies up to December 2014.This is because of its simplicity in operation. On the other hand, SGMD is the least studied MD technology, with a contribution of only 4.3% of the published studies [16]. Less than 1% of the total MD studies encompass the hybrid MD variants LGMD and TSGMD (see Fig. 2.3).

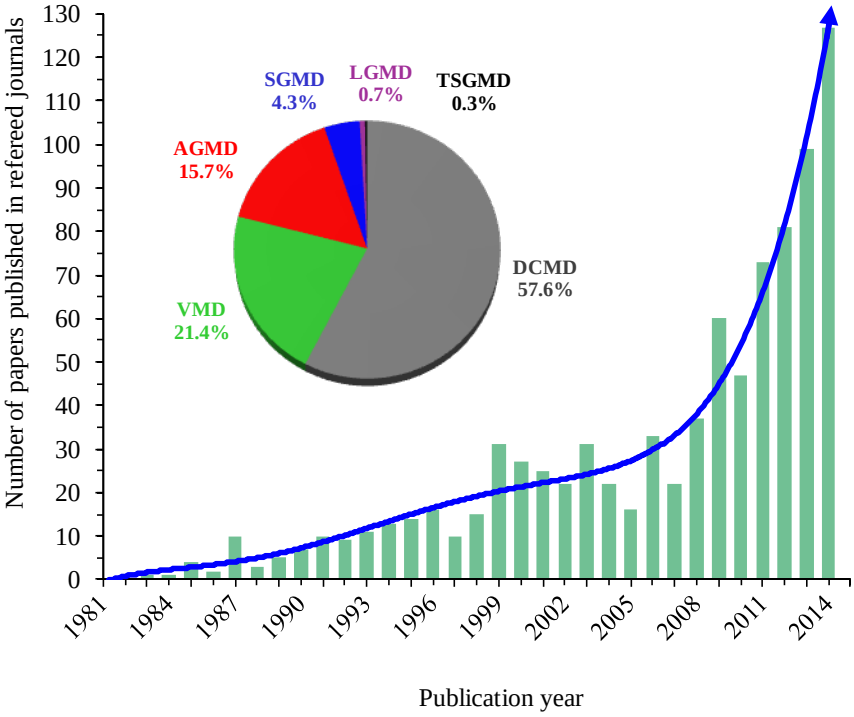

Figure 2.2. Number of published papers on membrane distillation (MD) technology annually and percentage contribution of each MD configuration since 1981 (DCMD, VMD, AGMD, SGMD) together with the two MD variants LGMD and TSGMD. DCMD, direct contact MD; AGMD, air gap MD; VMD, vacuum MD; SGMD, sweeping gas MD; TSGMD, thermostatic SGMD; LGMD, liquid gap MD.

Currently, MD technology is not fully viable in the commercial sense. The main reasons for this are (1) an uncertain water production cost (WPC) due to high energy consumption (SEC), (2) non-availability of membranes and modules designed specifically for MD, (3) a high risk of membrane pore wetting using membranes designed for other applications, e.g. microfiltration and (4) uncertain long-term operation because of membrane fouling and/or scaling.

2.2.2. MD configurations

MD is a non-isothermal evaporation/condensation separation process applied for the treatment of a contaminated aqueous solution, which is maintained in direct contact with one side of a porous and hydrophobic membrane. The process separation (e.g. salt rejection) is carried out mainly by a binary phase change phenomenon, i.e. simultaneous evaporation and condensation. The evaporation step occurs at the hot liquid/vapor interfaces formed at the feed/membrane surface, whereas the condensation step takes place either inside or outside the membrane module, depending on the MD variant, as it is explained later on.

The driving force of MD process is a vapor pressure difference established between both sides of the membrane pores. Depending on the method used to derive this driving force, MD is basically divided into four configurations plus two hybrid variants, as shown in Fig. 2.3.

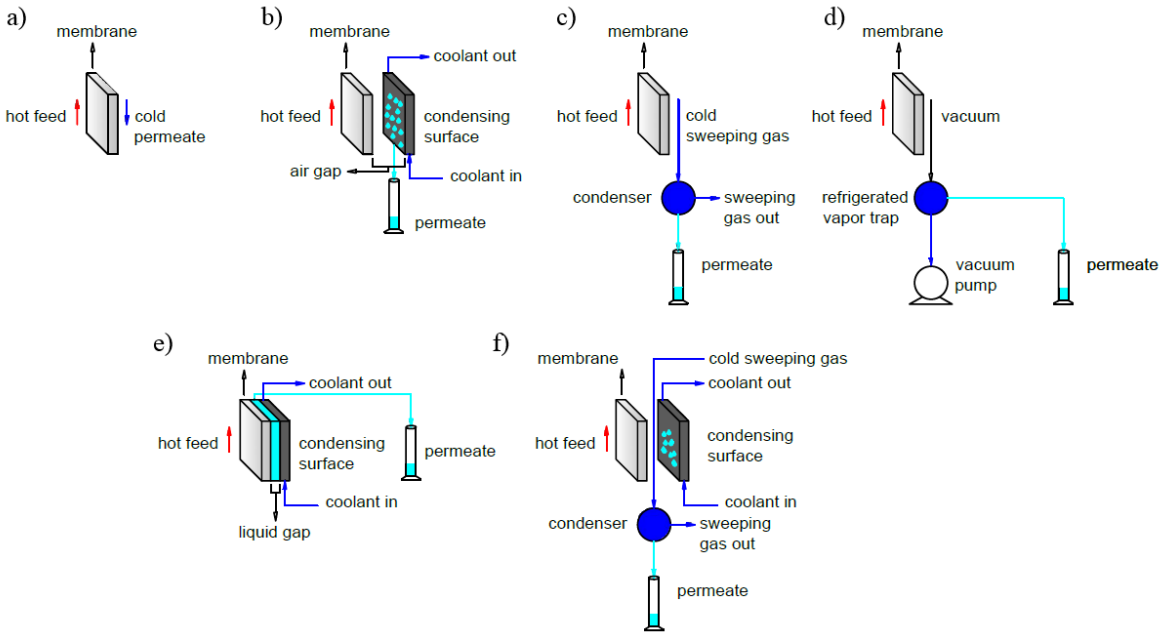

Figure 2.3. Principal membrane distillation (MD) configurations: a) DCMD, b) AGMD, c) SGMD, d) VMD and hybrid MD variants: e) LGMD, f) TSGMD. DCMD, direct contact MD; AGMD, air gap MD; VMD, vacuum MD; SGMD, sweeping gas MD; TSGMD, thermostatic SGMD; LGMD, liquid gap MD.

In DCMD, an aqueous solution colder than the feed one is maintained in direct contact with the permeate side of the membrane. The transmembrane temperature difference induces the necessary vapor pressure difference. In this case, volatile molecules evaporate at the hot liquid/vapor interface, cross the membrane pores in vapor phase and then condense in the cold liquid/vapor interface inside the membrane module.

In AGMD, a stagnant air gap is interposed between the membrane and a condensation surface. The evaporated volatile molecules cross both the membrane pores and the air gap to finally condense over a cold surface inside the membrane module.

In VMD, the driving force is applied by means of a vacuum pump. A hydrostatic pressure lower than the saturation pressure of the volatile compounds to be separated from the feed solution is considered in the permeate side of the membrane module. In contrast to both DCMD and AGMD configurations, condensation takes places outside of the membrane module.

In SGMD, a cold inert gas sweeps the permeate side carrying the evaporated molecules. Again, the condensation step takes place outside the membrane module.

Two other two hybrid MD configurations are also considered. If the air chamber of the AGMD configuration is replaced by a liquid, the process is termed LGMD. This is a combination of DCMD and AGMD. If any solid material is interposed between the membrane and the cold surface instead of air or liquid, the hybrid configuration is called material gap MD (MGMD) or permeate gap MD (PGMD). Because the temperature of the gas in SGMD process increases along the membrane length, a cold surface is built in the permeate side to increase the temperature difference across the membrane. This variant is known TSGMD.

2.2.3. Features and applications

MD technology presents a number of features that make MD an attractive process in comparison to the conventional membrane processes:

- Almost 100% rejection of non-volatile solutes (i.e. allowing production of not only distilled water but also high-purity water). Consequently, desalination of brackish water and seawater is the most likely MD application as well as in medical, pharmaceutical and semiconductor industrial sectors [11, 17].
- The treatment of brines and very high concentrated saline solutions, near their saturation concentration, facilitates the recovery of valuable by-products. On the other hand, pressure-driven membrane processes such as RO cannot treat concentrated brines because of their high osmotic pressures. MD can be used to improve the quality of RO and NF product water [18] and can be used for the recovery of valuable compounds in wastewaters from pharmaceutical, textile and metal industries. MD also enables the discharge of wastewaters less hazardous to the environment [11, 19, 20].
- The removal of trace volatile organic compounds from aqueous solutions in the chemical, petrochemical and biotechnological industries, as well as from dissolved gases such as oxygen and ammonia [11, 21, 22]. MD has also been applied for separating azeotropic mixtures [23].
- Low-operating hydrostatic pressures (near atmospheric pressure) and temperatures below the boiling points of the feed aqueous solutions.
- A lower membrane fouling propensity compared to the pressure-driven membrane processes.
- The feasibility to use waste heat and alternative energy sources (i.e. solar energy systems and geothermal energy).

Although MD technology exhibits all of the above-mentioned advantages, much work is still needed to increase its thermal efficiency and reduce SEC for industrial implementation [24].

2.2.4. Mechanisms of transport in MD

In MD the process, heat and mass transfer both take place simultaneously. As is well known, in all heat transfer systems a fluid boundary layer exists adjacent to both the feed and permeate membrane sides. This boundary layer leads to temperature polarization, which results in a reduction of the transmembrane temperature (because the temperature at the membrane surface (T_m) becomes different to that of the bulk solution (T_b)). This temperature polarization has a negative influence on the driving force. Similarly, the solute(s) concentration at the membrane surface (C_m) is different to that of the bulk feed solution (C_b), giving rise to concentration polarization. For example, during desalination, the concentration of salts at the membrane surface is higher than in the bulk feed aqueous solution. This reduces the water vapor pressure and, as a consequence, leads to a lower permeate flux.

The transport of heat in MD can be described by three steps: (1) heat transport through the feed boundary layer (Q_f), (2) heat transport through the membrane (Q_m) and (3) heat transport through the permeate boundary layer (Q_p) [10]. The total heat transferred through the membrane is due to both the latent heat associated to the produced vapor flux (Q_v) and the heat transferred by conduction following Fourier´s law (Q_c) across both the membrane matrix and its gas-filled pores [10, 11]. Electrical circuits analogy, containing heat transfer resistances corresponding to the heat transfer coefficients (h) of the different MD configurations, are shown in Fig. 2.4.

Between 50% and 80% of the required energy is consumed as latent heat for water vapor production associated with the mass flux, and the rest is lost by thermal conduction through the membrane [25]. This internal heat loss can be minimized by increasing the void volume fraction of the membrane, the size of the pores, the membrane thickness, or by using materials with low thermal conductivity coefficients [11, 26]. In the case of AGMD, the heat losses by conduction through the membrane are reduced because of the presence of the air gap between the membrane and the condensing surface [25]. In the case of VMD, this conductive heat is negligible. It is higher for DCMD and LGMD configurations compared to that for SGMD and TSGMD. This is because the thermal conductivity of liquids is an order of magnitude greater than that of gases.

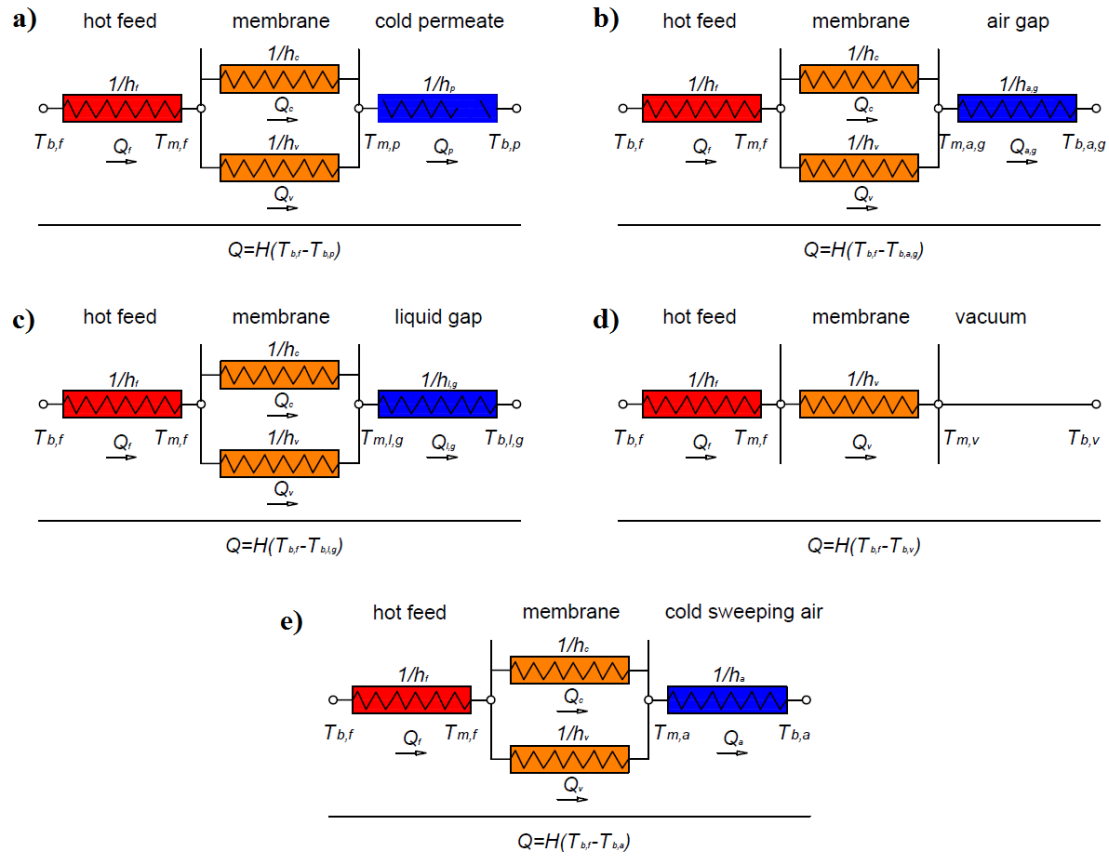

Figure 2.4. Heat transfer resistances in membrane distillation (MD) configurations using an electrical analogy: a) DCMD, b) AGMD, c) LGMD, d) VMD, e) SGMD and TSGMD. DCMD, direct contact MD; AGMD, air gap MD; VMD, vacuum MD; SGMD, sweeping gas MD; TSGMD, thermostatic SGMD; LGMD, liquid gap MD.

The transport of gases and vapors through porous and hydrophobic membranes has been studied extensively, based on the Kinetic Theory of Gases, and different theoretical models have been developed to predict the permeate flux of different types of membranes [10, 11, 13]. The different types of mechanisms proposed for the mass transport through MD membranes depend on (1) the pore size (d_p), (2) the mean free path of the molecules transported through the pores in vapor phase (λ) and (3) the presence of air in the pores. For example, in absence of air, Knudsen diffusion takes place when the pore size is smaller than λ; so that the probability of collisions between vapor molecules and pore wall is greater than the probability of collisions between the molecules themselves. A viscous-flow or Poiseuille-type mechanism of transport is considered when the pore size is higher than λ. In the presence of air inside the pores, the mass flux is described by the ordinary molecular diffusion model. Such models together with their combinations are detailed thoroughly elsewhere [10, 11, 27]. Fig. 2.5 shows schematically the mechanisms proposed for MD configurations.

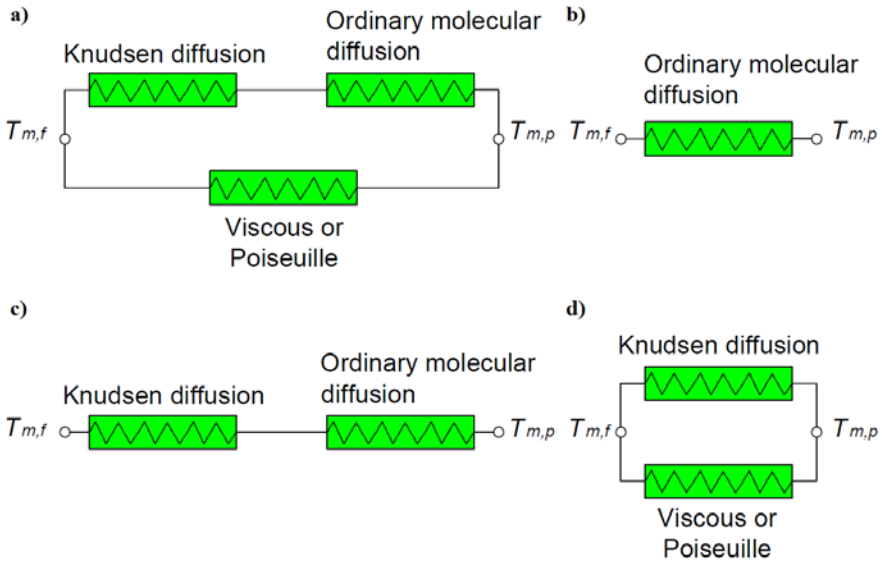

Figure 2.5. Mass transfer resistances in membrane distillation (MD) configurations using an electrical analogy described by the dusty gas model: a) DCMD, b) AGMD, c) LGMD, d) VMD, e) SGMD and TSGMD. DCMD, direct contact MD; AGMD, air gap MD; VMD, vacuum MD; SGMD, sweeping gas MD; TSGMD, thermostatic SGMD; LGMD, liquid gap MD.

The dusty gas model is a more general model that takes into account the above cited mechanisms of transport [10] and also includes a pathway for surface diffusion. However, this latter mechanism is considered negligible in MD because of high porosity and high hydrophobicity of the membrane (i.e. very low affinity between water and the membrane matrix) [13].

The Knudsen flow model and the ordinary molecular diffusion model are applicable in DCMD and in LGMD, when both the feed and permeate solutions are maintained in the membrane module at atmospheric pressure (i.e. no transmembrane hydrostatic pressure is applied). In this case, viscous flow is negligible [10, 11, 28]. Different contributions of each mass transfer resistance should be considered as reported by Essalhi and Khayet [29]. When a deaerated DCMD membrane module was considered (i.e. without air trapped within the membrane pores), Knudsen flow for membranes with small pore sizes was predominant, and the removal of air resulted only in a small increase of DCMD permeate flux. However, for membranes having larger pores, a substantial increase in DCMD flux was achieved [30].

In the SGMD or TSGMD configuration, if the total hydrostatic pressures on both sides of the membranes are similar, the viscous type of flow is negligible and the mass transport will take place via a combined Knudsen/ordinary molecular diffusion mechanism (Fig. 2.5c). In this case, ordinary molecular diffusion is the dominant mechanism and it is more important for membranes with wider pores [31]. For AGMD carried out under atmospheric pressure, ordinary molecular diffusion was reported as the dominant resistance to transport when taking into consideration the stagnant non-

condensable gases trapped within the membrane pores and in the gap between the membrane and the condensing surface (Fig. 2.5b).

In the VMD configuration (with a continuous vacuum applied in the permeate side), air is removed and, therefore, ordinary molecular diffusion resistance can be neglected since diffusion depends on the partial pressure of air in the membrane pores [10]. In this case, the model for the mass transport mechanisms is Knudsen flow, viscous flow or a combination of the two, depending on the pore size and the mean free path of the molecules transported through the pores in the vapor phase. The latter is a function of the applied temperature and pressure [11].

2.2.5. MD membranes

The MD membrane should be porous with a high porosity to allow a high permeate flux, it should be highly hydrophobic, it should possess a high LEP (liquid entry pressure) and it should possess a low thermal conductivity to minimize the heat loss by conduction through the membrane [11, 27, 32-34]. In addition, the membrane should exhibit a good thermal stability and a high resistance to chemicals such as those used in membrane cleaning [27].

Developments in the MD process were made particularly in the early 1980s when novel and more suitable membranes became available, for instance, hydrophobic polytetrafluoroethylene (PTFE) membranes [10]. Other polymers, such as polypropylene (PP) and polyvinylidene fluoride (PVDF), were also used to prepare membranes in tubular, capillary and flat-sheet forms [14]. Supported membranes have also been used in MD applications, but the support should not provide any significant resistance to mass transport [35].

To date, the membranes used for the fabrication of MD membrane modules and semi-pilot plants are those made for microfiltration applications. Very few laboratory researches have been performed on the preparation of membranes used specifically for MD [11]. Different techniques have been applied to prepare different types of flat sheet and hollow fiber membranes for MD. Different polymers or copolymers have been applied, the latter including poly(vinylidenefluoride-hexafluoropropylene) (PVDF-HFP) [36-38] or polyvinylidenefluoride-tetrafluoroethylene (PVDF-TFE) [39]. The membrane surface has been modified [40], and nano-fibrous and nanostructured membranes have also been employed [29, 41].

2.2.6. Commercial modules

Since 1963, when Bodell patented the first MD desalination test [42], numerous modules and devices have been developed; these include plate-and-frame, spiral wound

and shell-and-tube configurations. Plate-and-frame modules use flat sheet membranes that are easy to examine, clean and replace. This configuration requires supports to hold the membrane preventing its rupture and deflection. Both the membrane and the support along with the spacer are assembled forming different cassettes, which are normally stacked between two end plates [11]. *General Electric SEPA CF* [43], *Scarab Development AB* [44], *Keppel Seghers* [45] and *Memsys GmbH* [46] proposed plate-and-frame modules for different MD configurations.

Another type of module based on the use of flat sheet membranes is the spiral wound module. In this type of design, the membrane is integrated with the spacers so it is difficult to replace. One can find two types of spiral wound MD modules, these being fabricated by *SEP GmbH* [19] and *Fraunhofer ISE* [30], respectively.

Capillary fibers can also be assembled in a plate-and-frame module. *Membrana GmbH* designed modules with PP fibers in a cross-flow mode, to reduce the temperature polarization effects [47]. Normally, tubular, capillary and hollow fiber membranes are packed in shell-and-tube modules [11]. In this design, the membrane is an integrated part of the module. One of the important advantages of hollow fiber modules is their high membrane packing density. This type of modules is supplied by *Microdyn-Nadir GmbH* [26, 48].

MD modules must be fabricated with thermal insulating materials resistant to chemicals, high pressures and temperatures. Their design must permit the following: high and uniform flow rates of feed and permeate aqueous solutions, which move tangentially to the membrane surface or in cross-flow with a low pressure drop, high turbulence to reduce the effects of both temperature and concentration polarization, high packing density and good heat recovery. In cases where membrane pore wetting may occur, the MD module should provide an easy way to inspect and replace the membrane, if necessary.

2.3. Properties of saline aqueous solutions

2.3.1. Composition of seawater and brines

The ionic stoichiometry used in the determination of the reference composition of seawater is listed in Table 2.1. In general, the chemical composition of open sea is constant, and changes in the amount of total dissolved solids (TDS) are subject to geographical location as well as local conditions. The chemical composition of seawater also varies with the density of water and other physical and chemical parameters.

Salinity is the mass of dissolved salts in a unit mass of solution. Although the vast majority of seawater has salinity between 31 g/kg and 38 g/kg, seawater is not uniformly saline throughout the world. Nevertheless, a total salinity of 35,000 ppm (35 g/kg) is

commonly accepted as standard for seawater salinity. The main salt compounds reported in standard seawater are listed in Table 2.2. Table 2.3 shows the approximate salinity of different seas and oceans over the world.

Table 2.1. The ionic stoichiometry used in the determination of the reference composition of seawater, expressed in molar fractions and mass fraction [49, 50].

Solute	Molar fraction	Mass fraction
Na^+	0.4188071	0.3065958
Mg^{2+}	0.0471678	0.0365055
Ca^{2+}	0.0091823	0.0117186
K^+	0.0091159	0.0113495
Sr^{2+}	0.000081	0.000226
Cl^-	0.4874839	0.5503396
SO_4^{2-}	0.0252152	0.0771319
HCO_3^-	0.001534	0.0029805
Br^-	0.000752	0.001913
CO_3^{2-}	0.0002134	0.0004078
$B(OH)_4^-$	0.00009	0.0002259
F^-	0.000061	0.0000369
OH^-	0.0000071	0.0000038
$B(OH)_3$	0.0002807	0.0005527
CO_2	0.0000086	0.0000121
TOTAL	**~1**	**~1**

A significant amount of the rejected streams from desalination plants (i.e. brines) have a high salinity with a salt concentration ranging from 43 to 90 g/L. The brines also contain additives commonly used in the desalination process such as pretreatment anti-scalants or cleaning membrane agents, but they make a contribution of less than 1% of the total evacuated volume [58]. Table 2.4 summarizes the physical-chemical composition of brines of different desalination plants.

The discharged brines are, in effect, concentrated seawaters and will affect the marine environment. If the sea brine discharge is continuous, as occurs in numerous desalination plants currently, the salinity of the seawater in the vicinity of the discharge effluent will be elevated significantly. This in turn will disturb the local marine flora and fauna. Brines must therefore be recuperated or diluted to the seawater concentration before discharge.

Table 2.2. The main salt compounds of standard seawater (~35 g/L salinity) [49].

Salt compounds	Composition	Concentration (ppm)
Sodium chloride	NaCl	23,985
Magnesium chloride	$MgCl_2$	5,029
Sodium sulfate	Na_2SO_4	4,011
Calcium chloride	$CaCl_2$	1,141
Potasium chloride	KCl	699
Sodium bicarbonate	$NaHCO_3$	172
Potasium bromide	KBr	100
Boric acid	H_3BO_3	26
Strontium chloride	$SrCl_2$	14
Sodium fluoride	NaF	3
	TOTAL	**35,180**

Table 2.3. Average salinity of various seawaters [58-64].

Ocean/sea	Salinity (mg/L)
Baltic Sea	500-30,000
Red Sea	40,000
Atlantic Ocean	34,750-37,500
Mediterranean Sea	38,700
Pacific Ocean	32,500-36,250
Indic Ocean	32,000-36,000
Dead Sea	342,000

Table 2.4. Physicochemical characteristics of brines from RO desalination plants.

Brine physicochemical characteristics							
References	[59]	[60]		[61]	[62]	[63]	[64]
Parameters							
pH	-	7	8	-	4	7.2	6.2
TDS, mg/L	50200	-	-	-	-	28000	17124
Conductivity, µS/cm	-	-	-	-	13500	33000	25984
Hardness, mg/L ($CaCO_3$)	-	470	142	-	-	-	345
SiO_2, mg/L	-	116	72	103	56	-	15.6
Cations							
Na^+, mg/L	15500	991	5130	-	2084	5120	4160
Mg^{2+}, mg/L	2020	318	386	468	245	770	370
K^+, mg/L	-	-	-	-	79	-	134
Ca^{2+}, mg/L	625	1032	819	1020	540	2080	1537
Fe^{2+}, mg/L	-	-	-	-	-	-	0.4
Mn^{2+}, mg/L	-	-	-	-	-	-	0.2
Anions							
Cl^-, mg/L	28800	2823	8960	6710	4068	14170	8369
SO_4^{2-}, mg/L	3060	1553	1920	2688	2160	5920	2334
NO_3^-, mg/L	-	-	-	-	-	-	14.6
PO_4^{3-}, mg/L	-	0.4	2	-	0.04	-	-
HCO_3^-, mg/L	199	576	223	-	-	-	421

2.3.2. Thermodynamic properties of different saline aqueous solutions

As mentioned in section 2.1, the MD process is able to treat brines from other desalination processes for concentrating and further water production. This is done with a view towards ZLD to the environment. However, care must be taken during the treatment because of the high risk of membrane pore wetting. This can occur due to salt crystal formation and deposition over the membrane surface. Therefore, crystallization of salts over the membrane surface must be avoided and should, instead, be treated in an external container outside of the membrane module.

Since MD is a non-isothermal process, it is valuable to know the effects of the temperature on the solubility of different salts in water. Depending on the temperature, some salts dissolved in brines can precipitate and recovered without affecting the desalination process. Fig. 2.6 presents the solubility of different salt compounds in water with temperature at atmospheric pressure [65-68].

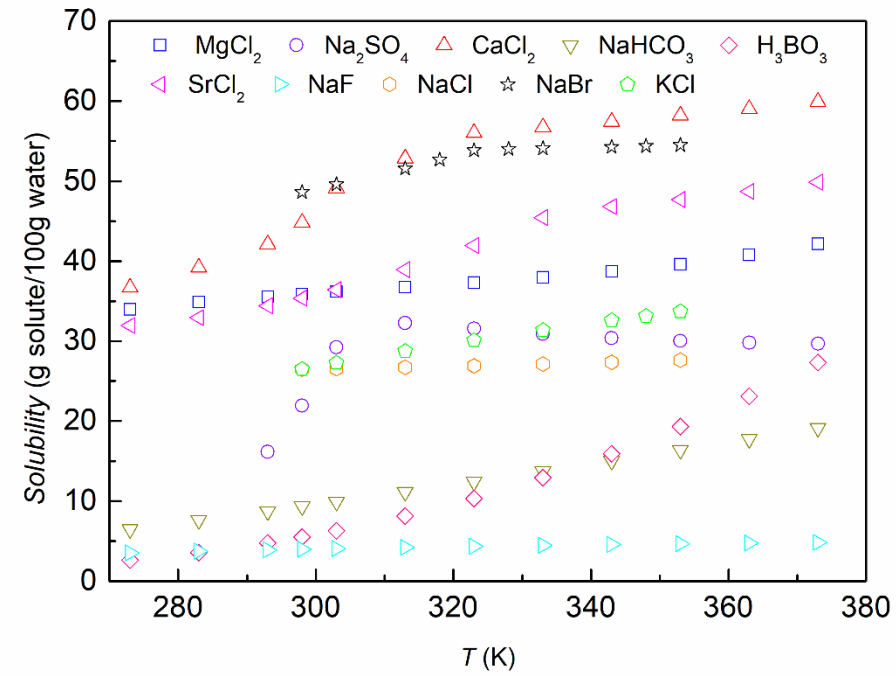

Figure 2.6. Solubility as a function of temperature for different compounds present in seawater (Solubility units are given in grams per 100 grams of water) [65-68].

The thermodynamic properties of saline waters depend on salinity, temperature and pressure. Some useful empirical functions are listed in Table 2.5.

Table 2.5. Thermodynamic properties of salt water.

Properties	Correlation	Parameters for correlation	Observations
Density ρ **(kg/m^3)**	$\rho = 10^3 \cdot \left(A_1 \cdot F_1 + A_2 \cdot F_2 + A_3 \cdot F_3 + A_4 \cdot F_4\right)$	$A_1 = 4.032219 \cdot G_1 + 0.115313 \cdot G_2 + 3.26 \cdot 10^{-4} \cdot G_3$ $A_2 = -0.108199 \cdot G_1 + 1.571 \cdot 10^{-3} \cdot G_2 - 4.23 \cdot 10^{-4} \cdot G_3$ $A_3 = -0.012247 \cdot G_1 + 1.74 \cdot 10^{-3} \cdot G_2 - 9 \cdot 10^{-6} \cdot G_3$ $A_4 = 6.92 \cdot 10^{-4} \cdot G_1 - 8.7 \cdot 10^{-5} \cdot G_2 - 5.3 \cdot 10^{-5} \cdot G_3$ $A = \frac{\left(2 \cdot T - 200\right)}{160}$ $F_1 = 0.5,\ F_2 = A,\ F_3 = 2 \cdot A^2 - 1,\ F_4 = 4 \cdot A^3 - 3 \cdot A$ $B = \frac{\left(\frac{2 \cdot s}{1000} - 150\right)}{150}$ $G_1 = 0.5,\ G_2 = B,\ G_3 = 2 \cdot B^2 - 1$	Correlation valid over this ranges: $0 < s < 160$ g/L $10 < T < 180$ ºC s is water salinity
Specific heat at constant pressure C_p **(kJ/kg K)**	$C_p = \left(A + B \cdot T + C \cdot T^2 + D \cdot T^3\right) \cdot 10^{-3}$	$A = 4206.8 - 6.6197 \cdot s + 1.2288 \cdot 10^{-2} \cdot s^2$ $B = -1.1262 + 5.4178 \cdot 10^{-2} \cdot s - 2.2719 \cdot 10^{-4} \cdot s^2$ $C = 1.2026 \cdot 10^{-2} - 5.3566 \cdot 10^{-4} s + 1.8906 \cdot 10^{-6} s^2$ $D = 6.8777 \cdot 10^{-7} + 1.517 \cdot 10^{-6} s - 4.4268 \cdot 10^{-9} s^2$	Correlation valid over this ranges: $20 < s < 160$ g/L $20 < T < 180$ ºC
Dynamic viscosity μ **(kg/m s)**	$\mu = (\mu_W)\ (\mu_R) \cdot 10^{-3}$	$Ln(\mu_w) = -3.79418 + 604.129 / (139.18 + T)$ $\mu_R = 1 + A \cdot s + B \cdot s^2$ $A = 1.474 \cdot 10^{-3} + 1.5 \cdot 10^{-5} \cdot T - 3.927 \cdot 10^{-8} \cdot T^2$ $B = 1.0734 \cdot 10^{-5} - 8.5 \cdot 10^{-8} \cdot T + 2.23 \cdot 10^{-10} \cdot T^2$	Correlation valid over this ranges: $0 < s < 130$ g/L $10 < T < 180$ ºC
Thermal conductivity k **(W/m K)**	$Log_{10}(k) = Log_{10}(240 + A \cdot s) + 0.434\left(2.3 - \frac{343.5 + B \cdot s}{T + 273.15}\right)\left(1 - \frac{T + 273.15}{647.3 + C \cdot s}\right)^{1/3}$	$A = 2 \cdot 10^{-4},\ B = 3.7 \cdot 10^{-2},\ C = 3 \cdot 10^{-2}$	Correlation valid over this ranges: $0 < s < 160$ g/L $20 < T < 180$ ºC
Enthalpy of saturated liquid water H **(kJ/kg)**	$H = -0.033635409 + 4.207557011 \cdot T - 6.200339 \cdot 10^{-4} \cdot T^2 + 4.459374 \cdot 10^{-6} \cdot T^3$		Correlation valid over this ranges: $5 < T < 200$ ºC
Enthalpy of saturated water vapor H**" (kJ/kg)**	$H'' = 2501.689845 + 1.806916015 \cdot T + 5.087717 \cdot 10^{-4} \cdot T^2 - 1.1221 \cdot 10^{-5} \cdot T^3$		Correlation valid over this ranges: $0.01 < T < 200$ ºC
Latent heat of water evaporation λ **(kJ/kg)**	$\lambda = 2501.897149 - 2.407064037 \cdot T + 1.192217 \cdot 10^{-3} \cdot T^2 - 1.5863 \cdot 10^{-5} \cdot T^3$		Correlation valid over this ranges: $5 < T < 200$ ºC
Entropy of saturated liquid water S **(kJ/kg ˚C)**	$S = -0.00057846 + 0.015297489 \cdot T - 2.63129 \cdot 10^{-5} \cdot T^2 + 4.11959 \cdot 10^{-8} \cdot T^3$		Correlation valid over this ranges: $5 < T < 200$ ºC

Table 2.5. (Continuation) Thermodynamic properties of salt water.

Properties	Correlation	Parameters for correlation	Observations
Entropy of saturated water vapor S" (kJ/kg K)	$S" = 9.149505306 - 2.581012 \cdot 10^{-2} \cdot T + 9.625687 \cdot 10^{-5} \cdot T^2 - 1.786615 \cdot 10^{-7} \cdot T^3$		Correlation valid over this ranges: $0.01 < T < 200$ ºC
Saturation pressure of water vapor *P* (kPa)	$\ln(P / P_c) = \left(\frac{T_c}{T + 273.15} - 1\right) \sum_{i=1}^{8} f_i (0.01(T + 273.15 - 338.15))^{(i-1)}$	$T_c = 647.286\ K$ $P_c = 22089\ kPa$ $f_1 = -7.419242,\ f_2 = 0.29721$ $f_3 = -0.1155286,\ f_4 = 0.008685635$ $f_5 = 0.001094098,\ f_6 = -0.00439993$ $f_7 = 0.002520658,\ f_8 = -0.000521868$	Correlation valid over this ranges: $5 < T < 200$ ºC
Saturation temperature of water vapor *T* (ºC)	$T = \left(42.6776 - \frac{3892.7}{(\ln(P / 1000) - 9.48654)}\right) - 273.15$		Correlation valid over this ranges: $0.8721 < P < 1553.8$ kPa $5 < T < 200$ ºC
Specific volume of saturated water vapor *V* (m^3/kg)	$V = V_c \left(\frac{T_c}{T + 273.15} - 1\right) \exp\left(\sum_{i=1}^{6} f_i (T + 273.15)^{(i-1)}\right)$	$T_c = 647.286\ K$ $V_c = 0.003172222\ m^3/kg$ $f_1 = 83.63213098,\ f_2 = -0.668265339$ $f_3 = 0.002495964,\ f_4 = -5.04185E^{-06}$ $f_5 = 5.34205E^{-09},\ f_6 = -2.3279E^{-12}$	Correlation valid over this ranges: $5 < T < 200$ ºC
Specific volume of saturated liquid vapor, *V* (m^3/kg)	$V = V_c \left(\frac{T_c}{T + 273.15} - 1\right) \exp\left(\sum_{i=1}^{6} f_i (T + 273.15)^{(i-1)}\right)$	$T_c = 647.286\ K$ $V_c = 0.003172222\ m^3/kg$ $f_1 = -2.781015567,\ f_2 = 0.002543267$ $f_3 = 9.845047E^{-06},\ f_4 = 3.636115E^{-09}$ $f_5 = -5.358938E^{-11},\ f_6 = 7.019341E^{-14}$	Correlation valid over this ranges: $5 < T < 200$ ºC
Dynamic viscosity of saturated liquid water, μ (kg/m s)	$\mu = \exp(-3.79418 + 604.129 / (139.18 + T)) \cdot 10^{-3}$		Correlation valid over this ranges: $10 < T < 115$ ºC
Dynamic viscosity of saturated water vapor, μ (kg/m s)	$\mu = \exp(-3.609417664 + 275.928958 / (-227.0446083 - 0.896081232 \cdot T - 0.002291383 \cdot T^2)) \cdot 10^{-3}$		Correlation valid over this ranges: $10 < T < 180$ ºC
Surface tension of saturated liquid water, σ (N/m)	$\sigma = 7.5798 \cdot 10^{-2} - 1.4691 \cdot 10^{-4} \cdot T - 2.2173 \cdot 10^{-7} \cdot T^2$		Correlation valid over this ranges: $0 < T < 136$ ºC

2.4. MD desalination

2.4.1. Most commonly used configurations and desalination performance

Weyl [17] was the first to propose the use of DCMD for desalination. However, the fluxes were much smaller than those achieved by RO technology (20-75 kg/m^{2}h). DCMD is the most studied MD configuration, and several authors have shown that the DCMD permeate fluxes are quite similar to those of RO. This is mainly attributed due to improvements in membranes and modules prepared especially for MD. For example, using a novel porous composite hydrophobic/hydrophilic membrane prepared for DCMD, Essalhi and Khayet [40] observed 99,98% NaCl rejection factor and 35 kg/m^{2}h permeate flux for a feed solution containing 30 g/L NaCl and a temperature difference of 60ºC. By using an electrospun nano-fibrous membrane (ENM) [69], a higher permeate flux, 53.5 kg/m^{2}h under the same operating conditions was achieved. By increasing the initial feed solution to 60 g/L NaCl (roughly twice the concentration of typical seawater) and applying the same DCMD operating conditions, the permeate flux of the ENM decreased only to 51.3 kg/m^{2}h. In both cases the rejection factor was higher than 99.94%. When using hollow fiber membranes, Wang *et al.* [70] reported permeate fluxes around 41 kg/m^{2}h, with a temperature difference of 60ºC and a rejection > 99.9% for a 35 g/L NaCl aqueous solution.

In general, AGMD has lower permeate fluxes than those of the other MD configurations. This is due to the mass transfer resistance associated to the stagnant air interposed between the membrane and the condensation surface. However, this stagnant air reduces the heat loss by conduction and it also reduces the temperature polarization effect. By applying the same operating conditions as those considered in DCMD, Essalhi and Khayet [40] obtained a salt rejection factor > 99.9% and a permeate flux of 11 kg/m^{2}h for AGMD. Guillén-Burrieza *et al.* [45] reported 5.9 kg/m^{2}h with a salt rejection > 99.8% for a feed aqueous solution of 35 g/L NaCl and a feed temperature of 81ºC. Similar AGMD desalination results may be found elsewhere [16, 71-74].

In LGMD, it can be postualted that the permeate flux should be higher than that in AGMD because the thermal conductivity coefficient of water is greater than that for air. Essalhi and Khayet [16] reported, for first time, a comparative study between AGMD and LGMD configurations used in desalination of a 30 g/L NaCl aqueous solution with a porous composite hydrophobic/hydrophilic flat-sheet membrane and temperature difference of 60ºC. The salt rejection was found to be quite similar for both MD variants (i.e. > 99.6%), whereas the permeate flux was slightly higher for the LGMD (9.5 kg/m^{2}h) when compared with the AGMD (i.e. 8 kg/m^{2}h).

The SGMD process was developed to provide an intermediate solution between DCMD and AGMD, combining a relatively low conductive heat loss through the

membrane with a reduced mass transfer resistance. Compared to the AGMD configuration, the gas is not stagnant but sweeps the membrane and carries the water vapor. This enhances the mass transfer coefficient and leads to a higher permeate flux. However, SGMD is the least studied MD configuration due to the need of external condensers to collect the permeate and a gas source to generate the sweeping gas. By using flat sheet PTFE membranes of different pore sizes (i.e. 0.2 and 0.45 μm), Khayet *et al.* [75] reported permeate fluxes of 17 and 21 kg/m^{2}h, respectively for distilled water as feed using a sweep gas velocity of 1.5 m/s and a feed temperature of 65ºC. For a 30 g/L NaCl feed solution, Khayet and Cojocaru [76] reported permeate fluxes of 5.37 kg/m^{2}h and a salt rejection > 99.94% at an air circulation velocity of 2.02 m/s and a feed inlet temperature of 69ºC. In another study, with the same membrane and the same salt feed solution, Khayet *et al.* [77] showed that, upon increasing the feed temperature to 71.6ºC and the air velocity to 2.11 m/s, the permeate flux increased to 8.32 kg/m^{2}h while maintaining the same salt rejection factor.

In TSGMD, a part of the vapor that permeates through the membrane condenses inside the module and the rest in an external condenser. García-Payo *et al.* [23] studied the effect of various parameters on the permeate flux achieving a maximum flux of 19 kg/m^{2}h at a sweep gas velocity of 2.6 m/s and a temperature difference of 50ºC.

Although VMD and SGMD exhibit high permeate fluxes (attributed mainly to the low heat transfer by conduction through the membrane), these configurations are the least used owing to the need for a pump or air generator and traps to collect the permeate. Li and Sirkar [47] obtained a permeate flux of 71 kg/m^{2}h for a feed temperature of 85ºC and a low concentration feed of 1 g/L NaCl, using a hollow fiber module. Meanwhile, Criscuoli *et al.* [78] attained initial permeate fluxes above 50 kg/m^{2}h using a flat-sheet membrane module with distilled water, 60ºC feed temperature and a vacuum pressure of 60 mbar. Lower permeate fluxes were obtained in other studies [9, 79, 80].

2.4.2. MD desalination of brines and high saline aqueous solutions

As stated earlier, MD technology can be used to treat brines and high salinity aqueous solutions (i.e. close to the saturation point of the salts). However, few studies have been performed with high salt concentrations solutions. Furthermore, not all MD configurations were tested and no study has been carried out using a feed aqueous solution containing salts with concentrations near their saturation point.

In the DMCD configuration, Gryta *et al.* [20] used PP commercial hollow fiber membranes to treat concentrated brine solutions (200 g/L of NaCl) at a temperature difference of 65ºC. The initial permeate flux obtained was 10.8 kg/m^{2}h, but rapid crystallization on the membrane surface was observed, and this lead to a decline in the permeate flux. Tun *et al.* [81] used a flat-sheet PVDF (0.22 μm) membrane and 260 g/L

NaCl brine solution, and achieved permeate flux up to 20 kg/m^{2}h at a temperature difference of 40ºC. However, the formation of crystals reduced the permeate flux drastically. Walton *et al.* [82] established the capability of the AGMD configuration to treat aqueous feed solutions with high NaCl concentrations (125 g/L and 270 g/L) at 70ºC, but the permeate flux was low (3.2 kg/m^{2}h and 2.5 kg/m^{2}h, respectively) producing distilled water quality permeate. Using two PTFE flat sheet commercial membranes with different pore sizes, lower permeate fluxes were reported by Alkhudhiri *et al.* [83] (0.17 kg/m^{2}h and 0.21 kg/m^{2}h for 0.2 μm and 0.45 μm, respectively) with salt rejections > 99.98%. In both cases, an aqueous solution of 180 g/L NaCl was used as feed at a temperature of 50ºC, and the air gap had a width of 8 mm. Safavi and Mohammadi [84] tested the VMD configuration to desalt 100, 200 and 300 g/L NaCl feed solutions using PP commercial hollow fiber membranes. At a feed temperature of 55ºC and a vacuum pressure of 40 mbar, the reported permeate fluxes were 14.2, 13.1 and 11 kg/m^{2}h, respectively, with salt rejection equal to 99.99%.

2.4.3. Effects of MD process conditions on MD desalination performance

2.4.3.1. Feed temperature

The feed temperature significantly affects the permeate flux and its effects have been widely investigated [9-11, 14, 75, 85, 86]. In general, the permeate flux increases with increasing feed temperature as a result of the exponential enhancement of the vapor pressure with temperature. The change of the partial vapor pressure (p_w^0) of pure water with absolute temperature can be determined using the Antoine equation [10]:

$$p_w^0(T) = \exp\left(\alpha - \frac{\beta}{T-\gamma}\right) \tag{2.1}$$

where α, β and γ are readily available constants). For water, for p_w^0 in units of Pa and T in units of K, α, β and γ values are 23.1964, 3816.44 K and 46.13 K, respectively.

In all MD configurations, an Arrhenius type of dependence is frequently considered to fit the permeate flux (J_w) variation with the temperature [11]:

$$J_w = a \cdot \exp\left(\frac{-b}{T}\right) \tag{2.2}$$

where T is the absolute temperature and a and b are constants. An example is shown in Fig. 2.7 for two PTFE flat-sheet membranes having different mean pore sizes.

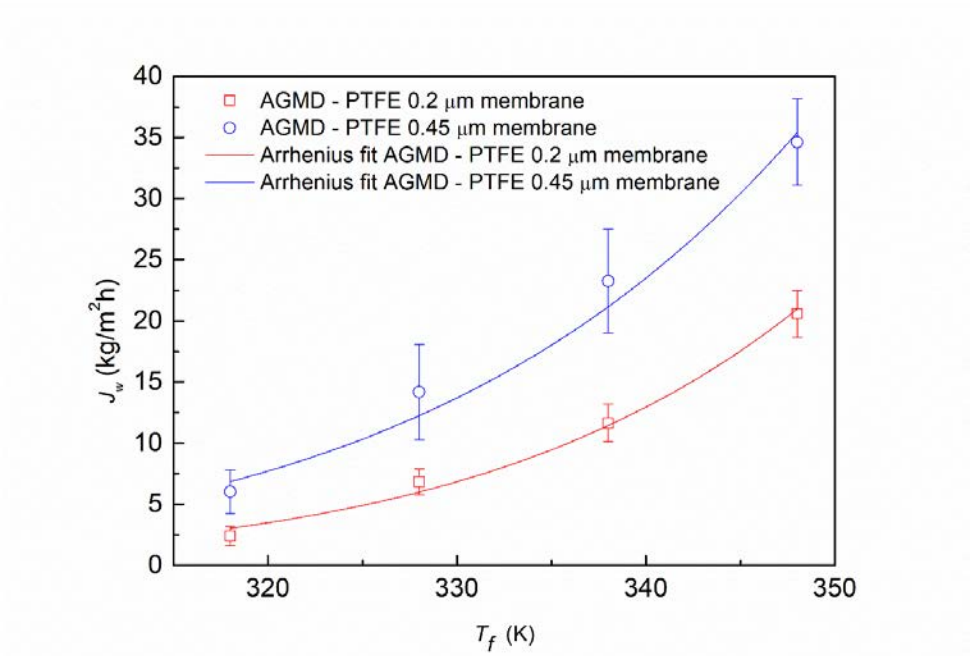

Figure 2.7. Air gap membrane distillation (AGMD) permeate flux as a function of the feed temperature for two different polytetrafluoroethylene (PTFE) flat-sheet membranes having a mean pore size of 0.2 μm and 0.45 μm. Operating parameters: 65 g/L NaCl feed solution, 25ºC condensation surface temperature and 3 mm air gap.

It is better to run the MD systems under high feed temperatures. This is because the thermal efficiency defined as the ratio of the heat that contributes to evaporation (i.e. the rate of mass transfer) to the total heat transferred through the membrane from the feed to the permeate side, is high, although the temperature polarization effect increases with feed temperature [13, 48, 87]. However, when increasing the feed temperature, there is a decrease of both the surface tension of water (γ_w) and the water contact angle (θ). This results in a reduction of the *LEP* and, therefore, increases the risk of membrane pore wetting [88-90]. If $\Delta P_{interface}$ exceeds the *LEP* value, the liquid can penetrate into and pass through the membrane pores. This scenario is quantified by the relationship between the maximum pore size of the membrane (d_{max}) and the transmembrane hydrostatic pressure given by Laplace equation [13, 90]:

$$P_{\text{liquid}} - P_{\text{vapor}} = \Delta P_{\text{interface}} < LEP = \frac{-B\gamma_w \cos\theta}{d_{\max}} \tag{2.3}$$

As mentioned earlier, the temperature polarization phenomenon reduces the mass transfer driving force and, hence, the water production rate of the MD process [13, 91]. The corresponding coefficient defined in Eq. (2.4) is generally used to quantify the magnitude of the boundary layer resistances over the total heat transfer resistance [11]:

$$\zeta = \frac{T_{m,f} - T_{m,p}}{T_{b,f} - T_{b,p}} \tag{2.4}$$

where $T_{m,f}$, $T_{m,p}$ represent the temperature at the membrane surfaces for the feed and the permeate, respectively, and $T_{b,f}$, $T_{b,p}$ represent the bulk temperature on the feed and the permeate sides, respectively. In the ideal case, ζ should be unity, but in reality, is always lower [11]. If the difference between the temperature at the membrane surfaces and that in the corresponding bulk phase is large (i.e. for severe temperature polarization), the transmembrane temperature difference is low, resulting in small values of both ζ and the permeate flux. In this case, the temperature polarization is the determining factor in the MD process.

Several methods have been adopted to minimize the heat transfer resistances of the boundary layers adjoining the membrane surfaces (i.e. the use of spacers, turbulence promoters and high flow rates) so that the fluid temperature at the membrane surface approaches that of the bulk fluid.

2.4.3.2. Feed concentration

The salt concentration of feed reduces the water vapor pressure, as indicated in Eqs. (2.5 and 2.6), and increases the concentration polarization effect, resulting in a decrease of the driving force and the permeate flux in all MD configurations. Water vapor pressure, besides depending on the temperature as seen in the Antoine equation, Eq. (2.1), also depends on the feed concentration (x) [11]:

$$p_w(T, x) = p_w^0(T) a_w(x) \tag{2.5}$$

Thus, the influence of the feed concentration of NaCl on the vapor pressure can be determined by the water activity, a_w [11, 13]:

$$a_w(x) = \gamma_w x_{NaCl} \tag{2.6}$$

where a_w can be written as a combination of the activity coefficient of water (γ_w) and the non-volatile solute (NaCl) mole fraction (x_{NaCl}). For an aqueous solution of NaCl, an empirical correlation between γ_w and x_{NaCl} is often used [11, 13]:

$$\gamma_w(x) = 1 - 0.5 x_{NaCl} - 10 x_{NaCl}^2 \tag{2.7}$$

For instance, an increase in feed salt concentration results in a decrease in both the water activity and the partial vapor pressure.

The effect of the concentration polarization (ξ_s) is quantified using the following equation [11, 92]:

$$\xi_s = \frac{C_{m,f}}{C_{b,f}} \tag{2.8}$$

where $C_{b,f}$ and $C_{m,f}$ is the salt concentration at the bulk feed solution and at the feed membrane interface, respectively.

It is worth noting that the contribution of the concentration polarization in the reduction of the permeate flux is small compared to that of the temperature polarization [91, 93-95].

2.4.3.3. Flow rate

High flow rate (i.e. circulation velocities of fluids tangentially to the membrane) results in high heat transfer coefficients. This reduce the thickness of the boundary layer at the membrane, and therefore, increases the driving force leading to higher permeate flux [14]. However, the response may differ among MD configuration and MD set-ups. The DCMD, AGMD and VMD configurations all show an increase of the permeate flux with feed flow rate, reaching in some cases asymptotic levels. In SGMD, the permeate flux is less affected by the feed flow rate and the effect is negligible when non-volatile solutes are present in the feed solution [75]. This is attributed mainly to the lower effect of temperature polarization on the feed side of the membrane module in SGMD compared to that of the permeate side, for which the effect is predominant [31, 75]. In general, in order to obtain a high-water production rate, it is better to operate under a turbulent flow regime [11, 13].

In the case of DCMD and SGMD configurations, high permeate flow rates must be also considered to reduce the temperature polarization effect and increase the permeate flux. In the SGMD process, the temperature polarization is localized on the permeate side of the membrane- There is an optimum permeate flow rate beyond which any increase may result in a reduction of the permeate. This ultimate reduction in flux is due to the increase of pressure on the permeate side of the membrane [31, 75]. In fact, the permeate side pressure must be lower than the feed side pressure.

2.4.3.4. Other MD operating parameters

The general effect of increasing the permeate inlet temperature is to lower permeate flux. This is related to the decrease of the transmembrane vapor pressure drop at constant feed temperature [14].

In DCMD and SGMD, the temperature increases along the length of the permeate side of the membrane module length from the inlet to the outlet. This variation depends strongly on the fluid type, on its flow velocity, and on the applied feed temperature. An increase of the permeate temperature results in a reduction of the transmembrane driving force, leading to a decrease of the permeate flux [11].

In the case of AGMD, the condensation surface temperature has little effect on the permeate flux compared to the feed inlet temperature. This is due to the presence of the stagnant air gap between the membrane and the cold surface. The air gap width and the feed temperature are the two most important factors affecting desalination performance. For instance, the AGMD gap is inversely proportional to the permeate flux [21]. By reducing the gap width, the temperature gradient within the gap compartment increases while the path of the transported evaporated molecules is reduced; both these effects lead to an enhancement of the permeate flux. However, a higher gap width results in a lower heat loss by conduction through the membrane, a higher process thermal efficiency and a greater mass transfer resistance. Thus, it is necessary to determine an optimum air gap thickness, most likely small, to obtain a high-water production rate and a high thermal efficiency [11].

As in the case of DCMD, for LGMD, the lower the liquid gap temperature the higher the permeate flux across the membrane [16]. The SGMD process presents a very high increase of the gas temperature along the membrane module length, leading to a reduction of the transmembrane vapor pressure. This leads consequently to a decline in permeate flux [31, 75]. In order to keep the driving force constant along the module length, a cold wall can be introduced inside the module (i.e. TSGMD variant) [23]. It is more convenient to increase the feed side temperature rather than to decrease the gas inlet temperature in order to achieve high water production rates by SGMD.

In the VMD configuration, the transmembrane hydrostatic pressure and the permeate flux both increase with a reduction of the downstream pressure. However, a large decrease in vacuum pressure induces a major risk of membrane pore wetting and a higher energy consumption. Therefore, it is preferable to operate at moderate downstream pressures, i.e. below the saturation pressure of the feed aqueous solution [11].

2.4.3.5. Operating time

During MD desalination operation, the salt concentration of the feed solution increases with time whereas the permeate flux decreases.

The variation of permeate flux with time has been divided into three states: sub-steady, pre-steady and steady state [96].

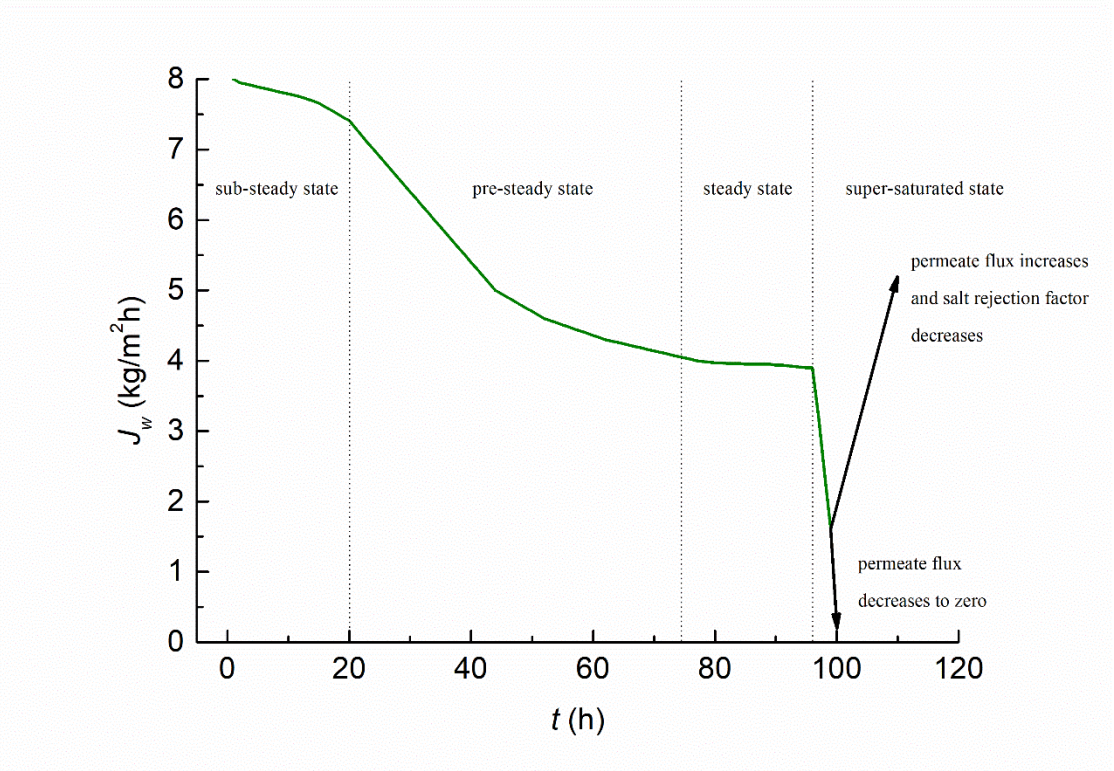

Figure 2.8. Possible change in permeate flux (J_w) with time during desalination by membrane distillation (MD).

As can be seen in Fig. 2.8, during the sub-steady state, the permeate flux drops slightly with time as the salt feed concentration increases. At the same time, salt particles start to deposit on the membrane surface. In the pre-steady state, the permeate flux begins to decline significantly and the salt particle deposition continues to cause fouling. This deposition results in membrane pore clogging, a higher pressure drop, a higher temperature polarization effect and consequently a considerable decay of the permeate flux [13]. In steady state, when the feed aqueous solution reaches its saturation point, no variation of the permeate flux with time can be detected. However, when a super-saturated state is reached, salt crystals start to penetrate and grow inside the pores. This leads to pore wetting, elimination of the gas entrapped within the pores and facilitation of direct diffusion of feed liquid aqueous solution across them. This may result in an increase in permeate flux and a reduction of salt rejection. In fact, the flux may also experience a sharp reduction to zero when the membrane surface becomes completely

covered by salt crystals deposits [81]. This last state is reversible by a simple mechanical washing of the membrane, using distilled water under tangential flow over the membrane surface. The initial permeate flux observed in the steady state zone is then recovered.

It must be pointed out that fouling problem in MD is significantly lower than the observed in pressure-driven membrane separation processes [27], and the phenomenon is controlled by feedwater pretreatment and/or membrane cleaning.

2.4.4. Influence of membrane characteristics on MD desalination performance

The parameters of the membranes such as pore size (d_p), porosity or void volume fraction (ε), pore tortuosity (τ) and thickness (δ) affect considerably the water production rate as well as salt rejection. Theoretically, the permeate flux (J_w) is written as function of these parameters as follows [87, 97]:

$$J_w \; \alpha \; \frac{r^{\alpha} \; \varepsilon}{\tau \; \delta} \tag{2.9}$$

where the characteristic constant α is unity for pores working under Knudsen type of flow and two under viscous type of flow.

To obtain a high-water production rate, the membrane should be as thin as possible. However, to achieve a better heat efficiency, the membrane should be as thick as possible, because conductive heat loss occurs through the membrane matrix [98, 99]. This is true for all MD configurations except for AGMD, in which the influence of thicker membranes is negligible because the predominant resistance to mass transfer is in the stagnant air gap [100].

Membranes with a higher porosity results in higher permeate fluxes, regardless of the configuration. In addition, membranes with high porosity exhibit low conductive heat transfer. This is because the thermal conductivity coefficient of air entrapped within the membrane pores is an order of magnitude smaller than that of the materials (i.e. polymers) [13, 101].

As stated in section 2.4, more than one mechanism of mass transport can take place simultaneously, depending on the pore size. The MD membrane pore sizes range between few nanometers and10 μm, the only condition being to maintain the pores dry during MD operation. Therefore, the maximum allowable pore size is limited by the wetting of the membrane, which is related to the LEP. It must be noted that the water production rate depends also on the pore size distribution, which must be uniform for a membrane to be used in MD applications.

Most of the membranes used in MD have tortuous pores (i.e. the pores do not go straight across the membrane thickness), and the permeate flux is smaller for membranes with more tortuous pores, as can be deduced from Eq. (4.9).

In order to form the vapor/liquid interfaces at the membrane pores and prevent their wetting, the membrane must be hydrophobic; hence, hydrophobic materials are used or the membrane surface is rendered hydrophobic using surface modification techniques [16, 41, 92, 101]. Membrane roughness also affects the MD performance and contributes to temperature and concentration polarization as well as fouling [102].

2.4.5. MD Hybrid systems and solar energy

Different hybrid systems in different combinations have been proposed to integrate the MD process and reduce the volume of discharged brine, increase the water recovery (water production rate) and improve the product water quality. Table 2.6 summarizes most of these integrated systems.

Several processes, membrane-based or not, can be coupled in order to overcome the limits of single units and thus achieve better performance, i.e. using hybrid systems. Numerous studies have mainly concerned brines from RO desalination plants [60, 62, 63, 103-109] because the recovery is slow (35-50% for seawater and 70-75% for brackish water) with brine TDS about 70,000 mg/L. Hybrid systems can be applied to any type of concentrate or reject streams.

The main limitation of hybrid systems is the low feasibility for implementation because of the investment and operating costs required. Although early economic calculations are encouraging, the profitability of these systems has only been demonstrated at the laboratory and pilot plant scales.

Some authors have investigated MD as the main stage in desalination of RO brine with pretreatment and posttreatment, achieving low separation factors [7, 44, 81, 106]. However, MD is most effective when used as a second stage, with recovery > 90% [8, 60]. This possibility is becoming quite attractive due to the capability of MD to concentrate saline solutions up to their supersaturated state. This allows crystallization of salts and enables MD to be coupled with a crystallization system (MDC) for salt recovery. MDC is a combination of MD and a membrane crystallizer (MCr). In MDC, distilled water is produced as permeate from the MD process while the concentrated solutes can be recovered as solids from the crystallizer [18].

Provided that an MD system operates below the boiling point of the feed aqueous solution, the use of renewable energies, especially solar thermal and geothermal, is feasible. However, very few MD studies have been performed (see Table 2.7) and it will be interesting to consider novel and emerging renewable energy systems in parallel with improvements in the MD process.

Table 2.6. Hybrid systems containing some stage of MD for the concentration and recovery of brines ("zero discharge").

Pretreatment 1	Pretreatment 2	Step 1	Step 2	Step 3	Fresh water recovery (%)	References
MF	NF + MCr	RO	-	-	71.6	[103, 104]
MF	NF	RO + MCr	-	-	70.4	
MF	NF + MCr	RO + MD	-	-	88.6	
MF	NF + MCr	RO + MCr	-	-	92.8	
-	-	NF	Membrane contact G/L (CO_2 added)	MCr	95	[105]
-	-	RO	VMD	-	89	[8]
-	-	RO	VEDCMD	-	96	[60]
-	-	RO	WAIV	MCr	77-89	[62]
UF	NF	RO	MCr	-	-	[103]
CO_2 addition	Crystallization	AGMD	-	-	80	[7]
Heating (thermic solar system)	-	AGMD	-	-	-	[44]
-	-	DCMD	MCr	-	-	[82, 106]

Abbreviations:

AGMD: Air gap membrane distillation
DCMD: Direct contact membrane distillation
MCr: Membrane crystallizer
MF: Microfiltration
NF: Nanofiltration
RO: Reverse osmosis
SGMD: Sweeping gas membrane distillation
UF: Ultrafiltration
VEDCMD: Vacuum-enhanced direct contact membrane distillation
WAIV: Wind aided intensified evaporation

Table 2.7. MD systems coupled to a renewable energy source. SEC, production capacity and GOR values.

Renewable energy source	MD configuration	Place/Company/Project	Year	*SEC* (kWh/m^3)	Production (m^3/d)	*GOR*	References
Solar thermal	MD not specified	University of New South Wales, Australia	1991	55.6	0.05	n.d.	[112]
Solar thermal	AGMD	Freiburg/ Fraunhofer ISE (Institute for Solar Energy Systems)	2003	117	0.2-20	5.5	[113]
Solar thermal	AGMD	Freiburg/ Fraunhofer ISE (Institute for Solar Energy Systems)	2003	140-200	0.2-20	4-6	[113]
Solar PV and solar thermal	LGMD	Gran Canaria, Spain/ Technological Institute of Canarias (ITC)/MEMDIS Project	2005	68.8–492	0.06-0.18	1.2-8.1 Average 2.6 ± 1.1	[114]
Geothermal water	AGMD	Tunisia	2005	30.8	n.d.	n.d.	[115]
Solar thermal and solar PV	AGMD	Alexandria, Egypt/ Mechanical Engineering Department of Alexandria University/SMADES Project	2006	650	0.02-0.06*	n.d.	[116]
Solar PV and solar thermal	AGMD	Marine Science Station (MSS) of Aqaba, Jordan/SMADES Project	2007	200-300	0.02-0.11*	0.3-0.9	[117]
Solar PV and solar thermal	AGMD	Marine Science Station (MSS) of Aqaba, Jordan/SMADES Project	2007	200-300	1.44*	0.4-0.7	[118]
Solar PV and solar thermal	LGMD	Gran Canaria, Spain/ Technological Institute of Canarias (ITC)/MEMDIS Project	2008	203.3–441.4	0.06-0.18*	0.8–5.6 Average 2.1 ± 0.6	[114]
Solar PV and solar thermal	AGMD	Fraunhofer ISE (Institute for Solar Energy Systems)	2009	100-200	0.1-0.5*	3-6	[119]
Solar PV	AGMD (multi-stage MD system)	Spain/MEDESOL Project	2009	638.9	0.5-50	n.d.	[33]
Solar thermal	VMD	Hangzhou, China	2009	91.1-318.9	0.4-1.4*	n.d.	[120]
Solar PV and solar thermal	LGMD	Gran Canaria, Spain/ Technological Institute of Canarias (ITC)/MEMDIS Project	2009/2010	138.5–499.1	0.06-0.18*	0.5–5.1 Average 3.4 ± 0.5	[114]

* Values calculated from original results (L/h or L/d)

n.d. values not determined.

2.5. Energy consumption and costs of MD desalination

Energy is the largest single variable cost for a desalination plant, varying from 30% to more than 50% of the cost of produced water [110]. The total energy depends on the system's design and engineering characteristics as well as its principle of operation, and the type of losses encountered during separation.

In general, the SEC and the gained output ratio (GOR) are two parameters used to compare different desalination systems. SEC is defined as the total energy input (E_i) required to produce 1 m^3 of desalinated water [11].

$$SEC = \frac{E_i}{J_w A} \tag{2.10}$$

where J_w is the permeate flux and A is the membrane area.

The GOR value indicates how well the energy input in the system is utilized to produce the permeate [24]. The higher the value of the GOR, the better is the performance of the system. In MD process the GOR is defined as [18]:

$$GOR = \frac{J_w A \Delta H_{v,w}}{E_i} \tag{2.11}$$

where $\Delta H_{v,w}$ is the enthalpy of evaporation of water. Unlike other desalination processes, such as RO, the SEC in MD has not been studied in detail because the few proposed systems and pilot plants are still under evaluation. The energy requirement of MD systems includes the thermal energy necessary to heat up the feed aqueous solution to be treated and to cool down or condense the permeate aqueous solution using heat exchangers. In addition, electrical energy is required to run the circulation pumps, the vacuum pumps for VMD and the gas compressors for SGMD and TSGMD [45].

The reported SEC values for MD systems range between 1.25 kWh/m^3 in cases using heat recovery systems and about 500 kWh/m^3 when renewable energy sources are used [24]. The SEC is much higher for small laboratory MD systems compared to larger pilot plants with larger membrane areas, exhibiting values which are three orders of magnitude greater [24]. It must be pointed out that there is still no agreement on any standard for calculating the SEC of MD processes. This also partly explains the large variation in the reported SEC values and, consequently, the WPC [24]. Values range from 0.5 \$/m^3 for a hybrid system consisting of an MD stage with heat recovery and using available thermal energy to 30-36 \$/m^3 for a MD process coupled to a solar energy system [111].

It must be pointed out that the GOR values for MD systems are still very small, ranging between 0.5 and 6 in the best cases. A considerable reduction in SEC with an increase of the GOR of MD processes can be expected, because MD has the advantage of using renewable energy sources such as solar energy, geothermal energy or industrial waste heat. Table 2.7 lists some pilot plants and laboratory systems coupled to renewable energy sources. It also reports their SEC and GOR values as well as their daily water production rates.

2.6. Conclusions and future perspectives in MD

During last ten years, tremendous progress has been made towards the implementation of MD and principally for desalination. However, commercial prototypes are still under evaluation and, therefore, SEC, WPC and GOR values are not specified yet. The use of commercial membranes designed for other applications rather than for MD in MD prototypes is one of the reasons for the high reported values of SEC. Thus, development of the membrane is among the areas that merit investigation for MD. In addition, it is important to optimize the coupling of renewable energy systems with MD plants. Recovery of waste heat as well as to improved designs of MD modules for reducing the SEC values is also warranted.

Other key issues of MD are the uncertainty long-term MD performance, and membrane scaling and fouling. More intensive research should be carried out in these areas along systematic lines in order to improve the membrane design and MD performance.

It is worth noting that the DCMD, AGMD and VCM configurations have been tested using commercial membranes and highly saline aqueous feed solutions; but others, such as SGMD, TSGMD and LGMD, have not yet been tested similarly. Such studies will broaden the possibility for the integration of MD technology with other separation processes, taking advantages of each other to achieve ZLD and increase the water production rate and water recovery.

2.7. References

[1] M. Shatat, M. Worall, S. Riffat, Opportunities for solar water desalination worldwide: Review, Sustainable Cities and Society, 9 (2013) 67.

[2] M.C. Mickley, Membrane concentrate disposal: Practices and regulation in: Desalination and Water Purification Research and Development Program Report No. 123 (Second Edition), Mickley & Associates, U.S. Department of Interior. Bureau of Reclamation. Denver, Co, 2006.

[3] D.A. Roberts, E.L. Johnston, N.A. Knott, Impacts of desalination plant discharges on the marine environment: A critical review of published studies, Water Research, 44 (2010) 5117.

[4] L. Henthorne, The Current State of Desalination, in: IDA World Congress, Dubai, UAE, 2009.

[5] A.D. Khawaji, I.K. Kutubkhanah, J.M. Wie, Advances in seawater desalination technologies, Desalination, 221 (2008) 47.

[6] Desaldata.com, in: Desaldata, Global Water Intelligence (G.W.I.) 2013.

[7] S. Bouguecha, D. Mahmoud, Fluidised bed crystalliser and air gap membrane distillation as a solution to geothermal water desalination, Desalination, 152 (2002) 237.

[8] J.P. Mericq, S. Laborie, C. Cabassud, Vacuum membrane distillation of seawater reverse osmosis brines, Water Research, 44 (2010) 5260.

[9] H. Fan, Y. Peng, Application of PVDF membranes in desalination and comparison of the VMD and DCMD processes, Chemical Engineering Science, 79 (2012) 94.

[10] M. Khayet, Membranes and theoretical modeling of membrane distillation: a review, Advances in Colloid and Interface Science, 164 (2011) 56.

[11] M. Khayet, T. Matsuura, Membrane Distillation. Principles and Applications, Elsevier B.V., The Netherlands, 2011.

[12] M. Khayet, Desalination by membrane distillation, in: Encyclopedia of Life Support Systems (EOLSS): Water and Wastewater Treatment Technologies, 2010.

[13] K.W. Lawson, D.R. Lloyd, Membrane distillation, Journal of Membrane Science, 124 (1997) 1.

[14] M.S. El-Bourawi, Z. Ding, R. Ma, M. Khayet, A framework for better understanding membrane distillation separation process, Journal of Membrane Science, 285 (2006) 4.

[15] K. Smolders, A.C.M. Franken, Terminology for membrane distillation, Desalination, 72 (1989) 249.

[16] M. Essalhi, M. Khayet, Application of a porous composite hydrophobic/hydrophilic membrane in desalination by air gap and liquid gap membrane distillation: A comparative study, Separation and Purification Technology, 133 (2014) 176.

[17] P.K. Weyl, Recovery of demineralized water from saline waters, in: United States Patent, 1967.

[18] E. Curcio, A. Criscuoli, E. Drioli, Membrane Crystallizers, Industrial & Engineering Chemistry Research, 40 (2001) 2679.

[19] G. Zakrzewska-Trznadel, M. Harasimowicz, A.G. Chmielewski, Concentration of radioactive components in liquid low-level radioactive waste by membrane distillation, Journal of Membrane Science, 163 (1999) 257.

[20] M. Gryta, M. Tomaszewska, K. Karakulski, Wastewater treatment by membrane distillation, Desalination, 198 (2006) 67.

[21] M.C. García-Payo, M.A. Izquierdo-Gil, C. Fernández-Pineda, Air gap membrane distillation of aqueous alcohol solutions, Journal of Membrane Science, 169 (2000) 61.

[22] M.S. El-Bourawi, M. Khayet, R. Ma, Z. Ding, Z. Li, X. Zhang, Application of vacuum membrane distillation for ammonia removal, Journal of Membrane Science, 301 (2007) 200.

[23] M.C. García-Payo, C.A. Rivier, I.W. Marison, U. von Stockar, Separation of binary mixtures by thermostatic sweeping gas membrane distillation II. Experimental results with aqueous formic acid solutions, Journal of Membrane Science, 198 (2002) 197.

[24] M. Khayet, Solar desalination by membrane distillation: Dispersion in energy consumption analysis and water production costs (a review), Desalination, 308 (2013) 89.

[25] A.G. Fane, R.W. Schofield, C.J.D. Fell, The efficient use of energy in membrane distillation, Desalination, 64 (1987) 231.

[26] S. Alobaidani, E. Curcio, F. Macedonio, G. Di profio, H. Alhinai, E. Drioli, Potential of membrane distillation in seawater desalination: Thermal efficiency, sensitivity study and cost estimation, Journal of Membrane Science, 323 (2008) 85.

[27] A. Alkhudhiri, N. Darwish, N. Hilal, Membrane distillation: A comprehensive review, Desalination, 287 (2012) 2.

[28] C. Fernández-Pineda, M.A. Izquierdo-Gil, M.C. García-Payo, Gas permeation and direct contact membrane distillation experiments and their analysis using different models, Journal of Membrane Science, 198 (2002) 33.

[29] M. Essalhi, M. Khayet, Self-sustained webs of polyvinylidene fluoride electrospun nanofibers at different electrospinning times: 2. Theoretical analysis, polarization effects and thermal efficiency, Journal of Membrane Science, 433 (2013) 180.

[30] D. Winter, J. Koschikowski, S. Ripperger, Desalination using membrane distillation: Flux enhancement by feed water deaeration on spiral-wound modules, Journal of Membrane Science, 423-424 (2012) 215.

[31] M. Khayet, P. Godino, J.I. Mengual, Nature of flow on sweeping gas membrane distillation, Journal of Membrane Science, 170 (2000) 243.

[32] H. Kurokawa, T. Sawa, Heat recovery characteristics of membrane distillation, Heat transfer-Japanese Research, 25 (1996) 135.

[33] J. Blanco Gálvez, L. García-Rodríguez, I. Martín Mateos, Seawater desalination by an innovative solar-powered membrane distillation system: the MEDESOL project, Desalination, 246 (2009) 567.

[34] D. Hou, J. Wang, X. Sun, Z. Ji, Z. Luan, Preparation and properties of PVDF composite hollow fiber membranes for desalination through direct contact membrane distillation, Journal of Membrane Science, 405-406 (2012) 185.

[35] M. Khayet, T. Matsuura, Preparation and Characterization of Polyvinylidene Fluoride Membranes for Membrane Distillation, Industrial & Engineering Chemistry Research, 40 (2001) 5710.

[36] M.C. García-Payo, M. Essalhi, M. Khayet, Preparation and characterization of PVDF–HFP copolymer hollow fiber membranes for membrane distillation, Desalination, 245 (2009) 469.

[37] L. García-Fernández, M.C. García-Payo, M. Khayet, Effects of mixed solvents on the structural morphology and membrane distillation performance of PVDF-HFP hollow fiber membranes, Journal of Membrane Science, 468 (2014) 324.

[38] M. Khayet, C. Cojocaru, M. Essalhi, M.C. García-Payo, P. Arribas, L. García-Fernández, Hollow fiber spinning experimental design and analysis of defects for fabrication of optimized membranes for membrane distillation, Desalination, 287 (2012) 146.

[39] C. Feng, B. Shi, G. Li, Y. Wu, Preparation and properties of microporous membrane from poly(vinylidene fluoride-co-tetrafluoroethylene) (F2.4) for membrane distillation, Journal of Membrane Science, 237 (2004) 15.

[40] M. Essalhi, M. Khayet, Surface segregation of fluorinated modifying macromolecule for ydrophobic/hydrophilic membrane preparation and application in air gap and direct contact membrane distillation, Journal of Membrane Science, 417-418 (2012) 163.

[41] M. Essalhi, M. Khayet, Self-sustained webs of polyvinylidene fluoride electrospun nano-fibers: Effects of polymer concentration and desalination by direct contact membrane distillation, Journal of Membrane Science, 454 (2014) 133.

[42] B.R. Bodell, Silicone rubber vapor diffusion in saline water distillation, in: United States Patent Serial, 285,032, 1963.

[43] SEPA CF II: Membrane Cell System, in: G.E. Water (Ed.) General Electric Water & Process Technologies, 2009.

[44] E. Guillén-Burrieza, J. Blanco, G. Zaragoza, D.-C. Alarcón, P. Palenzuela, M. Ibarra, W. Gernjak, Experimental analysis of an air gap membrane distillation solar desalination pilot system, Journal of Membrane Science, 379 (2011) 386.

[45] E. Guillén-Burrieza, G. Zaragoza, S. Miralles-Cuevas, J. Blanco, Experimental evaluation of two pilot-scale membrane distillation modules used for solar desalination, Journal of Membrane Science, 409-419 (2012) 264.

[46] K. Zhao, W. Heinzl, M. Wenzel, S. Büttner, F. Bollen, G. Lange, S. Heinzl, N. Sarda, Experimental study of the memsys vacuum-multi-effect-membrane-distillation (V-MEMD) module, Desalination, 323 (2013) 150.

[47] B. Li, K.K. Sirkar, Novel membrane and device for vacuum membrane distillation-based desalination process, Journal of Membrane Science, 257 (2005) 60.

[48] F. Laganà, G. Barbieri, E. Drioli, Direct contact membrane distillation: modelling and concentration experiments, Journal of Membrane Science, 166 (2000) 1.

[49] F.J. Millero, R. Feistel, D.G. Wright, T.J. McDougall, The composition of Standard Seawater and the definition of the Reference-Composition Salinity Scale, Deep Sea Research Part I: Oceanographic Research Papers, 55 (2008) 50.

[50] F.J. Millero, Chemical Oceanography, 4th ed., CRC Press. Taylor & Francis Group, United States of America, 2013.

[51] J.P. Ducrotoy, M. Elliott, The science and management of the North Sea and the Baltic Sea: natural history, present threats and future challenges, Marine pollution bulletin, 57 (2008) 8.

[52] J.C. Dauvin, The main characteristics, problems, and prospects for Western European coastal seas, Marine pollution bulletin, 57 (2008) 22.

[53] B. Malaizé, M.T. Vénec-Peyré, C. Joly, F. Bassinot, N. Caillon, K. Charlier, Imprints of high-salinity water plumes originating from the red sea during termination II, Palaeogeography, Palaeoclimatology, Palaeoecology, 276 (2009) 69.

[54] B. Subrahmanyam, V.S.N. Murty, D.M. Heffner, Sea surface salinity variability in the tropical Indian Ocean, Remote Sensing of Environment, 115 (2011) 944.

[55] M. Ezersky, I. Goretsky, Velocity–resistivity versus porosity–permeability inter-relations in Dead Sea salt samples, Engineering Geology, 183 (2014) 96.

[56] S.C. Painter, M.N. Tsimplis, Temperature and salinity trends in the upper waters of the Mediterranean Sea as determined from the MEDATLAS dataset, Continental Shelf Research, 23 (2003) 1507.

[57] T. Delcroix, M.J. McPhaden, A. Dessier, Y. Gouriou, Time and space scales for sea surface salinity in the tropical oceans, Deep Sea Research Part I: Oceanographic Research Papers, 52 (2005) 787.

[58] S. Lattemann, T. Höpner, Environmental impact and impact assessment of s eawater desalination, Desalination, 220 (2008) 1.

[59] X. Ji, E. Curcio, S. Alobaidani, G. Di Profio, E. Fontananova, E. Drioli, Membrane distillation-crystallization of seawater reverse osmosis brines, Separation and Purification Technology, 71 (2010) 76.

[60] C.R. Martinetti, A.E. Childress, T.Y. Cath, High recovery of concentrated RO brines using forward osmosis and membrane distillation, Journal of Membrane Science, 331 (2009) 31.

[61] E. Korngold, L. Aronov, N. Daltrophe, Electrodialysis of brine solutions discharged from an RO plant, Desalination, 242 (2009) 215.

[62] F. Macedonio, L. Katzir, N. Geisma, S. Simone, E. Drioli, J. Gilron, Wind-Aided Intensified eVaporation (WAIV) and Membrane Crystallizer (MCr) integrated brackish water desalination process: Advantages and drawbacks, Desalination, 273 (2011) 127.

[63] F. Hajbi, H. Hammi, A. M'nif, Reuse of RO Desalination Plant reject Brine, Journal of Phase Equilibria and Diffusion, 31 (2009) 341.

[64] M. Ahmed, A. Arakel, D. Hoey, M.R. Thumarukudy, M.F.A. Goosen, M. Al-Haddabi, A. Al-Belushi, Feasibility of salt production from inland RO desalination plant reject brine: a case study., Desalination, 158 (2003) 109.

[65] P. Novotny, O. Sohnel, Densities of binary aqueous solutions of 306 inorganic substances, Journal of Chemical & Engineering Data, 33 (1988) 49.

[66] M.A. Clynne, R.W. Potter, Solubility of some alkali and alkaline earth chlorides in water at moderate temperatures, Journal of Chemical & Engineering Data, 24 (1979) 338.

[67] B. Krumgalz, A. Starinsky, K. Pitzer, Ion-Interaction Approach: Pressure Effect on the Solubility of Some Minerals in Submarine Brines and Seawater, Journal of Solution Chemistry, 28 (1999) 667.

[68] S.P. Pinho, E.A. Macedo, Solubility of NaCl, NaBr, and KCl in Water, Methanol, Ethanol, and Their Mixed Solvents, Journal of Chemical & Engineering Data, 50 (2004) 29.

[69] M. Essalhi, M. Khayet, C. Cojocaru, M.C. García-Payo, P. Arribas, Response surface modeling and optimization of electrospun nanofiber membranes, The Open Nanoscience Journal, 7 (2013) 8.

[70] K.Y. Wang, T.-S. Chung, M. Gryta, Hydrophobic PVDF hollowfiber membranes with narrow pore size distribution and ultra-thin skin for the freshwater production through membrane distillation, Chemical Engineering Science, 63 (2008) 2587.

[71] H. Geng, H. Wu, P. Li, Q. He, Study on a new air-gap membrane distillation module for desalination, Desalination, 334 (2014) 29.

[72] D. Singh, K.K. Sirkar, Desalination by air gap membrane distillation using a two hollow-fiber-set membrane module, Journal of Membrane Science, 421-422 (2012) 172.

[73] M. Khayet, C. Cojocaru, Artificial neural network modeling and optimization of desalination by air gap membrane distillation, Separation and Purification Technology, 86 (2012) 171.

[74] A. El Amali, S. Bouguecha, M. Maalej, Experimental study of air gap and direct contact membrane distillation configurations: application to geothermal and seawater desalination, Desalination, 168 (2004) 357.

[75] M. Khayet, P. Godino, J.I. Mengual, Theory and experiments on sweeping gas membrane distillation, Journal of Membrane Science, 165 (2000) 261.

[76] M. Khayet, C. Cojocaru, Artificial neural network model for desalination by sweeping gas membrane distillation, Desalination, 308 (2013) 102.

[77] M. Khayet, C. Cojocaru, A. Baroudi, Modeling and optimization of sweeping gas membrane distillation, Desalination, 287 (2012) 159.

[78] A. Criscuoli, M.C. Carnevale, E. Drioli, Evaluation of energy requirements in membrane distillation, Chemical Engineering and Processing, 47 (2008) 1098.

[79] J.M. Li, Z.K. Xu, Z.M. Liu, W.F. Yuan, H. Xiang, S.Y. Wang, Y.Y. Xu, Microporous polypropylene and polyethylene hollow fiber membranes. Part 3. Experimental studies on membrane distillation for desalination, Desalination, 157 (2003) 153.

[80] Y.Y. Xu, B.-K. Zhu, Y.-Y. Xu, Pilot test of vacuum membrane distillation for seawater desalination on a ship, Desalination, 189 (2006) 165.

[81] C.M. Tun, A.G. Fane, J.T. Matheickal, R. Sheikholeslami, Membrane distillation crystallization of concentrated salts-flux and crystal formation, Journal of Membrane Science, 257 (2005) 144.

[82] J. Walton, H. Lu, C. Turner, S. Solis, H. Hein, Solar waste heat desalination by membrane distillation, in: Desalination and Water Purification Research and Development Program. Report No 81, Desalination and Water Purification Research and Development Program, 2004.

[83] A. Alkhudhiri, N. Darwish, N. Hilal, Treatment of high salinity solutions: Application of air gap membrane distillation, Desalination, 287 (2012) 55.

[84] M. Safavi, T. Mohammadi, High-salinity water desalination using VMD, Chemical Engineering Journal, 149 (2009) 191.

[85] A.M. Alklaibi, N. Lior, Membrane-distillation desalination: Status and potential, Desalination, 171 (2005) 111.

[86] L. Nghiem, F. Hildinger, F.I. Hai, T. Cath, Treatment of saline aqueous solutions using direct contact membrane distillation, Desalination and Water Treatment, 32 (2001) 234.

[87] J. Phattaranawik, R. Jiraratananon, A.G. Fane, Effect of pore size distribution and air flux on mass transport in direct contact membrane distillation, Journal of Membrane Science, 215 (2003) 75.

[88] R.B. Saffarini, H.A. Arafat, R. Thomas, Influence of pore estructure on membrane wettability in membrane distillation, in: The Sixth Jordan International Chemical Engineering Conference, Amman, Jordan, 2012.

[89] R.B. Saffarini, B. Mansoor, R. Thomas, H.A. Arafat, Effect of temperature-dependent microstructure evolution on pore wetting in PTFE membranes under membrane distillation conditions, Journal of Membrane Science, 429 (2013) 282.

[90] M.C. García-Payo, M.A. Izquierdo-Gil, C. Fernandez-Pineda, Wetting Study of Hydrophobic Membranes via Liquid Entry Pressure Measurements with Aqueous Alcohol Solutions, Journal of Colloid and Interface Science, 230 (2000) 420.

[91] L. Martínez-Diez, M.I. Vázquez-González, Temperature and concentration polarization in membrane distillation of aqueous salt solutions, Journal of Membrane Science, 196 (1999) 265.

[92] M. Khayet, T. Matsuura, Application of surface modifying macromolecules for the preparation of membranes for membrane distillation Desalination, 158 (2003) 51.

[93] C. Feng, K.C. Khulbe, T. Matsuura, R. Gopal, S. Kaur, S. Ramakrishna, M. Khayet, Production of drinking water from saline water by air-gap membrane distillation using polyvinylidene fluoride nanofiber membrane, Journal of Membrane Science, 311 (2008) 1.

[94] P. Peng, A.G. Fane, L. Xiaodong, Desalination by membrane distillation adopting a hydrophilic membrane, Desalination, 173 (2005) 45.

[95] M. Khayet, M.P. Godino, J.I. Mengual, Study of Asymmetric Polarization in Direct Contact Membrane Distillation, Separation Science and Technology, 39 (2005) 125.

[96] Y. Yun, R. Ma, W. Zhang, A.G. Fane, J. Li, Direct contact membrane distillation mechanism for high concentration NaCl solutions, Desalination, 188 (2006) 251.

[97] J. Woods, J. Pellegrino, J. Burch, Generalized guidance for considering pore-size distribution in membrane distillation, Journal of Membrane Science, 368 (2011) 124.

[98] M. Khayet, T. Matsuura, J.I. Mengual, M. Qtaishat, Design of novel direct contact membrane distillation membranes, Desalination, 192 (2006) 105.

[99] M. Gryta, Influence of polypropylene membrane surface porosity on the performance of membrane distillation process, Journal of Membrane Science, 287 (2007) 67.

[100] M.A. Izquierdo-Gil, M.C. García-Payo, C. Fernandez-Pineda, Air gap membrane distillation of sucrose aqueous solutions, Journal of Membrane Science, 155 (1999) 291.

[101] M. Khayet, T. Matsuura, J.I. Mengual, Porous hydrophobic/hydrophilic composite membranes: Estimation of the hydrophobic-layer thickness, Journal of Membrane Science, 266 (2005) 68.

[102] M. Khayet, K.C. Khulbe, T. Matsuura, Characterization of membranes for membrane distillation by atomic force microscopy and estimation of their water vapor transfer coefficients in vacuum membrane distillation process, Journal of Membrane Science, 238 (2004) 199.

[103] D.H. Kim, A review of desalting process techniques and economic analysis of the recovery of salts from retentates, Desalination, 270 (2011) 1.

[104] E. Drioli, E. Curcio, G. Di Profio, F. Macedonio, A. Criscuoli, Integrating membrane contactors technology and pressure-driven membrane operations for seawater desalination. Energy, Exergy and Costs Analysis, Chemical Engineering Research and Design, 84 (A3) (2006) 209.

[105] E. Drioli, E. Curcio, A. Criscuoli, G. Di Profio, Integrated system for recovery of $CaCO_3$, NaCl and $MgSO_4 \cdot 7H_2O$ from nanofiltration retentate, Journal of Membrane Science, 239 (2004) 27.

[106] L. Mariah, C.A. Buckley, C.J. Brouckaert, E. Curcio, E. Drioli, D. Jaganyi, D. Ramjugernath, Membrane distillation of concentrated brines—Role of water activities in the evaluation of driving force, Journal of Membrane Science, 280 (2006).

[107] A. Pérez-González, A.M. Urtiaga, R. Ibáñez, I. Ortiz, State of the art and review on the treatment technologies of water reverse osmosis concentrates, Water Research, 46 (2012) 267.

[108] R. Bond, S. Veerapaneni, Zeroing in on ZLD technologies for inland desalination, Journal American Water Works Association (AWWA) 100 (2008) 76.

[109] S.T. Reddy, A.E. Lewis, G.J. Witkamp, H.J.M. Kramer, J. van Spronsen, Recovery of Na2SO4·10H2O from a reverse osmosis retentate by eutectic freeze crystallisation technology, Chemical Engineering Research and Design, 88 (2010) 1153.

[110] A. Al-Karaghouli, L.L. Kazmerski, Energy consumption and water production cost of conventional and renewable-energy-powered desalination processes, Renewable and Sustainable Energy Reviews, 24 (2013) 343.

[111] F. Banat, N. Jwaied, Economic evaluation of desalination by small-scale autonomous solar-powered membrane distillation units, Desalination, 220 (2008) 566.

[112] P.A. Hogan, Sudjito, A.G. Fane, G.L. Morrison, Desalination by solar heated membrane distillation, Desalination, 81 (1981) 81.

[113] J. Koschikowski, M. Wieghaus, M. Rommel Solar thermal-driven desalination plants based on membrane distillation, Desalination, 156 (2003) 295.

[114] R.G. Raluy, R. Schwantes, V.J. Subiela, B. Peñate, G. Melián, J.R. Betancort, Operational experience of a solar membrane distillation demonstration plant in Pozo Izquierdo-Gran Canaria Island (Spain), Desalination, 290 (2012) 1.

[115] S. Bouguecha, B. Hamrouni, M. Dhahbi, Small scale desalination pilots powered by renewable energy sources: case studies, Desalination, 183 (2005) 151.

[116] H.E.S. Fatha, S.M. Elsherbinya, A.A. Hassana, M. Rommel, M. Wieghaus, J. Koschikowski, M. Vatansever, PV and thermally driven small-scale, stand-alone

solar desalination systems with very low maintenance needs, Desalination, 225 (2008) 58.

[117] F. Banat, N. Jwaied, M. Rommel, J. Koschikowski, M. Wieghaus, Desalination by a “compact SMADES” autonomous solar-powered membrane distillation unit, Desalination, 217 (2007) 29.

[118] F. Banat, N. Jwaied, M. Rommel, J. Koschikowski, M. Wieghaus, Performance evaluation of the “large SMADES” autonomous desalination solar-driven membrane distillation plant in Aqaba, Jordan, Desalination, 217 (2007) 17.

[119] J. Koschikowski, M. Wieghaus, M. Rommel, V. Subiela, B. Peñate, J.R. Betancort, Experimental investigations on solar driven stand-alone membrane distillation systems for remote areas, Desalination, 248 (2009) 125.

[120] X. Wang, L. Zhang, H. Yang, H. Chen, Feasibility research of potable water production via solar-heated hollow fiber membrane distillation system, Desalination, 247 (2009) 403.

Chapter 3

Treatment of brines by membrane distillation

3.1. Desalination and concentration of saline aqueous solutions up to supersaturation by air gap membrane distillation and crystallization fouling

The possibility to concentrate synthetic brines (65 g/L of NaCl) above the saturation concentration of NaCl at different feed inlet temperatures up to 355 K is studied, using the AGMD configuration and two different polytetrafluoroethylene (PTFE) membranes, TF200 and TF450. A good quality distillate (< 0.5 g/L NaCl) and high salt rejection factors (> 99.89%) were achieved when treating high saline aqueous solutions. When applying the highest feed inlet temperature, 355 K, better AGMD results were observed, permeate flux of 23.84 ± 0.09 kg/m^{2}h and 46.50 ± 0.21 kg/m^{2}h with a thermal efficiency of 80.97% and 96.06%, for the membranes TF200 and TF450, respectively. Once the saturation limit of NaCl was overpassed, crystallization fouling occurs by blocking or wetting the membrane pores due to the continued deposition and growth of salt crystals on the membrane surface and inside the membrane pores. Membrane properties changed with crystallization fouling and reduced the thermal efficiency of the AGMD process. When using NaCl aqueous solutions, a simple washing with water is enough to partially recover the initial properties of the membrane.

3.1.1. Introduction

Desalination of seawater and brackish water is considered nowadays an important solution to the problem of potable water shortage especially in coastal zones. At the present time, thermal and membrane processes are the two major used desalination processes. Thermal technology, like multi-stage flash distillation (MSF) or multi-effect distillation (MED) processes, dominates the desalination market in warm countries of the Middle East [1]. In the rest of the world, membrane processes especially reverse osmosis (RO) is well recognized as the most convenient desalination technology. It heads the membrane desalination processes with 2/3 of the contracted capacity [2]. The economic sustainability of desalination processes depends mainly on the reduction of energy consumption costs, the increase of the water recovery factor and the management of the generated wastes or brines. In general, brines have been always associated with the rejection of the desalination processes and discharged in seas. High saline content and additives of brine, with a concentration of total dissolved solids (TDS) over 70 g/L have direct effects over the marine environment due to the salt composition of brines, which is approximately the double of that of seawater [3]. As a result, the major effects of brine discharge are eutrophication, pH changes and heavy metals accumulation, among others [4, 5]. Therefore, new options to improve the management of concentrates from desalination plants are a current demand. Recent strategic research lines for brine management are focused on the accomplishment of the zero-liquid discharge (ZLD) concept [6, 7] and recovery of valuable byproducts such as salts through the combination of different individual technologies (i.e. hybrid systems), trying to make the desalination process environmentally more sustainable.

Among the proposed technologies, the non-isothermal process membrane distillation (MD) has emerged as an important process for desalination of high saline aqueous solutions and treatment of brines [8-15]. One of the main advantages of MD over other membrane processes in the field of desalination is its capability to operate under high salt concentrations (i.e. > 65 g/L of sodium chloride (NaCl), equivalent to the salt concentration of RO brines), producing relatively high permeate fluxes with high salts rejection factors. The most used MD configuration to achieve this purpose is direct contact membrane distillation (DCMD). Tun *et al.* [14] by using a flat sheet polyvinylidene fluoride (PVDF) membrane with a mean pore size of 0.22 μm, achieved permeate fluxes up to 20 kg/m^2h for a temperature difference of 40ºC and a feed aqueous solution of 260 g/L NaCl. Alkhudhiri *et al.* [10] used an air gap membrane distillation (AGMD) system with a polytetrafluoroethylene (PTFE) flat-sheet commercial membrane with a pore size of 0.2 μm. A permeate flux of 24.48 kg/m^2h and a NaCl rejection factor of 99.98% were obtained. An aqueous solution of 84.4 g/L NaCl was used as feed, at a temperature difference between feed and permeate membrane sides of 343 K and a feed flow rate of 90 L/h. Compared to DCMD and AGMD, vacuum membrane distillation (VMD) is less studied

due to the need of external condenser(s) and a vacuum pump. Safavi and Mohammadi [15] tested VMD for desalination of 100, 200 and 300 g/L NaCl feed aqueous solutions using PP commercial hollow fiber membranes of 0.2 μm mean pore size with a feed temperature of 55ºC and a vacuum pressure of 40 mbar. In this study, the NaCl feed concentration was kept nearly constant during the experiments. The reported permeate fluxes were 14.2, 13.1 and 11 $kg/m^2.h$ for the NaCl feed solutions 100, 200 and 300 g/L, respectively, with salt rejection factors of 99.99%.

Since MD can be applied for the treatment of high saline aqueous solutions, including those with concentrations above their saturation point, (i.e. supersaturated salt solutions), and due to its feasibility to be combined with other separation processes and crystallization systems [11, 13, 14, 16], this technology is suitable to achieve the above said ZLD [17]. However, the concentration and temperature polarization effects diminish the driving force of the process (i.e. transmembrane vapor pressure) and then facilitate the nucleation of inorganic salts with positive solubility coefficients, such as NaCl, near the membrane surface [14]. When supersaturated saline solutions are treated by MD, the formation and grow of salt crystals above the membrane surface and inside the pores is more pronounced [18], reducing the permeate flux [19] and the membrane hydrophobicity, limiting the operating conditions in MD systems and consequently decreasing the salt rejection performance [19] and the lifetime of the membranes. This phenomenon is defined as crystallization fouling.

The present study is intended to use AGMD configuration for desalination and the concentration of a feed saline aqueous solution having an initial NaCl concentration of 65 g/L, which is approximately the concentration of brine rejected by RO desalination plants, to values above the saturation concentration, using different feed inlet temperatures. It should be mentioned that there are only few published studies on MD separation using saline aqueous solutions with concentrations above the salt concentration saturation point. In this paper, systematic experiments were carried out with two commercial membranes having different pore sizes. Besides the concentration experiments, complementary experiments of membrane control (to check the reproducibility of different membrane samples) and membrane characterization (to check the membrane performance) were conducted in order to study the effects of supersaturation salt concentration on membrane fouling. The membranes were characterized before and after the concentration experiments. Inorganic fouling by crystallization of NaCl and its influence on the membrane parameters and on the thermal efficiency of the MD process were investigated.

3.1.2. Experimental

3.1.2.1. Membranes and characterization techniques

Two commercial polytetrafluroetylene (PTFE) flat sheet membranes (TF200 and TF450, Pall Corporation) supported by a PP net were used. Their characteristics as supplied by the manufacturer are summarized in Table 3.1.1.

Table 3.1.1. Initial parameters of the membranes TF200 and TF450 (δ: membrane thickness, d_p: mean pore size, ε: void volume fraction, θ: water contact angle and LEP_w: liquid entry pressure of water).

Membrane	Data	δ (µm)	d_p (nm)	ε (%)	θ (°)	LEP_w (kPa)
TF200	Manufacturer	139	200	80	-	282
	Measured in this study	107 ± 6	329 ± 18	78 ± 4	139.9 ± 2.8	290 ± 10
TF450	Manufacturer	135	450	80	-	138
	Measured in this study	98 ± 6	553 ± 4	78 ± 6	140.9 ± 1.0	150 ± 10

Both membranes were characterized before and after desalination tests by means of different techniques to determine the thickness (δ), pore size (d_p) and its distribution, void volume fraction (ε) (i.e. porosity), water contact angle (θ) and liquid entry pressure of water (LEP_w). The obtained initial characteristics of the membranes together with those given by the manufacturer are reported in Table 3.1.1.

The thickness was measured by an electronic micrometer *Schut* (*Schut Geometrical Metrology*) on different points of each membrane sample. At least 50 values were obtained and the average values together with their standard deviations were reported.

The mean pore size was measured by a flow porometer (*POROLUX™ 100 Porometer*) that considers the pressure scan method within a pressure range of 0-0.7 MPa at a room temperature. The gas used was compressed air and the effective membrane area was 2.7 10^{-4} m^2. POREFIL® was used as a wetting liquid agent due its low surface tension (16 mN/m). The applied method was reported elsewhere [20].

The void volume fraction of the membranes was determined at room temperature by measuring the density of each membrane sample using isopropyl alcohol (IPA, ACS reagent supplied by Sigma-Aldrich), which penetrates inside the membrane pores, and distilled water, which does not go into the pores as described elsewhere [21].

The water contact angle of the membrane surface was measured at room temperature by a computerized optical system *CAM200*, equipped with CCD frame grabber camera and image analysis software. Distilled water drops of about 3 µL were deposited on the membrane surface employing a tight syringe. The contact angles were performed at both left and right sides of each drop and were automatically calculated by fitting the captured drop shape to Young–Laplace equation. Five drops and five readings per drop

were obtained for each sample and an average value was calculated and reported together with its standard deviation.

The measurements of the LEP_w were carried out using the experimental system reported in [22]. The LEP_w could not be measured after desalination test providing that the membrane was wet at the end of the test.

The surface (i.e. active layer) and the support layer of the membranes were examined by a Field Emission Scanning Electron Microscopy (FESEM), model *JEOL 6335F*. The samples were first fractured in liquid nitrogen and then placed over a support and coated with gold under vacuum conditions. X-ray Energy Dispersive Spectroscopy (EDX) was considered to determine the elemental composition of carbon, fluorine, oxygen, sodium and chlorine at the top surface of the membrane sample.

3.1.2.2. AGMD desalination

The membranes were placed in a plate and frame membrane module (i.e. modified *Filtron Minisette*, Filtron Technology Corp.) that consists of two chambers, feed and permeate, and a stainless-steel condensation surface. For the permeate chamber, a layer of stagnant air (3.068 ± 0.001 mm) was formed between the membrane and the condensation surface with rubber separators. The feed chamber was also formed with rubber separators and its thickness was 4.369 ± 0.001 mm. The effective membrane area was $5.5\ 10^{-3} \pm 2\ 10^{-5}$ m^2. Fig. 3.1.1 shows a simplified schema of the used AGMD set-up.

The hot feed saline solution was circulated tangentially to the active PTFE layer of the membrane. A *Lauda K20 KS* thermostat was used to establish the temperature of the feed solution in the range 318 – 355 K through a heat exchanger placed at the outlet of the feed tank (2000 ± 10 mL). The condensation surface was maintained in all desalination tests at 298 K by a *PolyScience* chiller. All the temperatures at the inlets and outlets of the membrane module were measured by *Pt100* sensors connected to a *Fluke Hydra* digital multimeter. A peristaltic pump (*Cole Parmer Masterflex easy-load* model 7529-20) was used to circulate the liquid feed through the membrane module. The feed flow rate was measured by a flowmeter *Tecfluid* with an accuracy of ± 5 L/h. In order to prevent the membrane pores wetting, the hydrostatic pressure was controlled by a manometer *Wika*, having an accuracy of ± 0.2 bar, placed at the entrance of the feed membrane chamber. In all desalination tests, a feed flow rate of 100 L/h was considered. To minimize heat losses, all the pipes of the circuit, the heat exchanger, the membrane module and the feed tank were insulated.

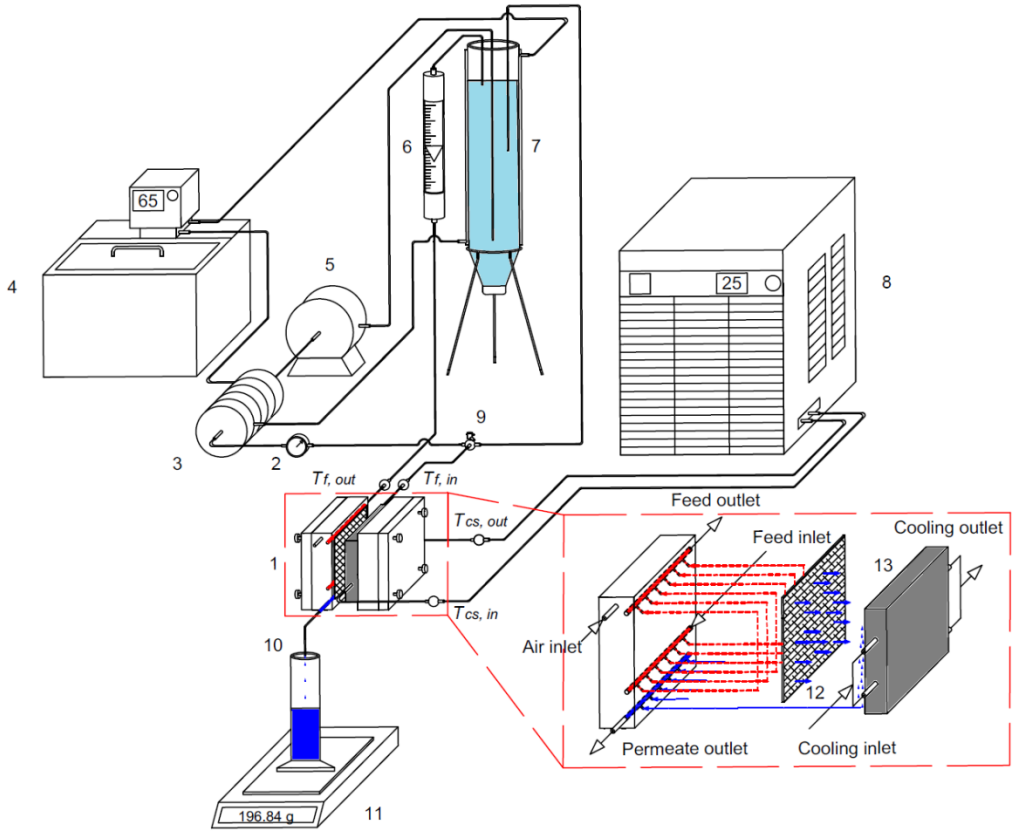

Figure 3.1.1. AGMD set-up: 1.- membrane module, 2.- manometer, 3.- heat exchanger, 4.- thermostat, 5.- peristaltic pump, 6.- flowmeter, 7.- feed tank, 8.- chiller, 9.- 3-ways valve, 10.- permeate, 11.- balance, 12.- membrane and 13.- condensation surface.

The used model brine feed solution was 65 g/L NaCl (ACS reagent ≥ 99%, supplied by *Sigma-Aldrich*) in water. The main objective is to produce distilled water and increase the concentration of the feed solution up to its saturation point and above. The weight of the permeate was registered every hour using a digital balance *Denver SI-2002* (± 0,01g) and the permeate flux (J) was calculated as:

$$J = \frac{m}{A \cdot t} \tag{3.1.1}$$

where m is the mass of the produced permeate, A is the effective membrane area and t is the operating time of the registered weights.

To measure the concentration of feed and permeate, a *712 Ω Metrohm* electrical conductivity meter was employed and the data were obtained with a reference temperature established at 298 K. A previous calibration curve was made using different NaCl aqueous solutions. The salt rejection factor (α) and the normalized concentration factor (β_h) were determined as follows:

$$\alpha = \left(1 - \frac{C_p}{C_f}\right) 100 \tag{3.1.2}$$

$$\beta_h = \frac{C_{f,t} / C_{f,0}}{h} \tag{3.1.3}$$

where C_p and C_f are the permeate and feed salt concentrations, respectively. $C_{f,t}$ is the feed salt concentration at time t, $C_{f,0}$ is the initial feed salt concentration and h is the total time of the concentration experiment.

For each membrane and feed temperature, a block of nine different experiments were realized as schematized in Fig. 3.1.2. The duration of the tests was different for each one. To study the initial state of the membrane and to ensure the reproducibility of the permeate fluxes for different membrane samples, the first two experiments were realized at a feed temperature of 338 K (Tests 1 and 2 in Fig. 3.1.2), one with distilled water and the next one with a salt feed solution of 30 g/L NaCl during two hours. Subsequently, two other similar experiments (Tests 3 and 4 in Fig. 3.1.2) were performed but with another feed temperature equal to that of the main concentration experiment (from 318 to 355 K). This permits to know the initial AGMD performance, based on the permeate flux and to study the membrane fouling, based on the decline of the permeate flux. As it is mentioned earlier, the main concentration experiment was carried out with an initial feed aqueous solution of 65 g/L NaCl at the desired temperature (T_f in Table 3.1.2) until saturation of the feed solution at time (t_s in Table 3.1.2).

Once achieved two options were considered, continue to concentrate the feed solution or stop at this point (i.e. saturation concentration of NaCl). Then the four previous experiments (Tests 1-4 in Fig. 3.1.2) were repeated again (i.e. experiments 6-9 in Fig. 3.1.2) to check the final state of the membrane and to compare it with the initial one. After each experiment, a simple washing with distilled water was done, as can be seen in Fig. 3.1.2, by circulating distilled water through the membrane system for at least one hour to remove the remaining salt residues in the membrane module and tubing until an electrical conductivity of the feed equals that of distilled water. At this point, it is considered that the system is clean and prepared to carry out the next experiment. If the membrane pores were not wetted after the main concentration experiment, the membrane fouling factor (FF) can be calculated using the following Eq. 3.1.4 FF is defined as the fouling that cannot be eliminated by a simple washing of the membrane with distilled water.

$$FF = \frac{J_{0,b} - J_{0,a}}{J_{0,b}} 100 \tag{3.1.4}$$

where $J_{0,b}$ and $J_{0,a}$ are the initial permeate flux of the experiments realized before and after the main concentration experiment, respectively. *FF* was calculated for both distilled water and 30 g/L NaCl aqueous solution used as feed solutions for the same feed temperature as that of the main concentration experiment (T^*).

Once all MD experiments were carried out, the used membranes were again characterized. The used membrane is either extracted from the MD system (without washing) or subjected to a stirred washing with distilled water at 500 rpm for 30 minutes. The post-characterization aims to check the effects of scaling/fouling phenomenon on the physical characteristics of the membranes as reported previously. Both washed and unwashed membranes with distilled water were characterized and the results were compared with those of the new membrane samples.

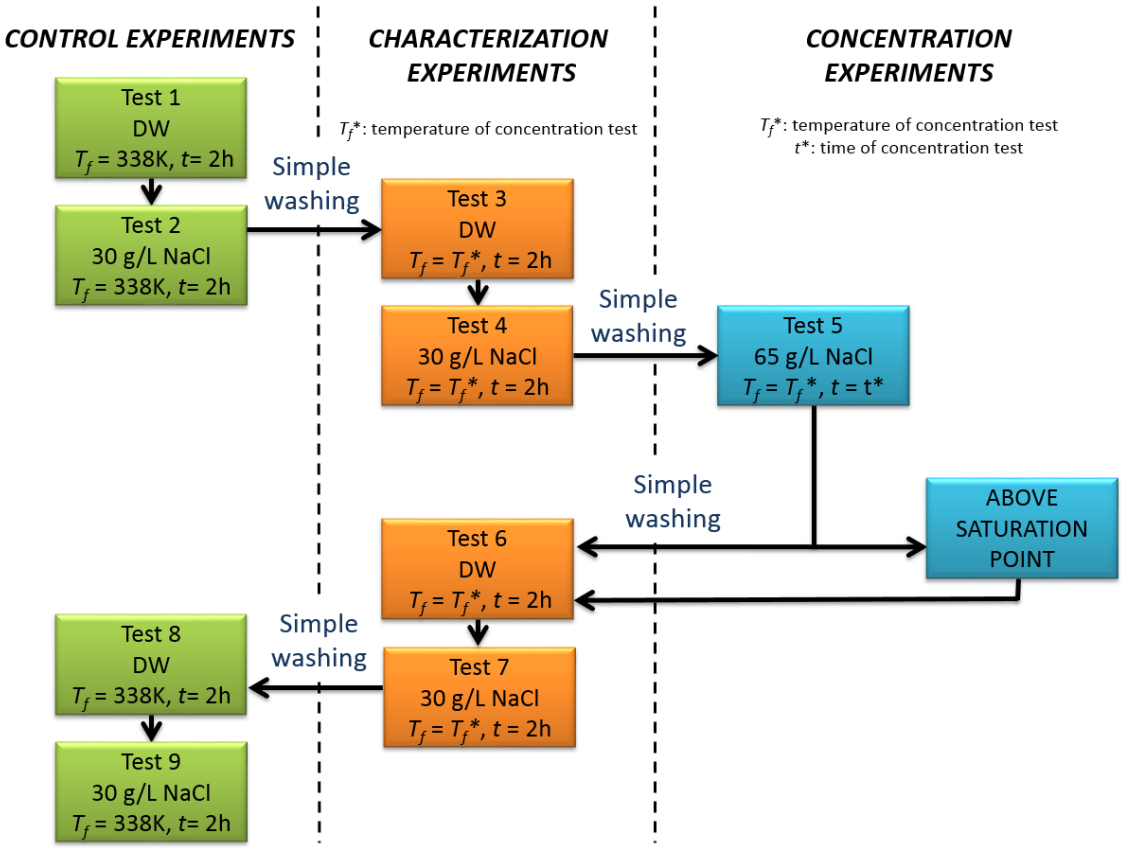

Figure 3.1.2. Block of nine different experiments realized for each new membrane (DW: distilled water; T_f^* feed temperature of concentration test; t^* time of concentration test). (Q_f = 100 L/h and T_{cs}= 298 K).

Table 3.1.2. Results of the AGMD desalination and concentration of the feed solutions when using different feed inlet temperatures and the two membranes (TF200 and TF450). (T_f: feed temperature; t_s: time to reach the saturation concentration; $J_{0:}$ initial permeate flux; J_s: permeate flux at the saturation concentration; ΔJ_h: average permeate flux decline per hour; $C_{f,s}$: feed concentration when the saturation concentration is reached; C_s: reported saturation concentration of NaCl [36]; α_0: initial salt rejection factor; α_s: salt rejection factor at the saturation concentration; $\beta_{h:}$ normalized concentration factor).

Membrane	T_f (K)	t_s (h)	J_0 (kg/m^{2}h)	J_s (kg/m^{2}h)	ΔJ_h (%/h)	$C_{f,s}$ (± 0.18 g/L NaCl)	C_s (g/L NaCl)	α_0 (%)	α_s (%)	β_h (%/h)
TF200	318	82	7.09 ± 0.03	4.54 ± 0.02	0.44	271.91	267.16	100	99.95	5.10
	328	37	8.51 ± 0.03	5.09 ± 0.02	1.09	274.45	269.18	99.88	99.89	11.41
	338	24	14.10 ± 0.05	9.02 ± 0.03	1.50	277.59	271.42	99.90	99.96	17.79
	348	13	20.18 ± 0.08	16.52 ± 0.06	1.40	287.29	273.90	99.98	100	34.00
	355	12	23.84 ± 0.09	17.05 ± 0.07	2.37	284.90	275.74	99.99	99.99	36.53
TF450	318	52	8.69 ± 0.03	3.83 ± 0.01	1.08	268.58	267.16	99.94	99.99	7.95
	328	19	19.89 ± 0.08	9.70 ± 0.04	2.70	273.60	269.18	99.98	99.99	22.15
	338	12	25.84 ± 0.10	17.11 ± 0.07	2.82	286.09	271.42	100	100	36.68
	348	9.5	35.03 ± 0.14	23.83 ± 0.11	3.37	276.44	273.90	100	100	44.77
	355	6	46.50 ± 0.21	35.06 ± 0.14	4.10	278.16	275.74	100	99.91	71.32

3.1.3. Results and discussion

3.1.3.1. Membrane parameters

Fig. 3.1.3 shows the FESEM images of the top (PTFE layer) and bottom (PP support) surfaces of the two membranes. Images of the contact angles (θ) of water drops deposited on the top surface of the membranes are also presented. The FESEM images reveal that the PTFE layer exhibits a network structure in which fine fibrils of diameters 112 ± 43 nm and 76 ± 25 nm and lengths of 2120 ± 1260 nm and 2240 ± 780 nm, for TF200 and TF450 membranes, respectively, are connected to each others at nodes and all the pores are interconnected.

The chemical elemental analysis carried out by EDX method indicates that both membranes have 20% carbon (C) and 80% fluorine (F), which gives it its hydrophobic character [23]. The measured water contact angle of the two membranes is quite similar (~140º in Table 3.1.1). Courel *et al.* [24] reported slightly higher water contact angle values of TF200 and TF450 membranes, 151.1º and 147.9º, respectively. This may be attributed to the followed characterization procedure.

Membrane code	PTFE layer		PP support layer
	x1000	x15000	
TF200	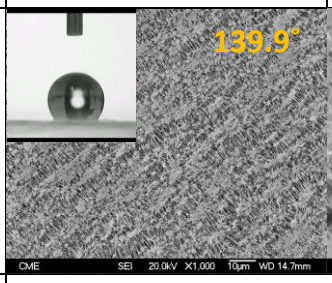	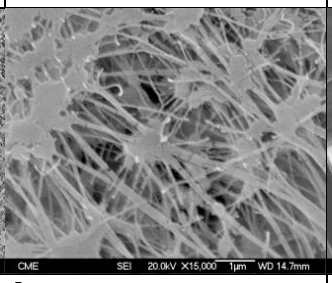	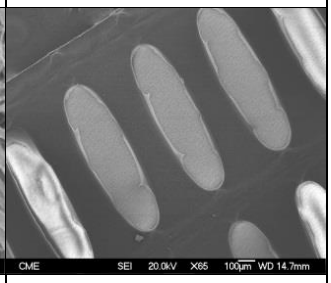
Membrane code	**PTFE layer**		**PP support layer**
	x1000	x15000	
TF450	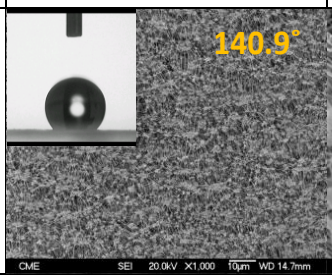	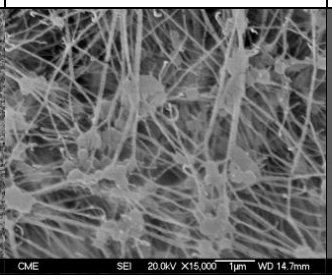	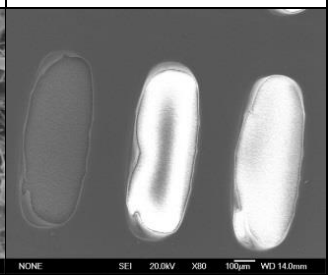

Figure 3.1.3. FESEM images of the top surface of the membranes TF200 and TF450 at two different magnifications and PP support layer together with water contact angles of the top PTFE surfaces.

The measured porosity of the two membranes are similar to those given by the manufacturer (78 ± 4% for TF200 membrane and 78 ± 6% for TF450 membrane, in comparison with 80% given by the manufacturer, see Table 3.1.1). Courel *et al.* [24] also measured the membrane porosity with a pycnometer, obtaining 67% and 58% for TF200 and TF450, respectively. Similar results were obtained by Khayet *et al.* [25], reporting values of 68.7% and 64.3% for TF200 and TF450 membranes, respectively. In other study, El-Abbassi *et al.* [26] characterized the TF200 membrane and obtained a value of 69 ± 5%.

The reported values for the membrane thickness by *Courel et al.* [24] determined by FESEM images were in the range 102-165 μm for the membrane TF200 and 110-178 μm for the membrane TF450. The measured thickness with an electronic micrometer in this study is more accurate and it is within the lower limit of these ranges. By means of a micrometer Khayet *et al.* [25] reported values of 54.8 μm and 60 μm for TF200 and TF450 membranes, respectively, for the PTFE active layer, with a thickness of the PP support layer of 110.4 μm for both membranes. The detected differences between the obtained thickness data may be attributed to the different measurements techniques.

The LEP_w results confirm that the membrane TF200 with a lower pore size has a greater LEP_w (Table 3.1.1). The measured values of the LEP_w are quite similar to those given by the manufacturer and close to those reported in other studies (i.e. 276 kPa and 149 kPa for the membranes TF200 and TF450, respectively [25]). The same value of the LEP_w for the TF200 membrane, 276 ± 9 kPa, was achieved by El-Abbassi *et al.* [26].

Finally, the mean pore size and its distribution were determined and the results are plotted in Fig. 3.1.4. Martínez *et al.* [27, 28] by using the gas transport model, obtained a mean pore size of 310 and 470 nm for TF200 and TF450 membranes, respectively. By the wet/dry flow method using IPA, Khayet *et al.* [25] reported a lower value for the membrane TF200, 198.96 nm, and a similar value for the membrane TF450, 418.82 nm. The mean pore sizes of the two membranes obtained in this study are greater than these values (see Table 3.1.1). The detected differences may be attributed principally to the different characterization techniques applied and also to the procedure followed in each technique.

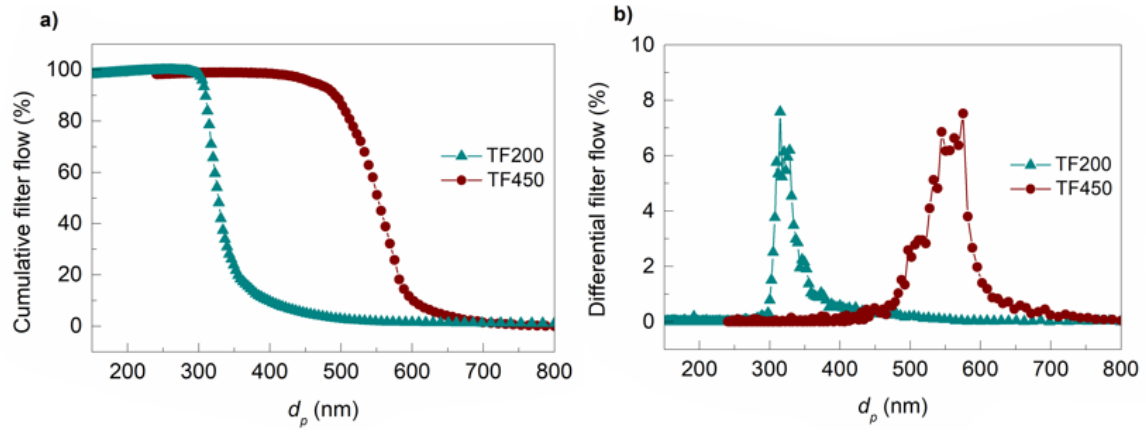

Figure 3.1.4. Cumulative (a) and differential (b) filter flow of the new TF200 and TF450 membranes obtained by porometry technique.

3.1.3.2. Experiments of concentration of feed saline solutions up to their saturation

As it was already mentioned, to know the initial AGMD performance of each membrane sample, Tests 1 and 2 (Fig. 3.1.2) were carried out. The obtained results showed a similar performance ensuring a good reproducibility of the obtained data with a maximum deviation of the initial permeate flux of 17% for TF200 membranes and always below 10% for TF450 membranes.

The concentration test of the saline feed aqueous solution was carried out as indicated in Fig. 3.1.2 (Test 5). Figs. 3.1.5-3.1.7 show the variation of the permeate flux, the salt feed concentration and the salt permeate concentration of the two membranes TF200 and TF450 during AGMD desalination and concentration of the feed solution up to the saturation concentration for different feed temperatures. The corresponding data are summarized in Table 3.1.2.

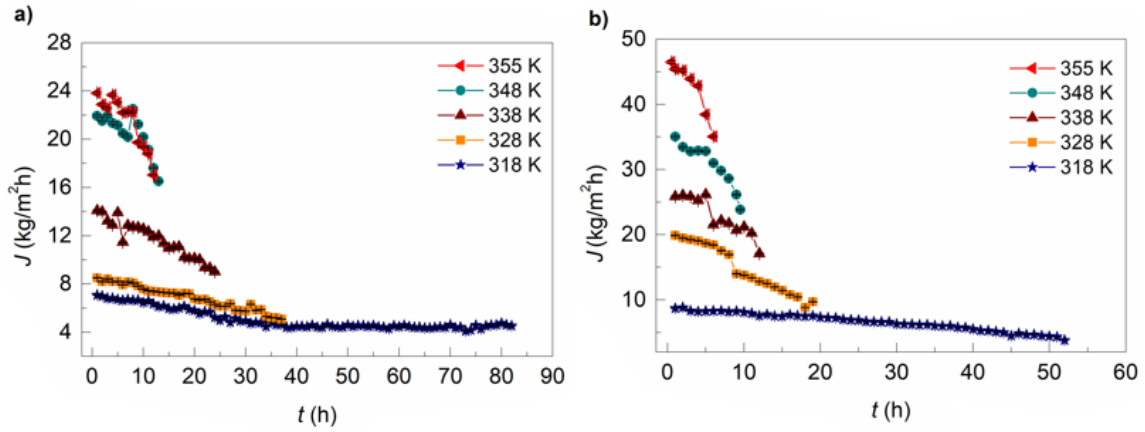

Figure 3.1.5. AGMD permeate flux as a function of time for different feed inlet temperatures (T_f): (a) TF200 and (b) TF450 membranes ($C_{f,0}$ = 65 g/L NaCl; Q_f = 100 L/h, T_{cs} = 298 K).

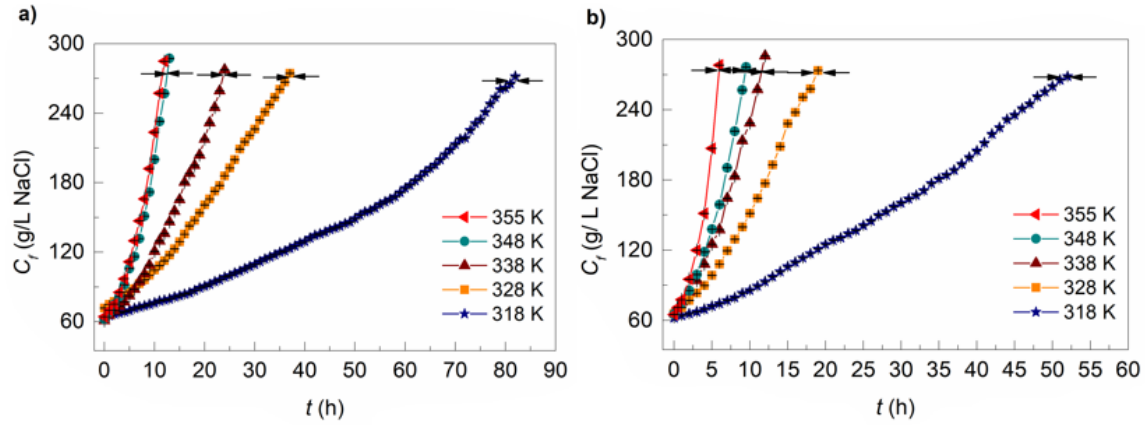

Figure 3.1.6. Concentration of the feed NaCl with time for different feed inlet temperatures (T_f) of the membranes TF200 (a) and TF450 (b). ($C_{f,0}$ = 65 g/L NaCl; Q_f = 100 L/h, T_{cs} = 298 K). The arrows represent the saturation concentration of NaCl (C_s) for each feed inlet temperature, low to high: 267.16; 269.18; 271.42; 273.90 and 275.74 g/L NaCl.

Considering that the initial concentration of the feed solution is the same in all the experiments, 65 g/L NaCl, the initial permeate flux is higher for higher feed temperature, as discussed previously. The feed solution is concentrated with time and the permeate flux decreases whereas the permeate concentration remains below the concentration limit of fresh water (0.5 g/L NaCl), as presented in Fig. 3.1.7. Therefore, high salt rejection factors at initial time were obtained as it is reported in Table 3.1.2. The reduction of the permeate flux with time is attributed to the increase of the salt feed concentration, the decrease of the driving force, the subsequent increase of the concentration polarization effect and to the salt crystallization on the surface of the membrane (i.e. external surface fouling), and/or inside the membrane pores (i.e. a partial blocking or gradual narrowing of the pores or a complete pore blocking [29]). This reduction of the permeate flux can be defined as the average permeate flux decline per hour:

$$\Delta J_h = \frac{J_0 - J_s}{J_0 \cdot h} 100 \qquad (3.1.5)$$

where J_0 is the initial permeate flux and J_s is the permeate flux at the saturation point of saline feed solution.

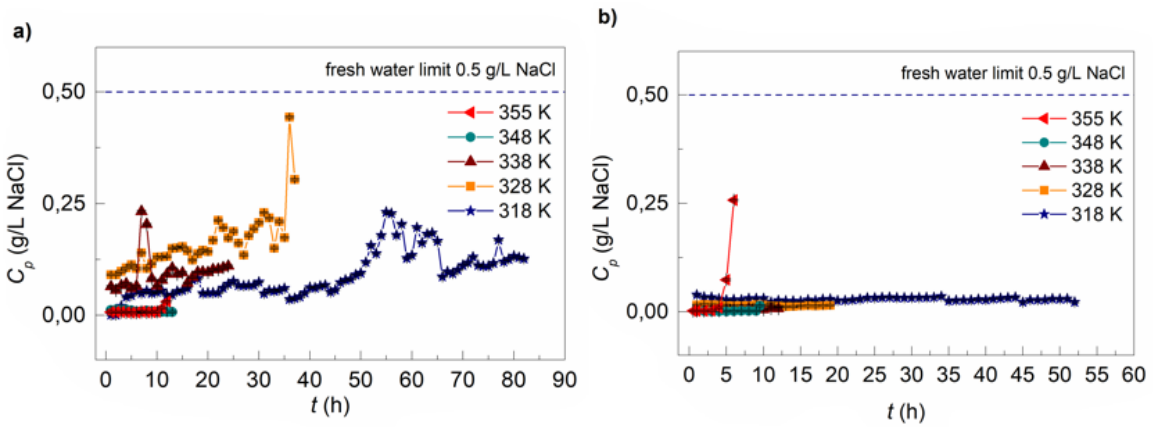

Figure 3.1.7. Permeate salt concentration during the concentration of the feed solution for different feed inlet temperatures (T_f) using the membranes TF200 (a) and TF450 (b). ($C_{f,0}$ = 65 g/L NaCl; Q_f = 100 L/h, T_{cs} = 298 K).

As it is expected, the higher the feed temperature, the higher is ΔJ_h as can be seen in Table 3.1.2. In addition, ΔJ_h is higher for the membrane TF450 having greater pore size. A higher permeate flux accelerates the concentration of the feed saline solution. Moreover, the duration of the concentration tests up to the saturation point is larger for lower feed inlet temperature and for smaller membrane pore size as can be seen in Fig. 3.1.8. Table 3.1.2 also indicates the reported saturation concentration of NaCl (C_s) for each feed temperature [30] and the feed concentration when the saturation point is reached ($C_{f,s}$), which is higher than C_s providing that the data were collected each hour. In these cases, all concentration experiments were carried out until the indicated NaCl saturation concentrations were reached maintaining the salt rejection factors at these points higher than 99.89%, or which is the same, the membranes do not suffer wetting while working below the saturation point of NaCl. The corresponding normalized salt concentration factor (β_h) was also calculated. As already mentioned, the greater is the membrane pore size or the higher is the feed temperature, the higher is the permeate flux. Consequently, the feed concentration increases faster up to the saturation concentration of NaCl, and therefore β_h increases as can be seen in Table 3.1.2.

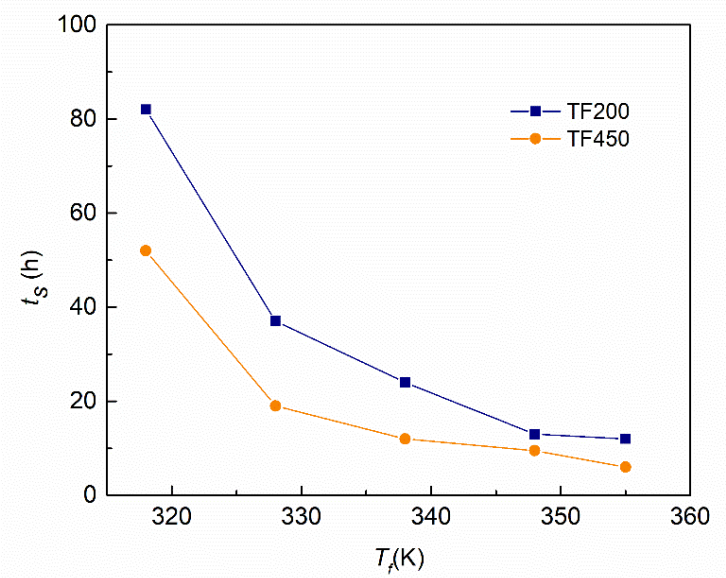

Figure 3.1.8. Decrease of the experiment time to reach the saturation concentration of NaCl with the feed inlet temperature (T_f) for the membrane TF200 and TF450.

After reaching the saturation concentration of salt, in some experiments it was decided to stop and check the membrane status by performing the four subsequent experiments indicated in Fig. 3.1.2 (Tests 6-9) followed by the characterization of the used membranes. For the membrane TF200 four experiments were performed at the feed inlet temperatures 328 K, 338 K, 348 K and 355 K. For the membrane TF450, only one experiment at the feed inlet temperature of 348 K was performed. Membrane fouling factor (*FF*) was calculated using Eq. (3.1.4) as explained previously and the results are summarized in Table 3.1.3. The detected crystallization fouling is small and irreversible with a simple distilled water washing. For a high feed inlet temperature (i.e. 355 K for the membrane TF200) and big pore size (i.e. the membrane TF450 at 348 K), the obtained initial permeate flux under the same operation conditions after the concentration experiment was higher than the initial permeate flux for both distilled water and 30 g/L feed salt solutions of the experiments realized before the concentration experiment. Therefore, *FF* could not be calculated. However, the obtained salt rejection factors of the subsequent experiments, 99.95%, discarded the possibility of a total membrane pore wetting. Thus, a partial pore wetting may explain why the permeate flux increases slightly in the subsequent experiments (within the margin of error). Therefore, it can be stated that *FF* is greater at lower feed inlet temperatures and smaller pore sizes. This may be attributed to the longer duration of the concentration experiment at low feed temperatures and small membrane pore size.

Table 3.1.3. Membrane fouling factor (*FF*) of the membranes TF200 and TF450 at different feed inlet temperatures for the concentration test performed up to the saturation point (T_f: feed temperature; $J_{0,b}$: initial permeate flux before the concentration test of the feed solution; $J_{0,a}$: initial permeate flux after of the concentration test of the feed solution, with distilled water (DW) and 30 g/L NaCl as feed solution; *FF*: membrane fouling factor and α_a: salt rejection factor of the characterization experiments realized after the concentration test of the feed solution).

Membrane	T_f (K)	$J_{0,b}$ DW (kg/m^{2}h)	$J_{0,a}$ DW (kg/m^{2}h)	*FF* (%)	$J_{0,b}$ 30 g/L NaCl (kg/m^{2}h)	$J_{0,a}$ 30 g/L NaCl (kg/m^{2}h)	*FF* (%)	α_a (%)
TF200	328	11.95 ± 0.05	11.86 ± 0.05	0.73	10.01 ± 0.05	9.52 ± 0.04	4.88	99.85
TF200	338	18.88 ± 0.09	17.12 ± 0.08	9.29	15.94 ± 0.07	14.61 ± 0.07	8.35	99.92
TF200	348	29.08 ± 0.13	26.93 ± 0.12	7.38	23.99 ± 0.11	22.43 ± 0.10	6.48	99.99
TF200	355	31.43 ± 0.14	31.63 ± 0.14	- *	25.36 ± 0.12	25.48 ± 0.12	- *	99.95
TF450	348	39.13 ± 0.18	39.61 ± 0.18	- *	36.88 ± 0.17	37.27 ± 0.17	- *	99.95

**FF* cannot be calculated if the permeate flux is higher after realized the concentration experiment.

3.1.3.3. Experiments of concentration of feed saline solutions above saturation concentration

Some desalination and concentration experiments were not stopped after reaching saturation points but were continued achieving very high salt concentrations. These experiments were carried out with the membrane TF200 at the lower feed temperature (318 K), and the membrane TF450 at the feed inlet temperatures 318, 328, 338 and 355 K. These experiments were stopped once membrane wetting was detected based on the sudden increase of the concentration of the permeate (i.e. sharp reduction of the salt rejection factor) or when a sharp reduction in the permeate flux was occurred. Some results are plotted in Fig. 3.1.9 and the corresponding data are listed in Table 3.1.4.

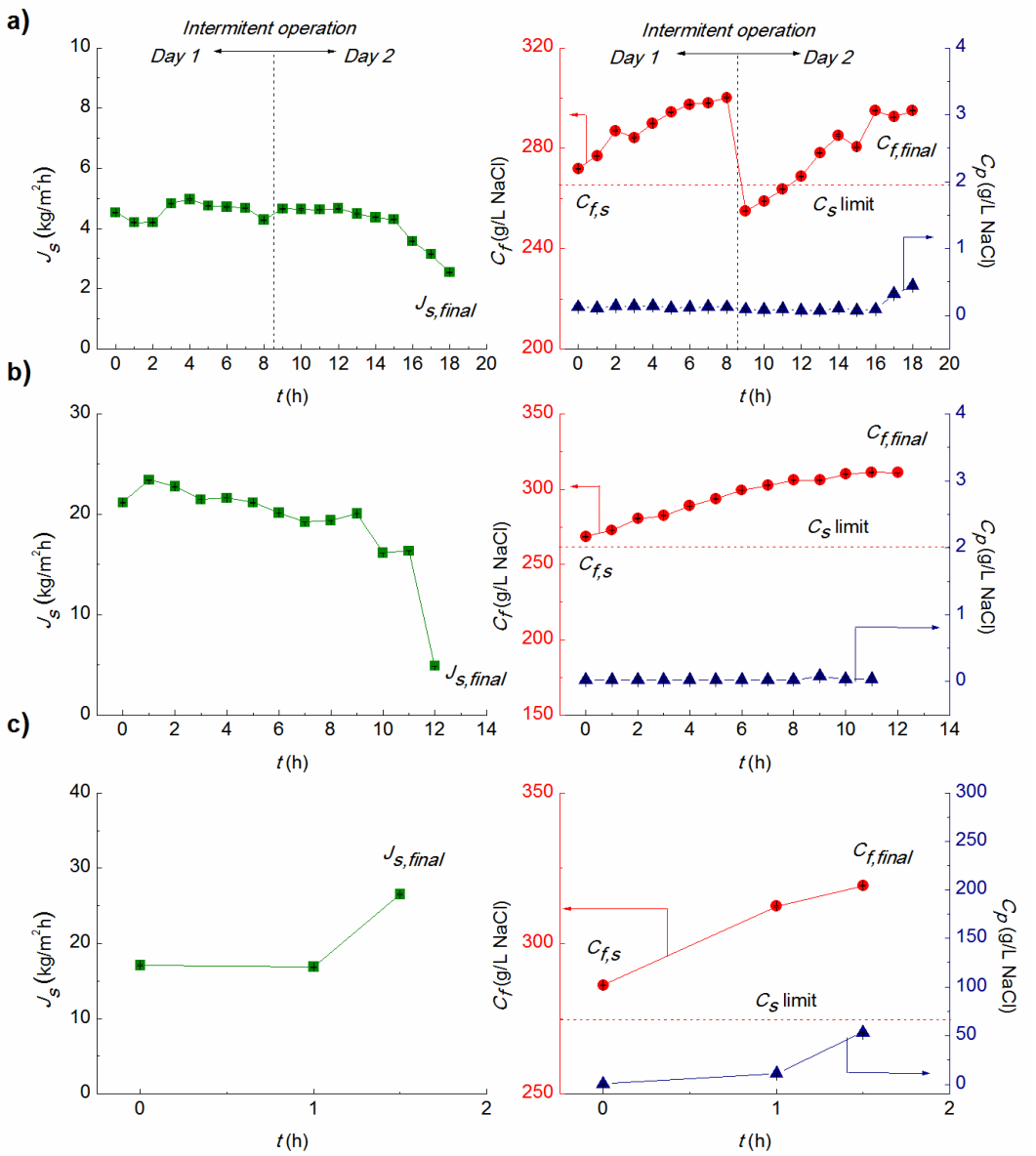

Figure 3.1.9. Permeate flux together with the feed and permeate salt concentrations of AGMD tests carried out after the feed solution reached the saturation concentration: a) TF200 (T_f=318 K), b) TF450 (T_f = 318 K) and c) TF450 (T_f = 338 K) (Q_f = 100 L/h, T_{cs} = 298 K).

It was proved that both PTFE membranes can continue separating water from salt during few hours after reaching the saturation point of the feed salt solution. As can be seen in Fig. 3.1.9, operating time is shorter for higher feed inlet temperatures, as it was expected. In Fig. 3.1.9(a), the feed concentration decreased below the saturation concentration of NaCl when the experiment was stopped. This was due to the crystallization and subsequent deposition of salt crystals at the bottom of the feed tank (Fig. 3.1.1). Fig. 3.1.9 (a and b) show the blockage effect of the membrane for 318 K as a feed inlet temperature of both membranes. The permeate flux decreased while a reasonably good salt rejection factor was maintained (Table 3.1.4).

Table 3.1.4. Results of the AGMD experiments collected above the saturation concentration and until wetting of the membrane pores (T_f: feed temperature; $t_{a,s}$: time of the experiment after saturation concentration; $J_{s:}$ permeate flux at the saturation concentration; $J_{s,final}$: final permeate flux of the saturated feed solution; ΔJ_h: average permeate flux decline per hour; $C_{f,s}$: feed concentration when the saturation concentration is reached; $C_{f,final}$: final feed concentration of the saturated feed solution; α_s: salt rejection factor corresponding to saturation concentration; $\alpha_{s,final:}$ final salt rejection factor of the saturated feed solution and $\beta_{h:}$ normalized concentration factor).

Membrane	T_f (K)	t_{as} (h)	J_s (kg/m^{2}h)	$J_{s,final}$ (kg/m^{2}h)	ΔJ_h (%/h)	$C_{f,s}$ (± 0.18 g/L NaCl)	$C_{f,final}$ (± 0.18 g/L NaCl)	α_s (%)	$\alpha_{s,final}$ (%)	β_h (%/h)
TF200	318	18	4.54 ± 0.02	2.54 ± 0.01	2.45	271.91	294.93	99.95	99.85	6.03
TF450	318	12	3.83 ± 0.01	0.88 ± 0.01	6.42	268.58	310.99	99.99	99.99	9.65
	328	1.5	9.70 ± 0.04	9.66 ± 0.04	0.27	273.60	290.31	99.99	96.00	70.74
	338	1.5	17.11 ± 0.07	26.52 ± 0.12	1.46[a]	286.09	319.09	100	83.36	74.36
	355	3	35.06 ± 0.14	66.38 ± 0.26	12.26[b]	278.16	323.94	99.91	73.81	38.82

[a] calculated with the last permeate flux measured before the membrane wet: 16.86 kg/m^{2}h

[b] calculated with the last permeate flux measured before the membrane wet: 26.46 kg/m^{2}h

The decreasing trend of the permeate flux with time is due to the reduction of the permeability of the membrane caused mainly by surface and/or pore blockage by an amorphous precipitate of salt deposits [31-33] as it is confirmed by the FESEM images presented in Fig. 3.1.10, where salt crystals of different sizes appear on the membrane surface. The FESEM images reveal the presence of salt crystals on the PTFE layer composed mainly by sodium (Na^+) and chlorine (Cl^-) ions as confirmed by the EDX qualitative analysis. The oxygen that appears in the EDX analysis corresponds to the hydrated salt crystals, as a result of the characterization of the membrane without preliminary drying (in blue). If the membrane is dried under vacuum conditions at 353 K (in red) the percentage of oxygen decreases considerably. This fact was corroborated by measuring the difference of oxygen percentage of an area containing a salt crystal (13.93%) in comparison with a net of fibrils area (1.36%) of the same membrane sample (Fig. 3.1.10 d).

Membrane code	PTFE layer		EDX spectrum
	x1500	x10000 / * x6000	
(a) TF200 T_f 318 K $C_{f,final}$ 294.93 g/L NaCl	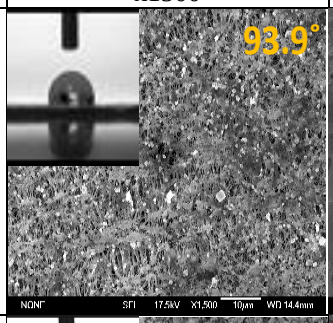	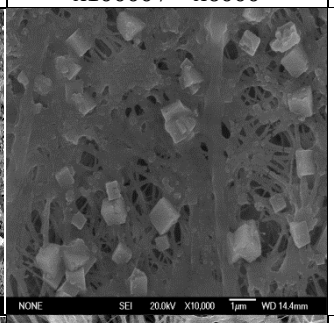	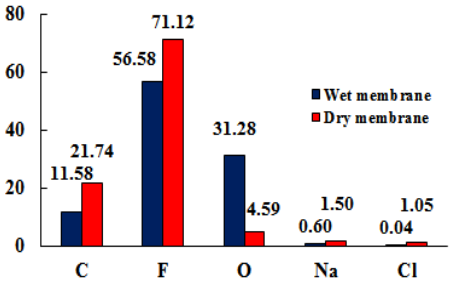
(b) TF450 T_f 318K $C_{f,final}$ 310.99 g/L NaCl	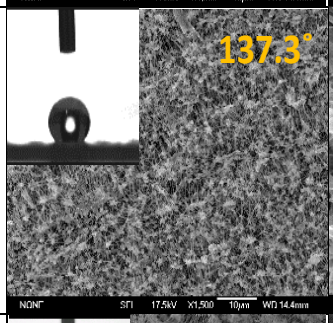	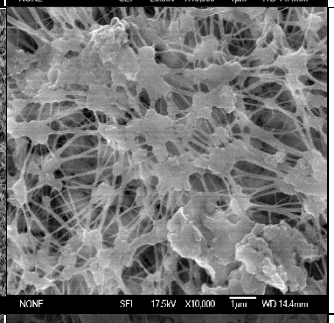	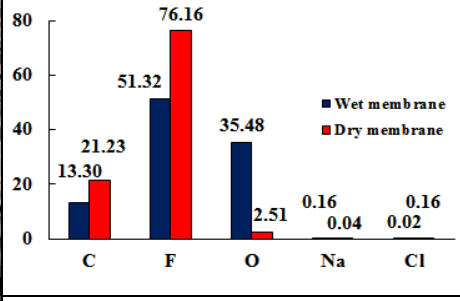
(c) TF450 T_f 328K $C_{f,final}$ 290.31 g/L NaCl	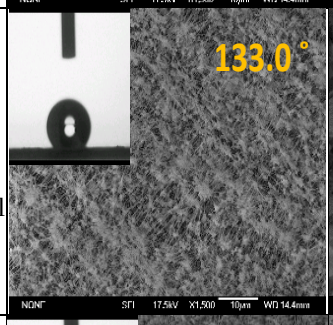	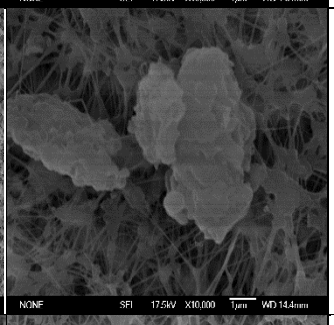	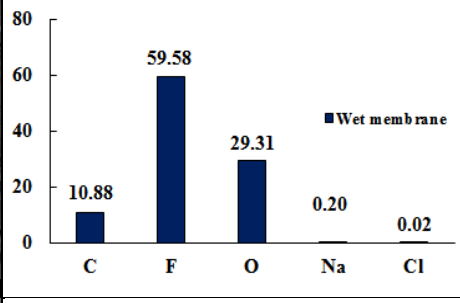
(d) TF450 T_f 338K $C_{f,final}$ 319.09 g/L NaCl	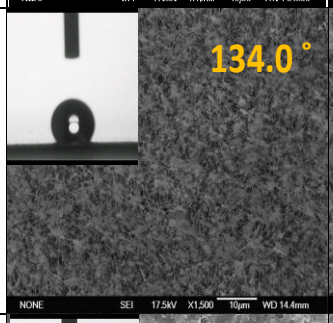	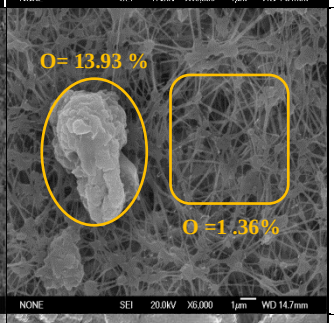	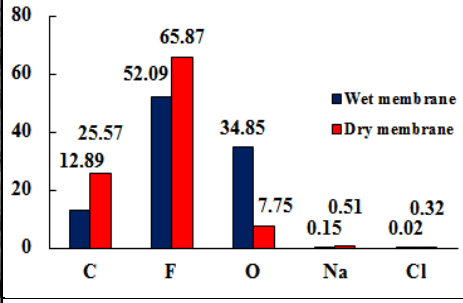
(e) TF450 T_f 355K $C_{f,final}$ 323.94 g/L NaCl	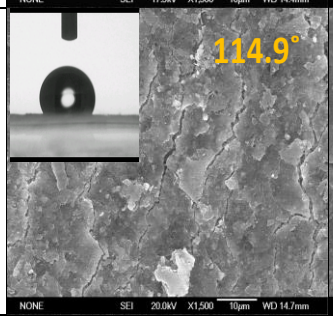	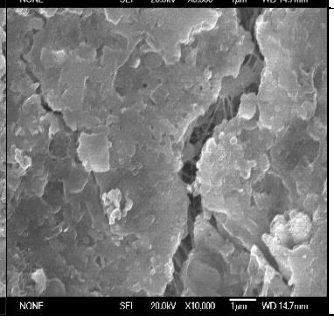	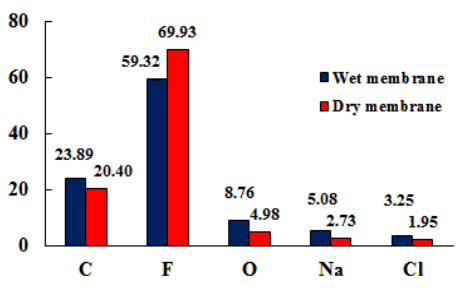

Figure 3.1.10. Salt deposition on the surface of the PTFE membrane top layer (at different magnifications), water contact angles and EDX spectra of the membranes TF200 and TF450 already used in AGMD.

The values of β_h in Table 3.1.4 were higher than the β_h values of Table 3.1.2, corresponding to a supersaturation condition where the nucleation and growth of crystals in the feed solution and on the membrane surface must be taken into account [34]. Taking into consideration that salt deposits usually start forming at the biggest pores of the membrane, this fact accelerates the wetting phenomenon [35-37]. For the TF450 membrane a break of the established vapor-liquid interfaces occurs, allowing the diffusion of feed solute in liquid phase through the membrane pores. This is corroborated by the sharply increase of the permeate flux, as can be seen in Fig. 3.1.9(c) and the reduction of the salt rejection factor (Table 3.1.4).

The *FF* was calculated for the membranes that were not finally wetted even after the use of supersaturated feed solutions. Only in the cases where the concentration experiment was carried out under the lower feed inlet temperature (318 K), for both membranes. It is worth quoting that in these cases, the membranes suffered a pore blockage phenomenon and the *FF* could be calculated. Values were 6.86% and 4.62% with distilled water as feed solution, for TF200 and TF450 membranes respectively, and 3.03% for the TF450 membrane with 30 g/L NaCl as feed solution. As occurs with experiments carried out up to the saturation point (Table 3.1.3), the *FF* is higher when the duration of the AGMD experiments is larger (i.e. low feed temperatures and small membrane pore size).

3.1.3.4. Effects on membranes characteristic morphology of salt fouling phenomenon

The used membranes in the AGMD concentration experiments carried out above the saturation concentration of NaCl were characterized by means of the methods specified previously. Fig. 3.1.10 shows the FESEM images of the PTFE top layer of the TF200 and TF450 membranes together with the corresponding EDX spectra and the water contact angle images. Table 3.1.5 summarizes the obtained characterization parameters.

Compared to the thickness of the new membranes, salt crystals depositions on the membrane surface increase the final thickness of the membranes already used (compare Tables 3.1.1 and 3.1.5). The PTFE membranes exhibit irregular interstices between fibrils (see Fig. 3.1.3) that may act as effective nucleation sites for crystal growth [32]. The higher area of the TF450 membrane pores permits a higher salt deposition, making thicker the salt layer on the membrane surface, especially when the feed inlet temperature is higher, due to the greater value of β_h and the feed concentration achieved (Fig. 3.1.10(e)).

Table 3.1.5. Parameters of the membranes after their use in AGMD above the saturation concentration including the membranes washed under turbulent flow in distilled water for 30 min before characterization (t: total time of the concentration experiment; $C_{f,final}$: final feed concentration of the saturated feed solution; δ: membrane thickness; d_p: mean pore size; ε: porosity; θ: water contact angle).

Membrane	T_f (K)	t (h)	$C_{f,final}$ (± 0.18 g/L NaCl)	δ (µm)	d_p (nm)	ε (%)	θ (°)	Membrane washed
TF200	318	100	294.93	108 ± 6	309 ± 7	71 ± 10	93.9 ± 7.8	No
		100	294.93	106 ± 7	303 ± 11	74 ± 6	100.4 ± 4.3	Yes
TF450	318	64	310.99	100 ± 6	519 ± 6	69 ± 9	137.3 ± 3.3	No
		64	310.99	101 ± 6	517 ± 10	70 ± 8	138.2 ± 0.6	Yes
	328	20.5	290.31	104 ± 6	536	65 ± 9	133.0 ± 1.6	No
		20.5	290.31	103 ± 6	539	68 ± 2	133.2 ± 1.4	Yes
	338	13.5	319.09	99 ± 6	525 ± 10	72 ± 8	134.0 ± 2.4	No
		13.5	319.09	99 ± 5	525 ± 4	73 ± 9	134.6 ± 1.6	Yes
	355	9	323.94	105 ± 5	580 ± 24	59 ± 4	114.9 ± 3.1	No
		9	323.94	104 ± 4	615	73 ± 4	134.7 ± 2.3	Yes

After a stirr washing of the membranes described above the membrane thickness decreased slightly due to the elimination of some salt particles from the membrane surface, but the majority of the salt layer remains on the membrane surface.

The water contact angles of all used membranes are smaller than those of the new membranes (Tables 3.1.1 and 3.1.5). After mechanical washing with distilled water, the water contact angles increased slightly tending to reach the initial θ values especially for the membrane TF450.

It must be pointed out that the membrane having the higher values of *FF* (6.86% for the membrane TF200 at 318 K), presents the lower value of the water contact angle (93.9 ± 7.8º). The formed partial or total crystal layer on the membrane surface reduces its hydrophobicity that is confirmed by the water contact angle measurement. The same behavior is observed for the membrane TF450 at 355 K. It is to point out that crystallization within the pores (i.e. salt crystals growing inside the pores) increases the risk of membrane wetting [32, 38]. As the pores of the membrane are blocked or filled with salt crystals the void volume fraction or porosity also decreases (Tables 3.1.1 and 3.1.5). The reduction of the porosity respect to the initial value of the membrane differs about 9% for the membrane TF200 and between 8% and 24% for the membrane TF450. This reduction is greater for the membrane having bigger pore size because it is easier for the salt feed solution to penetrate and therefore induces crystal growth inside the big pores. After mechanical washing a slight increase of ε values was observed, 4% for the membrane TF200 and between 1 and 19% for the membrane TF450, due to the facility to clean the bigger pores.

The initial ε value was not recovered due partially to the presence of salt crystals inside the membrane pores.

Salt crystals fouling may also cause an alteration of the membrane structure, due to the damage of some fibrils and crack formation [32], that contribute to the decrease of the mechanical strength of the membrane [31, 32], and subsequently changes in the pore size distribution [32]. The greater percentage of salt ions present in the membrane TF450 at 355 K (see Fig. 3.1.10(e)), denotes the presence of a thicker salt layer deposited on the membrane surface that increases the membrane thickness compared to a new membrane. An increase of the mean pore size of the respective membrane was achieved due to the effect of salt crystals in the pores structure (Fig 3.1.11(b)).

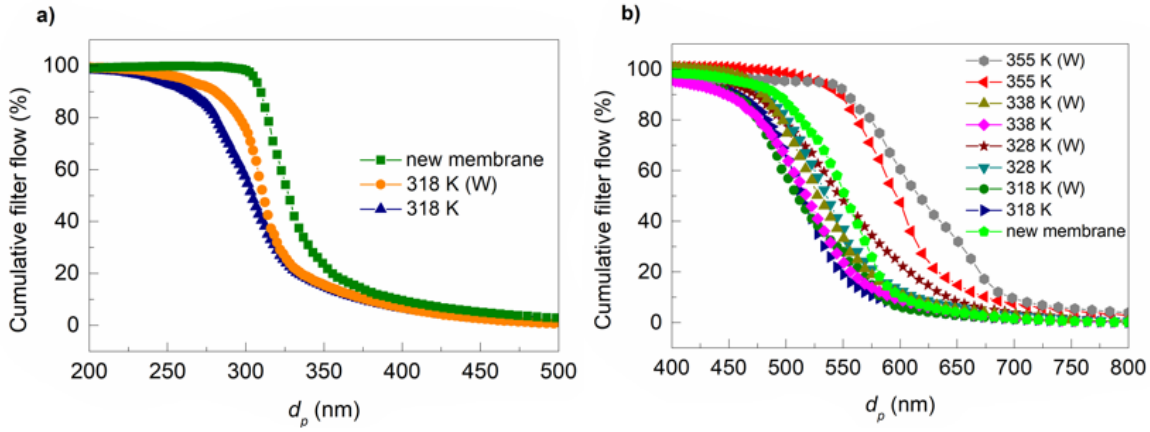

Figure 3.1.11. Cumulative filter flow obtained by porometry technique of a) TF200 and b) TF450 membranes, new or once used in AGMD above the saturation concentration of NaCl and washed under turbulent flow (W) before characterization. ($C_{f,0}$ = 65 g/L NaCl, Q_f = 100 L/h, T_{cs} = 298 K).

After washing, the mean pore size increases, as it was expected, due to the partially removal of salt crystals from the membrane pores. A similar case occurs for the membrane TF450 with a feed temperature of 328 K. After washing, the mean pore size increases and it is higher than the mean pore size of the new membrane. This difference is greater for bigger pore sizes due to its higher facility to be cleaned. In the rest of the cases, a reduction of the gas flow through the used membranes and a decrease of the pore size were observed in general (Fig. 3.1.11(a) and (b)) due to the pore blockage effect. After washing, the mean pore size value becomes quite similar except for the membranes that suffered some cracks (i.e. TF450 328 K and 355K).

3.1.3.5. Thermal efficiency

Not only it is important to maximize the permeate flux but also to reduce the energy consumption and therefore improve the thermal efficiency of the MD systems. The total heat flux transferred through the membrane is due to the heat transfer by conduction through both the membrane material and to its gas-filled pores and the latent heat associated

to the involved mass transfer. It is worth quoting that between 50 and 80% of thermal energy is consumed as latent heat for water production while the remaining is lost by conduction [39]. The thermal efficiency (η_T) is defined as [40]:

$$\eta_T = \frac{J\ A\ \Delta H_{v,w}}{Q_f\ c_{p,f}\ (T_{f,in} - T_{f,out})}\ 100 \qquad (3.1.6)$$

where $\Delta H_{v,w}$ is the enthalpy of evaporation of water, Q_f is the feed flow rate, $c_{p,f}$ is the specific heat of the feed solution and $T_{f,in}$ and $T_{f,out}$ the mean inlet and outlet feed temperatures.

Fig. 3.1.12(a) shows the initial thermal efficiency at the beginning of each concentration experiment of a feed aqueous solution of 65 g/L NaCl as a function of the feed inlet temperature. For the same membrane, feed flow and feed solution, the thermal efficiency depends mainly on the feed inlet temperature and the permeate flux. As it can be seen in Fig. 3.1.12(a) the thermal efficiency increases with the feed temperature [41, 42] and it is higher for the membrane TF450 having greater pore size. A similar thermal efficiency value was reported by Liu et *al.* [43], 98%, by using an AGMD system with a flat sheet PTFE membrane of 100 nm as mean pore size, a temperature difference between feed and permeate sides of 55 K, 4 mm of air gap and 228 L/h feed flow rate. Lower thermal efficiency values were reported by Gryta [44] when using DCMD configuration, due to the higher thermal losses that occurs in this configuration (i.e. thermal efficiencies of 72% and 55% at 358 K and 293 K feed and distillate inlet temperatures were obtained using PP S6/2 hollow fiber membrane with a mean pore size of 200 nm, 50 L/h feed and distillate flow rates, and distilled water and 167 g/L NaCl as feed aqueous solutions, respectively).

Fig. 3.1.12(b) shows the trend of η_T with time of the experiments realized with the membranes TF200 and TF450. An initial feed concentration of 65 g/L NaCl and a feed inlet temperature of 355 K were used. The observed decline of η_T with time is attributed to the decrease in the permeate flux due the concentration polarization and the fouling layer, as discussed previously. The decrease of η_T is more pronounced after saturation of the feed solution.

The calculated initial thermal efficiency for the previous and subsequent experiments to the concentration test is summarized in Table 3.1.6, for both distilled water and 30 g/L NaCl as feed solutions. As it was expected, the initial thermal efficiency of the experiments carried out with distilled water as feed solutions are higher due to the permeate flux is also higher. Differences between the thermal efficiencies measured before and after the concentration experiment are given by the *FF* values. The higher is the *FF* the higher is the decrease of the thermal efficiency. It is to be noted that the thermal efficiency cannot be calculated in wetted membranes.

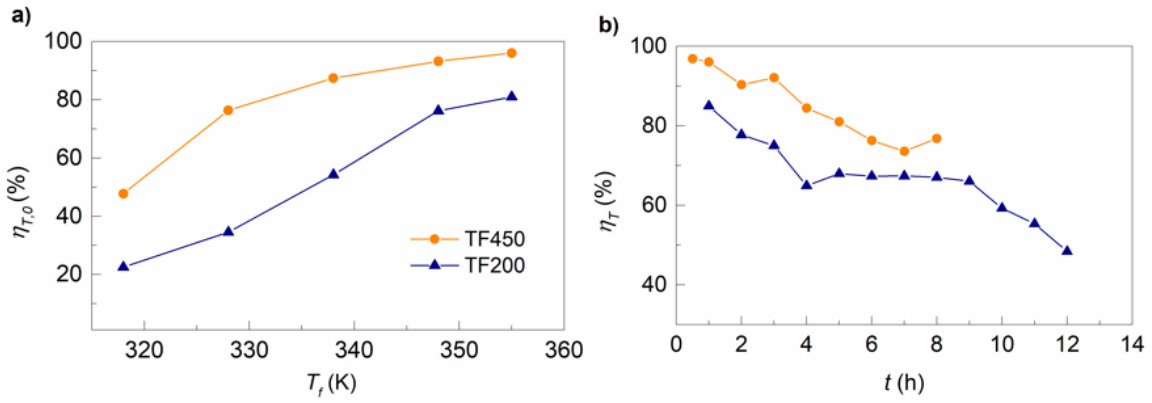

Figure 3.1.12. (a) Initial thermal efficiency of the AGMD test of the membranes TF200 and TF450 ($C_{f,0}$ = 65 g/L NaCl; Q_f = 100 L/h; T_{cs} = 298 K). (b) Tendency of the thermal efficiency with time of the experiments realized with the membranes TF200 and TF450 ($C_{f,0}$ = 65 g/L NaCl; T_f = 355 K; Q_f = 100 L/h; T_{cs} = 298K).

Table 3.1.6. Thermal efficiency (η_T) of the membranes TF200 and TF450 (T_f: feed inlet temperature; ηT_0: initial thermal efficiency of the characterization experiments realized before (b) and after (a) the concentration test, respectively; with distilled water (DW) and 30 g/L NaCl as feed solutions; $\Delta\eta T_0$: decrease of initial thermal efficiency).

			DW			***30 g/L NaCl***		
Main experiment duration	**Membrane**	**T_f (K)**	**$\eta T_{0,b}$ (%)**	**$\eta T_{0,a}$ (%)**	**$\Delta\eta T_0$ (%)**	**$\eta T_{0,b}$ (%)**	**$\eta T_{0,a}$ (%)**	**$\Delta\eta T_0$ (%)**
Up to the Saturation point of NaCl	TF200	328	50.75	50.38	0.73	43.01	40.88	4.95
	TF200	338	62.97	57.12	9.29	53.71	49.23	8.3
	TF200	348	82.56	78.60	4.80	71.40	68.02	4.73
	TF200	355	85.83	86.39	-	76.68	77.05	-
	TF450	348	94.15	95.30	-	89.83	-	-
Above the saturation point of NaCl	TF200	318	26.74	25.25	5.57	-	-	-
	TF450	318	50.18	47.86	4.62	45.05	43.68	3.04
	TF450	328	80.47	83.43	-	79.35	81.17	-
	TF450	338	90.28	-	-	88.72	-	-
	TF450	355	97.52	-	-	93.83	-	-

3.1.4. Conclusions

AGMD configuration has been proved to be a very useful process in water desalination and concentration of feed saline solutions including those of concentrations above their saturation points, rejecting more than 99.9% of salt and producing therefore a high-quality distillate, less than 0.5 g/L NaCl. The membrane TF450, due its larger mean pore size, exhibits higher permeate fluxes (e.g., for 355 K, the obtained permeate fluxes at the saturation salt concentration were 17 and 36 kg/m^{2}h for the TF200 and TF450 membranes, respectively). The permeate flux decline, ΔJ_h, caused by the continuous

deposition of salt over the membrane surface was observed with time, being more remarkable with an increase in the feed temperature (from 0.44 %/h, at 318 K, to 2.37 %/h, at 355 K for the membrane TF200, and from 1.08 %/h, at 318 K, to 4.10 %/h, at 355 K, for the membrane TF450). When saturation concentration of the NaCl is overpassed, salt crystals fouling can block or wet the membrane pores reducing the permeate flux or increasing it with a decrease of the permeate quality. Based on the post-characterization studies, crystallization fouling effect causes changes of the initial properties of the membrane. The observed changes of the water contact angle and porosity due to the deposition of salt crystals above the membrane surface and inside the pores indicate the reduction of the hydrophobic character of the membrane. This must be cleaned to recover its initial properties. The thermal efficiency of the AGMD process, affected mainly by the feed inlet temperature and the pore size of the membranes, decreases due to fouling effect. When using a high feed temperature, both the permeate flux and the thermal efficiency are higher for both PTFE membranes (the initial thermal efficiency after the concentration test was up to 77% for the TF200 membrane in experiments up to the saturation point), but crystallization fouling is also higher (around 6.5-8.4%) reducing the lifetime of the membranes.

3.1.5. References

[1] G.W.I., in: IDA Desalination Yearbook 2014-2015, Global Water Intelligence (G.W.I.) and International Desalination Association (IDA) 2014.

[2] J.P. Ducrotoy, M. Elliott, The science and management of the North Sea and the Baltic Sea: natural history, present threats and future challenges, Marine pollution bulletin, 57 (2008) 8.

[3] S. Lattemann, T. Höpner, Environmental impact and impact assessment of seawater desalination, Desalination, 220 (2008) 1.

[4] G.L. Meerganz von Medeazza, “Direct” and socially-induced environmental impacts of desalination, Desalination, 185 (2005) 57.

[5] D.A. Roberts, E.L. Johnston, N.A. Knott, Impacts of desalination plant discharges on the marine environment: A critical review of published studies, Water Research, 44 (2010) 5117.

[6] M. Ezersky, I. Goretsky, Velocity–resistivity versus porosity–permeability inter-relations in Dead Sea salt samples, Engineering Geology, 183 (2014) 96.

[7] B. Malaizé, M.T. Vénec-Peyré, C. Joly, F. Bassinot, N. Caillon, K. Charlier, Imprints of high-salinity water plumes originating from the red sea during termination II, Palaeogeography, Palaeoclimatology, Palaeoecology, 276 (2009) 69.

[8] H. Geng, H. Wu, P. Li, Q. He, Study on a new air-gap membrane distillation module for desalination, Desalination, 334 (2014) 29.

[9] D. Singh, K.K. Sirkar, Desalination of brine and produced water by direct contact membrane distillation at high temperatures and pressures, Journal of Membrane Science, 389 (2012) 380.

[10] A. Alkhudhiri, N. Darwish, N. Hilal, Treatment of saline solutions using air gap membrane distillation: Experimental study, Desalination, 323 (2013) 2.

[11] F. Edwie, T.-S. Chung, Development of simultaneous membrane distillation–crystallization (SMDC) technology for treatment of saturated brine, Chemical Engineering Science, 98 (2013) 160.

[12] L. Mariah, C.A. Buckley, C.J. Brouckaert, E. Curcio, E. Drioli, D. Jaganyi, D. Ramjugernath, Membrane distillation of concentrated brines—Role of water activities in the evaluation of driving force, Journal of Membrane Science, 280 (2006) 937.

[13] C.R. Martinetti, A.E. Childress, T.Y. Cath, High recovery of concentrated RO brines using forward osmosis and membrane distillation, Journal of Membrane Science, 331 (2009) 31.

[14] C.M. Tun, A.G. Fane, J.T. Matheickal, R. Sheikholeslami, Membrane distillation crystallization of concentrated salts—flux and crystal formation, Journal of Membrane Science, 257 (2005) 144.

[15] M. Safavi, T. Mohammadi, High-salinity water desalination using VMD, Chemical Engineering Journal, 149 (2009) 191.

[16] X. Ji, E. Curcio, S. Alobaidani, G. Di Profio, E. Fontananova, E. Drioli, Membrane distillation-crystallization of seawater reverse osmosis brines, Separation and Purification Technology, 71 (2010) 76.

[17] G. Chen, Y. Lu, W.B. Krantz, R. Wang, A.G. Fane, Optimization of operating conditions for a continuous membrane distillation crystallization process with zero salty water discharge, Journal of Membrane Science, 450 (2014) 1.

[18] S. Meng, Y. Ye, J. Mansouri, V. Chen, Crystallization behavior of salts during membrane distillation with hydrophobic and superhydrophobic capillary membranes, Journal of Membrane Science, 473 (2015) 165.

[19] L.D. Tijing, Y.C. Woo, J.S. Choi, S. Lee, S.-H. Kim, H.K. Shon, Fouling and its control in membrane distillation-A review, Journal of Membrane Science, 475 (2015) 215.

[20] M. Essalhi, M. Khayet, Self-sustained webs of polyvinylidene fluoride electrospun nano-fibers: Effects of polymer concentration and desalination by direct contact membrane distillation, Journal of Membrane Science, (2013).

[21] M. Khayet, T. Matsuura, Membrane Distillation. Principles and Applications, Elsevier B.V., The Netherlands, 2011.

[22] M. Essalhi, M. Khayet, Self-sustained webs of polyvinylidene fluoride electrospun nanofibers at different electrospinning times: 1. Desalination by direct contact membrane distillation, Journal of Membrane Science, 433 (2013) 167.

[23] M. Essalhi, M. Khayet, Surface segregation of fluorinated modifying macromolecule for ydrophobic/hydrophilic membrane preparation and application in air gap and direct contact membrane distillation, Journal of Membrane Science, 417-418 (2012) 163.

[24] M. Courel, E. Tronel-Peyroz, G.M. Rios, M. Dornier, M. Reynes, The problem of membrane characterization for the process of osmotic distillation Desalination, 140 (2001) 15.

[25] M. Khayet, J. Mengual, G. Zakrzewska-Trznadel, Direct contact membrane distillation for nuclear desalination. Part I: Review of membranes used in membrane distillation and methods for their characterisation, International Journal of Nuclear Desalination, 1 (4) (2005) 435.

[26] A. El-Abbassi, A. Hafidi, M.C. García-Payo, M. Khayet, Concentration of olive mill wastewater by membrane distillation for polyphenols recovery, Desalination, 245 (2009) 670.

[27] L. Martínez, F.J. Florido-Díaz, A. Hernández, P. Prádanos, Characterisation of three hydrophobic porous membranes used in membrane distillation. Modelling and evaluation of their water vapour permeabilities, Journal of Membrane Science, 203 (2002) 15.

[28] L. Martínez, J.M. Rodríguez-Maroto, Membrane thickness reduction effects on direct contact membrane distillation performance, Journal of Membrane Science, 312 (2008) 143.

[29] T.V. Knyazkova, A.A. Maynarovich, Recognition of membrane fouling: testing of theoretical approaches with data on NF of salt solutions containing a low molecular weight surfactant as a foulant, Desalination, 126 (1999) 163.

[30] S.P. Pinho, E.A. Macedo, Solubility of NaCl, NaBr, and KCl in Water, Methanol, Ethanol, and Their Mixed Solvents, Journal of Chemical & Engineering Data, 50 (2004) 29.

[31] M. Gryta, Fouling in direct contact membrane distillation process, Journal of Membrane Science, 325 (2008) 383.

[32] E. Guillen-Burrieza, R. Thomas, B. Mansoor, D. Johnson, N. Hilal, H. Arafat, Effect of dry-out on the fouling of PVDF and PTFE membranes under conditions simulating intermittent seawater membrane distillation (SWMD), Journal of Membrane Science, 438 (2013) 126.

[33] M. Gryta, Influence of polypropylene membrane surface porosity on the performance of membrane distillation process, Journal of Membrane Science, 287 (2007) 67.

[34] A.M. Alklaibi, N. Lior, Membrane-distillation desalination: Status and potential, Desalination, 171 (2005) 111.

[35] M. Gryta, M. Tomaszewska, K. Karakulski, Wastewater treatment by membrane distillation, Desalination, 198 (2006) 67.

[36] K.W. Lawson, D.R. Lloyd, Membrane distillation, Journal of Membrane Science, 124 (1997) 1.

[37] K. Schneider, W. Hölz, R. Wollbeck, S. Ripperger, Membranes and modules for transmembrane distillation, Journal of Membrane Science, 39 (1988) 25.

[38] D.M. Warsinger, J. Swaminathan, E. Guillen-Burrieza, H.A. Arafat, J.H. Lienhard V, Scaling and fouling in membrane distillation for desalination applications: A review, Desalination, 356 (2015) 294.

[39] A.G. Fane, R.W. Schofield, C.J.D. Fell, The efficient use of energy in membrane distillation, Desalination, 64 (1987) 231.

[40] M. Qtaishat, T. Matsuura, B. Kruczek, M. Khayet, Heat and mass transfer analysis in direct contact membrane distillation, Desalination, 219 (2008) 272.

[41] Y. Zhang, Y. Peng, S. Ji, Z. Li, P. Chen, Review of thermal efficiency and heat recycling in membrane distillation processes, Desalination, 367 (2015) 223.

[42] H. Fan, Y. Peng, Application of PVDF membranes in desalination and comparison of the VMD and DCMD processes, Chemical Engineering Science, 79 (2012) 94.

[43] G.L. Liu, C. Zhu, C.S. Cheung, C.W. Leung, Theoretical and experimental studies on air gap membrane distillation, Heat and Mass Transfer, 34 (1998) 329.

[44] M. Gryta, Effectiveness of water desalination by membrane distillation process, Membranes, 2 (2012) 415.

3.2. Treatment of reverse osmosis brines: chemical pretreatments and direct contact membrane distillation

Different chemical pretreatment (CPT) strategies followed by direct contact membrane distillation (DCMD) process were adopted for the processing of reverse osmosis (RO) brine. CPT with Na_2CO_3 + NaOH allowed scale reduction, removing both permanent calcium hardness and temporary calcium hardness whereas CPT with $BaCl_2$ permitted to remove sulfate ions from RO brine. This last CPT was found to be the most efficient pretreatment improving the DCMD performance owing to the highest permeate flux, lowest permeate flux decline and best permeate quality. However, it is relatively an expensive pretreatment not recommended for consumption because of the toxic residual barium. The brine was concentrated up to 37 wt% of salts in water, which is above the limiting salt (NaCl) saturation concentration. Therefore, the volume of discharged RO brine can be reduced considerably facilitating its efficient management.

3.2.1. Introduction

Due to the exponential growth of the world population, seawater desalination has become a necessity to supply drinking water to certain areas. Reverse osmosis (RO) is currently the most used seawater desalination technology all over the world [1-3]. More than 50% of the worldwide installed desalination plants use RO technology because of its simplicity, a relatively low energy cost compared to other processes and its continuous advancement attributed to the use of novel membrane materials, design of improved membranes and modules, coupling with other processes and optimization studies reducing further the specific energy consumption and the cost of water production [3]. Nevertheless, RO cannot be used for the treatment of high saline concentration effluents (> 65 g/L) since the osmotic pressure increases considerably with the salt concentration (above 80 10^5 Pa) leading to a significant enhancement of the specific energy consumption.

However, the major drawback of RO is the management of the high volume of the produced brine. Untreated or improperly managed brines can result in adverse environmental effects, due to their high salinity, organic and inorganic contaminants [4]. In fact, RO desalination plants usually discharge the concentrated brine to the sea, contributing to the pollution of the marine environment. In this sense, two new lines for the management of brines, zero-liquid discharge (ZLD) [5] or near-ZLD (feed water recovery of 95–98%) and zero desalination discharge (ZDD) [6] can be considered. ZLD aims to avoid the liquid waste to the ocean while it generates saline solid products. In contrast, the ZDD usually reintroduces the liquid waste to the process or converts it into saline solids for raw material.

Research studies dealing with the treatment of emerging RO concentrate are needed in order to develop cost-effective methods to minimize the potential impacts on the environment as well as alternative strategies to extract available salts and to recover purified water. Several strategies have been adopted for the treatment technologies of RO brines and some review papers have been published in the last 7 years [4, 7-10]. Traditional disposal options for RO concentrate are surface water discharge, deep well injection and evaporation ponds [4, 11]. Membrane-based, thermal-based or emerging technologies are capable not only to reduce RO concentrate volume, but when they are combined ZLD can be achieved [12]. The selection of the best available technology for concentrate volume minimization depends mainly on the characteristics of RO concentrate, the treated water quality, energy consumption and costs [4, 9, 13]. Emerging technologies, such as electrodialysis (ED) [14, 15], forward osmosis (FO) [16-18], membrane distillation (MD) [19-23] or even its coupling with crystallization (MDC) [24, 25], and eutectic freeze crystallization (EFC) [26-28], have been developed recently to reduce RO concentrate volume with the objective to achieve ZLD and to recover some valuable compounds present in RO concentrate. However, these technologies are still under development and operational data on large-scale facilities are limited.

MD is considered an efficient alternative, either alone or combined with FO or MDC, in terms of increasing water production whilst minimizing the volume of the generated brines as much as possible [18, 19, 22, 25]. However, as it is well known, among other drawbacks of MD technology such as membrane pore wetting, it is limited by fouling and scaling phenomena [29-31]. Zhang, *et al.* [32] observed by means of scanning electron microscopy coupled with an energy dispersion spectroscopy (SEM-EDS) and inductively coupled plasma (ICP) analysis that permeate flux reduction during processing of seawater RO brine was firstly caused by precipitation of calcium carbonate ($CaCO_3$) and calcium sulfate ($CaSO_4$) due to their low solubility forming mixed crystal deposits on the membrane surface. The concentration of brine above the saturation point of salts resulted in the formation of crystals and the subsequent damage of the membrane [33, 34]. These crystals could modify the membrane structure breaking the membrane fibrils and allowing the passage of liquid brine through the membrane pores (i.e. wetting of the membrane pores) [31]. Therefore, it would be necessary to find an appropriate procedure for the pretreatment of RO brines avoiding high energy consumption and/or obstruction or deterioration of the MD membranes.

Chemical treatments have been demonstrated to be a viable method for salt recovery from RO brines by using different precipitants as sodium carbonate (Na_2CO_3) [7, 35], sodium hydroxide (NaOH) [36], or calcium hydroxide ($Ca(OH)_2$) [25]. Drioli, *et al.* [37] preformed a research study to recover $CaCO_3$, NaCl and $MgSO_4 \cdot 7H_2O$ from nanofiltration (NF) retentate using reactive precipitation by adding $NaHCO_3/Na_2CO_3$ aqueous solutions to the NF retentate. Ca^{2+} ions were precipitated as carbonates, which causes the reduction

of SO_4^{2-} content in the solution, limiting the recovery of magnesium sulfate. Calcium and magnesium by-products recovery from an RO brine was carried out by Casas *et al.* [36] using Na_2CO_3 and NaOH precipitants at 25ºC and 65ºC. Ji *et al.* [25] used lime/soda ash ($Ca(OH)_2$/ NaOH) softening to the RO concentrate in order to reduce calcium and magnesium hardness and limit scaling problems in MDC process. Qu *et al.* [38] could control calcium scaling by accelerated precipitation softening (APS) prior direct contact membrane distillation (DCMD) process of the RO brine. The APS process involved pH adjustment with sodium hydroxide along with calcite seeding, followed by microfiltration (MF) to avoid seeds clogging of the DCMD module.

In this paper, different chemical pretreatments of seawater RO brine have been considered prior MD application in order to increase the water production rate and minimize the volume of RO brine. The treated RO brine has a concentration of 55 g/L total dissolved solids (TDS) being the most abundant salt the NaCl. The first step consisted on chemical pretreatments of RO brine in order to remove permanent calcium hardness, temporary calcium hardness and/or to reduce sulfates. These chemical pretreatments do not require solvents and/or inert dispersion agents, which prevent nucleation and crystal growth and minimize, as far as possible, the risk of incrustation formation on the membrane surface. Once the RO brine has been treated, the precipitates were removed by filtration techniques. The second step consisted on the application of DCMD at a temperature below the boiling point of the RO brine using two membranes with different mean pore sizes.

3.2.2. Material and methods

3.2.2.1. RO brine composition

The treated RO brine was supplied by the company Abengoa Water S.L.U. and corresponds to the brine discharged by a RO desalination plant located in Almería (Spain). The RO brine composition was determined in the *Geochemical and Environmental Analysis Lab* of the University Complutense of Madrid (UCM), by using different techniques: ionic Ionic Chromatography (IC) for the determination of chlorides and sulfates; potentiometry to measure the alkalinity; Atomic Emission Spectrometry with Inductively Coupled Plasma (ICP-AES) to determine the concentration of Ca, Mg, Na, Si ions; and UV-Vis Spectrometry to determine the anionic detergents following the methylene blue active substances (MBAS) method. The obtained concentrations of the different components present in the RO brine are summarized in Table 3.2.1.

In order to characterize the non-volatile solutes of the RO brine, a semi-quantitative X-Ray diffraction analysis (XRD) was employed using a diffractometer X'Pert-MPD (Philips) at a wavelength of the Cu Kα (λ = 1.54 Å). The scanning range was varied from 5° to 70° in steps of 0.4°, with a scanning speed of 1 step/s. The operating conditions were 45 kV and 40 mA. The characterized solids were obtained once the liquid brine was

evaporated. The results are presented in Table 3.2.2. A majority of NaCl is observed (Halite, 66.7%), followed by magnesium chloride bi hydrate (Bischofite, 15.2%) and calcium sulfate (10.1%). Calcium carbonate ($CaCO_3$) is associated with magnesium forming Dolomite ($CaMg(CO_3)_2$) in less proportion. As it can be seen, in the used RO brine it was detected a major presence of sulfates than carbonates.

Among all salts present in the RO brines, both calcium sulfate ($CaSO_4$) and $CaCO_3$ are the less soluble salts. In addition, the solubility of these salts decreases with the increase of temperature, making it difficult for the treatment by DCMD. As it can be seen in Fig. 3.2.1, the solubility of $CaSO_4$ has a maximum value of 0,208g/100g solvent at 303 K [39], while $CaCO_3$ presents a maximum of 0,005g/100g solvent at 298 K [40].

Table 3.2.1. Concentration of the main components of the RO brine used in this study with the corresponding used techniques (IC: ionic chromatography; ICP-AES: atomic emission spectrometry with inductively coupled plasma; UV-Vis: UV-Vis spectrometry).

Component	Concentration	Technique
Cl^- (mg/L)	31150 ± 2400	IC
SO_4^{-2} (mg/L)	5264 ± 390	IC
Alkalinity (mg/L $CaCO_3$)	432 ± 39	Potentiometry
Ca (mg/L)	879 ± 53	ICP- AES
Mg (mg/L)	1864 ± 56	ICP- AES
Na (mg/L)	15270 ± 460	ICP- AES
Si (mg/L)	11 ± 1	ICP- AES
Anionic detergents (µg/L MBAS)	119 ± 7	UV-Vis
pH	7.9	pH meter
Total Dissolved Solids (TDS, g/L)	55.0 ± 2.5	

Table 3.2.2. Identification of the phases of the non-volatile solutes presents in the used RO brine by semi-quantitative analysis of the characteristic peaks obtained by X-ray diffraction (XRD) technique.

Compound name	Chemical formula	Factor (%)
Halite, syn	NaCl	66.7
Bischofite, syn	$MgCl_2$ - 6 H_2O	15.2
Calcium sulfate(VI)	$Ca(SO_4)$	10.1
Magnesium bis(sulfate(VI)) dihydroxide	$Mg_3(SO_4)_2$ $(OH)_2$	3.0
Thenardite, syn	Na_2SO_4	3.0
Dolomite	$CaMg(CO_3)_2$	2.0

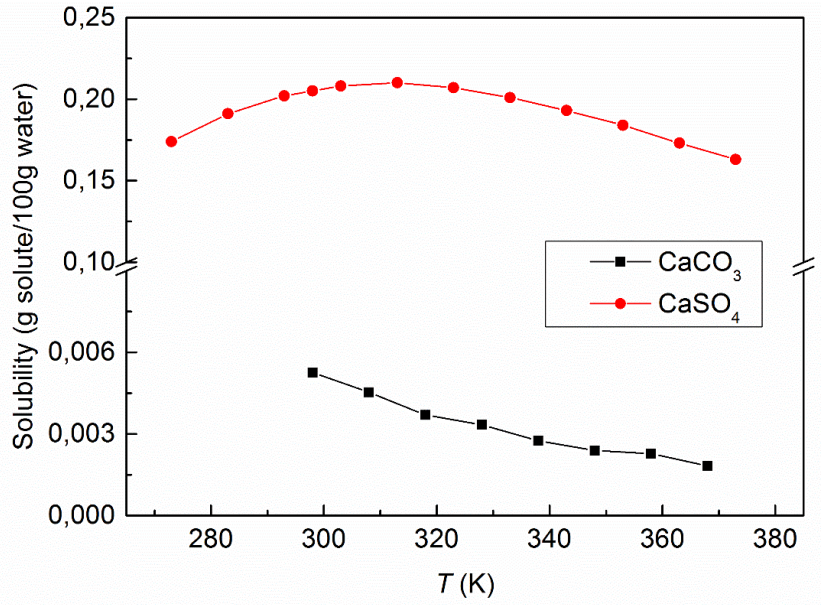

Figure 3.2.1. $CaCO_3$ and $CaSO_4$ solubility as a function of temperature [39, 40].

3.2.2.2. Chemical pretreatments of brine

Based on the chemical composition of the RO brine, a list of possible pretreatments was suggested to remove some type of salts before applying DCMD experiments. The proposed chemical pretreatments do not require the use of any solvents and/or inert dispersing agent for inhibiting the nucleation or crystal growth in order to minimize as much as possible the risk of fouling of the membranes used in the DCMD process. After salt(s) addition to the RO brine, in all cases a filtration process was carried out in order to separate the precipitate(s) from the RO brine before its treatment by DCMD. The precipitate(s) was analyzed after drying by means of XRD to determine its composition. The followings are the considered CPTs:

CPT-1: Sodium hydroxide (NaOH) is added to remove the "temporary calcium hardness", also known as "carbonate calcium hardness" and to neutralize the carbonic acid. The aim of this CPT is to remove the carbonic species present in the RO brine that may react with the calcium ions also present in the RO brine to form calcium carbonate ($CaCO_3$). This pretreatment may be useful for treating brines with a high carbonic species content and low calcium content. The involved reaction is the following:

$$CO_3^{2-} + NaOH \rightarrow Na_2CO_3 + 2OH^- \quad (3.2.1)$$

Taking into account the stoichiometry and the brine composition, 0.4g of NaOH per liter of solution is needed. The reaction was carried out for 45-60 minutes under stirring. Then, the obtained solution was filtered through a glass microfibers filter, supplied by Fisherbrand™, having a mean pore size of 1 µm.

CPT-2: This is a simple pretreatment consisting on the addition of Na_2CO_3. The "permanent calcium hardness" or "non-carbonate hardness" is associated with the presence of anions like sulfates. The Na_2CO_3 can react with the sulfates ions that form $CaSO_4$. This reaction is easier at high temperatures (from 323 to 353 K approximately). Therefore, the process requires heating the solution during stirring. This treatment may be useful for RO brines with high alkalinity and low carbonic species content. In order to remove completely calcium, an excess of sodium carbonate over the stoichiometry would be required (20-30%). The excess amount will depend on the ionic force and the pH of the RO brine to be treated.

CPT-3: This pretreatment consists in the addition of NaOH and Na_2CO_3. Specifically, NaOH is added to neutralize the carbonic acid and to remove the carbonate calcium hardness, as in CPT-1. The NaOH also contributes to increase the pH of the solution to a basic value (over 9) to favor the precipitation of Ca^{2+} when the Na_2CO_3 is added. The Na_2CO_3 is needed to react with sulfates and form $CaSO_4$ removing the non-carbonate calcium hardness. In this way, both types of hardness can be removed. Two chemical reactions take place in this case:

$$2Ca^{2+} + 2HCO_3^- + 2\,NaOH \rightarrow 2CaCO_3(s) + 2Na^+ + 2H_2O \quad (3.2.2)$$

$$Ca^{2+} + \left[\frac{SO_4^{2-}}{2Cl^-}\right] + Na_2CO_3 \rightarrow CaCO_3(s) + 2Na^+ + \left[\frac{SO_4^{2-}}{2Cl^-}\right] \quad (3.2.3)$$

Taking into account the stoichiometry of the reactions and the brine composition, the quantities needed for NaOH and Na_2CO_3 are 0.4 and 2.5 g/L of brine, respectively. Similar to CPT-1, before filtration, the reaction was performed by stirring the solution 45-60 min.

CPT-4: After observing the precipitation of $CaCO_3$ particles during DCMD process at high feed temperatures (i.e. > 348K), the CPT-4 pretreatment was proposed. This consists on heating the solution during stirring, in order to promote the precipitation of residual $CaCO_3$ at high temperature, since the solubility of this crystalline phase decreases with temperature. In this case, the selected temperature is the same as that of the feed solution used in DCMD experiment. The procedure is the same as that followed in CPT-3, but here during stirring the temperature was increased, at least, to 348 K. In this way, it can be assumed than all Ca^{2+} ions precipitate during the pretreatment step.

CPT-5: Other strategy to remove sulfates consists in the addition of barium chloride ($BaCl_2$) to produce insoluble barium sulfate ($BaSO_4$), according to the following reactions:

$$CaSO_4 + BaCl_2 \rightarrow BaSO_4(s) + CaCl_2 \quad (3.2.4)$$

$Na_2SO_4 + BaCl_2 \rightarrow BaSO_4(s) + 2NaCl$ (3.2.5)

In accordance with the stoichiometry of the reaction and brine composition, 9 g of $BaCl_2$ per liter of brine should be added. To prevent the $BaCl_2$ precipitation, the pH must be decreased to 5 using a buffer solution of hydrochloric acid (HCl). The system must react during 45-60 min under stirring conditions followed by filtration. Two different pH values of pretreated brine were used in these experiments, 5 and 9, to study the pH effect.

3.2.2.3. Membranes used in DCMD

Two commercial polytetrafluoroethylene (PTFE) flat sheet membranes (TF200 and TF450, Pall Corporation) supported by a polypropylene (PP) net were used. Their characteristics were determined by different characterization methods as described elsewhere [31, 41-43]. Both membranes exhibit practically the same porosity value, (78 ± 4 % for TF200 and 78 ± 6 % for TF450), similar water contact angle values (140 ± 3º for TF200 and 141 ± 1º for TF450), lower thickness for the membrane TF450 (98 ± 6 μm) compared to 107 ± 6 μm for TF200, different mean pore sizes (329 ± 18 nm for TF200 and 553 ± 4 nm for TF450) and different liquid entry pressure (*LEP*) values (290 ± 10 kPa for TF200 and 150 ± 10 kPa for TF450).

In this study, the top and bottom membrane surfaces (i.e. PTFE layer and PP support layer) as well as the membrane cross-section were examined by a Field Emission Scanning Electron Microscopy (FESEM), model JEOL 6335F. The samples were first fractured in liquid nitrogen and then placed over a support and coated with gold under vacuum conditions. X-ray Energy Dispersive Spectroscopy (EDS) was considered to determine the elemental composition of salt crystals at the PTFE membrane surfaces.

3.2.2.4. DCMD experiments

The DCMD experimental setup is schematized in Fig. 3.2.2. The membrane is placed in the middle of a plate and frame membrane module prepared for DCMD configuration (Millipore, Minitan^{TM} System). This consists of two chambers, one for the feed solution and the other one for the permeate. The effective membrane area is (3.94 ± 0.03) 10^{-3} m^2. The setup has two symmetric circuits, a hot feed circuit and a cold permeate circuit. The hot is circulated tangentially to the PTFE layer of the membrane surface by means of a peristaltic pump (Cole Parmer Masterflex easy-load model 7529-20). A Lauda K20 KS thermostat is required to heat up the feed solution through a glass heat exchanger. The brine is also heated up through a double wall feed tank (2000 ± 10 mL), connected to the heater. The permeate solution (i.e. distilled water) is maintained at 298 K by a chiller (PolyScience) connected to the double wall permeate tank (2000 ± 10 mL) and to a heat

exchanger. All temperatures at the inlets and outlets of the membrane module are measured by Pt100 sensors connected to a Fluke Hydra digital multimeter. The permeate is also circulated tangentially to the PP membrane support, by another peristaltic pump, in counter current regime with respect to the feed solution. The feed and the permeate flow rates are 31 and 36 L/h, respectively. Both feed and permeate flows are measured by flowmeters Tecfluid with an accuracy of ± 5 L/h. In order to prevent the membrane pores wetting, the hydrostatic pressure was controlled by a manometer Wika, having an accuracy of ± 0.2 10^5 Pa, placed at the entrance of the feed membrane module. To minimize heat losses, all the pipes of the circuit, the heat exchangers, the membrane module and the feed and permeate tanks were insulated. The variation of the permeate with time permits to calculate the permeate flux (J) as follows:

$$J = \frac{\Delta V_p}{S \times \Delta t} \tag{3.2.6}$$

where ΔV_p is the increase of the permeate tank volume in the interval of time Δt, while S is the effective membrane area.

To measure the concentration of feed and permeate solutions, a 712 Ω Metrohm electrical conductivity meter was employed and the data were obtained with a reference to a temperature of 298 K. A previous calibration curve was obtained by drying and then weighing brine samples subjected to different evaporation times in order to get the total dissolved solids (TDS) as a function of the electrical conductivity. It is necessary to take into account that the different applied chemical pretreatments to the brine resulted in different salts precipitation. Therefore, different calibration curves were needed depending on the type of the considered chemical pretreatment.

The brine rejection factor (α) was determined as follows:

$$\alpha = \left(1 - \frac{C_p}{C_f}\right) \times 100 \tag{3.2.7}$$

where C_p and C_f are the permeate and feed brine concentrations (in TDS), respectively.

A brine concentration factor (β) was defined as follows:

$$\beta = \left(\frac{C_{f,f}}{C_{f,0}}\right) \tag{3.2.8}$$

where $C_{f,f}$ and $C_{f,0}$ are the brine concentrations at the end and the beginning of the DCMD experiment, respectively. Provided that the necessary DCMD tests were carried out during

different times, an effective concentration factor (β_{ef}) of 6 hours, which corresponds to the shorter duration of the DCMD experiment, was adopted as follows:

$$\beta_{ef} = \left(\frac{\beta}{t}\right) \times 6 \tag{3.2.9}$$

where t is the total duration of the experiment in hours. In this way, different DCMD experiments can be compared despite their different durations.

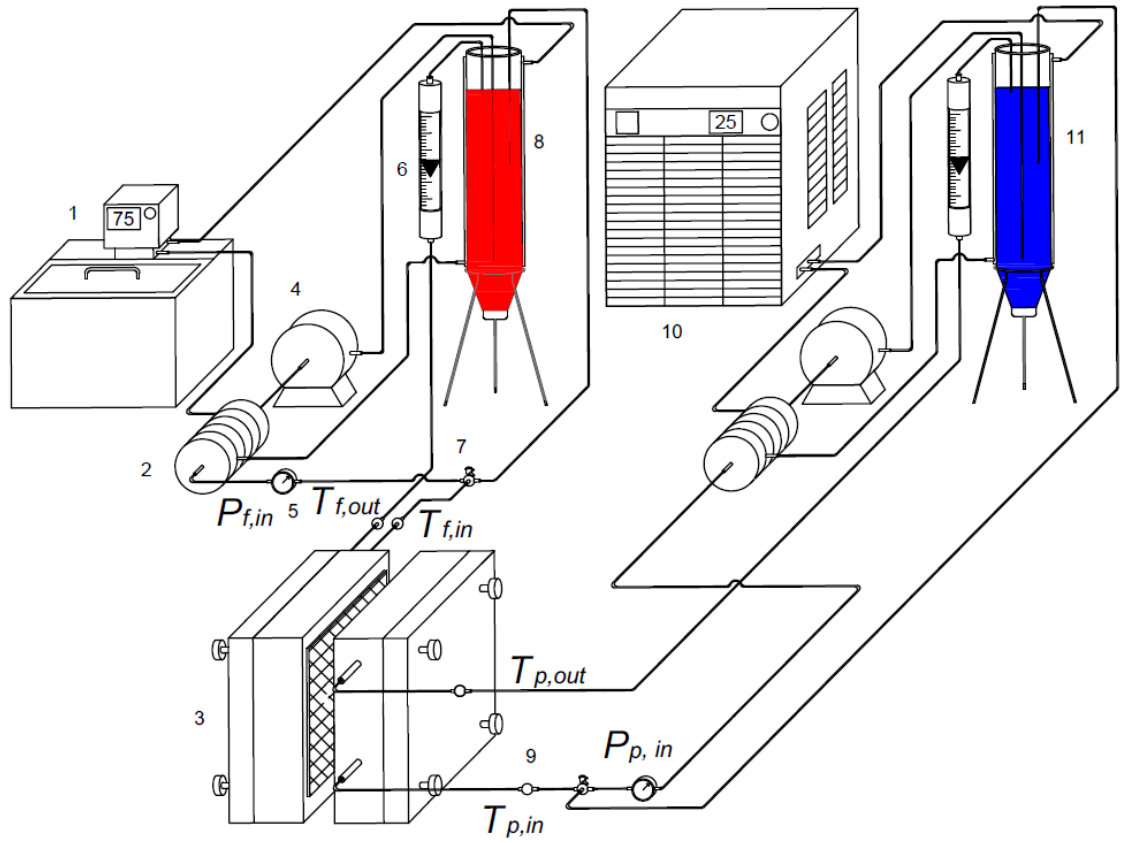

Figure 3.2.2. DCMD experimental setup: 1.- thermostat, 2.- heat exchanger, 3.- membrane module, 4.- peristaltic pump, 5.- pressure sensor, 6.- flowmeter, 7.- 3-way valve, 8.- feed tank, 9.- temperature sensor (PT-100 probes), 10.- chiller, 11.- permeate tank.

3.2.3. Results and discussion

3.2.3.1. DCMD test without chemical pretreatment

Various DCMD tests at different feed temperatures, in the range 318-348 K, were carried out to evaluate the DCMD performance when using RO brine directly without any pretreatment, keeping constant the permeate temperature at 298 K. Figs. 3.2.3 and 3.2.4 show the obtained results in terms of the permeate flux, feed and permeate concentrations together with the separation factor of the two membranes TF200 and TF450, respectively.

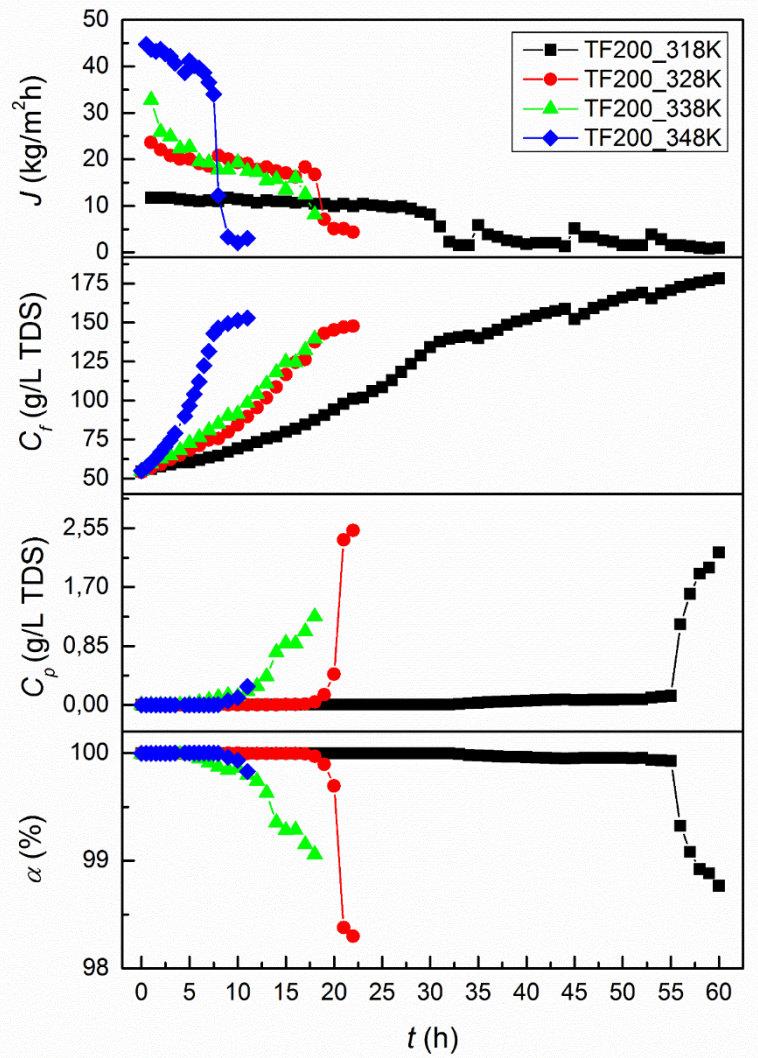

Figure 3.2.3. Permeate flux, feed and permeate concentrations and separation factor as a function of DCMD operating time at different feed inlet temperatures for the membrane TF200 using RO brine without any CPT as feed solution. T_p = 298K; Q_f = 31 L/h; Q_p = 36 L/h.

As it was expected, a higher feed temperature together with a higher pore size (TF450 membrane) contributed to achieve a higher permeate flux. Therefore, among all tested feed temperatures, the results of the initial permeate flux when using the feed temperature 348 K were the highest (i.e. 44.7 ± 0.3 and 50.3 ± 0.4 kg/m^{2}h, for the TF200 and TF450 membranes, respectively).

For both membranes, the brine concentration increased during all DCMD tests. As it can be seen in Figs. 3.2.3 and 3.2.4, the higher is the permeate flux, the higher is the brine concentration slope. It seems to be a limit of the maximum brine concentration, between 150 and 170 g/L TDS, which corresponds to an increase in the permeate concentration due to the membrane pore wetting. The final values of the brine concentration at 348 K feed temperature were 152.9 and 136.3 g/L TDS, for the membranes TF200 and TF450 respectively. These values were exceeded by those obtained when the feed temperature was

318 K. The total duration of the DCMD tests explained this result. The experiments at 348 K feed temperature lasted around 11 hours for both membranes while the total duration at 318 K feed temperature, were 32 and 60 hours for TF200 and TF450 membranes, respectively.

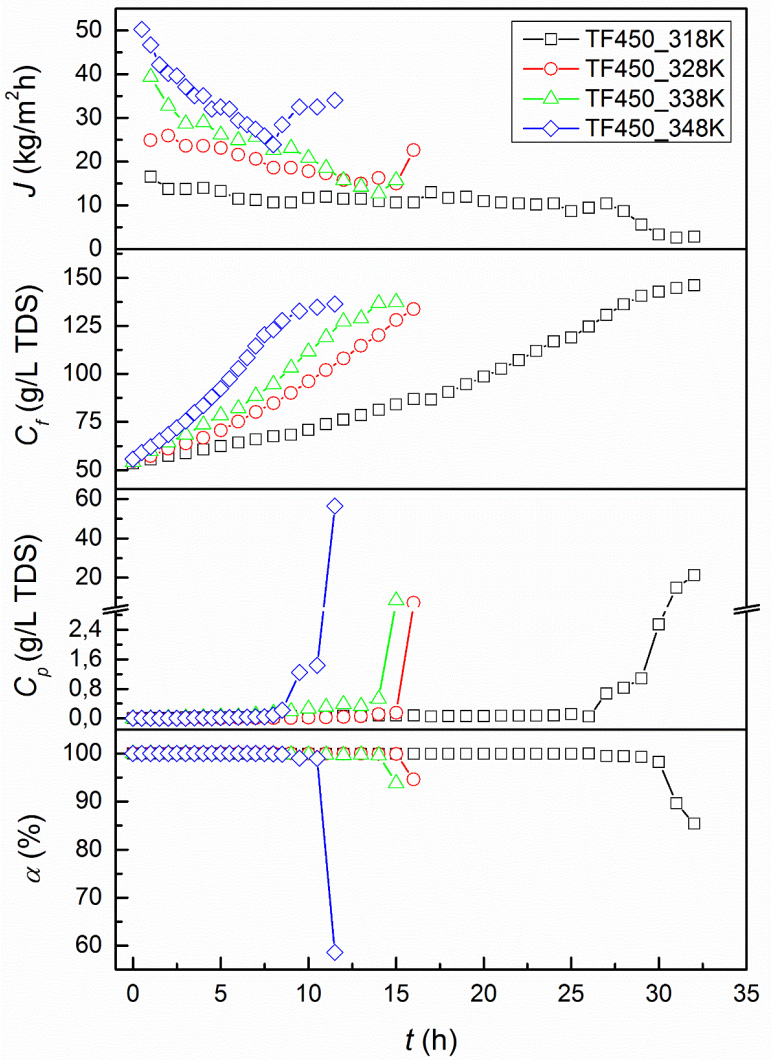

Figure 3.2.4. Permeate flux, feed and permeate concentrations and separation factor as a function of DCMD operating time at different feed inlet temperatures for the membrane TF450 using RO brine without any CPT as feed solution. T_p = 298K; Q_f = 31 L/h; Q_p = 36 L/h.

The study of the effective brine concentration factor (β_{ef}) indicated low value for both membranes at 318 K feed temperature (i.e. 0.3 and 0.2 for TF200 and TF450 membranes, respectively). When the temperature was 348 K, β_{ef} values were higher (i.e. 1.4 and 1.2 for TF200 and TF450 membranes respectively). Both the final brine concentration and the DCMD operating time affected their calculation and should be taken into account.

Because of the chemical composition of the RO brine, as it was already explained, some salts precipitated in crystal form, especially as $CaSO_4$ and $CaCO_3$ crystals, which are

the less soluble salts, when the RO brine TDS was increased. This salt precipitation contributed to form a fouling layer during the DCMD test, blocking the membrane pores if their size is relatively small or penetrating in them if the pore size is big. It is to point out that fouling reduced the permeate flux significantly when using membranes with small pore size. The higher permeate flux decline due to pore blocking was observed for the TF200 membrane at 348 K feed temperature (from 44.7 ± 0.3 to 3.0 ± 0.1 kg/m^{2}h, i.e. a reduction of 93.2%). For the same feed temperature, the permeate flux decline was lower when using the TF450 membrane due its greater pore size (i.e. from 50.3 ± 0.4 to 23.9 ± 0.2 kg/m^{2}h after 8 hours, i.e. a reduction of 52.5%). Membrane fouling due to salt deposition also caused a reduction of the hydrophobicity of the membrane active layer resulting in a significant increase of the permeate concentration and a decrease of the separation factor (α), as shown in Figs. 3.2.3 and 3.2.4. Therefore, it is worthy to note that wetting of the membrane pores occurred in both tested membranes. The increase of the permeate concentration is more evident in the TF450 membrane due to its bigger pore size and lower *LEP* value. As the permeate concentration was increased, α was decreased. These effects were investigated in previous studies and were confirmed in the present study before applying the necessary CPTs [29, 44-46].

A semi-quantitative analysis using X-ray diffraction (XRD) of the solids deposited on both the feed and permeate sides of the membrane permitted to figure out that practically all the salt crystals were $CaSO_4$ (98%) and NaCl (2%) and both salts were detected also on the permeate side of the membrane. Fig. 3.2.5 shows the FESEM images of the PTFE layer as well as the support layer (PP) and cross-section of both TF200 and TF450 membranes after their use in DCMD process. As can be seen in Fig. 3.2.5, the salt crystals form a compact cake on the PTFE membrane surface and, as confirmed by the EDS qualitative analysis, this is composed mainly by calcium, carbon and sulfur in a complete agreement with the obtained results from XRD. Zhang *et al.* [32] also observed by SEM-EDS and ICP analysis that $CaCO_3$ and $CaSO_4$ formed mixed crystal deposits on the membrane surface.

The retentate and permeate of the DCMD experiment at 348 K were also analyzed by IC, ICP-AES, potentiometry and UV-Vis spectrometry and the obtained results are summarized in Table 3.2.3.

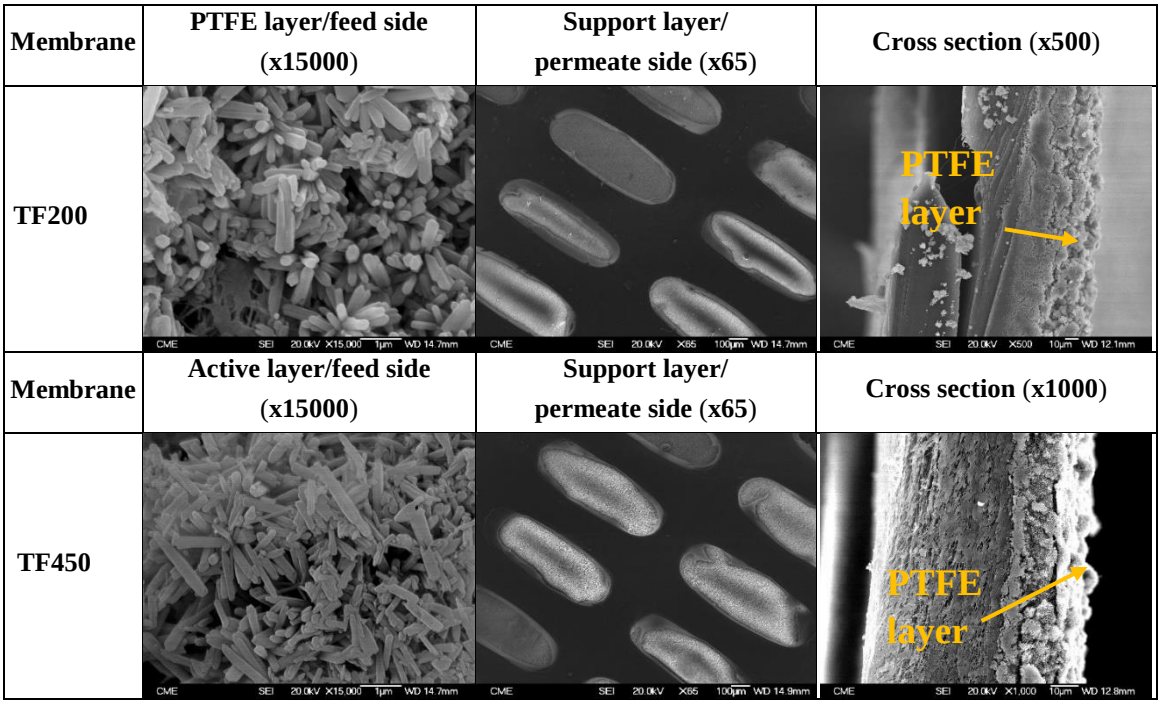

Figure 3.2.5. FESEM images of the PTFE layer, support layer and cross-section of the TF200 and TF450 membranes used in DCMD at different magnifications. Feed solution: RO brine. T_f = 348 K; T_p = 298 K; Q_f = 31 L/h; Q_p = 36 L/h.

Table 3.2.3. Analytical results of the retentate and permeate composition of the DCMD experiment carried out with RO brine at T_f = 348 K without any CPT for the TF200 membrane.

Component	Retentate brine	Permeate brine
Cl^- (mg/L)	94300 ± 7300	0.63 ± 0.05
SO_4^{-2} (mg/L)	11430 ± 850	< 4
Alkalinity (mg/L $CaCO_3$)	88 ± 8	< 20
Ca (mg/L)	1213 ± 73	0.30 ± 0.03
Mg (mg/L)	4650 ± 140	< 0.02
Na (mg/L)	37800 ± 1100	< 0.1
Si (mg/L)	21 ± 2	0.58 ± 0.06
Anionic detergents (µg/L MBAS)	349 ± 19	50 ± 3

As it was expected, the permeate reveals a very small presence of the components present in the used RO brine. Anionic detergents were the brine components that most passed through the membrane pores (i.e. 50 µg/L compared to 349 µg/L present in the retentate, which represents a separation factor of only 85.7%). This is due to the fact that detergents have low surface tension values and wet easily hydrophobic porous membranes. The concentration factor of each brine component varied between 3 for chlorine ion and 1.4 for calcium. It is worth noting that the alkalinity of the retentate is lower than that of the RO brine die to the $CaCO_3$ precipitation at high temperatures.

The low DCMD performance achieved for both membranes, together with the presence of salts deposited in both sides of the membranes at the end of the DCMD experiments indicated that it is mandatory to apply pretreatments of RO brines before performing DCMD. As it was already described, compared to other low feed temperatures applied, a feed temperature of 348 K showed better results in terms of higher permeate fluxes and higher final brine concentration. Consequently, this feed temperate was selected to carry out the experiments with the chemical pre-treated brines.

3.2.3.2. CPT-1: addition of NaOH

The used RO brine has a pH value of 7.9 (see Table 3.2.1). With the addition of NaOH the brine pH was increased to 9.4. After filtration, according to the XRD results the precipitated components revealed that around 87.9% was $CaCO_3$, 4% was NaCl and 8.1% was calcite magnesium, $Mg_{0.03}Ca_{0.97}(CO_3)$. This indicated that CPT-1 was able to reduce $CaCO_3$ precipitation inside the membrane module. Despite the fact that the DCMD performance was enhanced when NaOH was added to the RO brine, especially in terms of a higher initial permeate flux, a higher final brine concentration and a lower permeate flux decline with DCMD operating time, the pore blocking and even the pore wetting effects persisted (see Figs. 3.2.6-3.2.9 and Table 3.2.4). The initial permeate flux of the membrane TF200 was 13.6% higher than that obtained without CPT, but it was also reduced significantly with time (i.e. 72.6% compared to 93% obtained without CPT, see Table 3.2.4). After 9 hours of DCMD operation (CPT-1), the initial permeate flux decreased from 50.8 ± 0.7 kg/m^{2}h to 13.9 ± 0.2 kg/m^{2}h. As it can be seen in Fig. 3.2.6, a slight increase of the permeate flux was detected at the ninth hour, indicating pore wetting due to foulants precipitation. The increase of the corresponding permeate concentration will be discussed later on.

For the membrane TF450, the initial permeate flux was also higher than that obtained without CPT (i.e. a 21% higher, see Fig. 3.2.6 and Table 3.2.4). However, 60.8% permeate flux decline was observed at the seventh hour of DCMD experiment, and after that, a sharp increase of the permeate flux was registered (i.e. 139.5 ± 2.3 kg/m^{2}h, see Fig. 3.2.6 and Table 3.2.4) due to pore wetting phenomenon.

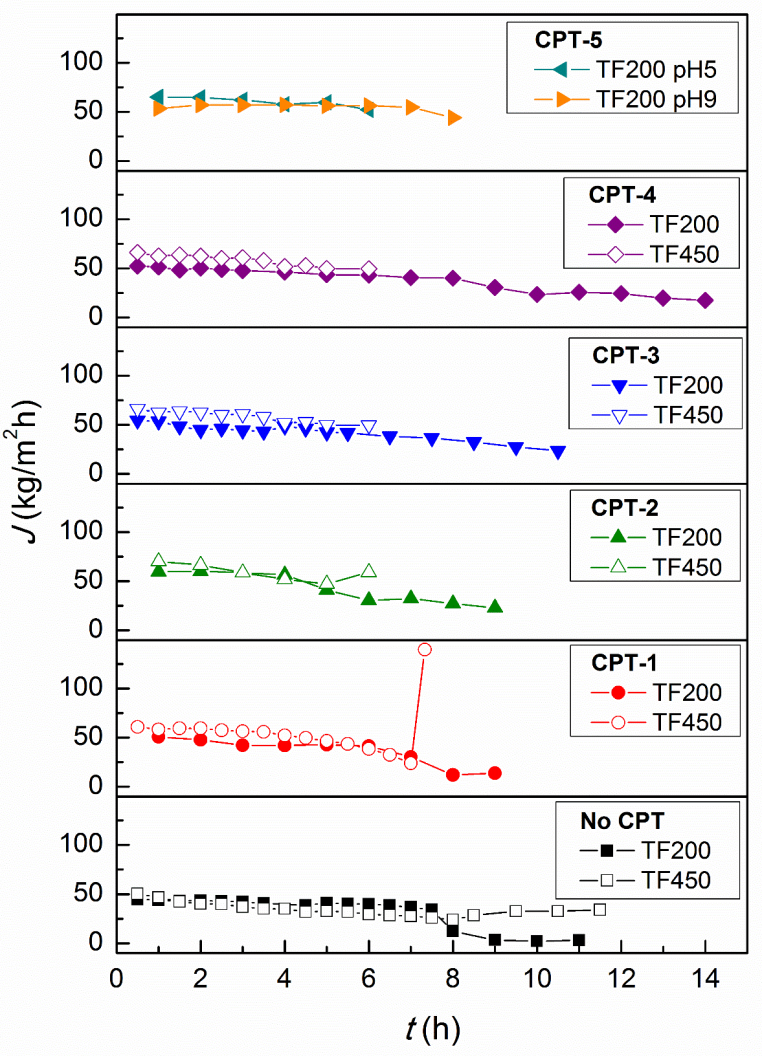

Figure 3.2.6. Change of the permeate flux with DCMD operating time when using TF200 and TF450 membranes for the treatment of RO brine applied as a feed solution without CPT and with different CPTs as feed solution. T_f = 348 K; T_p = 298 K; Q_f = 31 L/h; Q_p = 36 L/h.

Compared to the membrane TF200, the slope of the brine concentration was slightly higher for the membrane TF450 due to its higher permeate flux, as can be seen in Fig. 3.2.7. Consequently, the membrane TF450 was able to concentrate the RO brine up to 190 g/L TDS, whereas for the membrane TF200 the final RO brine concentration was lower, 164 g/L of TDS (see Table 3.2.4). In both cases, the final value of the brine concentration was higher than that achieved without CPT (i.e. 153 and 136 g/L of TDS for the TF200 and TF450 membranes, respectively). As it was expected, the values of β_{ef} were greater than those corresponding to the same DCMD test but without CPT (i.e. 1.8 h^{-1} for the TF200 membrane and 2.6 h^{-1} for the TF450 membrane, due to the higher final brine concentration obtained when using the membrane TF450, see Table 3.2.4). Moreover, the permeate concentration (Fig. 3.2.8) was maintained low for both membranes with good values in

terms of water quality until the pore wetting was occurred. Therefore, at the end of the DCMD experiments, the separation factor was decreased (Fig. 3.2.9).

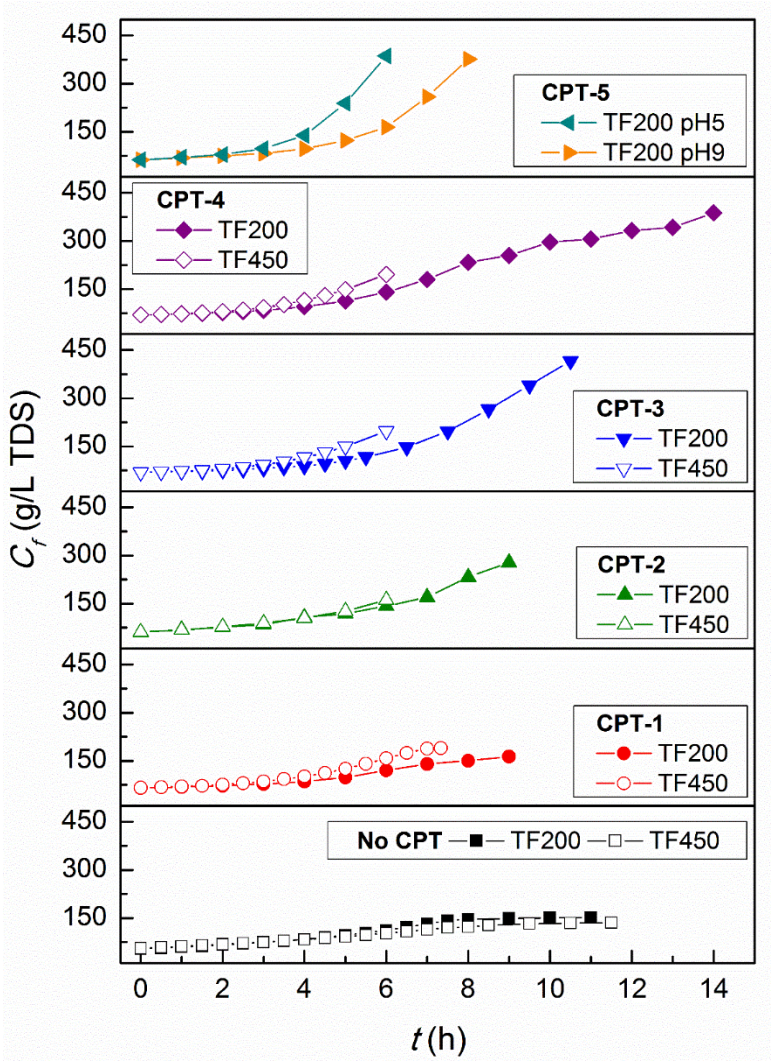

Figure 3.2.7. Concentration of RO feed brine with the operating DCMD time when using TF200 and TF450 membranes for the treatment of RO brine applied as a feed solution without CPT and with different CPTs as feed solution. T_f = 348 K; T_p = 298 K; Q_f = 31 L/h; Q_p = 36 L/h.

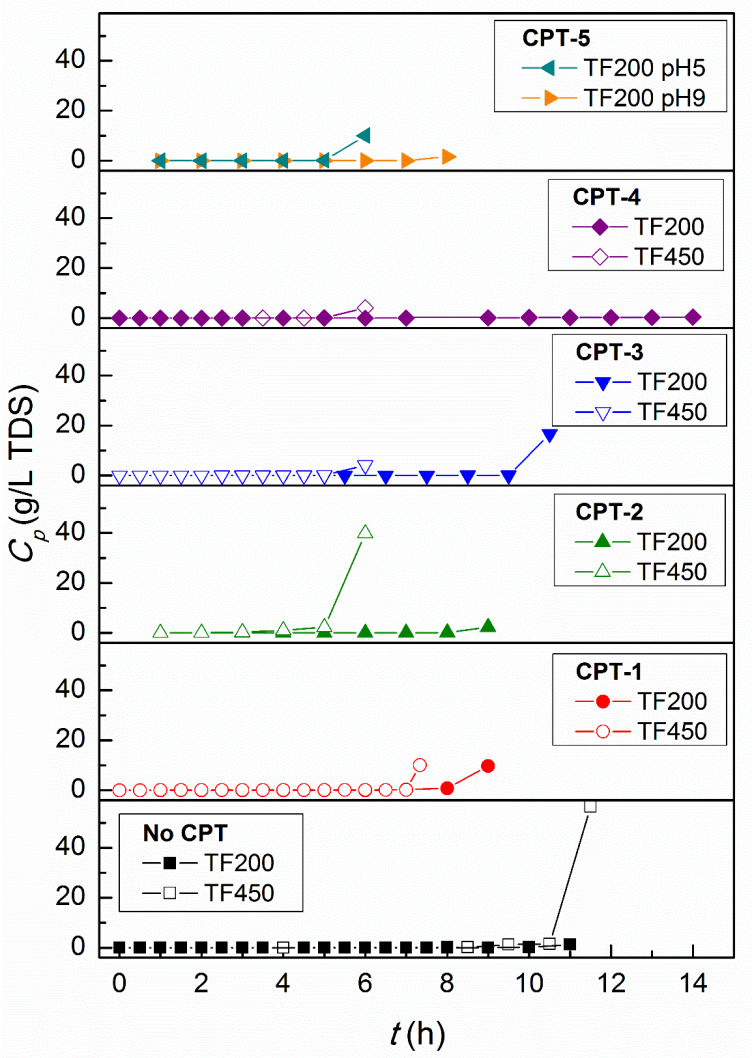

Figure 3.2.8. Change of the permeate concentration with DCMD operating time when using TF200 and TF450 membranes for the treatment of RO brine applied as a feed solution without CPT and with different CPTs. T_f = 348 K; T_p = 298 K; Q_f = 31 L/h; Q_p = 36 L/h.

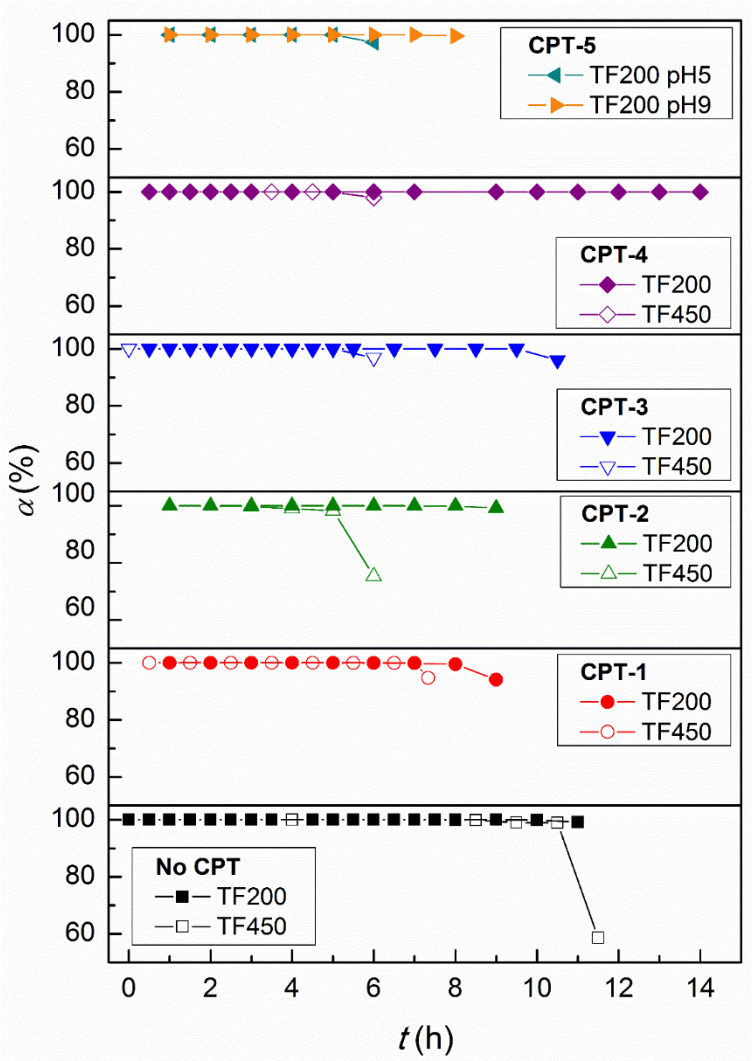

Figure 3.2.9. Change of the separation factor with DCMD operating time when using TF200 and TF450 membranes for the treatment of RO brine applied as a feed solution without CPT and with different CPTs. T_f = 348 K; T_p = 298 K; Q_f = 31 L/h; Q_p = 36 L/h.

Taking into account the above-mentioned results, CPT-1 does not seem to be a good option due to the small improvement observed for the RO brine concentration by DCMD process that was much lower than the expected value, about 300 g/L TDS, which would allow NaCl to precipitate.

Table 3.2.4. DCMD results obtained for both the TF200 and TF450 membranes without CPT and with the different CPTs used in this study (t: time of the DCMD experiment; J_0: initial permeate flux; J_{final}: final permeate flux; $C_{f,max}$: maximum brine concentration; β: concentration factor (Eq. 3.2.8); β_{ef}: effective concentration factor (Eq. 3.2.9) and α_{final}: final separation factor).

Membrane	Variables	Without CPT	CPT-1	CPT-2	CPT-3	CPT-4	CPT-5 pH5	CPT-5 pH9
TF200	*t*	11	9	9	10.5	14	6	8
	pH	8.3	9.4	8.4	9.7	9.4	5	9
	J_0 (kg/m^{2}h)	44.7 ± 0.3	50.8 ± 0.7	59.7 ± 0.5	54.4 ± 0.6	52.3 ± 0.6	65.2 ± 0.5	53.6 ± 0.4
	J_{final} (kg/m^{2}h)	3.0 ± 0.1	13.9 ± 0.2	23.0 ± 0.2	23.6 ± 0.2	17.5 ± 0.1	52.3 ± 0.4	44.3 ± 0.4
	$C_{f,max}$ (g/L TDS)	153	164	278	416	388	387	377
	β_{ef} (h^{-1})	1.4	1.8	3.1	4.0	2.8	6.4	4.7
	α_{final} (%)	99.2	94.5	99.1	96.0	99.9	97.4	99.6
TF450	*t*	11.5	7.3	6	6	6	-	-
	pH	8.3	9.4	8.4	9.7	9.4	-	-
	J_0 (kg/m^{2}h)	50.3 ± 0.4	61.0 ± 0.9	70.0 ± 0.6	66.0 ± 0.5	66.1 ± 0.7	-	-
	J_{final} (kg/m^{2}h)	34.0 ± 0.2	139.5 ± 2.1	59.2 ± 0.5	49.5 ± 0.8	49.5 ± 0.4	-	-
	$C_{f,max}$ (g/L TDS)	136	190	161	197	196	-	-
	β_{ef} (h^{-1})	1.2	2.6	2.7	3.3	3.3	-	-
	α_{final} (%)	58.6	94.7	75.4	96.7	97.9	-	-

3.2.3.3. CPT-2: addition of Na_2CO_3

As it was explained previously, the Na_2CO_3 reacts with sulfates ions to form $CaSO_4$, removing therefore the permanent calcium hardness. The pH of the used brine after this CPT was 8.4. Compared with CPT-1, an enhancement of the initial permeate fluxes was detected for both membranes (i.e. about 15% in the both cases as it can be seen in Table 3.2.4). In the DCMD test carried out with the membrane TF200, 61% of the permeate flux decline was observed (i.e. from 59.7 ± 0.5 kg/m^{2}h to 23.0 ± 0.1 kg/m^{2}h, see Table 3.2.4). This value is lower than the obtained one with CPT-1. For the membrane TF450, 33% permeate flux reduction was achieved (i.e. from 70.0 ± 0.6 kg/m^{2}h to 47.3 ± 0.4 kg/m^{2}h registered at the fifth hour of DCMD test) due to the higher pore size of this membrane. At the end of this experiment, the pore wetting effect due to brine crystals precipitation on the membrane and inside its pores appeared causing an increase of the permeate flux to 59.2 ± 0.5 kg/m^{2}h (see Fig. 3.2.6).

As can be seen in Fig. 3.2.7, similar to CPT-1, it is not possible to concentrate the RO brine over 300 g/L TDS with both membranes. The obtained values of the final brine concentration were 278 and 161 g/L of TDS, for the TF200 and TF450 membranes respectively (see Table 3.2.4). Despite the fact that the brine concentration slope was quite similar for both membranes, due the greater pore size of the membrane TF450, the feed solution penetrated easily inside the membrane pores due to crystallization fouling reducing therefore the necessary DCMD operating time to achieve the desired brine concentration.

By applying CPT-2, the obtained β_{ef} values were greater than those corresponding to CPT-1 (i.e. 3.1 h^{-1} and 2.7 h^{-1} for the TF200 and TF450 membranes, respectively). This result is attributed to the higher final brine concentration achieved using the membrane TF200 during a longer DCMD operating time. For the membrane TF450, the final brine concentration was lower than that achieved when applying CPT-1, but the DCMD operating time applied after CPT-2 was shorter.

As it was stated previously, pore wetting appeared at the end of the DCMD experiment performed with the membrane TF450. This increased the permeate concentration (Fig. 3.2.8) and reduced the separation factor (Fig. 3.2.9) from 99.9 to 75.3%. The membrane TF200 exhibited better DCMD performance with a final separation factor of 99.2%.

3.2.3.4. CPT-3: addition of $NaOH+Na_2CO_3$

With the addition of NaOH and Na_2CO_3 to the RO brine, the pH increased to 9.7. As occurred in the case of CPT-1 and due to the addition of NaOH to the brine, 88% of $CaCO_3$ and 12% of NaCl were found as precipitates according to the XRD analysis. The

addition of Na_2CO_3 contributed to the precipitation of $CaCO_3$ eliminating all calcium ions and preventing the formation of $CaSO_4$ as consequence. With the precipitation of the less soluble salts outside the membrane module, before carrying out the DCMD test, the final brine concentration was increased significantly (see Fig. 3.2.7 and Table 3.2.4).

The initial permeate fluxes were similar to those obtained when applying CPT-2. However, the percentage of the permeate flux decline was lower when applying CPT-3. Thus, only 57% was obtained for the membrane TF200 (i.e. a decrease from 54.4 ± 0.6 kg/m^{2}h to 23.6 ± 0.2 kg/m^{2}h) and 25% for the membrane TF450 (i.e. a decrease from 66.0 ± 0.5 kg/m^{2}h to 49.5 ± 0.8 kg/m^{2}h). The permeate flux reduction is higher for the membrane TF200 due to its larger duration of the DCMD test (i.e. 10.5 hours in comparison to 6 hours when using the membrane TF450, see Fig. 3.2.6) and to the easily pore blocking effect suffered by the membrane due to its smaller pore size.

A high final brine concentration was achieved when using the membrane TF200. It can be seen in Fig. 3.2.7 an increasing variation of the slope of the brine concentration with time when CPT-3 was used. The brine concentration was increased up to 416 g/L of TDS. This value is much higher than those obtained without CPT (153 g/L of TDS), with the CPT-1 (164 g/L of TDS) and with CPT-2 (278 g/L of TDS). This enhancement was reflected into a high β_{ef} value of 4.0. However, for the membrane TF450, CPT-3 improved only slightly the final brine concentration (i.e. 197 g/L of TDS) with respect to the previous CPTs (see Table 3.2.4). Thus, as it was expected from the final brine concentration, the obtained β_{ef} value for the membrane TF450, 3.3, was lower than that of TF200 membrane.

Despite the use of CPT-3, a complete elimination of calcium ion was not accomplished and salts (may be $CaSO_4$) continue precipitating on the membrane surface causing pore wetting, especially if the pore size is large (TF450 membrane). When pore wetting took place, the brine passed through the membrane pores to the permeate, as it can be seen in Fig. 3.2.8, increased the permeate concentration and reduced the separation factor (Fig. 3.2.9).

3.2.3.5. CPT-4: addition of $NaOH+Na_2CO_3$ at high temperature

Compared to the previous applied CPTs, with CPT-4 a higher salt precipitation prior DCMD test was obtained because the solubility of $CaCO_3$ and $CaSO_4$ decreased with temperature (see Fig. 3.2.1). The XRD analysis showed that the majority of the precipitated salts corresponded to NaCl (31.6%), followed by $CaSO_4$ (18.8%.), $CaCO_3$ (18.5%) Na_2CO_3 (17.3%) and Na_2SO_4 (13.9%). In this case, before carrying out DCMD process, more salt types were removed compared with the previous studied CPTs, including carbonates and sulfates. This contributed to reduce the amount of foulants and the subsequent scaling on the membrane surface, while the DCMD operating time was extended especially when

using the membrane TF200. However, neither a higher initial permeate flux nor a greater final brine concentration were achieved. For the TF200 membrane, the permeate flux decreased in 14 hours from 52.3 ± 0.6 kg/m^{2}h to 17.5 ± 0.1 kg/m^{2}h (i.e. a 67%) while the final brine concentration was increased up to 388 g/L of TDS (see Table 3.2.4). Thus, the β_{ef} value was 2.8 h^{-1}, which is lower than that obtained in CPT-3 due to the lower final brine concentration achieved. The performance of the membrane TF450 was very similar to that obtained for the same membrane when applying CPT-3. A permeate flux reduction of 25% (i.e. from 66.1 ± 0.7 kg/m^{2}h to 49.5 ± 0.4 kg/m^{2}h) was achieved. The final brine concentration was increased up to 196 g/L of TDS in 6 hours, being the β_{ef} value 3.3 h^{-1}. Nevertheless, the principal benefit of the application of CPT-4 is the good separation factor achieved. The membrane TF200 maintained a value of 99.9% for the separation factor during all the performed DCMD test and the membrane was also maintained in good conditions, unlike what happened with the same membrane subjected to the CPT-3 (Fig. 3.2.8). This was the best result collected in terms of the separation factor among all applied CPTs in this study. However, the membrane TF450 after the fifth hour of DCMD test was wetted increasing slightly the permeate concentration as can be seen in Fig. 3.2.8. This enhancement could be due to the fact that RO brine has anionic detergents that easily penetrates into the membrane pores of the TF450 membrane because of their low surface tension, favouring the wetting as consequence. According to the obtained DCMD results, heating and stirring the brine seems to be better than CPT-3.

3.2.3.6. CPT-5: addition of $BaCl_2$

$CaSO_4$ seems to be the most influential non-volatile solute in the final state of the MD membrane. Therefore, it is necessary to remove its involved ions before carrying out the DCMD test. The main objective of CPT-5 application is to remove SO_4^{2-} ions by precipitation in form of barium sulfate ($BaSO_4$) salt. To achieve it, $BaCl_2$ bi-hydrated was added to the RO brine and then tested at two different pH values, 5 and 9. The first pH value was the pH obtained after the addition of $BaCl_2$, while the pH 9 was achieved by adding a buffer solution of NaOH. Based on the XRD analysis performed after filtration, around 85% of $BaSO_4$ was precipitated in both cases.

The best initial permeate flux together the lowest permeate flux decline was obtained for the membrane TF200 when applying CPT-5 at pH 5 (i.e. the permeate flux was reduced from 65.2 ± 0.5 kg/m^{2}h to 52.3 ± 0.4 kg/m^{2}h after 6 hours, which is a reduction of 20%, see Table 3.2.4). At pH 9, the initial permeate flux was found to be lower but it was declined by only 17% in eight hours (i.e. from 53.6 ± 0.4 kg/m^{2}h to 44.3 ± 0.4 kg/m^{2}h). These results may be attributed to the different interactions between the membrane surface and the RO brine particles (i.e. attractive or repulsive electrostatic forces) depending on the pH effect [47]. As the isoelectric point of the PTFE membrane material is around 3.7 [48],

when the pH of the RO brine was 5 the membrane/particle electrostatic repulsive forces were lower than those at a pH value of 9. In addition, the contact angle of the membrane exhibited a minimum around this isoelectric point [49] and the surface tension of water showed a minimum in the same pH region [50]. Therefore, less separation took place at pH 5, which caused a greater initial permeate flux but a worse DCMD performance as shown in Figs. 3.2.6, 3.2.8 and 3.2.9.

Fig. 3.2.7 shows that, in both cases, the final brine concentration surpasses clearly the limit of 300 g/L TDS (i.e. 387 and 377 g/L TDS, for pH 5 and pH 9, respectively, as shown in Table 3.2.4). Therefore, it seems that the final brine concentration does not depend on the pH value. A higher permeate flux at acid pH permits to achieve early the maximum brine concentration. However, when working under acidic pH the membrane was finally wetted reducing the separation factor value to 97.4% (Table 3.2.4). In the case of pH 9, the wetting of the membrane pores was also occurred, but later and to a lesser extent, decreasing the separation factor (i.e. 99.6%, as shown in Table 3.2.4).

CPT-5 results show a combination of high permeate flux, final brine concentration and good permeate quality. Despite of these interesting DCMD results, CPT-5 has a couple of inconveniencies. It is relatively expensive compared with the other applied CPTs in this study and it is not recommended when treating wastewaters for water production consumption due to the toxicity of the residual barium formed during the pretreatment process.

3.2.3.7. Comparative study between CPTs

In order to choose the adequate CPT, some parameters obtained during DCMD tests are summarized in Table 3.2.4. It seems to be clear that the membrane TF200 permits to work for longer time than the TF450 membrane. Lower pore size helps to prevent pore wetting. In terms of the initial permeate flux, CPT-5 showed the best results for the membrane TF200 and the lowest permeate flux decline with DCMD operating time. In the case of the membrane TF450, no much difference exists between all applied CPTs, being CPT-3 the one that presented the lowest permeate flux decline for this membrane. This could be due to the fact that the presence of anionic detergents strongly affected the membrane with bigger pore sizes resulting in an easy wetting. On the other hand, the final brine concentration obtained with the TF200 membrane surpassed the limit of NaCl precipitation (i.e. 300 g/L of TDS) when using CPT-3, CPT-4 and CPT-5. This NaCl precipitation was not achieved when using the membrane TF450, being the maximum attained value near 200 g/L of TDS obtained when using CPT-3 and CPT-4.

Regarding β_{ef}, this depends on both the final brine concentration and the DCMD operating time. The greatest values were obtained in those CPTs that achieved higher final

brine concentrations in lower DCMD operating time, namely, CPT-5 at pH 5 with the membrane TF200 membrane, CPT-3 and CPT-4 with the membrane TF450.

Despite the fact that all DCMD tests were continued until an increase of the permeate concentration was detected, different separation factors were obtained. In general, better values were obtained when using the membrane TF200 due to its lower pore size. Among all registered values of the final separation factors, 99.9% was obtained when using CPT-4 and 99.6% when using CPT-5 at pH 9. For the membrane TF450, the best value of the final separation factor, 97.9%, was obtained when applying CPT-4. Therefore, it may be stated that both CPTs, CPT-4 and CPT-5, that allow to precipitate SO_4^{2-} ions are pretreatments reducing the risk of membrane wetting.

Due to the differences of the resultant brine concentration after carrying out the above mentioned CPTs, for sake of comparison the value of the concentration was normalized so that one can determine which CPTs contributed more in the brine concentration. This normalized brine concentration was calculated as follows:

$$C_{f,n} = \left(\frac{C_{f,t}}{C_{f,0}} \right) \tag{3.2.13}$$

where $C_{f,t}$ and $C_{f,0}$ are the feed brine concentration at time t and at the beginning of the DCMD process, respectively.

It must be pointed out that a decrease of the permeate flux with time does not mean necessary a bad DCMD performance. In some DCMD experiments, the initial permeate flux was higher than in other cases. Due to the different initial permeate fluxes obtained for the same tested membranes when applying different CPTs, a normalized permeate flux was defined in order to analyze all the permeate fluxes under the same criteria:

$$J_n = \left(\frac{J_t}{J_0} \right) \tag{3.2.14}$$

where J_t and J_0 are the DCMD permeate fluxes at time t and at the beginning of the DCMD process, respectively.

These obtained results are shown in Figs. 3.2.10 and 3.2.11 for the both membranes TF200 and TF450, respectively. It can be seen that the higher value of the normalized brine concentration corresponds to CPT-5, at both pH values, and also the higher normalized permeate flux corresponds to CPT-5, at pH 9 for the membrane TF200 (Fig. 3.2.10). Taking into account these results and those given in Table 3.2.4, CPT-5 can be considered as the best pretreatment for the RO brine when using the membrane TF200. However, if the

produced water is for consumption it is recommended to choose CPT-4, due the toxicity of the residual barium, as it was mentioned previously.

In the case of TF450 membrane, this has worse performance than the membrane TF200. The normalized brine concentration factor does not exceed the value of 3, except when using CPT-4 (Fig. 3.2.11). This pretreatment also shows better trend in the normalized permeate flux. Despite these results, the membrane TF450 does not seems to be adequate for RO brine treatment by DCMD.

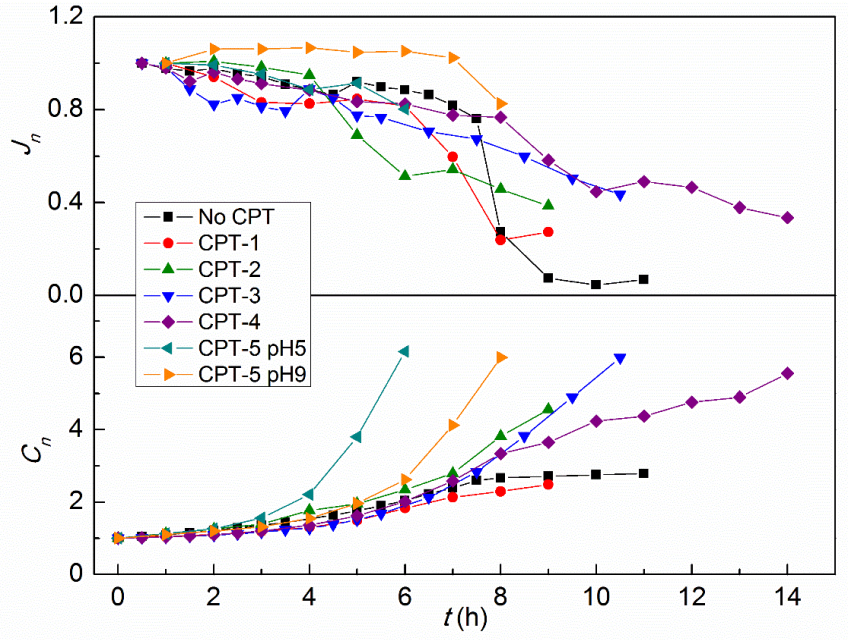

Figure 3.2.10. Normalized DCMD permeate flux (J_n) and normalized brine concentration (C_n) of the TF200 membrane used for the treatment of RO brine without CPT and with different CPTs application.

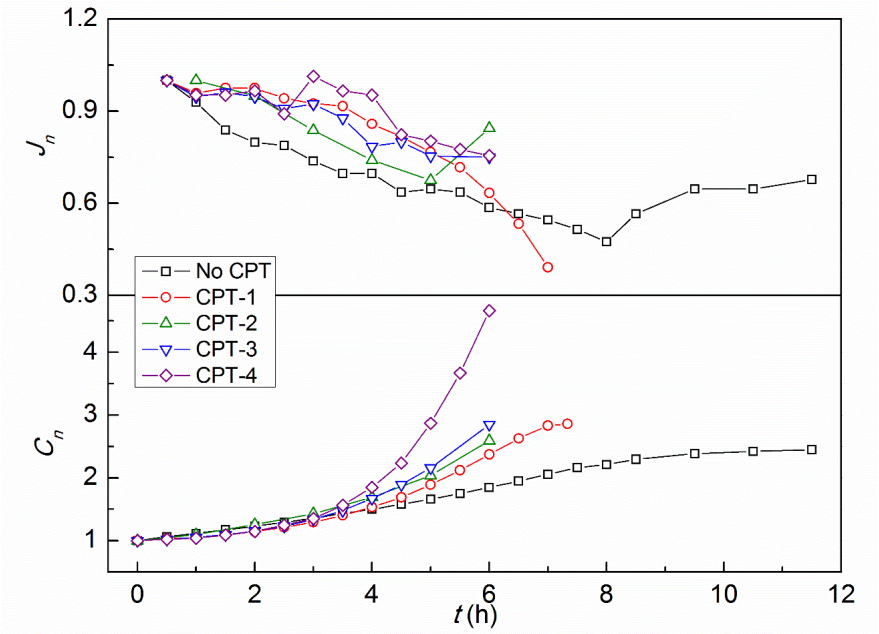

Figure 3.2.11. Normalized DCMD permeate flux (J_n) and normalized brine concentration (C_n) of the TF450 membrane used for the treatment of RO brine without CPT and with different CPTs application.

3.2.4. Conclusions

It has been shown that RO brines can be treated by DCMD, but it is necessary to apply a previous adequate chemical pretreatment (CPT) in order to extend the lifetime of the membrane and prevent pore wetting. This CPT consists on the removal of calcium ions by adding Na_2CO_3 and sulfate ions by adding $BaCl_2$. In this way, $CaCO_3$ and $CaSO_4$ salts, the less soluble salts present in the RO brines, can be eliminated before carrying out the DCMD test by means of a simple filtration procedure. These salts are the responsible of membrane fouling (i.e. salt crystals precipitation) and lead to a continuous decline of the permeate flux with time and a final wetting of the membrane pores. Thus, the DCMD process ends early limiting the possibility to concentrate the RO brine sufficiently to precipitate the NaCl.

CPT-1 (addition of NaOH) and CPT-2 (addition of addition of Na_2CO_3) did not permit to get good DCMD results. However, the application of these CPTs were capable to increase the initial permeate flux in at least 12% for the membrane TF200 and 18% for the membrane TF450. CPT-2 was also able to increase considerably the final concentration of the RO brine, especially when the membrane TF200 was used, but not enough to precipitate NaCl. In both cases, low permeate quality was achieved (i.e. pore wetting occurred in all DCMD tests), especially for the membrane TF450.

However, when both CPTs were combined in an unique chemical pretreatment, CPT-3 (addition of NaOH+Na_2CO_3) and CPT-4 (addition of NaOH+Na_2CO_3 at high temperature), better results were obtained. A similar increase of the initial permeate flux was observed in both cases compared with the DCMD test carried out with RO brine without CPT (i.e. 15-18% for the CPT-3 and CPT-4 using the TF200 membrane, and 24% for the membrane TF450). Also, the final RO brine concentration was increased significantly and overpassed clearly the NaCl precipitation concentration when the TF200 membrane was used. However, despite the fact that both CPT-3 and CPT-4 show the best results achieved for TF450 membranes, only managed to concentrate the brine until around 200 g/L TDS. This reveals that this type of membranes seems not adequate for the RO brines treatment due to the higher pore size. A better permeate quality and separation factor were observed when CPT-4 was used, due to the fact that more salt types were removed compared with the previously studied CPTs. Among all considered CPTs in this study, the best results in terms of permeate quality were obtained when applying CPT-4.

Finally, CPT-5 (addition of $BaCl_2$) permitted to remove sulfate ions from the RO brines and improved considerably the DCMD performance in terms of both the permeate flux (i.e. the highest registered values) and the permeate flux decline (i.e. the lowest decrease achieved) with a good permeate quality, especially when using RO brine at a pH value of 9. However, this CPT is not recommended when treating wastewaters for water

production consumption due to the toxicity of the residual barium formed during the pretreatment process.

3.2.5. References

[1] K.P. Lee, T.C. Arnot, D. Mattia, A review of reverse osmosis membrane materials for desalination—Development to date and future potential, Journal of Membrane Science, 370 (2011) 1.

[2] B. Peñate, L. García-Rodríguez, Current trends and future prospects in the design of seawater reverse osmosis desalination technology, Desalination, 284 (2012) 1.

[3] S.S. Shenvi, A.M. Isloor, A.F. Ismail, A review on RO membrane technology: Developments and challenges, Desalination, 368 (2015) 10.

[4] A. Subramani, J.G. Jacangelo, Treatment technologies for reverse osmosis concentrate volume minimization: A review, Separation and Purification Technology, 122 (2014) 472.

[5] K. Nakoa, K. Rahaoui, A. Date, A. Akbarzadeh, Sustainable zero liquid discharge desalination (SZLDD), Solar Energy, 135 (2016) 337.

[6] H.W. Chung, K.G. Nayar, J. Swaminathan, K.M. Chehayeb, J.H. Lienhard V, Thermodynamic analysis of brine management methods: Zero-discharge desalination and salinity-gradient power production, Desalination, 404 (2017) 291.

[7] D.H. Kim, A review of desalting process techniques and economic analysis of the recovery of salts from retentates, Desalination, 270 (2011) 1.

[8] A. Perez-Gonzalez, A.M. Urtiaga, R. Ibanez, I. Ortiz, State of the art and review on the treatment technologies of water reverse osmosis concentrates, Water Research, 46 (2012) 267.

[9] A. Giwa, V. Dufour, F. Al Marzooqi, M. Al Kaabi, S.W. Hasan, Brine management methods: Recent innovations and current status, Desalination, 407 (2017) 1.

[10] S.H. Joo, B. Tansel, Novel technologies for reverse osmosis concentrate treatment: a review, Journal of Environmental Management, 150 (2015) 322.

[11] J.M. Arnal, M. Sancho, I. Iborra, J.M. Gozálvez, A. Santafé, J. Lora, Concentration of brines from RO desalination plants by natural evaporation, Desalination, 182 (2005) 435.

[12] S. Shanmuganathan, M.A.H. Johir, A. Listowski, S. Vigneswaran, J. Kandasamy, Sustainable Processes for Treatment of Waste Water Reverse Osmosis Concentrate to Achieve Zero Waste Discharge: A Detailed Study in Water Reclamation Plant, Procedia Environmental Sciences, 35 (2016) 930.

[13] J. Morillo, J. Usero, D. Rosado, H. El Bakouri, A. Riaza, F.-J. Bernaola, Comparative study of brine management technologies for desalination plants, Desalination, 336 (2014) 32.

[14] K. Loganathan, P. Chelme-Ayala, M. Gamal El-Din, Treatment of basal water using a hybrid electrodialysis reversal–reverse osmosis system combined with a low-temperature crystallizer for near-zero liquid discharge, Desalination, 363 (2015) 92.

[15] M. Reig, S. Casas, O. Gibert, C. Valderrama, J.L. Cortina, Integration of nanofiltration and bipolar electrodialysis for valorization of seawater desalination brines: Production of drinking and waste water treatment chemicals, Desalination, 382 (2016) 13.

[16] S. Jamil, S. Jeong, S. Vigneswaran, Application of pressure assisted forward osmosis for water purification and reuse of reverse osmosis concentrate from a water reclamation plant, Separation and Purification Technology, 171 (2016) 182.

[17] R.L. McGinnis, N.T. Hancock, M.S. Nowosielski-Slepowron, G.D. McGurgan, Pilot demonstration of the NH3/CO2 forward osmosis desalination process on high salinity brines, Desalination, 312 (2013) 67.

[18] C.R. Martinetti, A.E. Childress, T.Y. Cath, High recovery of concentrated RO brines using forward osmosis and membrane distillation, Journal of Membrane Science, 331 (2009) 31.

[19] J.A. Bush, J. Vanneste, T.Y. Cath, Membrane distillation for concentration of hypersaline brines from the Great Salt Lake: Effects of scaling and fouling on performance, efficiency, and salt rejection, Separation and Purification Technology, 170 (2016) 78.

[20] H. Geng, J. Wang, C. Zhang, P. Li, H. Chang, High water recovery of RO brine using multi-stage air gap membrane distillation, Desalination, 355 (2015) 178-185.

[21] J.P. Mericq, S. Laborie, C. Cabassud, Vacuum membrane distillation of seawater reverse osmosis brines, Water Research, 44 (2010) 5260.

[22] J. Minier-Matar, A. Hussain, A. Janson, F. Benyahia, S. Adham, Field evaluation of membrane distillation technologies for desalination of highly saline brines, Desalination, 351 (2014) 101.

[23] G. Naidu, S. Jeong, Y. Choi, S. Vigneswaran, Membrane distillation for wastewater reverse osmosis concentrate treatment with water reuse potential, Journal of Membrane Science, 524 (2017) 565.

[24] H. Guo, H.M. Ali, A. Hassanzadeh, Simulation study of flat-sheet air gap membrane distillation modules coupled with an evaporative crystallizer for zero liquid discharge water desalination, Applied Thermal Engineering, 108 (2016) 486.

[25] X. Ji, E. Curcio, S. Al Obaidani, G. Di Profio, E. Fontananova, E. Drioli, Membrane distillation-crystallization of seawater reverse osmosis brines, Separation and Purification Technology, 71 (2010) 76.

[26] D.G. Randall, J. Nathoo, A succinct review of the treatment of Reverse Osmosis brines using Freeze Crystallization, Journal of Water Process Engineering, 8 (2015) 186.

[27] D.G. Randall, J. Nathoo, A.E. Lewis, A case study for treating a reverse osmosis brine using Eutectic Freeze Crystallization-Approaching a zero waste process, Desalination, 266 (2011) 256.

[28] P.M. Williams, M. Ahmad, B.S. Connolly, Freeze desalination: An assessment of an ice maker machine for desalting brines, Desalination, 308 (2013) 219.

[29] M. Gryta, Fouling in direct contact membrane distillation process, Journal of Membrane Science, 325 (2008) 383.

[30] J.A. Sanmartino, M. Khayet, M.C. García-Payo, Desalination by Membrane Distillation, in: R. Singh, N. Hankins (Eds.) Emerging Membrane Technology for Sustainable Water Treatment, Elsevier, 2016.

[31] J.A. Sanmartino, M. Khayet, M.C. García-Payo, H. El Bakouri, A. Riaza, Desalination and concentration of saline aqueous solutions up to supersaturation by air gap membrane distillation and crystallization fouling, Desalination, 393 (2016) 39.

[32] P. Zhang, P. Knötig, S. Gray, M. Duke, Scale reduction and cleaning techniques during direct contact membrane distillation of seawater reverse osmosis brine, Desalination, 374 (2015) 20.

[33] E. Curcio, X. Ji, G. Di Profio, A.O. Sulaiman, E. Fontananova, E. Drioli, Membrane distillation operated at high seawater concentration factors: Role of the membrane on $CaCO_3$ scaling in presence of humic acid, Journal of Membrane Science, 346 (2010) 263.

[34] C. Tzotzi, T. Pahiadaki, S. Yiantsios, A. Karabelas, N. Andritsos, A study of CaCO3 scale formation and inhibition in RO and NF membrane processes, Journal of Membrane Science, 296 (2007) 171.

[35] M.H. Sorour, H.A. Hani, H.F. Shaalan, G.A. Al-Bazedi, Schemes for salt recovery from seawater and RO brines using chemical precipitation, Desalination and Water Treatment, (2014) 1.

[36] S. Casas, C. Aladjem, E. Larrotcha, O. Gibert, C. Valderrama, J.L. Cortina, Valorisation of Ca and Mg by-products from mining and seawater desalination brines for water treatment applications, Journal of Chemical Technology and Biotechnology, 89 (2014) 872.

[37] E. Drioli, E. Curcio, A. Criscuoli, G.D. Profio, Integrated system for recovery of $CaCO_3$, NaCl and $MgSO_4 \cdot 7H_2O$ from nanofiltration retentate, Journal of Membrane Science, 239 (2004) 27.

[38] D. Qu, J. Wang, L. Wang, D. Hou, Z. Luan, B. Wang, Integration of accelerated precipitation softening with membrane distillation for high-recovery desalination of primary reverse osmosis concentrate, Separation and Purification Technology, 67 (2009) 21.

[39] CRC Handbook of Chemistry and Physics, CRC Press, Cleveland, Ohio, 1975.

[40] B. Coto, C. Martos, J.L. Peña, R. Rodríguez, G. Pastor, Effects in the solubility of $CaCO_3$: Experimental study and model description, Fluid Phase Equilibria, 324 (2012) 1.

[41] M. Khayet, T. Maatsura, Membrane Distillation. Principles and Applications, Elsevier B.V., Amsterdam, The Netherlands, 2011.

[42] M. Essalhi, M. Khayet, Self-sustained webs of polyvinylidene fluoride electrospun nanofibers at different electrospinning times: 1. Desalination by direct contact membrane distillation, Journal of Membrane Science, 433 (2013) 167.

[43] M. Essalhi, M. Khayet, Self-sustained webs of polyvinylidene fluoride electrospun nano-fibers: Effects of polymer concentration and desalination by direct contact membrane distillation, Journal of Membrane Science, 454 (2014) 133.

[44] F. He, K.K. Sirkar, J. Gilron, Studies on scaling of membranes in desalination by direct contact membrane distillation: $CaCO_3$ and mixed $CaCO_3/CaSO_4$ systems, Chemical Engineering Science, 64 (2009) 1844.

[45] F. He, J. Gilron, H. Lee, L. Song, K.K. Sirkar, Potential for scaling by sparingly soluble salts in crossflow DCMD, Journal of Membrane Science, 311 (2008) 68.

[46] M. Gryta, Calcium sulphate scaling in membrane distillation process, Chemical Papers, 63 (2009) 146.

[47] C. Duclosorsello, Neutral adsorptive capture of particles by membranes: network modeling near the membrane isoelectric point, Journal of Membrane Science, 237 (2004) 167.

[48] T. Preočanin, A. Selmani, P. Lindqvist-Reis, F. Heberling, N. Kallay, J. Lützenkirchen, Surface charge at Teflon/aqueous solution of potassium chloride interfaces, Colloids and Surfaces A: Physicochemical and Engineering Aspects, 412 (2012) 120.

[49] F. Hamadi, H. Latrache, M. Zekraoui, M. Ellouali, J. Bengourram, Effect of pH on surface energy of glass and Teflon and theoretical prediction of Staphylococcus aureus adhesion, Materials Science and Engineering C: Materials for Biological Applications, 29 (2009) 1302.

[50] M. Manciu, E. Ruckenstein, Ions near the air/water interface. II: Is the water/air interface acidic or basic? Predictions of a simple model, Colloids and Surfaces A: Physicochemical and Engineering Aspects, 404 (2012) 93.

Chapter 4

Reuse of discarded membrane distillation membranes in wastewater treatment by microfiltration

Membrane distillation (MD) technology is being implemented in industry thanks to the incessant progress made so far in membrane modules, membrane design and their fabrication. The main drawback of MD is the irreversible membrane pore wetting. Special care must be made in order to maintain the membrane pores dry. Once the pores are getting wet and/or blocked the efficiency of the MD process is reduced and the membrane is finally discarded. It is to be noted that MD membranes are more expensive than the membranes used in other membrane processes (e.g. pressure driven membrane processes microfiltration, MF; ultrafiltration, UF or reverse osmosis, RO). Reusing of disposed MD membranes is a possible solution to prevent membrane disposal and save costs. In this study, polytetrafluoroethylene (PTFE) membranes were used for the treatment of synthetic and RO brines at different feed temperatures by air gap membrane distillation (AGMD) until the membrane pores were blocked or wetted. These membranes were proposed for MF considering as a feed solution example humic acid (HA) aqueous solutions. Fouling of the discarded PTFE membranes for use in AGMD was studied and compared with that of new PTFE membranes. Depending on the membrane characteristics and its initial state, MF results are different in terms of the permeate flux, separation factor or performance index. It was observed that the recycled AGMD membranes could exhibit even better MF performance than the new ones.

4.1. Introduction

Membrane distillation (MD) technology has been proposed as a solution for desalination of high saline aqueous solutions and treatment of reverse osmosis (RO) brines producing relatively high permeate fluxes with high salt rejection factors if the pores of the used hydrophobic membranes are maintained dry [1, 2]. A lot of progress has been made during last 10 years on the improvements of membrane modules and MD membrane engineering. This progress results in an industrial implementation of MD technology using different types of membrane modules [3-9]. However, the common drawback of MD technology is the risk of the irreversible membrane pores wetting that occurs due to various reasons: application of a hydrostatic pressure higher than the liquid entry pressure of the membrane (*LEP*), membrane scaling or fouling (i.e. organic, inorganic of biological) that may be produced on the membrane surface or inside the pores with the subsequent loose of the hydrophobic character of the membrane, use of membranes designed for other processes rather than for MD, use of feed solutions with low surface tension contaminants such as alcohols, production of concentrated volatile organic compounds that may wet the membrane pores from the permeate side, application of very low vacuum pressure in the permeate side of the membrane in vacuum membrane distillation (VMD) configuration, use of higher pressure of the sweeping gas than the hydrostatic pressure of the feed side in sweeping gas membrane distillation (SGMD), etc. Depending on the cause of wetting, only large pores or all pores can be flooded with the liquid feed or permeate solution provided that the membranes exhibit pore size distribution. Once the membrane pores are getting wet, the MD permeate flux is increased and the separation factor or concentration factor are reduced considerably. Consequently, the membrane must be changed by a new one.

Some laboratory strategies have been adopted in order to restore the MD wetted or blocked membranes due to fouling: cleaning with distilled water or using some cleaning agents followed by drying directly the membrane in air, blowing with inert gas, changing the liquid entrapped inside the pores with another lower surface tension liquid such as alcohols followed by drying, etc. These procedures were carried out directly on the membrane by taking it out from the module or keeping it inside the module and applying the cleaning/restoration in the whole installation. However, none of the followed methods proved to be completely successful and finally the membranes were discarded for use in MD process. The frequent raised question in MD laboratories: What should we do with these rejected MD membranes?

It is worth quoting that different propositions were considered in waste management for recycling, reuse and disposal of discarded reverse osmosis (RO) membranes in order to reduce desalination costs [10, 11]. However, in MD no strategy has been proposed yet for the recycling and reuse of discarded MD membranes.

In order to reduce water treatment costs and at the same time take care of the environment, the discarded MD membranes can be recycled as support for the fabrication of other membranes especially those membranes having big pores (i.e. 1 μm), low tortuosity factor (i.e. near unity), good mechanical properties and thin. Another possibility is to reuse the membranes in another independent membrane separation process or integrated as a pretreatment membrane process prior to MD process. In this study, we propose using these membranes in microfiltration (MF).

MF membranes are porous hydrophilic or hydrophobic, with pore sizes ranging between 0.05 and 10 μm, used to separate contaminants from aqueous solutions under a low hydrostatic pressure in the range of 0.1-3 MPa [12]. When hydrophobic porous membranes are used, these must be wetted first using alcohols for example and then compacted at pressures higher than the *LEP* of the membrane before carrying out MF separation.

This paper aims to analyze the possibility to reuse discarded MD membranes in MF for the treatment of humic acid (HA) aqueous solutions. Polytetrafluorethylene (PTFE) commercial flat sheet membranes were considered as a case of study. These membranes were previously used in air gap membrane distillation (AGMD) for water production and concentration of synthetic or real RO brines until their pores were finally wet or blocked due to fouling/scaling phenomena.

4.2. Materials and methods

4.2.1. Membranes, brines and HA aqueous solutions

Two porous hydrophobic flat sheet membranes (*Pall Scientific*) having a thin polytetrafluoroethylene (PTFE) layer of 6-10 μm thickness, supported by a polypropylene (PP) net, and different mean pore sizes, 0.2 μm (TF200) and 0.45 μm (TF450), were used in this study. Their morphological characteristics were reported elsewhere [2]. These membranes were used in AGMD for the concentration of saline solutions (i.e. synthetic brines, SB) up to the concentration limit of salt in water and for the treatment of RO brines (ROB) [2].

The SB were prepared by dissolving 65 g/L NaCl (ACS reagent ≥ 99%, supplied by *Sigma-Aldrich*) in water. To measure the concentration of SB in both the feed and permeate, an electrical conductivity meter (712 Ω *Metrohm*) was employed and a calibration with NaCl aqueous solutions of different concentrations was performed. The ROB used in this study were discharged by an RO desalination plant located in Almeria (Spain) and analyzed in the Geochemical and Environmental Analysis Laboratory of the University Complutense of Madrid (UCM). The concentration of the components present in the RO brines was determined by means of different techniques: ionic chromatography to determine chlorides

and sulfates, potentiometry to measure alkalinity, atomic emission spectrometry with inductively coupled plasma (ICP- AES) to get the concentration of Ca, Mg, Na and Si ions, and UV-Vis spectrometry to determine the anionic detergents following the methylene blue active substances (MBAS) assay. The obtained concentrations of the different components are summarized in Table 4.1. During AGMD experiments, the ROB concentration was also determined by means of the electrical conductivity meter. In this case, the calibration curve was obtained by drying and then weighing ROB samples subjected to different evaporation times in order to get the total dissolved solids (TDS) as a function of the electrical conductivity.

Table 4.1. Analytical characteristics of the used RO brine (ROB).

Component	Concentration	Technique
Cl^- (mg/L)	31150 ± 2400	ionic chromatography
SO_4^{-2} (mg/L)	5264 ± 390	ionic chromatography
Alkalinity (mg/L $CaCO_3$)	432 ± 39	potentiometry
Ca (mg/L)	879 ± 53	ICP- AES
Mg (mg/L)	1864 ± 56	ICP- AES
Na (mg/L)	15270 ± 460	ICP- AES
Si (mg/L)	11 ± 1	ICP- AES
Anionic detergents (μg/L MBAS)	119 ± 7	UV-Vis Spectrometry
pH	7.9	pH meter
Total Dissolved Solids (TDS mg/L)	55000 ± 2500	

The feed solution used in MF was a dilute aqueous solution of 15 mg/L of HA (molecular weight 4.1 kDa, supplied by *Fluka*) at two different pH values 3 and 11. The pH value was measured using a pH/Ion meter (692, *Metrohm*) and adjusted by adding either 2M HCl or 2M NaOH as needed, since the main HA solution has a pH value of 10. The HA concentration was determined by means of UV-Vis spectrophotometer (7315, *Jenway*).

4.2.2. Membrane characterization techniques

Before carrying out MF process, all the membranes were characterized by means of different techniques as it was described elsewhere [2]. The membrane thickness (δ) was determined by an electronic micrometer (*Schut Geometrical Metrology*), the mean pore size (d_p) was obtained by a flow porometer (POROLUX™100 Porometer) and the water contact angle (θ) of the membrane surface by a computerized optical system (CAM200), equipped with CCD frame grabber camera and image analysis software. The top surface and the support layer of the membranes were analyzed by a field emission scanning electron microscope (FESEM, *JEOL* 6335F). After their use in MF, the morphological characteristics of the membranes were again determined in order to study the HA fouling.

4.2.3. MF tests

The experimental MF setup is schematized in Fig 4.1. The membrane, with an effective area of (217.58 ± 0.14) 10^{-5} m^2, was placed in the filtration module. The feed solution was kept in the feed tank at a constant temperature of 298 K by a thermostat (*Lauda* K20 KS). The feed solution was circulated tangentially to the membrane surface by a magnetic gear pump (*Danfoss*, APP 0.6). After passing the filtration module, both permeate and retentate were turned back to the feed tank. To control the feed flow rate and the pressure at the inlet of the membrane module a frequency variator (*ABB Industrial Drives*, ACS355) together with a pressure controlling valve were used. Two pressure transmitters (*Wika*) connected to digital indicators (*Junior*20-PRC) permit the measurement of the pressure at the inlet and outlet of the membrane module. The feed flow rate was measured by a flow-meter (*RS-Amidata*, 5111-3892). A pre-filter (*Millipore Corporation*) that holds a nylon filter (*Millipore*, NY20) having a pore size of 20 μm was placed between the pump and the membrane module in order to retain undesirable large particles present in the feed solution and therefore protect the membrane.

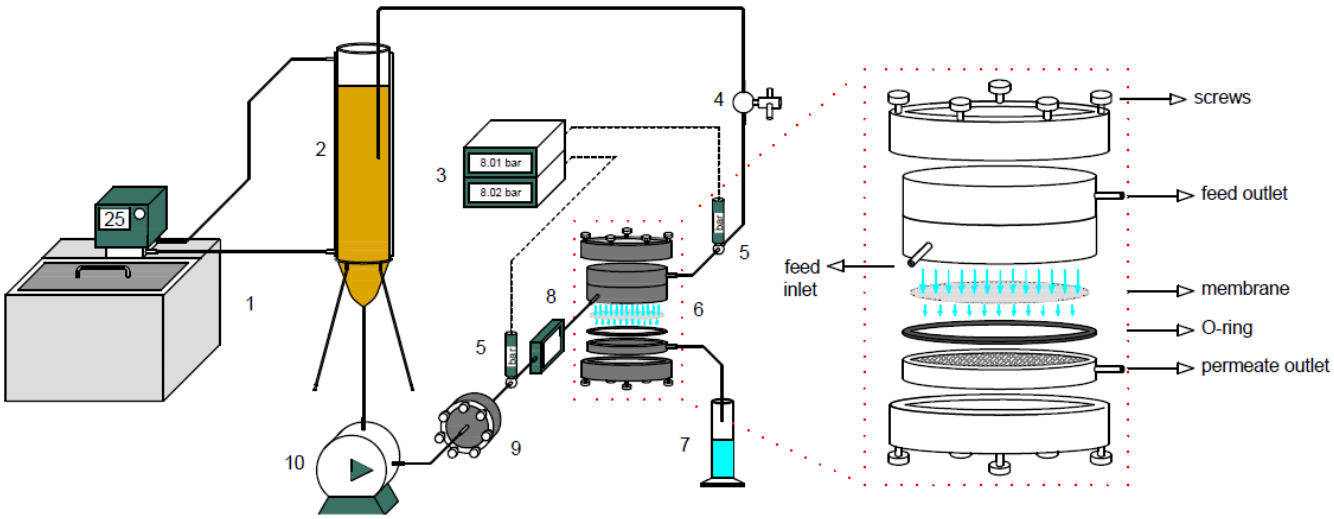

Figure 4.1. MF experimental setup: 1.- thermostat, 2.- feed tank, 3.- pressure digital indicators, 4.- valve, 5.- pressure transmitters, 6.- filtration module, 7.- permeate container, 8.- flow-meter, 9.- pre-filter holder and 10.- magnetic pump.

Membrane compaction was carried out using distilled water as feed and a pressure that was increased stepwise from 1 to 9 10^5 Pa, for a period of 30 min each pressure. The permeation tests with HA feed aqueous solutions were carried out at an applied pressure of 8 10^5 Pa, maintaining the pump at 2500 rpm, and a feed flow rate of 0.7-0.8 L/min. It is worth noting that the *LEP* values of the used TF200 and TF450 membranes are 2.9 and 1.5 10^5 Pa, respectively [2].

In all performed MF experiments the permeate flux (J), the separation factor (α) and the water flux reduction factor (FR_W) were determined as follows. An electronic balance (*Denver SI-2002*, ± 0,01 g) was used to calculate the permeate flux [13]:

$$J = \frac{m}{S_{ef} \cdot \Delta t} \tag{4.1}$$

where m is the permeate mass, S_{ef} is the effective membrane area and Δt is the permeate collection time.

The measured feed and permeate HA concentrations were used to calculate the separation factor of the membranes as [13]:

$$\alpha = \left(1 - \frac{C_p}{C_f}\right) \cdot 100 \tag{4.2}$$

where C_f and C_p are the feed and permeate HA concentrations, respectively.

The permeate fluxes of distilled water before ($J_{w,b}$) and after ($J_{w,a}$) each HA filtration experiments were measured during 30 min under the same applied pressure as that applied to perform the HA experiments (i.e. 8 10^5 Pa). FR_W was calculated as [14]:

$$FR_W = \frac{J_{w,b} - J_{w,a}}{J_{w,b}} \cdot 100 \tag{4.3}$$

4.3. Results and discussion

4.3.1. AGMD experiments

Fig. 4.2 shows the evolution with AGMD operating time of the permeate fluxes and both the feed and permeate concentrations of the membranes TF200 and TF450. The calculated mean permeate flux and the final concentration of the feed solution together with the reason to discard the use of the membranes in AGMD are summarized in Table 4.2. As can be seen in Fig. 4.2, in all cases the permeate flux decreased with time due to the increase of the salt feed concentration (i.e. reduction of the driving force, the vapor pressure of the feed solution) and to fouling or salt crystallization on the surface of the membrane and inside the membrane pores producing a partial or a complete pore blocking as reported elsewhere [2]. The reduction of the permeate flux is more significant when using SB as feed solution instead of ROB. Other than the type of the saline feed solution, this difference may be attributed partly to the higher feed temperature applied for the concentration of SB (348 and 328K), instead of 318K used to concentrate ROB. As it is well known [2], the

higher is the feed temperature and the membrane pore size, the higher is the permeate flux. In addition, as can be seen in Fig. 4.2, when the permeate flux is high the slope of the feed concentration curve is also high. The observed sharp enhancement of the final permeate flux of the membrane TF450_SB_328K (Fig. 4.2) indicated pore wetting, which reduced considerably the quality of the produced water.

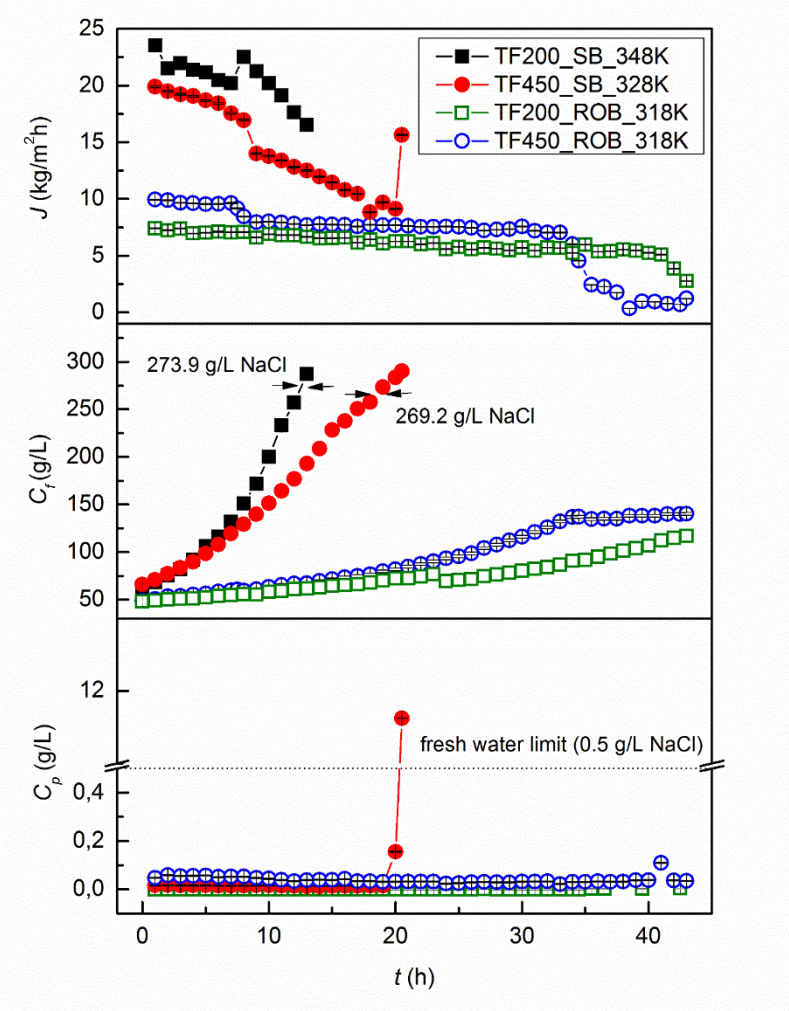

Figure 4.2. AGMD permeate flux, feed (C_f) and permeate (C_p) concentration as a function of operating time for the membranes TF200 and TF450 when using SB (NaCl concentration) and ROB (TDS concentration) feed solutions at different feed temperatures (318K, 328K, 348K). The arrows represent the saturation concentration of NaCl (C_s) for each feed temperature: 269.2 g/L NaCl at 328 K and 273.9 g/L NaCl at 348 K.

The saturation concentration limit of NaCl [15], mentioned in Fig. 4.2, for each feed temperature was reached when using SB solution. This was not the case for ROB solution because of the obtained lower permeate fluxes and feed concentration slopes than those of the SB solution, attributed partly to fouling and pore blocking with the different components present in ROB (Table 4.1). The permeate concentration remained below the

concentration limit of fresh water (i.e. 0.5 g/L NaCl) for all the AGMD membranes except for the membrane TF450_SB_328K, whose pores were wet.

Table 4.2. Membranes and operating parameters used in AGMD experiments (T_f: feed temperature, J: mean permeate flux, C_f: final concentration of feed solution and T_p: temperature of the condensation surface kept constant at 298 K).

Membrane	Feed solution	T_f (K)	J (kg/m^{2}h)	C_f (g/L)	Reason to discard the membrane from use in AGMD
TF200_SB_348K	Synthetic brine (65 g/L NaCl)	348	20.6 ± 1.9	287.29 ± 0.18	Membrane pores blocked
TF200_ROB_318K	RO brine (50 g/L TDS)	318	5.9 ± 0.9	133.6 ± 1.4	Membrane pores blocked
TF450_SB_328K	Synthetic brine (65 g/L NaCl)	328	14.7 ± 3.8	290.31 ± 0.18	Membrane pores wetted
TF450_ROB_318K	RO brine (50 g/L TDS)	318	6.0 ± 3.2	134.3 ± 1.4	Membrane pores blocked

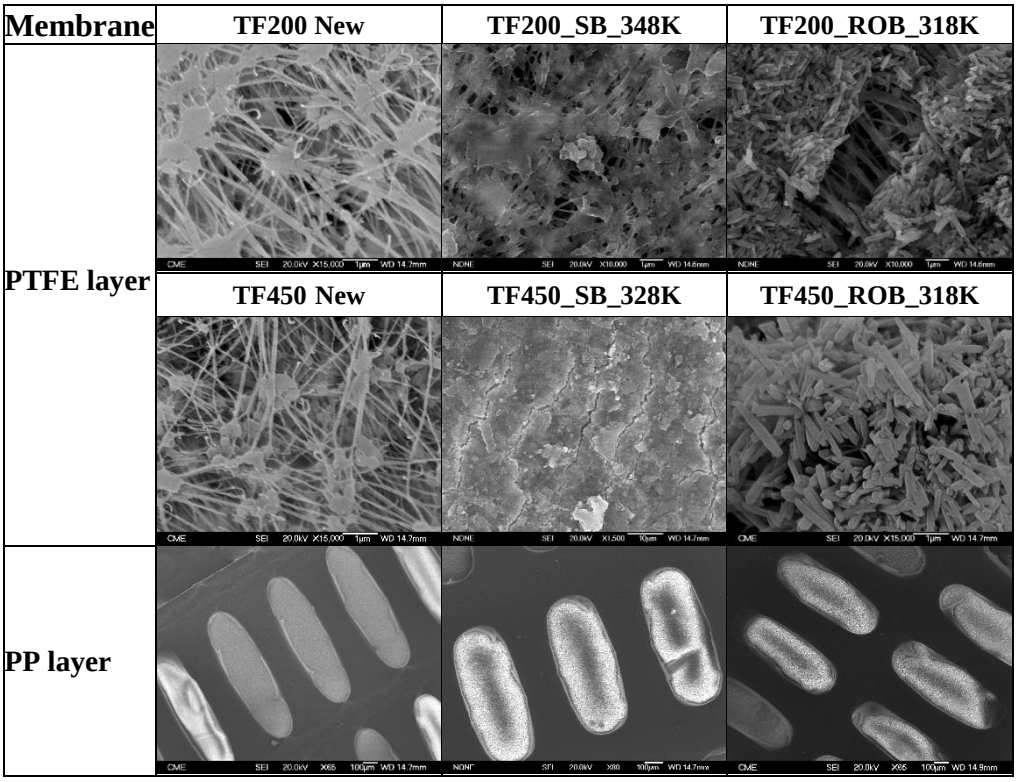

Figure 4.3. SEM images (at different magnifications) of the PTFE layer and the PP support layer of the membranes TF200 and TF450 (new ones and after AGMD process using SB and ROB feed solutions).

The membranes used in AGMD presented a fouling layer on their surface as can be seen in Fig. 4.3. Independently of the feed solution used, a layer of salt crystals was formed

on the membrane surface and some crystals penetrate into the membrane pores as it will be explained later on. In addition, the FR_W values were found to be higher when using ROB as feed (i.e. 13.1% for the membrane TF200_ROB_318K and 37.6% for the membrane TF450_ROB_318K) than those corresponding to SB used as feed. This result indicated that the degree of irreversible fouling of the PTFE membranes is more significant when using ROB as feed and for the membrane having greater pore size. For both feed solutions, the morphological characteristics of the membranes changed in comparison with the new ones as can be seen in Table 4.3.

Table 4.3. Morphological characteristics (thickness (δ), mean pore size (d_p) and water contact angle (θ)) of the new membranes and those used in AGMD and recycled in MF.

Membrane	δ (µm)			d_p (nm)			θ (º)		
	New [a]	After AGMD	After MF	New [a]	After AGMD	After MF	New [a]	After AGMD	After MF
TF200_SB_348K	107 ± 6	114 ± 6	119 ± 7	329 ± 18	377 ± 20	212 ± 22	140 ± 3	126 ± 15	118 ± 8
TF200_ROB_318K		117 ± 5	112 ± 4		339 ± 3	206 ± 28		138 ± 3	128 ± 7
TF450_SB_328K	98 ± 6	104 ± 6	110 ± 9	553 ± 4	536 ± 15	298 ± 22	141 ± 1	133 ± 2	119 ± 2
TF450_ROB_318K		109 ± 5	113 ± 9		389 ± 18	285 ± 3		134 ± 5	129 ± 11

[a] Values reported in [2].

Compared to the thickness of the new membranes, salt or brine crystal deposited on the membrane surface increased the final thickness of the membranes. As a result of fouling, smaller water contact angles were measured indicating a lower hydrophobicity of all studied membranes. The membrane pore size also changed being small for the membrane TF450 due to the pore constriction by salt crystals. This indicates the easy penetration of the salts crystals in the pores of the membrane exhibiting large pore size. In addition, damage of some fibrils and crack formation were observed in the PTFE layer. These contributed also to the reduction of the mechanical properties of the membrane, and subsequently to the change of the membrane pore size as reported in [16, 17].

Taking into consideration the reduced MD performance of the tested membranes in AGMD and the failed trials looking at their regeneration following different strategies [18-23], these membranes were finally discarded for further use in MD and proposed for MF applications.

4.3.2. MF preliminary experiments

In order to design the MF experiments for recycling MD membranes, preliminary MF tests were performed applying different MF operation parameters with new PTFE

membranes. As it was expected the pH value of the HA solutions and the compaction of the PTFE membranes affects considerably the MF performance as shown below.

4.3.2.1. Effects of the pH value of HA solutions on the MF performance

It is worth quoting that there exists a pH-dependence of the HA solution on MF performance [13, 14, 24, 25]. This was explained by HA-HA and HA-membrane material interactions. In addition, the macromolecular structure and particle size of HA depend on the degree of charge neutralization and vary with the pH value, ionic strength and degree of complexation with metal ions [26]. In acidic media HA particles tend to aggregate forming chains by hydrogen bonding and other attractive forces (i.e. van der Waals interactions and π-electron interactions). As an example, at pH 3 the average size of HA particles ranges between 1 and 27 nm [27]. In contrast, in alkaline media deprotonation of HA functional groups induces higher intra- and intermolecular electrostatic repulsive forces and the HA forms stretched linear and flat structures without aggregates resulting in lower sizes of HA particles (e.g. at pH 8 the average size of HA particles ranges between 0.3 and 4 nm [27]).

Particle-membrane interactions in liquids are governed among others by electrostatic attractive or repulsive forces [28]. Electrostatic interactions may be attractive or repulsive depending on the charge of the electrostatic potential of the HA and the membrane material. The isoelectric point of PTFE is around 3.7 [29]. Thus, the used membranes are almost electrically neutral at pH 3. In addition, the contact angle of the membrane exhibits a minimum around this isoelectric point [30] and the surface tension of water shows a minimum in the same pH region [31]. Moreover, the inter- and intra-molecular electrostatic repulsive forces of HA are also very low or close to zero [32]. Therefore, when the pH of the HA aqueous solution is 3, the electrostatic repulsive forces between the PTFE material and the HA particles and/or between the HA particles are negligible resulting in HA adsorption on the membrane material [32, 33]. In this case, the hydrophobic interaction is the predominant interaction compared to the electrostatic interaction. On the contrary, at pH 11 the electrostatic repulsive forces increase between HA macromolecules and between HA-membrane material (i.e. both membrane and HA are negatively charged) leading to a lower adsorption of HA on the membrane surface [24]. In this case, the electrostatic interaction is the predominant mechanism affecting HA separation phenomenon from water.

To verify the above cited statements, new TF200 and TF450 membranes were considered using HA feed solutions at pH 3 and pH 11. Based on the model developed by Astaraee *et al.* [34], the initial fouling of the MF membrane is due to pore blockage caused by the physical deposition of large HA aggregates on the surface of the MF membranes,

and the subsequent cake formation in the last stage exerting the main mass transport resistance of the MF process and resulting in a significant reduction of the permeate flux.

Different behaviors can be seen in Fig. 4.4 for the two membranes in acid and basic HA aqueous solutions, in terms of permeate flux, feed and permeate concentrations and separation factor.

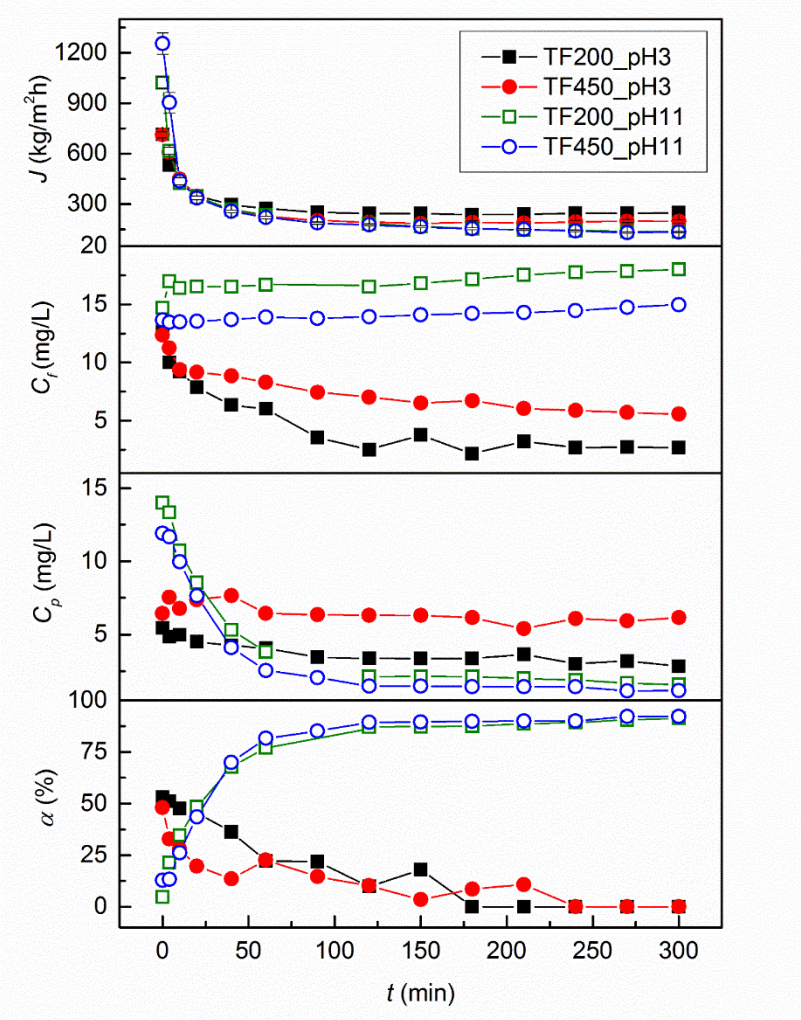

Figure 4.4. Evolution with time of the permeate flux (J), feed concentration (C_f), permeate concentration (C_p) and HA separation factor (α) of the new membranes TF200 and TF450 during MF tests of 15 mg/L HA aqueous solution at different pH values.

Both membranes were not able to separate HA from water at pH 3. Similar results were reported by Arribas *et al.* [13] when using polysulfone (PS) nanofibrous membranes. As stated previously, the adsorption phenomenon of HA on the membrane surface in acidic media is the responsible of about 50% separation factor achieved at the beginning of the MF experiments, and the observed lower initial permeate flux. The significant decrease of the HA feed concentration with time approaching an asymptotic value equal to that of the permeate resulted in no HA separation from water. This result indicated that the used PTFE membranes are not selective to HA in acidic environment.

At basic pH, an opposite tendency was detected for the HA feed and permeate concentration as well as for the HA separation factor. At the beginning of the MF experiments, both the feed and permeate concentrations were quite similar. Then, both the HA feed concentration and the HA separation factor increased with time, whereas the HA permeate concentration was reduced approaching asymptotic values. In this case, the final HA separation factor was higher than 90% (i.e. 91.3% and 92.3% for TF200 and TF450 new membranes, respectively) This fact could be justified by the lower adsorption of HA on PTFE membrane occurs at pH 11 compared to that at pH 3 due to the increase of the electrostatic repulsive forces between HA macromolecules and between HA and PTFE material as stated previously. This proves the bad initial HA separation from water. During MF, the continuous deposition of HA on the PTFE material increased further the negative charge of both the membrane surface and the pores and consequently the electrostatic repulsion effect becomes greater with time leading to an enhancement of the HA separation factor.

As it was stated earlier, the HA fouling was quantified by means of the FR_W. The PTFE membrane is not able to retain the HA particles at pH 3 and as a result a small reduction of the water permeate flux was detected after the MF test. Therefore, both TF200 and TF450 membranes presented lower FR_W values when using HA solutions at pH 3 (i.e. 59.8% and 63.8% for TF200 and TF450, respectively) in comparison with the FR_W values obtained with HA solutions at pH 11 (i.e. 80.2% for the TF200 membrane and 93.0% for the TF450 membrane). The higher FR_W value of TF450 membrane is due to its higher water permeate flux obtained before HA MF experiment.

4.3.2.2. Effect of membrane compaction on MF performance

As it was explained previously, membrane compaction was performed using distilled water as feed under a transmembrane pressure exceeding the *LEP* of the membrane. The reduction of the mean pore size after compaction was found to be similar for both TF200 and TF450 membranes. A 12% reduction was found for the TF200 new membrane (i.e. from 329 ± 18 to 290 ± 3 nm) and a 14% for the TF450 new membrane (i.e. from 553 ± 4 to 477 ± 2 nm). A higher pore size reduction was observed for the recycled membranes previously used in AGMD (e.g. the membrane pore size decreased by 42%, from 357 to 206 ± 24 nm for the membrane TF450_ROB_328K after its compaction). This may be attributed to the foulants that block or reduce the pore size during compaction. In fact, the use of distilled water as feed for compaction contributed to clean the membrane surface from foulants and crystals.

Compaction effect on membrane surfaces is illustrated in Fig. 4.5 by means of SEM images of both compacted and uncompacted new and recycled membranes. The PTFE layer was compacted against its PP support. The fibrillar structure of the PTFE layer was reduced

in those supported zones and disappeared from the free zones (i.e. unsupported zones of the PTFE layer) that suffered more compaction. In fact, the areas of the PTFE layer supported by PP fiber were less compacted than the free zones.

Membrane	PTFE layer before compaction	PTFE layer after compaction (x40)	Supported zone of compacted PTFE layer (x10000)	Free zone of compacted PTFE layer (x10000)
TF200 new membrane	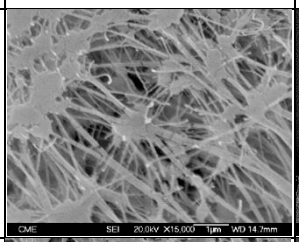	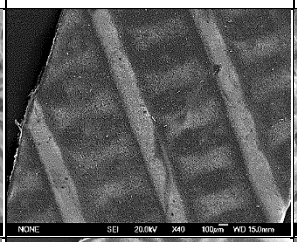	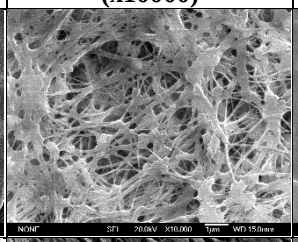	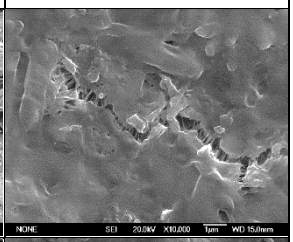
TF200_SB_348K	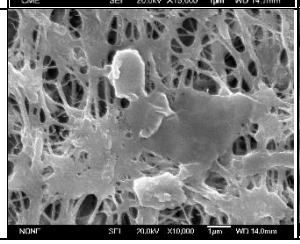	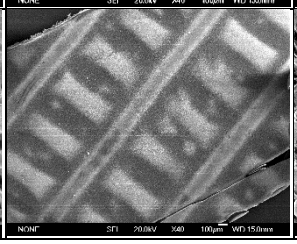	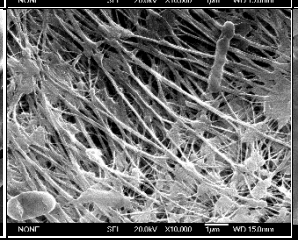	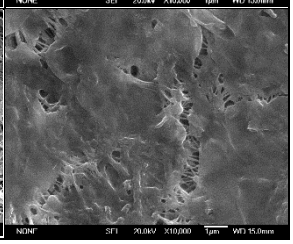

Figure 4.5. SEM images of uncompacted and compacted PTFE layer at different zones of new and recycled membranes.

Other than the reduced pore size detected after compaction, the water contact angle was reduced, 20% for the TF200 new membrane (e.g. from 140º ± 3º to 112º ± 11º), 11% for the TF450 new membrane (e.g. from 141º ± 1º to 125º ± 3º) and 27% for the TF450_ROB_328K membrane (e.g. from 132º ± 6º to 97º ± 4º). This can be attributed to the disappearance of the fibrillar structure and the subsequent decrease of the membrane surface roughness.

Fig. 4.6 shows the permeate flux, the feed and permeate concentrations together with the HA separation factor of both compacted and uncompacted new TF200 membranes. The initial permeate flux of the compacted membrane was lower than that of the uncompacted one due to the reduction of the pore size as indicated previously. However, during MF of HA solution the permeate fluxes of both membranes were declined and became almost similar after 30 min due to fouling effect. As it was expected the increase of the HA separation factor was faster and greater for the compacted membrane. Therefore, it can be concluded that a previous compaction process is completely necessary in order to improve the MF separation factor and to clean both the membrane surface and the pores of the recycled membranes previously used in AGMD.

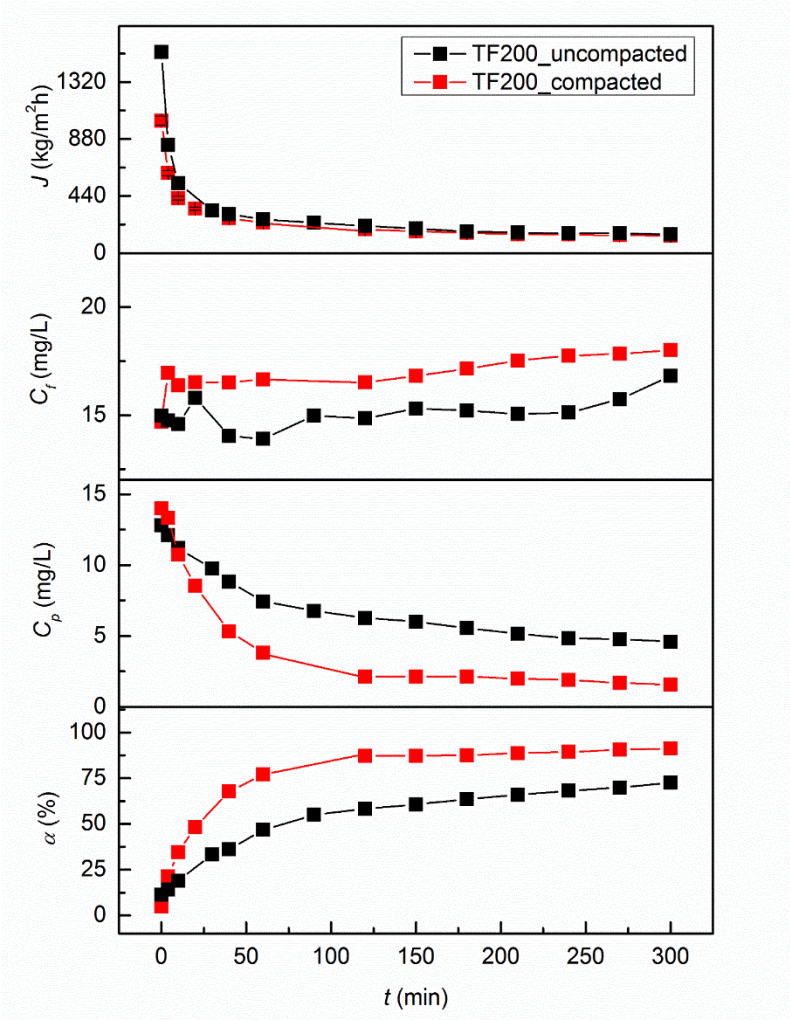

Figure 4.6. Effects of the membrane compaction of the new TF200 membrane on the MF permeate flux (*J*), feed (C_f) and permeate (C_p) concentration together with the HA separation factor (α) when using 15 mg/L HA solution at pH 11.

4.3.3. MF performance and fouling of reused AGMD membranes

The discarded AGMD membranes were first compacted as stated in the previous section. The results of the MF experiments using the recycled AGMD membranes are presented in Fig. 4.7. As it was expected, the initial permeate fluxes are higher for TF450 membranes due their greater pore size. The initial permeate flux value of the membrane TF450_SB_328K was slight higher (i.e. 2210 ± 110 kg/m^{2}h) than that of the membrane TF450_ROB_318K (i.e. 2098 ± 47 kg/m^{2}h). This is due to the higher fouling effect of ROB compared to SB as it was indicated previously, and to the fact that the membrane TF450_SB_328K was finally wetted due to crystals deposition. The same fouling effect can be confirmed for the TF200 membranes (i.e. 1800 ± 360 kg/m^{2}h for the membrane TF200_SB_348K and 1130 ± 80 kg/m^{2}h for the membrane TF200_ROB_318K). It was observed practically the same initial permeate concentration for the four membranes (i.e. ≈ 12 mg/L in Fig. 4.7).

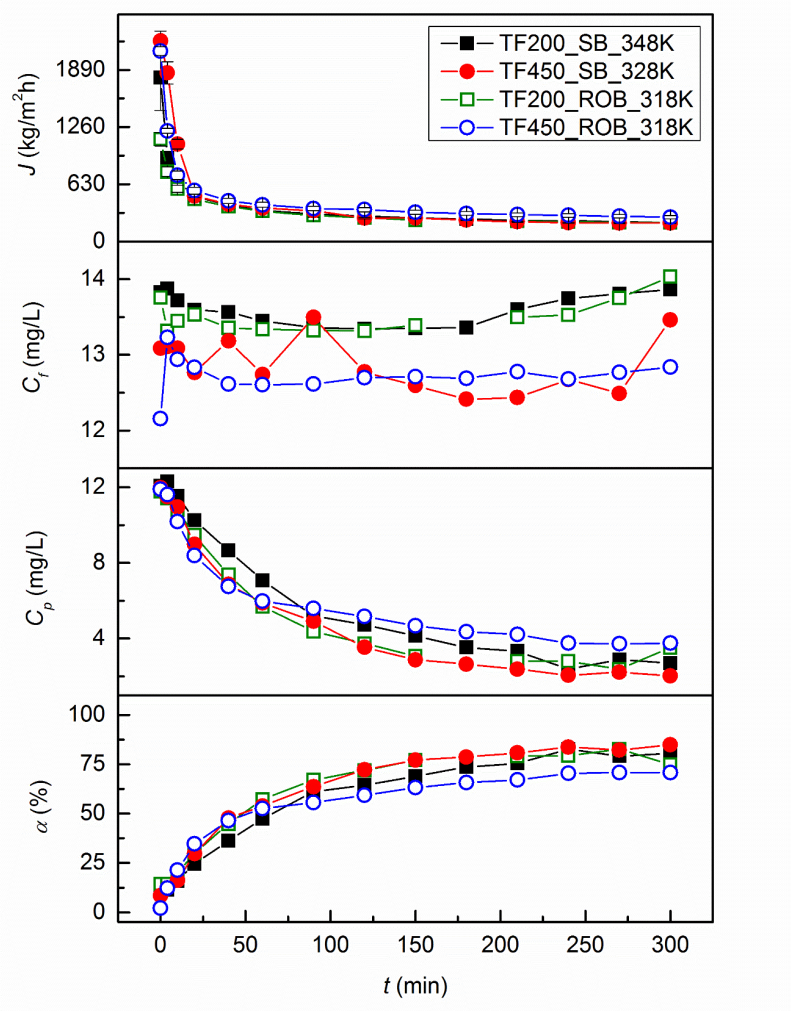

Figure 4.7. Evolution with time of the permeate flux (J), feed (C_f) and permeate (C_p) concentration together with the HA separation factor (α) of the recycled AGMD membranes during MF experiments using 15 mg/L HA solution at pH 11.

From Fig. 4.7, all used membranes in AGMD showed a rapid permeate flux decay with time principally at the beginning of the MF process and then a decrease of the rate of this reduction tending to asymptotic values. As it was indicated previously this is due to pore blockage caused by the physical deposition of large HA aggregates on the surface of the MF membrane and the subsequent cake formation in the last stage exerting therefore the main mass transport resistance of the MF process. For all recycled membranes, the operating time corresponding to the predominant change of the permeate flux decline was 30 min and the final permeate fluxes became almost the same for all membranes.

Similar tendencies as those observed for new TF200 and TF450 membranes at pH 11 (Fig. 4.4) were obtained for the recycled AGMD membranes (Fig. 4.7). The HA separation factor increased over time from zero to at least 70.8% in the worst case (i.e. for TF450_RO_318K membrane). The recycled membranes previously used in AGMD for the treatment of SB exhibited slightly higher separation factor values (i.e. 80.5% for the membrane TF200_SB_3248K and 85.0% for the membrane TF450_SB_328K) than those

of the recycled membranes used in AGMD for the treatment of ROB (i.e. 75.0% for the membrane TF200_ROB_318K and 70.8% for the membrane TF450_ROB_318K). This slight difference detected for the HA separation factor is associated to the initial state of the used membranes related with the change of the structure of the recycled membranes due to the effects of fouling effect.

The performance index ($PI = J_{final} \times \alpha_{final}$) of all membranes was calculated. For the new membranes TF200 and TF450, the *PI* values were quite similar, 122.7 and 123.9 kg/m^{2}h, respectively. For the recycled membranes, the *PI* values were higher (166.3 for the membrane TF200_SB_348K, 155.0 kg/m^{2}h for the membrane TF200_ROB_318K, 173.3 for the membrane TF450_SB_328K and 189.2 kg/m^{2}h for the membrane TF450_ROB_318K). In spite of the slightly lower HA separation factors achieved with the recycled AGMD membranes, their higher permeate fluxes resulted in better MF performance.

It was observed that the recycled TF200 membranes exhibited FR_W values of 92.2 and 86.2% depending on the previously used feed solution in the AGMD process, SB and ROB, respectively. The recycled TF450 membranes showed FR_W values of 91.1 and 89.5% when using SB and ROB, respectively. The new membranes had FR_W values of 80.2% for the membrane TF200 and 93.0% for the membrane TF450 due the higher permeate flux registered before carrying out MF experiment. The lower FR_W values of the recycled membranes used with ROB as feed in AGMD were attributed to the higher fouling effect (i.e. lower permeate fluxes of water before performing MF experiment).

The morphological characteristics of the recycled membranes were determined after MF experiments in order to study the HA fouling phenomena. Table 4.3 compares the final state of the membranes (after MF treatment) with their initial state (after AGMD treatment) and with the new membranes. The membrane thickness increased slightly after MF test due to the HA deposition on the membrane surface although compaction might reduce the PTFE layer thickness provided that PP support was practically incompressible under MF conditions.

After MF test, the mean pore size decreased by 44% for the membranes used in MF after AGMD with SB. The mean pore size reduction is lower for the membranes used in AGMD with ROB (39% for the membrane TF200_ROB_318K and 27% for the membrane TF450_ROB_318K) compared with that used in AGMD with SB. In addition, as result of the previous compaction process and the HA fouling layer, the water contact angle measurements were smaller than those obtained after AGMD test. The decrease in the contact angle values indicated the reduction of the hydrophobic character of the membrane surface layer.

4.4. Conclusions

Discarded wet and fouled PTFE membranes from use in AGMD process can be recycled and reused in MF for wastewater pretreatment. In general, it was found that the PTFE recycled membranes exhibited even better MF performance than the new membranes used for the treatment of HA aqueous solution at pH 11.

Compaction of the recycled membranes not only reduced the pore size and improved the HA separation factor as it occurred for the new membranes, but it also permitted to clean the membrane from foulants and crystals.

The pores of the TF450 membranes were more prone to be fouled and blocked either by ROB or SB foulants and HA particles than the smaller pores of the TF200 membranes. The membranes used in AGMD for the treatment of ROB showed lower initial MF permeate fluxes than those previously used in AGMD for the concentration of SB.

The discarded PTFE membranes from use in AGMD demonstrated to be useful in MF for the treatment of HA aqueous solutions, offering an economic and environmental important possibility for the future of both MD and MF technologies.

4.5. References

[1] M. Khayet, T. Maatsura, Membrane Distillation. Principles and Aplications, Elsevier B.V. , The Netherlands, 2011.

[2] J.A. Sanmartino, M. Khayet, M.C. García-Payo, H. El Bakouri, A. Riaza, Desalination and concentration of saline aqueous solutions up to supersaturation by air gap membrane distillation and crystallization fouling, Desalination, 393 (2016) 39.

[3] G. Zakrzewska-Trznadel, M. Harasimowicz, A.G. Chmielewski, Concentration of radioactive components in liquid low-level radioactive waste by membrane distillation, Journal of Membrane Science, 163 (1999) 257.

[4] B. Li, K.K. Sirkar, Novel membrane and device for vacuum membrane distillation-based desalination process, Journal of Membrane Science, 257 (2005) 60.

[5] D. Winter, J. Koschikowski, S. Ripperger, Desalination using membrane distillation: Flux enhancement by feed water deaeration on spiral-wound modules, Journal of Membrane Science, 423-424 (2012) 215.

[6] G.E.W.P. Technologies, I.m.c.s. C.F. SEPA, C.F. SEPA, II: membrane cell system, (2009).

[7] E. Guillén-Burrieza, J. Blanco, Z. G, D.C. Alarcón, P. Palenzuela, M. Ibarra, W. Gernjak, Experimental analysis of an air gap membrane distillation solar desalination pilot system, Journal of Membrane Science, 379 (2011) 386.

[8] E. Guillén-Burrieza, G. Zaragoza, S. Miralles-Cuevas, J. Blanco, Experimental evaluation of two pilot-scale membrane distillation modules used for solar desalination, Journal of Membrane Science, 409-410 (2012) 264.

[9] K. Zhao, W. Heinzl, M. Wenzel, S. Büttner, F. Bollen, G. Lange, S. Heinzl, N. Sarda, Experimental study of the memsys vacuum-multi-effect-membrane-distillation (V-MEMD) module, Desalination, 323 (2013) 150.

[10] J. Landaburu-Aguirre, R. García-Pacheco, S. Molina, L. Rodríguez-Sáez, J. Rabadán, E. García-Calvo, Fouling prevention, preparing for re-use and membrane recycling. Towards circular economy in RO desalination, Desalination, 393 (2016) 16.

[11] W. Lawler, Z. Bradford-Hartke, M.J. Cran, M. Duke, G. Leslie, B.P. Ladewig, P. Le-Clech, Towards new opportunities for reuse, recycling and disposal of used reverse osmosis membranes, Desalination, 299 (2012) 103.

[12] N. Hankins, R. Singh, Emerging Membrane Technology for Sustainable Water Treatment, Elsevier B.V., 2016.

[13] P. Arribas, M. Khayet, M.C. García-Payo, L. Gil, Self-sustained electro-spun polysulfone nano-fibrous membranes and their surface modification by interfacial polymerization for micro- and ultra-filtration, Separation and Purification Technology, 138 (2014) 118.

[14] M.N.A. Seman, M. Khayet, N. Hilal, Nanofiltration thin-film composite polyester polyethersulfone-based membranes prepared by interfacial polymerization, Journal of Membrane Science, 348 (2010) 109.

[15] S.P. Pinho, E.A. Macedo, Solubility of NaCl, NaBr, and KCl in water, methanol, ethanol, and their mixed solvents, Journal of Chemical & Engineering Data 50 (1) (2004) 29.

[16] M. Gryta, Fouling in direct contact membrane distillation process, Journal of Membrane Science, 325 (2008) 383.

[17] E. Guillen-Burrieza, R. Thomas, B. Mansoor, D. Johnson, N. Hilal, H. Arafat, Effect of dry-out on the fouling of PVDF and PTFE membranes under conditions simulating intermittent seawater membrane distillation (SWMD), Journal of Membrane Science, 438 (2013) 126.

[18] M. Gryta, Long-term performance of membrane distillation process, Journal of Membrane Science, 265 (2005) 153.

[19] M. Gryta, Alkaline scaling in the membrane distillation process, Desalination, 228 (2008) 128.

[20] D.M. Warsinger, J. Swaminathan, E. Guillen-Burrieza, H.A. Arafat, J.H. Lienhard V, Scaling and fouling in membrane distillation for desalination applications: A review, Desalination, 356 (2015) 294.

[21] A. Al-Amoudi, R.W. Lovitt, Fouling strategies and the cleaning system of NF membranes and factors affecting cleaning efficiency, Journal of Membrane Science, 303 (2007) 4.

[22] E. Guillen-Burrieza, A. Ruiz-Aguirre, G. Zaragoza, H.A. Arafat, Membrane fouling and cleaning in long term plant-scale membrane distillation operations, Journal of Membrane Science, 468 (2014) 360.

[23] L.D. Tijing, Y.C. Woo, J.S. Choi, S. Lee, S.-H. Kim, H.K. Shon, Fouling and its control in membrane distillation—A review, J. Membr. Sci., 475 (2015) 215-244.

[24] A.E. Childress, M. Elimelech, Effect of solution chemistry on the surface charge of polymeric reverse osmosis and nanofiltration membranes, Journal of Membrane Science, 119 (1996) 253.

[25] S. Hong, M. Elimelech, Chemical and physical aspects of natural organic matter (NOM) fouling of nanofiltration membranes, Journal of Membrane Science, 132 (1997) 159.

[26] R.S. Swift, Humic Substances II, In Search of Structure, Molecular Weight, Size, Shape, and Charge Characteristics of Humic Substances: Some Basic Considerations. Herausgeber, 1989.

[27] M. Plaschke, J. Römer, R. Klenze, J.I. Kim, In situ AFM study of sorbed humic acid colloids at different pH, Colloids and Surfaces A: Physicochemical and Engineering Aspects, 160 (1999) 269.

[28] C. Duclosorsello, Neutral adsorptive capture of particles by membranes: network modeling near the membrane isoelectric point, Journal of Membrane Science, 237 (2004) 167.

[29] T. Preočanin, A. Selmani, P. Lindqvist-Reis, F. Heberling, N. Kallay, J. Lützenkirchen, Surface charge at Teflon/aqueous solution of potassium chloride interfaces, Colloids and Surfaces A: Physicochemical and Engineering Aspects, 412 (2012) 120.

[30] F. Hamadi, H. Latrache, M. Zekraoui, M. Ellouali, J. Bengourram, Effect of pH on surface energy of glass and Teflon and theoretical prediction of Staphylococcus aureus adhesion, Materials Science and Engineering C: Materials for Biological Applications, 29 (2009) 1302.

[31] M. Manciu, E. Ruckenstein, Ions near the air/water interface. II: Is the water/air interface acidic or basic? Predictions of a simple model, Colloids and Surfaces A: Physicochemical and Engineering Aspects, 404 (2012) 93.

[32] W. Yuan, A.L. Zydney, Effects of solution environment on humic acid fouling during microfiltration, Desalination, 122 (1999) 63.

[33] K. Xiao, X. Wang, X. Huang, T.D. Waite, X. Wen, Combined effect of membrane and foulant hydrophobicity and surface charge on adsorptive fouling during microfiltration, Journal of Membrane Science, 373 (2011) 140.

[34] R. S. Astaraee, T. Mohammadi, N. Kasiri, Analysis of BSA, dextran and humic acid fouling during microfiltration, experimental and modeling, Food and Bioproducts Processing, 94 (2015) 331.

Chapter 5

Modelling and optimization of a solar forward osmosis pilot plant by response surface methodology

Forward osmosis (FO) is a water treatment/separation technology of emerging interest. Due to its complex nature involving various operating parameters, modelling of this separation process is challenging. A solar thermal and photovoltaic-powered FO pilot plant has been optimized by means of a statistical experimental design and response surface methodology. Predictive models were developed for simulation and optimization of different responses such as the water permeate flux, the reverse solute permeate flux and the FO specific performance index that includes the water and reverse solute permeate fluxes together with the energy consumption. The considered input variables of the FO pilot plant were the feed flow rate, the permeate flow rate and the temperature. The developed response models have been tested using the analysis of variance. A Monte Carlo simulation method has been conducted to determine the optimum operating conditions of the FO pilot plant. The obtained optimum parameters were confirmed experimentally. Regeneration of the draw solution can be performed by means of an optimized solar powered reverse osmosis (RO) pilot plant with an optimum FO specific performance index ranging from 25.79 to 0.62 L/g.kWh achieved under the FO optimal conditions, 0.83 L/min feed flow rate, 0.31 L/min draw solution flow rate and 32.65ºC temperature. The FO energy consumption is only 14.1% the total energy consumption of the FO/RO hybrid system.

5.1. Introduction

Membrane technologies experienced important developments during last decades allowing significant increases in water production with high quality and low energy consumption. These are attributed mainly to a wide range of available advanced materials, novel and efficient technologies as well as to the well-known increasing demand of water supply and sanitation. The worldwide renewed interest in the osmotically driven membrane processes such as forward osmosis (FO) and pressure retarded osmosis (PRO) has increased tremendously in the last few years [1-8].

Osmosis is the transport of water across a semi-permeable water selective membrane from a feed solution of higher water chemical potential to a solution of lower water chemical potential (i.e. higher osmotic pressure or higher salt concentration) known as a draw solution. The membrane ideally permits the passage of water rejecting solute(s) molecules or ions. Fig. 5.1 shows four possible situations that can occur when a semi-permeable water selective membrane is placed in direct contact with pure water and a saline aqueous solution given here as an example. Once water starts moving through the membrane, the hydrostatic pressure at the permeate side of the membrane becomes higher than that of the feed side, resulting in a transmembrane hydrostatic pressure (ΔP) higher than zero. The water flux stops when ΔP equals the osmotic pressure difference ($\Delta\pi$) established between the feed and the permeate. This is the pressure which, if applied to the saline solution, would prevent transport of water across the membrane.

FO occurs when the only transmembrane driving force for water flux is the osmotic pressure difference ($\Delta\pi$) (see Fig. 5.1). In other words, no transmembrane hydrostatic pressure is applied ($\Delta P = 0$). In this case, a high concentration solution (i.e. draw solution) is separated from a low concentration solution by a water selective semi-permeable membrane. The concentration gradient between both the feed and draw solution induces a transmembrane $\Delta\pi$. Consequently, water flows spontaneously through the membrane from the low concentration side to the draw solution side. In FO mode, generally both the feed solution to be treated and the draw solution are circulated tangentially to each side of the membrane module. The used membranes have an asymmetric structure consisting of an active dense or porous layer with pore sizes below 10 nm and a support layer. Various types of osmotic solutions are considered (i.e. sucrose, glucose, $MgCl_2$, $CaCl_2$, NaCl, KCl, etc.) [3, 9]. Some advantages of FO are its potential low energy consumption (i.e. electric energy) to run the circulation pumps as well as its high rejection of a wide range of contaminants. One of the problems of FO is the reverse permeate flux of the draw solute, which must be minimal. FO is being applied in various separation processes such as in wastewater treatment, food processing, seawater or brackish water desalination [4, 6-8].

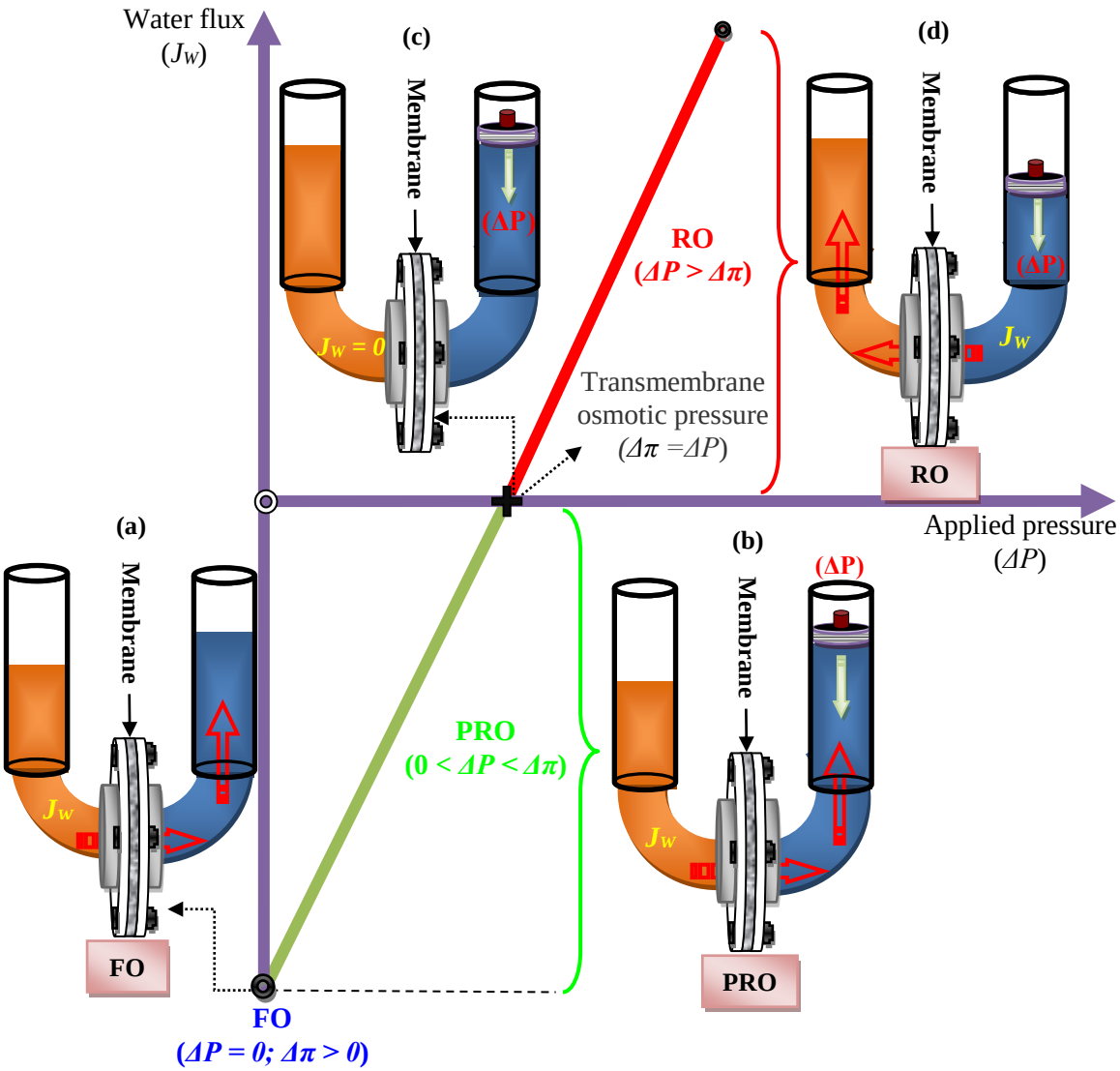

Figure 5.1. Schematic presentation of possible osmotic situations showing the water permeate flux (J_w) as a function of the transmembrane hydrostatic pressure (ΔP): (a) FO, (b) PRO, (c) No water permeate flux (J_w=0) and (d) RO.

PRO is an intermediate process between FO and the well-known reverse osmosis (RO) technology, where the hydraulic pressure is applied in the opposite direction of the osmotic pressure gradient. In this case, water from a low salinity aqueous solution permeates through a semi-permeable water selective membrane into a pressurized high salinity solution (i.e. seawater). The additional water volume increases the pressure in the permeate side of the PRO membrane module. The power (termed also osmotic power) is then obtained by depressurizing the permeate through, for example, a hydro-turbine. PRO is similar to RO, but in PRO process the applied pressure is maintained below $\Delta\pi$. It must be pointed out that when the applied ΔP is lower than $\Delta\pi$ (Fig. 5.1), the water permeate flux is still driven by $\Delta\pi$ in the direction of the concentrated draw solution. The interesting application area of PRO is the generation of electricity [1, 5]. When the

applied hydrostatic pressure ΔP is greater than $\Delta\pi$ (Fig. 5.1), the direction of the water flux is reversed leading to the well-known RO separation process used mainly in seawater desalination [10-13]. Since 1990s the development of low pressure (i.e. high permeability) RO membranes has progressed rapidly [12, 14].

FO technology is still in continuous improvements trying to overcome the many-faced challenges and barriers in order to extend its fields of industrial application. As stated previously, the growing interest of FO is attributed mainly to its lower energy consumption compared to other technologies and to its wider possibility to be coupled to other separation processes including RO for water production and regeneration of the used draw solution [7, 15-21]. It is worth quoting that actual improvements of FO technology, that can contribute to more competitive FO plants achieving significant reductions of energy consumption and water production cost, are focused on the development of FO fouling resistant membranes with low internal concentration polarization coefficients (*ICP*), the design of non-toxic draw solutions with higher osmotic pressures, the combination of FO installation to solar energy systems and the optimization of FO operating factors. As far as we know still there is no published paper on the utilization of renewable energy sources such as wind energy and solar energy systems (i.e. thermal collectors and photovoltaic panels, PV) to run FO plants. Schrier [7] used the solar evaporation for regeneration of the draw solution by removing excess of water using FO for production of fuel-grade ethanol. It is also noted that all the studies reported so far on FO deal with the conventional method of experimentation, in which the effect of an operation variable on the FO system performance is investigated keeping the other variables fixed. This classical or conventional method of experimentation requires many experimental runs, which take a lot of time especially for FO pilot plant tests, ignores the interaction effects between the operating parameters and leads to a low efficiency in optimization resulting in a high-energy consumption. These limitations of the classical method of experimentation can be avoided by applying the response surface methodology (RSM) that involves statistical design of experiments (DoE) in which all factors are varied simultaneously over a set of experimental runs. In fact, RSM is a collection of mathematical and statistical techniques useful for developing, improving and optimizing processes, and can be used to evaluate the relative significance of several affecting factors even in the presence of complex interactions between them using a minimum number of experiments [12, 22, 23]. In this methodology, all factors are simultaneously varied between minimum and maximum values. It is worth quoting that RSM has been applied successfully in various scientific and technical fields [12, 24-31]. In the present study, the central composite experimental design (CCD) and RSM has been applied to model and optimize a solar FO pilot plant. The objective is to ensure a high-water production rate of the FO pilot plant with a low reverse solute permeability and reduced energy consumption.

5.2. Experimental

5.2.1. Description of the solar FO pilot plant

A schematic diagram of the FO pilot plant used for experimental design is shown in Fig. 5.2. It is equipped with a commercial spiral wound membrane module (2521FO-CS, Hydration Technology Innovation LLC, HTI, Albany, OR, USA) having an effective membrane area of 0.35 m^2. This is fabricated using a corrugated spacer (CS) with 2.5 mm polystyrene chevron design flow path and the membrane 120629-ES-2(CTA-ES). The temperature limit of the membrane as indicated by the manufacturer (HTI) is 0 - 43ºC. The membrane housing is Axeon 2521 PVC and GTX material (AXEON Water Technologies, Temecula, USA). The maximum differential pressure through the side ports of the feed solution (outlet and inlet of the feed solution) is recommended to be below 50 kPa. The maximum pressure of the draw solution entering the end port of the membrane module is recommended to be 70 kPa. The feed and draw solution circulates tangentially to the membrane surfaces in a co-current configuration. The FO plant consists of feed and permeate double wall containers, two circulation pumps (Totton magnetically coupled centrifugal pumps DC 40/0, 12 Volt DC 12 Amps) connected to each container. As can be seen in Fig. 5.2, the pilot plant is equipped with vents, temperature sensors, pressure gauges, flow-meters, etc. The temperatures and pressures were measured at the inlets and outlets of the membrane module by Pt100 sensors connected to a digital multimeter (FLUKE HYDRA) and manometers (Wika, 0-250 kPa), respectively. The flow rates of the feed and permeate were recorded by pulse flow controllers (RS 511-3892). The temperatures of the circulating liquids were adjusted through glass heat exchangers. The energy consumption of the circulation pumps, thermostat and the whole FO pilot plant (electrical and thermal) were measured independently by means of Velleman NETBSEM2 (wattage 5 W – 4416 W) apparatus.

The operating variables of the FO pilot plant are the flow rate of the feed aqueous solution (ϕ_F), the flow rate of the draw solution or permeate (ϕ_P) and the inlet temperature of both the feed and permeate (T). The feed inlet pressure (P_F), the permeate inlet pressure (P_P) and the initial concentration of the draw solution (C_p) were maintained the same. In this study, the used draw solution is a saline aqueous solution of 35 g/L (NaCl) and the inlet feed and permeate pressures were kept below 30 kPa.

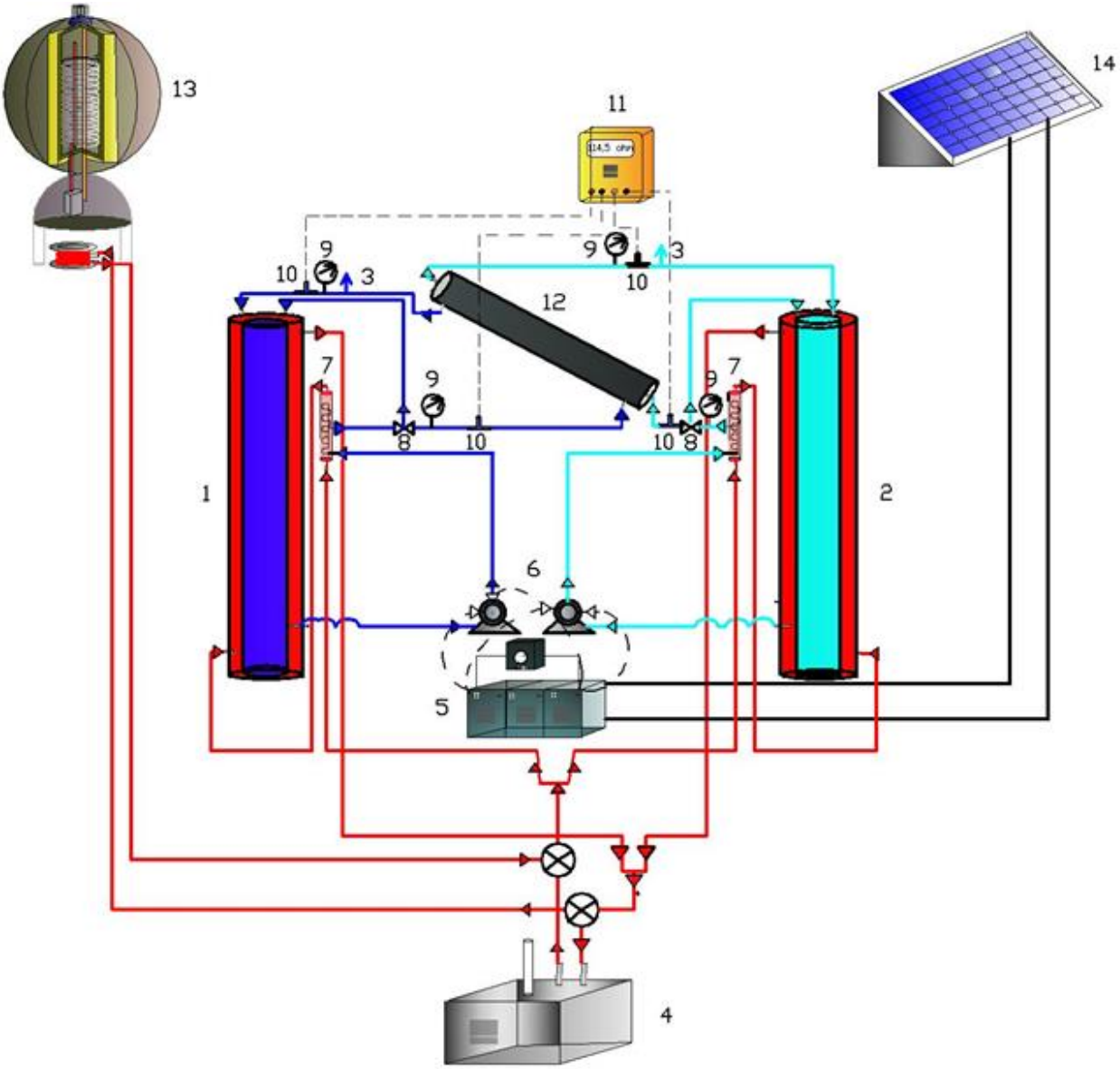

Figure 5.2. Basic scheme of the FO pilot plant used to carry out the experimental design: 1-Feed container; 2-Permeate container; 3-Liquid sample collector for analysis; 4-Thermostat; 5-Batteries; 6-Circulation pumps; 7-Heat exchanger; 8-Valves; 9-Manometers; 10-Temperature sensors; 11-Digital multimeter; 12-Membrane module; 13-Thermal solar collector; 14-Photovoltaic panel.

To carry out the first part of the study dealing with experimental design, either a thermostat (Tamson Holland, Type: TX 3/150, Gomensoro S.A.) was used to maintain the inlet temperature between 31ºC and 42ºC or a cryostat (Polyscience Recirculator, Hz/A/Ph: 50/5.6/1) for lower temperatures than 31ºC. In the second part of the study, the temperature of the feed and permeate solution were controlled by coupling a solar thermal collector to the containers of the FO pilot plant through their jackets and glass heat exchangers permitting to adjust the temperature at the required value. The solar thermal collector has a spherical geometry with a diameter of 1.05 m and an effective collection area of 4 m^2. The absorber plate is made of copper with a selective coating layer of

titanium oxide. The whole collector is protected by a methacrylate cover of 3 mm thickness. The liquid solution used for heat transfer is made of water and glycol with a working temperature range of -10 ºC to 100ºC. The collector contains an internal thermal tank made of stainless steel (AISI 304) coated with polyurethane with a capacity of 150 L. Inside the tank, there is a heat exchanger, also made of stainless steel. The hydraulic circuit of the collector is connected to a circulation pump (40 W). The controller unit Multical 401 provided by the company Kamstrup (Germany) was used to record the temperatures as well as the liquid flow-rates. An automatic data acquisition system (SAD, DC-100, Yogagawa) was used to record every 5 seconds the temperatures using Pt-100 sensors and the liquid flow-rate. A pyranometer (Skye-TORN) was employed to measure the global irradiation on horizontal plane. More details may be found in [12].

The two circulation pumps (for feed and permeate in Fig. 5.2) working on DC voltage were run by a set of 3 batteries (Master Vision AGM, MV100Ah–12V) powered by a PV flat panel (monocrystalline silicon of 33 Wp). In order to minimize the heat loss of the FO pilot plant, the membrane module, the containers and pipes were insulated.

The water permeate flux (J_w) was determined by recording the height (i.e. volume) variation (ΔV) of both the feed and permeate during a predetermined time (Δt = 30 min in this study). This can be calculated from:

$$J_w = \frac{\Delta V}{A\ \Delta t} \tag{5.1}$$

where A is the effective membrane area.

The salt concentrations of the feed or retentate and permeate were determined in real time by a calibrated electrical conductivimeter (Ω Metrohm) every 30 minutes. The reverse solute permeate flux (J_s) can be calculated for a predetermined time from the concentration (C_f) and volume (V_f) of the feed solution using the following equation:

$$J_s = \frac{\Delta(C_f V_f)}{A\ \Delta t} \tag{5.2}$$

5.2.2. Experimental statistical design

The statistical design of experiments (DoE) is a structured method of experimentation in which all factors are varied simultaneously. In this study, an orthogonal central composite design (CCD) with star points was employed with 3 factors and 5 levels. Table 5.1 shows the controllable variables (i.e. factors) and their levels in actual and coded values calculated as follows:

$$x_i = \frac{z_i - z_i^0}{\Delta z_i} \quad \forall\ i = 1,2,3 \tag{5.3}$$

$$z^0 = \frac{z_{max} + z_{min}}{2} \tag{5.4}$$

$$\Delta z = \frac{z_{max} - z_{min}}{2} = z_{max} - z^0 = z^0 - z_{min} \tag{5.5}$$

where z is the actual value of the operating variable, x is the coded value, z_{max} is the maximum actual value corresponding to x = +1, z_{min} is the actual minimum value corresponding to x = -1 and the subscript i refers to the feed flow rate, ϕ_F (i = 1), draw solution flow rate, ϕ_P (i = 2) and the inlet temperature, T (i = 3).

The CCD design consists of 16 experiments with 8 orthogonal design points (i.e. factorial points), 6 star points to form the central composite design with $\alpha = \pm 1.215$ and 2 centre points for replication. α is the star point in the experimental design that gives the limits of the valid region of experimentation, Ω [$x_j \in \Omega$; $\Omega = \{x_j \mid -\alpha \leq x_j \leq +\alpha\}$; $\forall j$=1,2,3]. The experimental design matrix is summarized in Table 5.2. The 8 top experiments in this table correspond to the orthogonal design, the 6 following are the axial experiments with "star points" to form the central composite design and finally the last two experiments are replicate experiments to estimate the experimental error for each response. Each experimental run was performed for 4 hours and the volumes (i.e. heights of the feed and permeate containers) together with the salt concentrations of the feed and draw solution, their flow rates, temperatures and pressures were registered with time together with the energy consumption.

Table 5.1. Actual and coded values of the independent variables used for the experimental design of the solar powered FO pilot plant.

Variable	Symbol	Real values of coded levels				
		$-\alpha$ [a]	-1	0	+1	$+\alpha$ [a]
ϕ_F (L/min)	x_1	0.050	0.121	0.450	0.779	0.850
ϕ_P (L/min)	x_2	0.050	0.094	0.300	0.506	0.550
T (ºC)	x_3	20.07	22.00	31.00	40.00	41.94

[a] α = 1.215 (star or axial point for orthogonal CCD in the case of 3 independent variables).

Fig. 5.3 shows as an example the determined permeate flux (J_w) from the volume of the permeate container. The decrease of J_w with time is not linear due to the reduction of the salt concentration of the draw solution indicating that the dilution of the draw solution is not negligible in this case. The high permeate fluxes correspond to the runs 1 and 13, which were carried out applying the highest temperatures (40-41.94ºC) and moderate/high feed and permeate flow rates (0.300-0.779 L/min). In contrast, the lowest permeate fluxes were observed for the runs 6 and 8, which corresponds to the lowest temperature (22ºC) and the lowest feed and permeate flow rates (0.094-0.121 L/min). In order to determine the average permeate flux J_w of each experimental run, $J_w(t)$ was first fitted to the following polynomial regression equation:

$$J_w(t) = a_0 + a_1 t + a_2 t^2 + a_3 t^3 \tag{5.6}$$

where the regression coefficients a_0, a_1, a_2 and a_3 were computed via the least square method. All the experimental data were fitted well with reasonably high correlation coefficients (i.e. $R^2 > 0.972$). Then the average permeate flux J_w was calculated as:

$$J_w = \frac{1}{t_n} \int_{t_1}^{t_n} J_W(t) dt \tag{5.7}$$

where t_1 is the initial time, 30 minutes in this study, and t_n is the final time, 4 hours. The results are summarized in Table 5.2.

The reverse solute flux (J_s) was calculated using Eq. (5.2). Providing that the variation of ($C_f V_f$) is not linear with time, the average value of J_S was determined following the same procedure as J_w (i.e. regression analysis using Eqs. 5.6 and 5.7). It was also noted that the variation with time of the salt concentration of both the feed (C_f) and permeate (C_p) aqueous solutions were not linear. The obtained average value of J_s for each experimental run is also reported in Table 5.2. During any FO process, there is a loss of the draw solute due to the reverse solute permeate flux (J_s) and the ratio (J_w/J_s), termed the reverse solute flux selectivity, must be maximized [8].

In this study, the output responses of the FO pilot plant are J_w, J_s, the ratio (J_w/J_s), the total energy consumption (E_c), the specific water permeate flux ($J_{w,sp}$) defined as:

$$J_{w,sp} = \frac{J_w}{E_c} \tag{5.8}$$

and the specific FO performance index (Y_{sp}) defined as:

$$Y_{sp} = \frac{J_w}{J_s \, E_c} \tag{5.9}$$

It is worth quoting that in FO process, J_W must be high whereas J_s and E_c must be as low as possible. Providing that $J_{w,sp}$ does not take into consideration J_s, Y_{sp} was used as response, since it takes into consideration J_w, J_s and E_c and must be as high as possible.

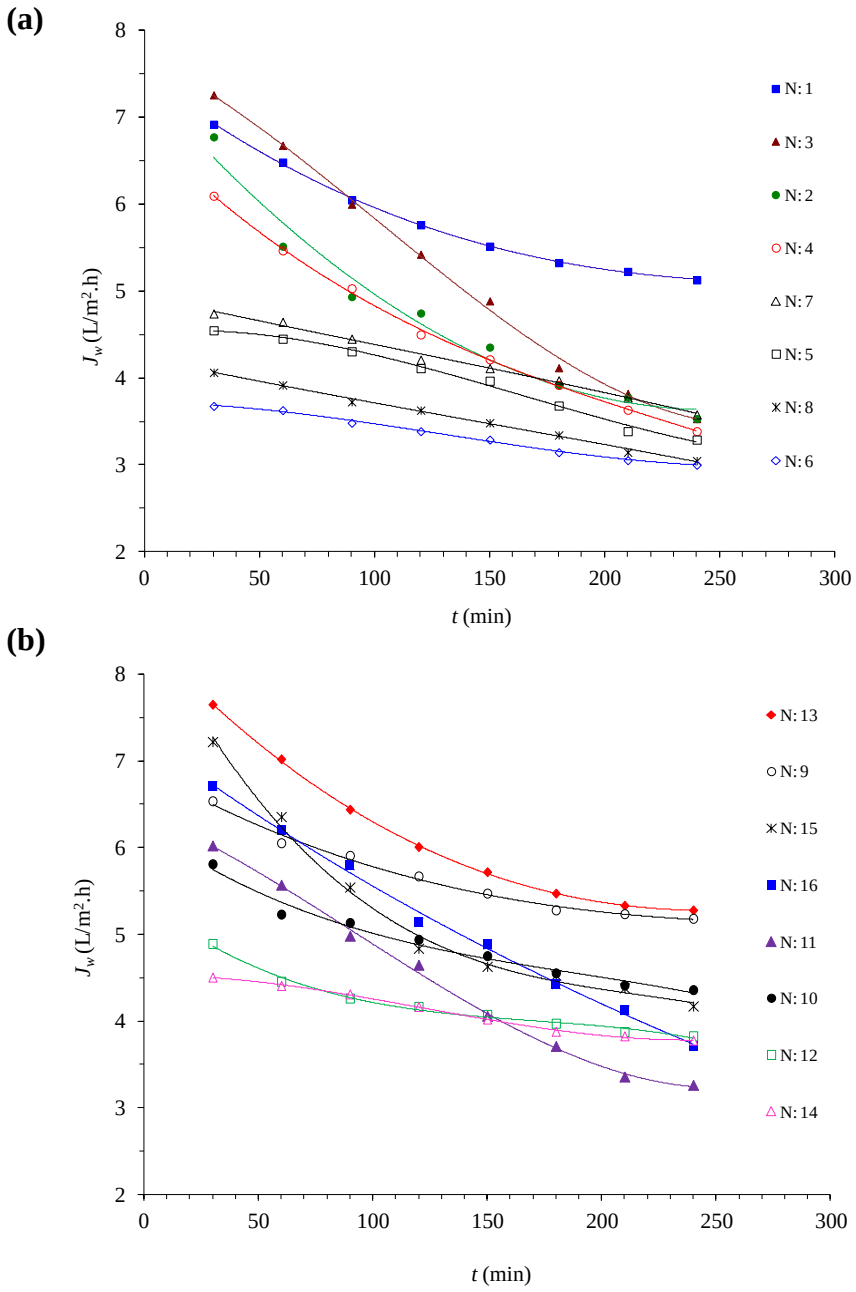

Figure 5.3. FO water permeate flux (J_w) of different experimental runs versus time. The solid lines represent the fitting curves to Eq. (5.6). (a) Orthogonal design tests and (b) Axial and centre design tests.

Table 5.2. CCD experimental design (DoE) used to model the solar powered FO pilot plant and the obtained responses.

Run number and type [a]		Design factors						Responses					
		ϕ_F (L/min)		ϕ_P (L/min)		T (ºC)		J_W (L/m^2.h)	J_S (g/m^2.h)	J_W/J_S (L/g)	E_c (kWh)	$J_{W,sp}$ (L/kwh)	Y_{sp} (L/g.kwh)
N		x_1 [b]	ϕ_F (L/min)	x_2 [b]	ϕ_P (L/min)	x_3 [b]	T (ºC)						
1	O1	+1	0.779	+1	0.506	+1	40.00	5.77	2.89	1.996	1.081	7.47	1.846
2	O2	-1	0.121	+1	0.506	+1	40.00	4.63	3.08	1.504	1.079	6.01	1.394
3	O3	+1	0.779	-1	0.094	+1	40.00	5.19	2.97	1.745	1.080	6.73	1.616
4	O4	-1	0.121	-1	0.094	+1	40.00	4.50	3.43	1.311	1.304	4.83	1.005
5	O5	+1	0.779	+1	0.506	-1	22.00	3.98	2.99	1.334	2.119	2.63	0.629
6	O6	-1	0.121	+1	0.506	-1	22.00	3.33	3.20	1.042	2.069	2.26	0.504
7	O7	+1	0.779	-1	0.094	-1	22.00	4.19	3.09	1.355	2.185	2.69	0.620
8	O8	-1	0.121	-1	0.094	-1	22.00	3.55	3.53	1.004	2.231	2.23	0.450
9	S1	+α	0.850	0	0.300	0	31.00	5.64	3.11	1.812	0.582	13.55	3.111
10	S2	-α	0.050	0	0.300	0	31.00	4.87	3.62	1.346	0.584	11.69	2.306
11	S3	0	0.450	+α	0.550	0	31.00	4.42	2.68	1.651	0.800	7.73	2.064
12	S4	0	0.450	-α	0.050	0	31.00	4.16	3.03	1.374	0.584	9.98	2.351
13	S5	0	0.450	0	0.300	+α	41.94	6.06	3.25	1.866	1.284	6.60	1.453
14	S6	0	0.450	0	0.300	-α	20.07	4.11	3.18	1.290	2.032	2.83	0.635
15	C1	0	0.450	0	0.300	0	31.00	5.11	3.14	1.627	0.593	12.06	2.745
16	C2	0	0.450	0	0.300	0	31.00	5.12	3.13	1.633	0.584	12.26	2.795

[a] O= orthogonal design points, C= centre points, S = star or axial points.
[b] −1 = low value, 0 = centre value, +1 = high value, +/−α = star point value.

5.3. Results and discussions

5.3.1. RSM models

FO experiments have been carried out according to the experimental design summarized in Table 5.2. The obtained results (responses) are also presented in Table 5.2.

The RSM models have been developed for the responses, J_w, J_s, J_w/J_s, $J_{w,sp}$ and Y_{sp} defined in the previous section. Each response has been linked to the coded factors x_1, x_2 and x_3 by a 2nd order polynomial model with interactions as shown in the following equation [23, 27, 28]:

$$\hat{Y} = \beta_0 + \sum_{i=1}^{k} \beta_i x_i + \sum_{i=1}^{k} \beta_{ii} x_i^2 + \sum_{j} \sum_{i=1(i<j)}^{k} \beta_{ij} x_i x_j + \varepsilon \quad (5.10)$$

where $\hat{Y}$ is the predicted response, x_i and x_j ($j = k+1$, $i < j$) are the coded independent variables (factors), β_0, β_1, …, β_k, β_{ij} are the regression coefficients and ε is the statistical error.

The regression coefficients of the RSM model were computed by means of Multiple Linear Regression (MLR) method in order to minimize the sum of squares of the residuals. The least square estimations of the regression coefficients were calculated by the following matrix equation [23, 27, 28, 32]:

$$B = (X^T X)^{-1} X^T Y \quad (5.11)$$

where B is the vector formed by the regression coefficients, X is the matrix ($N \times u$) of the independent variables, u is the number of regression coefficients in the RSM model (Eq. 10) and Y is a vector ($N \times 1$) formed by the responses of the N experiments. According to this method the β coefficients are determined by the method of least squares (i.e. the β values are chosen in order to minimize the sum of squared residuals). For each response, first the regression coefficients using the coded variables have been determined. Subsequently, the regression coefficients corresponding to the actual variables have been calculated as shown below.

5.3.1.1. RSM model of the water permeate flux (J_w)

The obtained regression equation of J_w in terms of the coded variables is:

$$\hat{Y} = 5.2261 + 0.3692x_1 + 0.0547x_2 + 0.676x_3 - 0.6733x_2^2 - 0.1387x_3^2 + 0.056x_1x_2 + 0.0666x_1x_3 + 0.1414x_2x_3 \quad (5.12)$$

The regression coefficients were tested for significance using Student's *t*-test. Therefore, in the above equation only the significant coefficients were maintained. The regression coefficient b_{11} is found to be negligible. The empirical model obtained in terms of actual parameters is determined and written in general form as follows:

$$J_w = 0.3741 + 0.177\phi_F + 7.0492\phi_P + 0.1483T - 15.8662\phi_P^2 - 1.712310^{-3}T^2 + 0.8263\phi_F\phi_P + 0.0225\phi_F T + 0.0763\phi_P T \quad (5.13)$$

where: 0.050 L/min ≤ ϕ_F ≤ 0.850 L/min; 0.050 L/min ≤ ϕ_P ≤ 0.550 L/min and 20.07 ºC ≤ T ≤ 41.94 ºC.

The RSM model was validated statistically for adequacy by analysis of variance (ANOVA) and the obtained results are summarized in Table 5.3.

Table 5.3. Analysis of variance (ANOVA) for the developed RSM model of J_w.

Source	***DF***[a]	***SS***[b]	***MS***[c]	***F-value***	***F-tab***	R^2	R_{adj}^2
Model	9	9.017826	1.00198	38.206	3.8	0.9828	0.957
Residual	6	0.157356	0.02623				
Total	15	9.175182					

[a]*DF* - degree of freedom; [b]*SS* - sum of squares; [c]*MS* – mean square.

The statistical significance of the second-order regression model was determined by *F*-value, which is a measurement of variance of data about the mean, based on the ratio of mean square of group variance due to error. If the model gives a good prediction of the experimental data then the calculated *F*-value should be greater than the tabulated *F*-value, 3.8 in this case. For the RSM model of J_w, the calculated *F*-value is found to be much greater than 3.8 (i.e. three variables). This means that the developed model is valid from statistical standpoint and it is a good predictor of the experimental data. Moreover, the R^2-value is 0.9828, which is desirable. This implies that more than 98.28% of the data deviation can be explained by the developed empirical model. Furthermore, the predicted R^2 values are in agreement with the adjusted statistics R^2_{adj}. This means that only significant terms have been included in the empirical model. All the above cited statistical estimators show that the RSM model for J_w is statistically accepted for prediction of J_w in

a wide range of the valid region of experimentation. Figure 5.4 presents the comparison of J_w calculated by the RSM model and the experimental one obtained in each test (Table 5.2). This comparison shows a good agreement between the predicted J_w values and the corresponding experimental ones.

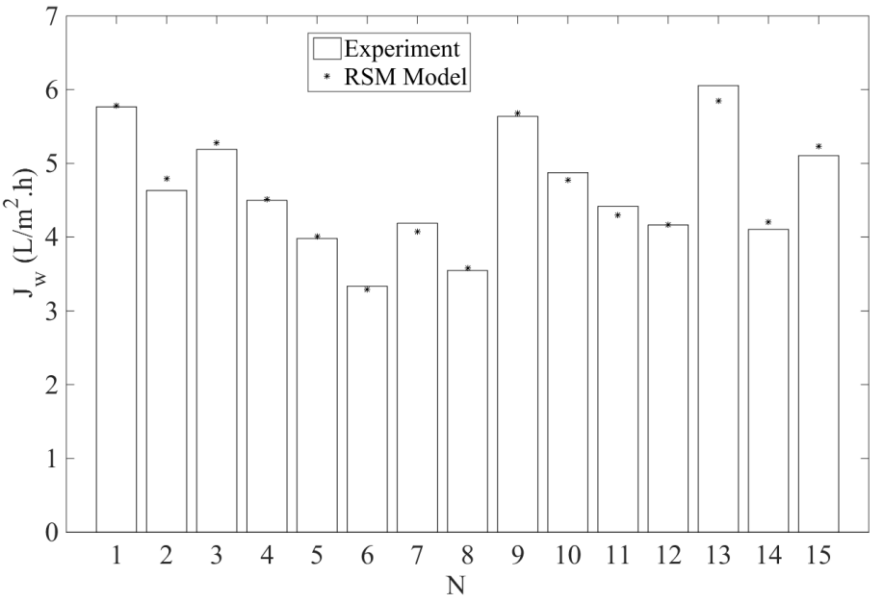

Figure 5.4. Experimental and predicted FO water permeate flux (J_w) of different experimental runs indicated in Table 5.2.

The effects of the FO operating variables on J_w are shown in Fig. 5.5. The curves were obtained using the RSM model (Eq. 5.13). It can be seen the gradual increase of J_w with the increase of both ϕ_F and T for all values of ϕ_P. These results are due to the reduction of the thickness of the feed boundary layer with the increase of ϕ_F leading to lower polarization effect and to the increase of both the solubility and diffusivity membrane parameters with the increase of T [33]. However, a maximum J_w is observed with the variation of ϕ_P for all ranges of ϕ_F and T. The increase of J_w up to a maximum with the increase of ϕ_P is due to the reduction of both temperature and concentration polarization effects. The increase of ϕ_P reduced the external concentration polarization effect and therefore increased both J_w and J_s. The subsequent decline of J_w may be attributed to the rapid loss of the draw solute of the permeate for higher ϕ_P values.

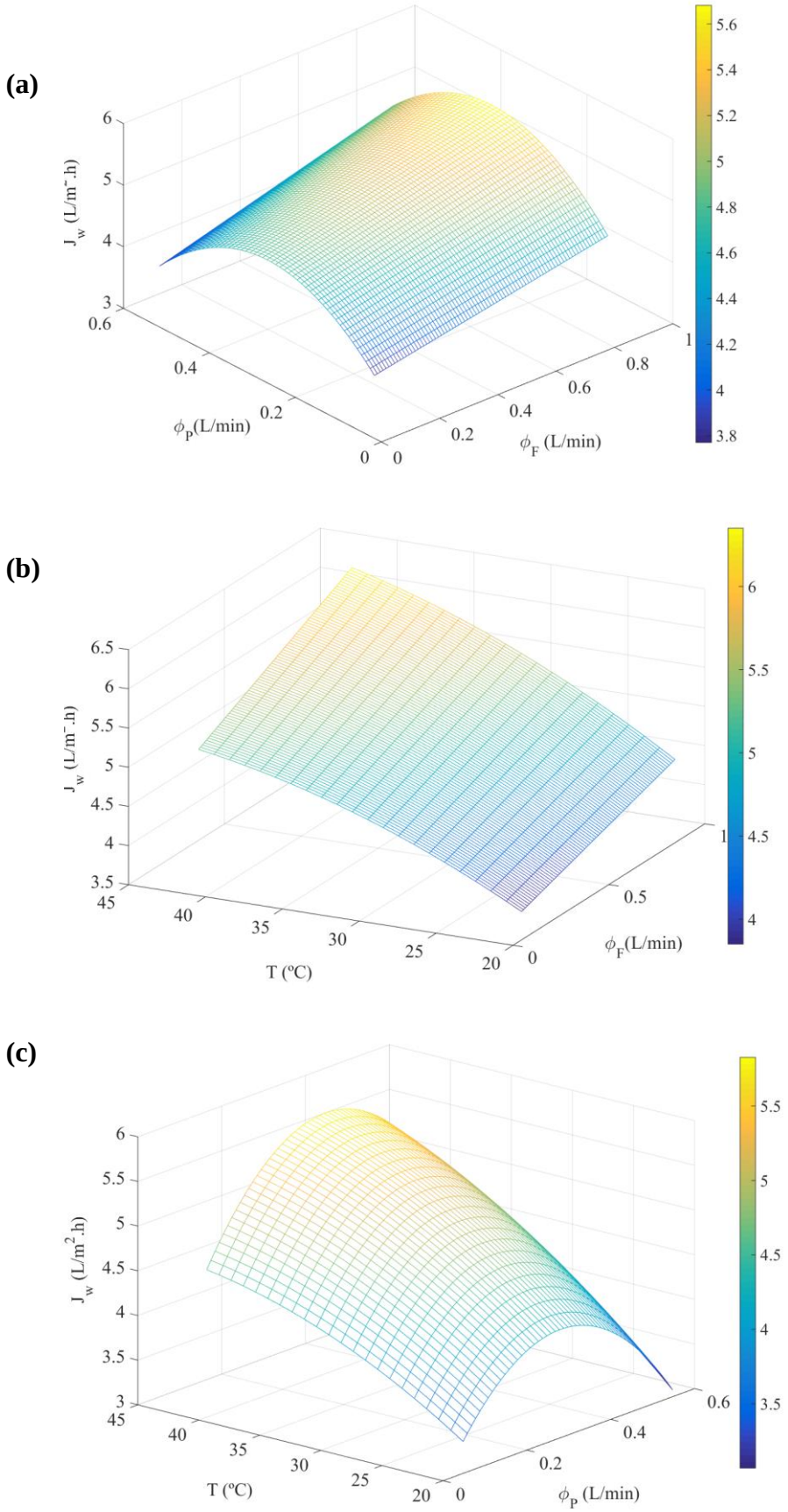

Figure 5.5. Response surface plots of the water permeate flux (J_w) as a function of the temperature (T), feed flow rate (ϕ_F) and permeate flow rate (ϕ_P): (a) T = 31 ºC; (b) ϕ_P = 0.3 L/min; (c) ϕ_F = 0.45 L/min.

5.3.1.2. RSM model of the reverse solute permeate flux (J_s)

The developed RSM model of J_s in terms of the coded variables is:

$$\hat{Y} = 3.14 - 0.1757x_1 - 0.1191x_2 - 0.0326x_3 + 0.1534x_1^2 - 0.1943x_2^2 + 0.0491x_3^2 + 0.0615x_1x_2 \quad (5.14)$$

The regression coefficients corresponding to the interaction terms b_{13} and b_{23} are found to be negligible. In terms of the actual variables the RSM model is written as:

$$J_s = 4.246 - 2.0818\phi_F + 1.7607\phi_P - 0.0412T + 1.4172\phi_F^2 - 4.5787\phi_P^2 + 6.061710^{-4}T^2 + 0.9074\phi_F\phi_P \quad (5.15)$$

where: 0.050 L/min ≤ ϕ_F ≤ 0.850 L/min; 0.050 L/min ≤ ϕ_P ≤ 0.550 L/min and 20.07 ºC ≤ T ≤ 41.94 ºC.

The RSM model was validated statistically for adequacy by means of ANOVA and the results are summarized in Table 5.4. The calculated F-value is found to be greater than the tabulated one and the R^2-value (0.9737) is greater than R^2_{adj} indicating that the developed RSM model for J_s is valid from statistical standpoint and only the significant terms have been considered in the model. As can be seen in Eqs. (5.14 and 5.15), the only interaction term affecting J_s is the feed and permeate flow rates (b_{12}). The other interactions between parameters are negligible. In addition, compared to ϕ_F and ϕ_P, the effect of the temperature on J_s is less significant. A comparison between the J_s response calculated by the RSM model and the experimental one obtained in each test (Table 5.2) is plotted in Fig. 5.6. A good agreement was found between both responses.

Table 5.4. Analysis of variance (ANOVA) for the developed RSM model of J_S.

Source	*DF*[a]	*SS*[b]	*MS*[c]	*F-value*	*F-tab*	R^2	R_{adj}^2
Model	9	0.812429	0.09027	24.645	3.8	0.9737	0.934
Residual	6	0.021977	0.0036628				
Total	15	0.834406					

[a]*DF* - degree of freedom; [b]*SS* - sum of squares; [c]*MS* – mean square.

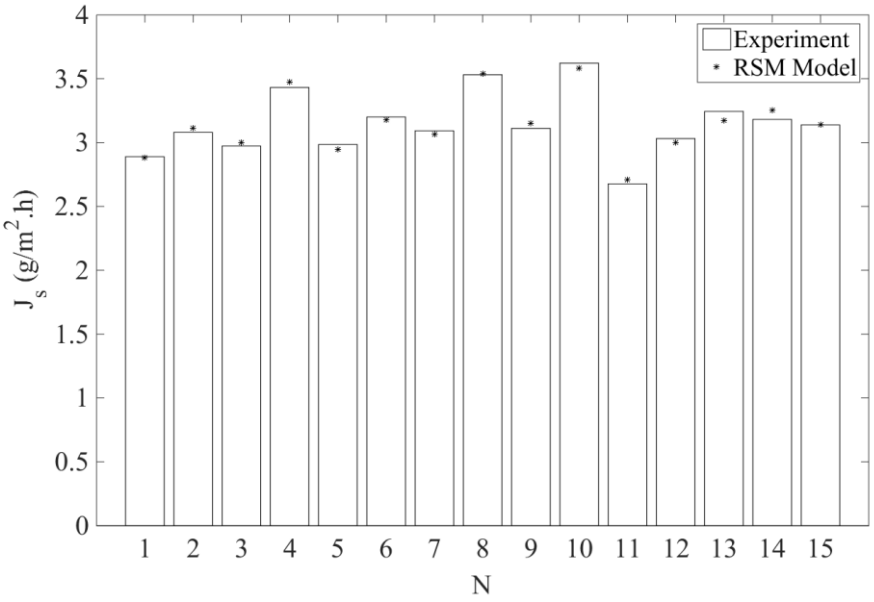

Figure 5.6. Experimental and predicted reverse solute permeate flux (J_s) of different experimental runs indicated in Table 5.2.

The effects of the three variables (ϕ_F, ϕ_P and T) on J_s are shown in Fig. 5.7. The increase of ϕ_F clearly leads to a strong reduction of J_s tending to asymptotic values and therefore, as it is required by FO process, the solute flux selectivity (J_w/J_s) is high. As can be seen in Figs. 5.5 and 5.7, the effects of ϕ_P on J_s and J_w are similar. Interestingly it was observed an increase of J_w/J_s with the increase of T and ϕ_F for all ϕ_P values. However, for low values of T and ϕ_F the ratio J_w/J_s increased up to a maximum with the increase of ϕ_P and then decreased; whereas for high values of T and ϕ_F it shows a continuous gradual increase attributed meanly to the much higher J_w compared to that of J_s.

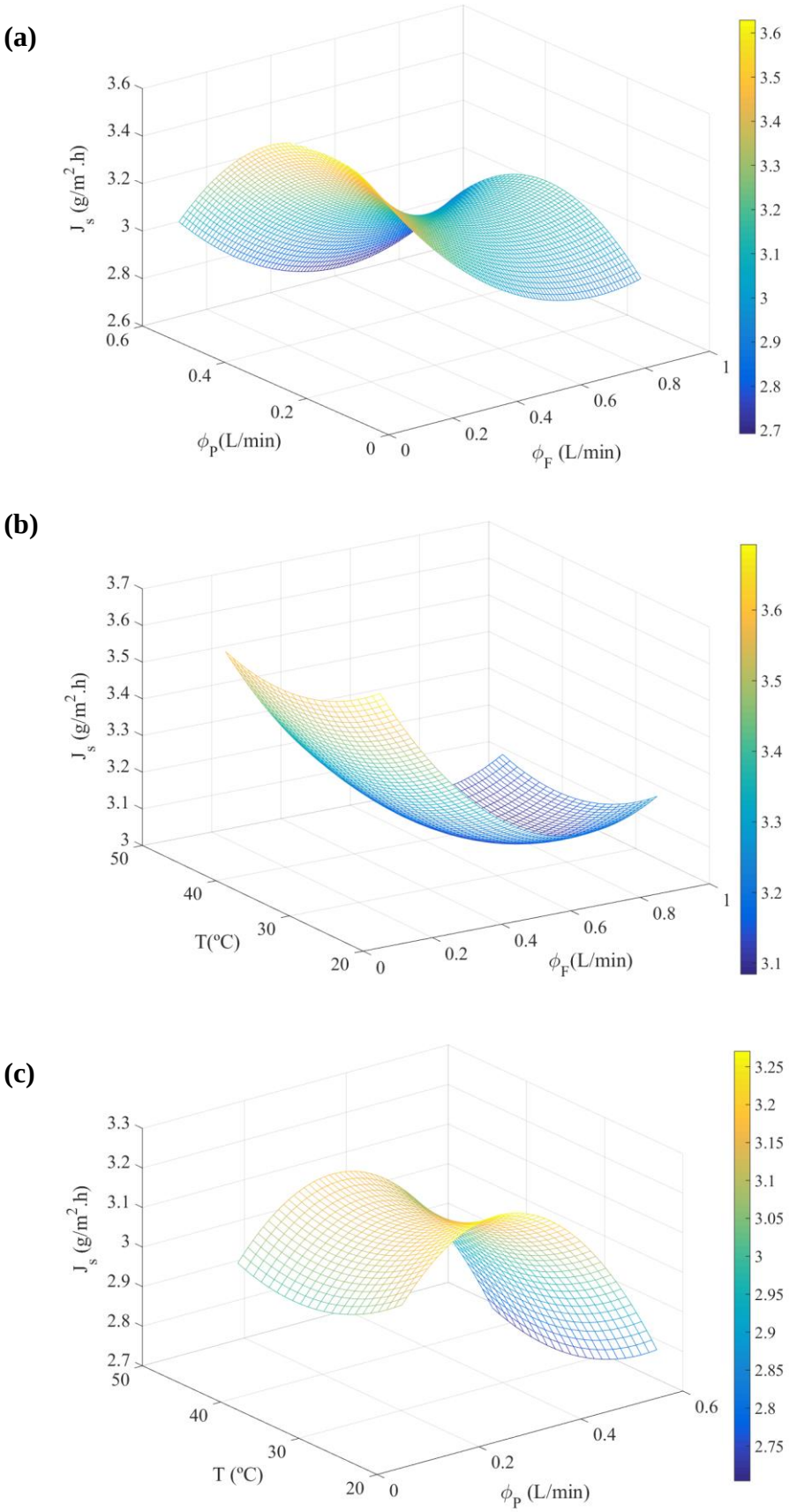

Figure 5.7. Response surface plots of the reverse solute permeate flux (J_s) as a function of the temperature (T), feed flow rate (ϕ_F) and permeate flow rate (ϕ_P): (a) T = 31 ºC; (b) ϕ_P = 0.3 L/min; (c) ϕ_F = 0.45 L/min.

5.3.1.3. RSM model of the specific FO performance index (Y_{sp})

The specific FO performance index (Y_{sp}) that takes into account all FO responses (J_w, J_s, E_c) was calculated by means of Eq. (5.9). The obtained RSM model of Y_{sp} is as follows in terms of the coded variables:

$$\hat{Y} = 2763.6 + 213.3881x_1 + 424.8272x_3 - 460.5659x_2^2 - 1249.1x_3^2 \quad (5.16)$$

The regression coefficient b_2, b_{11} and all the interaction terms b_{12}, b_{13} and b_{23} are found to be negligible. In terms of the actual variables, the RSM model is written as:

$$Y_{sp} = -1.4788\,10^4 + 648.596\phi_F + 6.5119\,10^3\phi_P + 1003.3T - 1.0853\,10^4\phi_P^2 - 15.421T^2 \quad (5.17)$$

where: 0.050 L/min ≤ ϕ_F ≤ 0.850 L/min; 0.050 L/min ≤ ϕ_P ≤ 0.550 L/min and 20.07 ºC ≤ T ≤ 41.94 ºC.

The response surface model was validated statistically for adequacy by ANOVA. The results are presented in Table 5.5. The calculated F-value is greater than 3.8 and the R^2-value is reasonably high (i.e. 0.9679). This R^2 value is in agreement with the adjusted statistics R^2_{adj} indicating that only significant terms have been included in the RSM model of the FO response Y_{sp}. These statistical estimators show that the RSM model of Y_{sp} is valid from statistical standpoint and it is a good predictor of the experimental data. Fig. 5.8 shows the comparison of the response Y_{sp} calculated by the RSM model and the experimental one obtained in each test (Table 5.2). A good agreement can be seen between the predicted Y_{sp} values and the corresponding experimental data.

Table 5.5. Analysis of variance (ANOVA) for the developed RSM model of Y_{sp}.

Source	*DF*[a]	*SS*[b]	*MS*[c]	*F-value*	*F-tab*	R^2	R_{adj}^2
Model	9	$1.17449\,10^7$	$1.30499\,10^6$	20.072	3.8	0.9679	0.92
Residual	6	390096.9	65016.1				
Total	15	$1.2135\,10^7$					

[a]*DF* - degree of freedom; [b]*SS* - sum of squares; [c]*MS* – mean square.

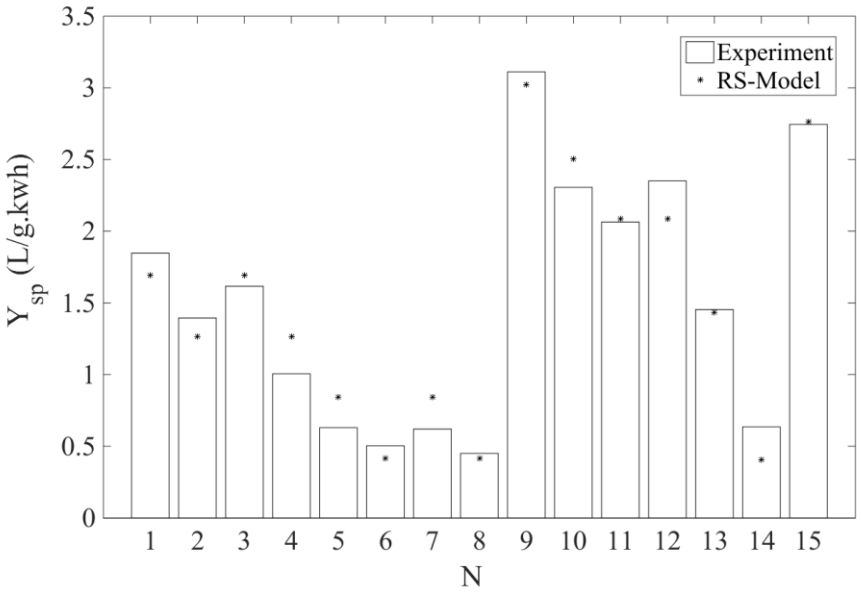

Figure 5.8. Experimental and predicted specific FO performance index (Y_{sp}) of different experimental runs indicated in Table 5.2.

The effects of the operating FO variables on the response Y_{sp} are plotted in Fig. 5.9. The increase of T and ϕ_P results in an enhancement of Y_{sp} up to a maximum, and then for higher values the trends are declined suggesting the existence of an optimal Y_{sp} value. It is to be noted that the effect of T upon Y_{sp} is the most significant one especially for high ϕ_F values. It can be observed a gradual increase of Y_{sp} with the increase of ϕ_F for all T and ϕ_P ranges. This result is due to the reduction of the polarization effect (i.e. narrowing of the feed boundary layer thickness) and the subsequent enhancement of the ratio J_w/J_s for practically the same energy consumption (E_c).

It was also observed that the effects of the FO operating parameters on the specific water permeate flux ($J_{w,sp}$ calculated by means of Eq. (5.8) are similar to those observed for the response Y_{sp} . In fact, the regression coefficient b_2, b_{11} and all the interaction terms b_{12}, b_{13} and b_{23} were also found to be negligible.

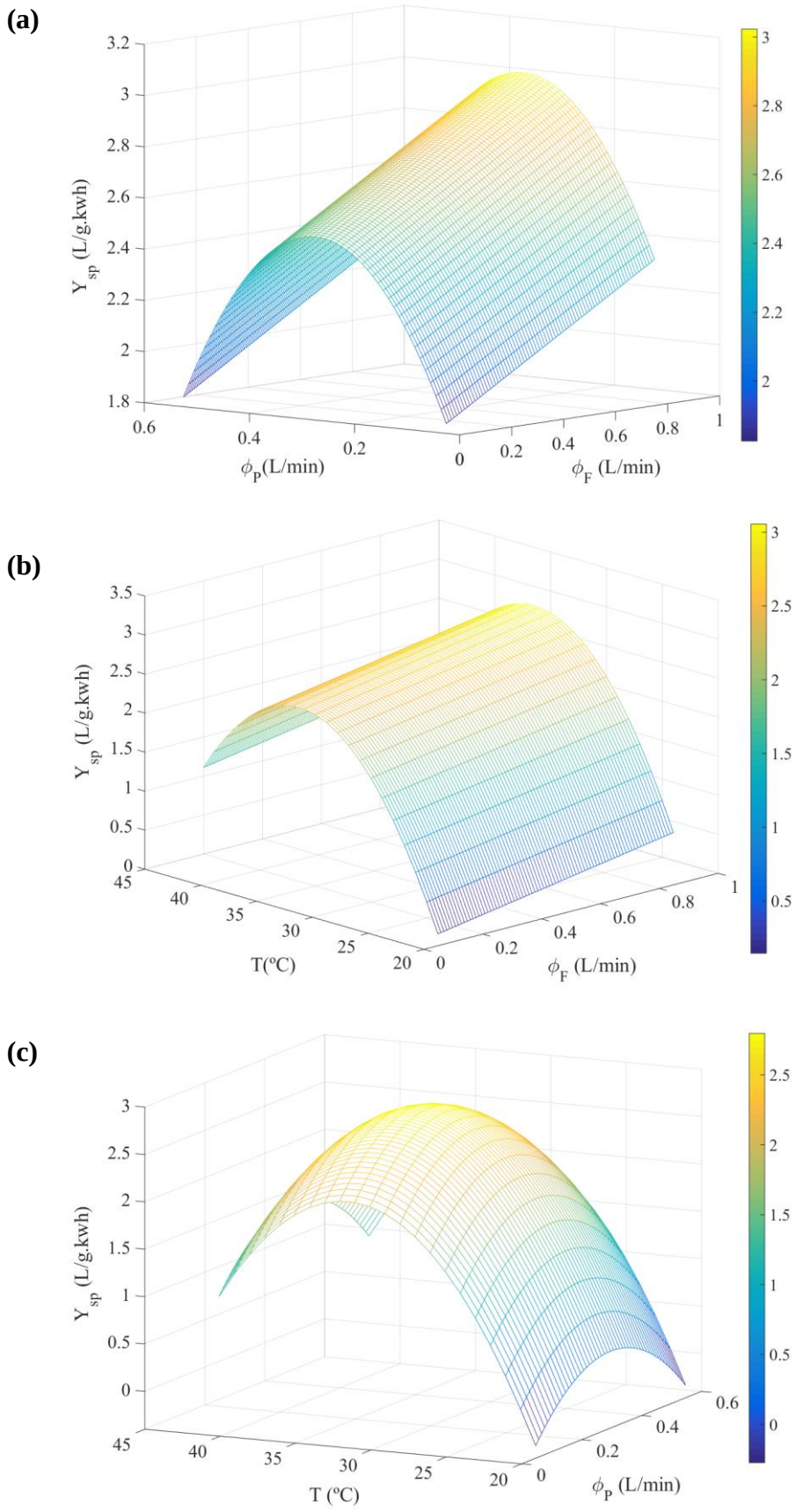

Figure 5.9. Response surface plots of the Y_{sp} as a function of the temperature (T), feed flow rate (ϕ_F) and permeate flow rate (ϕ_P): (a) T = 31 ºC;(b) ϕ_P = 0.3 L/min;(c) ϕ_F = 0.45 L/min.

5.3.2. Optimization of the FO pilot plant

One of the main objectives of this study is to determine the optimum operating conditions of the FO pilot plant in order to maximize the specific FO performance index (Y_{sp}) (i.e. maximize J_w, J_w/J_s and $J_{w,sp}$ and minimize J_s and E_c). This has been performed by means of Monte Carlo simulation (MCS) method, which is a stochastic optimization technique that generates the random coded values of the input FO variables and correspondingly generates a response inside the valid experimental region [24, 25, 29, 34]. 13 optimal points were obtained and the mean values of the optimum variables together with their standard deviations are summarized in Table 5.6 in terms of the actual operating variables as well as the predicted value of Y_{sp}.

Table 5.6. Optimal point of the Y_{sp} in terms of the actual operating variables and the output response, Y_{sp}.

ϕ_F (L/min)	ϕ_P (L/min)	T (°C)	Y_{sp} (L/g.kWh)	
			Predicted	Experimental
0.83 ± 0.01	0.31 ± 0.03	32.65 ± 0.86	3.027 ± 0.011	3.049 (+0.7%)

The experimental confirmation run was carried out under the optimum operating variables and the Y_{sp} response deviates only 0.7% from the predicted value. This experimental value of Y_{sp} together with that of the test number 9 (Table 5.2) represent the best (maximal) values throughout all the conducted experimental tests inside the region of experimentation.

The other experimental data of this optimum point are 2.94 g/m^2.h for J_s, 5.81 L/m^2.h for J_w, 1.976 L/g for J_w/J_s and 12.55 L/g.kWh for $J_{w,sp}$. These responses were also predicted by the developed RSM models of each response and the obtained values were quite similar to the experimental ones (i.e. 3.14 g/m^2.h for J_s, 5.80 L/m^2.h for J_w, 1.850 L/g for J_w/J_s and 13.32 L/g.kWh for $J_{w,sp}$).

5.3.3. Solar-powered FO pilot plant operation under optimum conditions

The FO solar-powered pilot plant is investigated under the determined optimal operating condition given in Table 5.6. It should be noted that the connection between the solar heat spherical collector and the feed and permeate aqueous solutions has been designed in such way to ensure a fixed temperature throughout the required testing period required. Fig. 5.10 shows as an example the instantaneous global solar radiation on horizontal plane (I) and the adjusted temperature (T) for the solar FO pilot plant to the determined optimum value during the entire period of experimentation together with the calculated responses J_w, J_s, $J_{w,sp}$ and Y_{sp}.

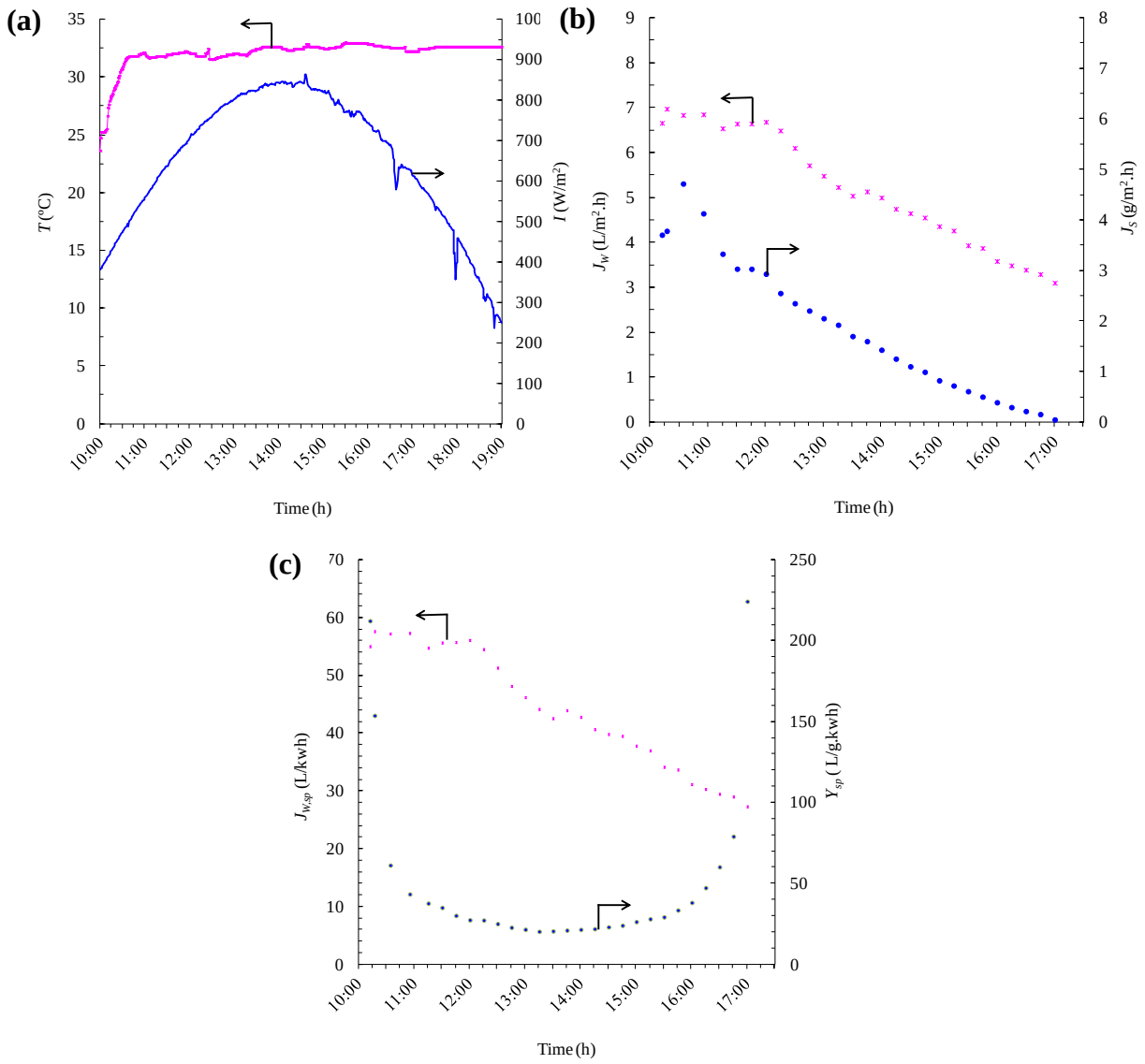

Figure 5.10. Evolution of: (a) Temperature (T) and instantaneous global solar radiation on horizontal plane (I) with time, (b) Obtained responses J_w and J_s, and (c) Obtained responses $J_{w,sp}$ and Y_{sp} of the solar FO pilot plant.

Except this last response, the other three responses are reduced with the operating time due to the dilution of the draw solution reducing the FO driving force. As a consequence, the calculated response Y_{sp} is reduced quickly after 30 min of operation of the FO pilot plant (i.e. 79.6%) reaching then a minimum value of 20.19 L/g.kWh at 3h15min operation time and then is increased. The determined values of Y_{sp} are higher than those obtained without using solar systems (Table 5.2 and Figs. 5.8 and 5.9). This is expected due to the considered energy consumption of the used thermostats or cryostat to carry out the designed experimental runs. Since the solar FO pilot plant is autonomous and operates without using thermostat or cryostat, energy consumption has been reduced. Therefore, Y_{sp} values plotted in Fig. 5.10(c) are higher than those presented in Fig. 5.9(c). Because of the dilution of the draw solution, another separation process such as

membrane distillation (MD) [19, 21, 35] or RO [15, 16] can be used as a second step for draw solution regeneration and water production. In this study, the solar RO pilot plant detailed elsewhere [12] is considered under optimum conditions forming a hybrid FO/RO plant as schematized in Fig. 5.11. In order to maintain constant the salt concentration of the draw solution, the RO water permeate flux must be similar to the FO permeate flux. As an example, the determined responses for a typical sunny day are plotted in Fig. 5.12. As can be seen J_w, J_s and $J_{w,sp}$ are maintained almost the same (i.e. 7.1 ± 0.4 L/m^2.h for J_w, 3.6 ± 0.4 g/m^2.h for J_s and 8.5 ± 0.5 L/kWh for $J_{w,sp}$). The observed slight decline of these responses is attributed mainly to the reverse solute. However, Y_{sp} is reduced with time from 25.79 L/g.kWh to an asymptotic value 0.62 L/g.kWh. This is due to the fact that the ratio J_w/J_s is maintained around a value of 2.0 ± 0.1 L/g whereas the total energy consumption (E_c) of the hybrid FO/RO system is increasing with time. Compared to the Y_{sp} data given in Fig. 5.10(c), these low values plotted in Fig. 5.12(c) are attributed to the consideration of the RO energy consumption [12]. For instance, the FO energy consumption is only 14.1 ± 0.2 % the total energy consumption of the FO/RO plant. It is to point out that the main benefit of using the FO/RO plant instead of RO plant is the possibility to treat a wide range of wastewater types not only desalination taking advantage of the low energy consumption of FO technology and its lower fouling effects [15-17, 20].

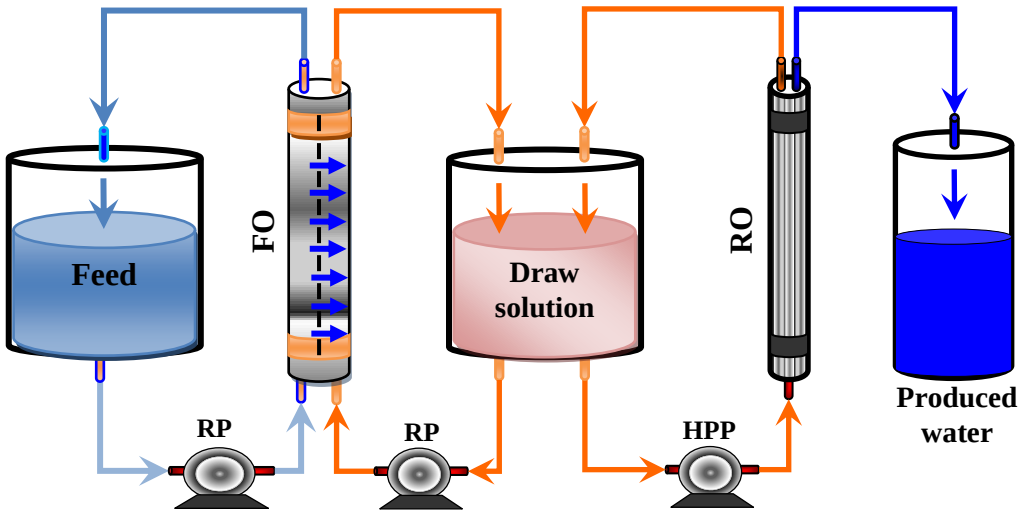

Figure 5.11. FO/RO simplified schema for regeneration of the draw feed solution (RP: circulation pump, HPP: high pressure pump).

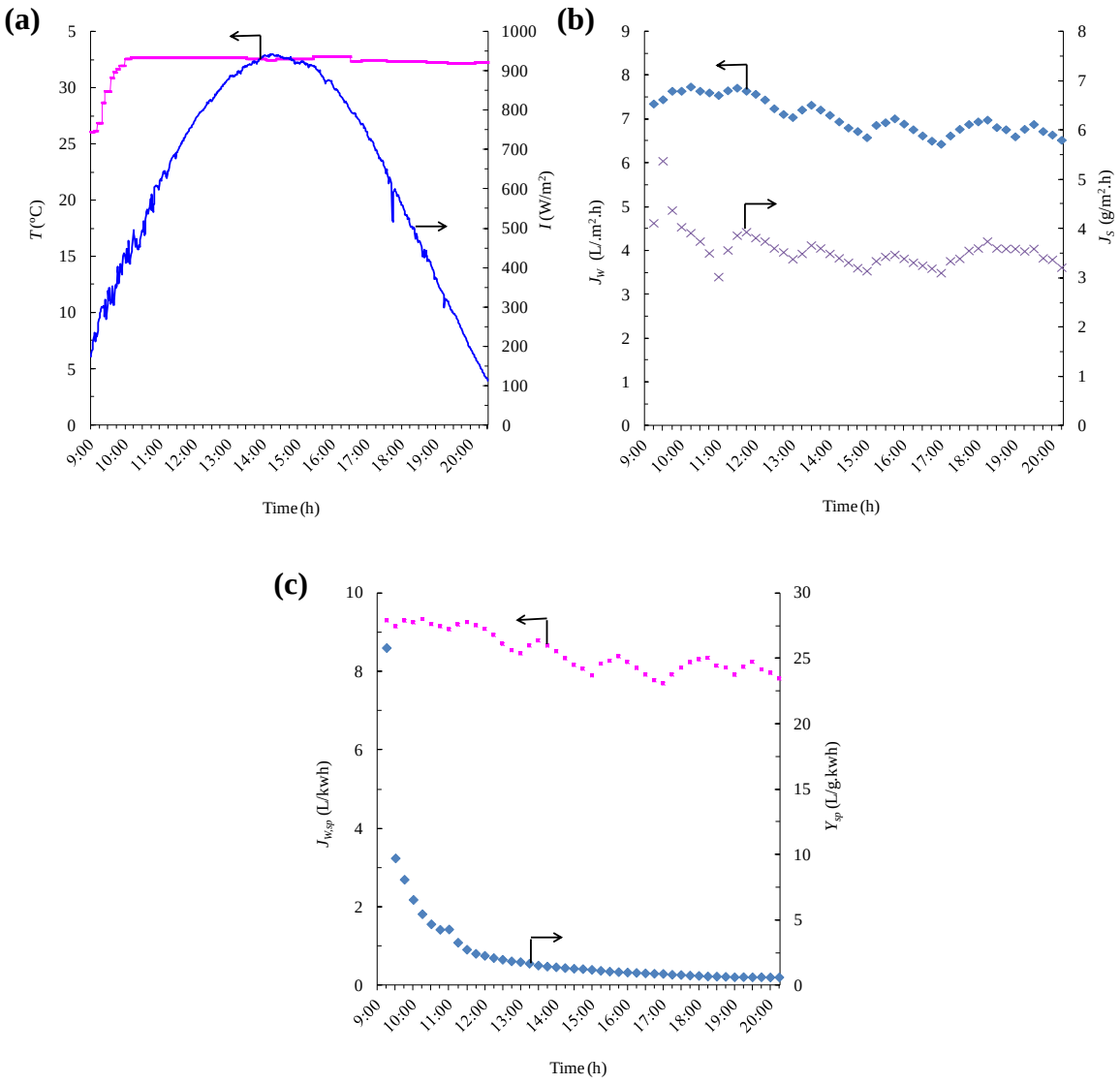

Figure 5.12. Evolution of: (a) Temperature (T) and instantaneous global solar radiation on horizontal plane (I) with time, (b) Obtained responses J_W and J_S, (c) Obtained responses $J_{W,sp}$ and Y_{sp} of the solar FO/RO hybrid pilot plant.

5.4. Conclusions

The statistical design of experiment (DoE) and response surface methodology (RSM) proved to be a useful and effective method for modelling and optimization of a solar FO pilot plant using a minimal number of experimental runs. Predictive RSM models of different FO responses were developed and confirmed their statistical validations by analysis of variance (ANOVA).

The observed gradual increase of J_w with the increase of both ϕ_F and T at all ranges of ϕ_P and the increase of J_w up to a maximum with the increase of ϕ_P, is due to the reduction of the thickness of the feed boundary layer leading to lower polarization effect and to the increase of both the solubility and diffusivity membrane parameters (i.e.

permeability) with the increase of T. The increase of ϕ_P reduced the external concentration polarization effect and thus increased both J_w and J_s. The only interaction term affecting J_s is the feed and permeate flow rates ($\phi_F.\phi_P$). Compared to ϕ_F and ϕ_P, the effect of T on J_s is less significant. The increase of ϕ_F clearly leads to a strong reduction of J_s tending to asymptotic values and therefore the solute flux selectivity (J_w/J_s) is high. Interestingly it was observed an increase of J_w/J_s with the increase of T and ϕ_F for all ϕ_P values. However, for low values of T and ϕ_F the ratio J_w/J_s increased up to a maximum with the increase of ϕ_P and then decreased; whereas for high values of T and ϕ_F it shows a continuous gradual increase attributed meanly to the much higher J_w compared to that of J_s.

The increase of T and ϕ_P results in an enhancement of Y_{sp} up to a maximum, and the effect of T upon Y_{sp} is the most significant one especially for high ϕ_F values. A gradual increase of Y_{sp} was observed with the increase of ϕ_F for all T and ϕ_P ranges.

The optimal FO operating variables of the pilot plant corresponding to the maximum of the Y_{sp} were determined by Monte Carlo Simulation (MCS) method. The obtained optimal operational conditions are 0.83 L/min feed flow rate, 0.31 L/min draw solution flow rate and 32.65ºC temperature. By applying these values, maximal Y_{sp} value was predicted and confirmed experimentally.

The FO solar-powered pilot plant was investigated under the determined optimal operation conditions. Except Y_{sp} the other responses of the FO pilot plant (J_w, J_s, $J_{w,sp}$) are reduced with the operating time due to the dilution of the draw solution reducing therefore the FO driving force. The regeneration of the draw solution can be performed by means of an optimized solar powered reverse osmosis (RO) pilot plant with an optimum FO Y_{sp} index ranging from 25.79 to 0.62 L/g.kWh achieved under the FO optimal conditions. The FO energy consumption is only 14.1% the total energy consumption of the FO/RO plant.

The solar FO pilot plant has been optimized using 35 g/L NaCl as a draw solution. Similar studies can be applied to any FO plant with other concentrations, feed and draw solutions.

5.5. References

[1] A. Achilli, A.E. Childress, Pressure retarded osmosis: From the vision of Sidney Loeb to the first prototype installation-Review, Desalination, 261 (2010) 205.

[2] I. Alsvik, M.-B. Hägg, Pressure Retarded Osmosis and Forward Osmosis Membranes: Materials and Methods, Polymers, 5 (2013) 303.

[3] Q. Ge, M. Ling, T.-S. Chung, Draw solutions for forward osmosis processes: Developments, challenges, and prospects for the future, Journal of Membrane Science, 442 (2013) 225.

[4] S. Gormly, Forward osmosis: Introduction and applications for wastewater processing, energy conservation and energy generation, in: A. Gugliuzza, A. Basile (Eds.) Membranes for Clean and Renewable Power Applications, Woodhead Publishing, Cambridge (UK), 2014, pp. 379.

[5] F. Helfer, C. Lemckert, Y.G. Anissimov, Osmotic power with Pressure Retarded Osmosis: Theory, performance and trends-A review, Journal of Membrane Science, 453 (2014) 337.

[6] K. Lutchmiah, A.R. Verliefde, K. Roest, L.C. Rietveld, E.R. Cornelissen, Forward osmosis for application in wastewater treatment: a review, Water Research, 58 (2014) 179.

[7] J. Schrier, Ethanol concentration by forward osmosis with solar-regenerated draw solution, Solar Energy, 86 (2012) 1351.

[8] D.L. Shaffer, J.R. Werber, H. Jaramillo, S. Lin, M. Elimelech, Forward osmosis: Where are we now?, Desalination, 356 (2015) 271.

[9] Y. Cai, W. Shen, S.L. Loo, W.B. Krantz, R. Wang, A.G. Fane, X. Hu, Towards temperature driven forward osmosis desalination using Semi-IPN hydrogels as reversible draw agents, Water Research, 47 (2013) 3773.

[10] A.A.A. Attia, Thermal analysis for system uses solar energy as a pressure source for reverse osmosis (RO) water desalination, Solar Energy, 86 (2012) 2486.

[11] A.M. Delgado-Torres, L. García-Rodríguez, Design recommendations for solar organic Rankine cycle (ORC)-powered reverse osmosis (RO) desalination, Renewable and Sustainable Energy Reviews, 16 (2012) 44.

[12] M. Khayet, M. Essalhi, C. Armenta-Déu, C. Cojocaru, N. Hilal, Optimization of solar-powered reverse osmosis desalination pilot plant using response surface methodology, Desalination, 261 (2010) 284.

[13] D. Manolakos, G. Kosmadakis, S. Kyritsis, G. Papadakis, On site experimental evaluation of a low-temperature solar organic Rankine cycle system for RO desalination, Solar Energy, 83 (2009) 646.

[14] M. Elimelech, W.A. Phillip, The Future of Seawater Desalination: Energy, Technology, and the Environment, Science, 333 (2011) 712.

[15] A. Altaee, G. Zaragoza, H.R. van Tonningen, Comparison between Forward Osmosis-Reverse Osmosis and Reverse Osmosis processes for seawater desalination, Desalination, 336 (2014) 50.

[16] G. Blandin, A.R.D. Verliefde, C.Y. Tang, P. Le-Clech, Opportunities to reach economic sustainability in forward osmosis–reverse osmosis hybrids for seawater desalination, Desalination, 363 (2015) 26.

[17] Y.-J. Choi, J.-S. Choi, H.-J. Oh, S. Lee, D.R. Yang, J.H. Kim, Toward a combined system of forward osmosis and reverse osmosis for seawater desalination, Desalination, 247 (2009) 239.

[18] H. Luo, Q. Wang, T.C. Zhang, T. Tao, A. Zhou, L. Chen, X. Bie, A review on the recovery methods of draw solutes in forward osmosis, Journal of Water Process Engineering, 4 (2014) 212.

[19] C.R. Martinetti, A.E. Childress, T.Y. Cath, High recovery of concentrated RO brines using forward osmosis and membrane distillation, Journal of Membrane Science, 331 (2009) 31.

[20] R.K. McGovern, J.H. Lienhard V, On the potential of forward osmosis to energetically outperform reverse osmosis desalination, Journal of Membrane Science, 469 (2014) 245.

[21] S. Zhang, P. Wang, X. Fu, T.S. Chung, Sustainable water recovery from oily wastewater via forward osmosis-membrane distillation (FO-MD), Water Research, 52 (2014) 112.

[22] D. Montgomery, Design and Analysis of Experiments, fifth ed., New York, 2001.

[23] D.C. Montgomery, R.H. Myers, Response Surface Methodology: Process and Product in Optimization Using Designed Experiments, New York, 1995.

[24] C. Cojocaru, M. Khayet, G. Zakrzewska-Trznadel, A. Jaworska, Modeling and multi-response optimization of pervaporation of organic aqueous solutions using desirability function approach, Journal of Hazardous Materials, 167 (2009) 52.

[25] C. Cojocaru, G. Zakrzewska-Trznadel, A. Jaworska, Removal of cobalt ions from aqueous solutions by polymer assisted ultrafiltration using experimental design approach. part 1: optimization of complexation conditions, Journal of Hazardous Materials, 169 (2009) 599.

[26] E. Kacan, Exergetic optimization of basic system components for maximizing exergetic efficiency of solar combisystems by using response surface methodology, Energy and Buildings, 91 (2015) 65.

[27] M. Khayet, C. Cojocaru, C. Garcia-Payo, Application of Response Surface Methodology and Experimental Design in Direct Contact Membrane Distillation, Industrial & Engineering Chemistry Research, 46 (2007) 5673.

[28] M. Khayet, M.N.A. Seman, N. Hilal, Response surface modeling and optimization of composite nanofiltration modified membranes, Journal of Membrane Science, 349 (2010) 113.

[29] M. Khayet, A.Y. Zahrim, N. Hilal, Modelling and optimization of coagulation of highly concentrated industrial grade leather dye by response surface methodology, Chemical Engineering Journal, 167 (2011) 77.

[30] A.V. Schenone, L.O. Conte, M.A. Botta, O.M. Alfano, Modeling and optimization of photo-Fenton degradation of 2,4-D using ferrioxalate complex and response

surface methodology (RSM), Journal of Environmental Management, 155 (2015) 177.

[31] H. Zamani, M. Moghiman, A. Kianifar, Optimization of the parabolic mirror position in a solar cooker using the response surface method (RSM), Renewable Energy, 81 (2015) 753.

[32] A.F. Ismail, P.Y. Lai, Development of defect-free asymmetric polysulfone membranes for gas separation using response surface methodology, Separation and Purification Technology, 40 (2004) 191.

[33] M. Xie, W.E. Price, L.D. Nghiem, M. Elimelech, Effects of feed and draw solution temperature and transmembrane temperature difference on the rejection of trace organic contaminants by forward osmosis, Journal of Membrane Science, 438 (2013) 57.

[34] M. Khayet, C. Cojocaru, M. Essalhi, Artificial neural network modeling and response surface methodology of desalination by reverse osmosis, Journal of Membrane Science, 368 (2011) 202.

[35] M. Khayet, Membranes and theoretical modeling of membrane distillation: a review, Advances in Colloid and Interface Science, 164 (2011) 56.

Chapter 6

Conclusions and future perspectives

6.1. Conclusions

The present PhD Thesis is focused on the use of membrane technologies of actual interests, membrane distillation (MD) and forward osmosis (FO) for the treatment of both synthetic brines and reverse osmosis (RO) brines. In addition, the possibility to reuse discarded membranes by MD in microfiltration (MF) process for the treatment of wastewater has been proposed for the first time obtaining promising results.

Among the various advantages of MD technology presented in chapter 2, MD proved to be useful in desalination field for the treatment of high saline solutions. In chapter 3, it was found that MD could be used for the treatment of RO discharged brines, not only for water production but also to concentrate their volume and therefore minimize their discharges to the environment.

First, a synthetic brine consisting of a high saline solution (i.e. initial concentration of 65 g/L sodium chloride solution) was treated by air gap membrane distillation (AGMD) using two polytetrafluoroethylene (PTFE) membranes with different pore sizes (i.e. TF200 and TF450). AGMD process proved to be an useful method to concentrate the synthetic brine up to the saturation point of NaCl salt with rejection factors greater than 99.9% (i.e. production of high quality distillate).

Both high feed temperatures and membrane pore sizes (i.e. TF450 membrane) showed to be the two most influential factors affecting the permeate flux, which increased with the increase of the feed temperature and the membrane pore size. During AGMD

processing, a permeate flux decline was observed due to the continuous deposition of salt over the membrane surface, which was more remarkable at a high feed temperature.

When the saturation concentration of the NaCl was overpassed, two different facts occurred in the membrane: i) a pore blockage due to salt crystal fouling that induced a significant decline of the permeate flux or ii) a pore wetting effect that permitted the synthetic brine to pass in liquid phase through the membrane pores increasing sharply the permeate flux and decreasing its quality. Both membranes, either blocked or wetted, were discarded from their use in AGMD.

The effect of crystallization fouling on membrane characteristics was analyzed. It was observed a decrease of both the void volume fraction (i.e. porosity) and the water contact angle indicating a reduction of the hydrophobic character of the membrane and the increasing risk of membrane pore wetting. In addition, the thermal efficiency of the AGMD process, which was affected mainly by the feed temperature and the membrane pore size, was decreased due to crystallization fouling effect.

Based on the results obtained with synthetic brines, a direct contact membrane distillation (DCMD) process was proposed for the treatment of an RO brine at high temperature. The expected DCMD performance was not achieved and some chemical pretreatment steps were proposed. Other than NaCl (halite, 66.7%), various other compounds were present in RO brines, magnesium chloride hexa-hydrate (bischofite, 15.2%), calcium sulfate ($CaSO_4$, 10.1%) and calcium carbonate ($CaCO_3$) alone or associated with magnesium (dolomite, $CaMg(CO_3)_2$) as salts in major proportion. It was detected a major presence of sulfates than carbonates. These salts, especially calcium carbonate ($CaCO_3$) and calcium sulfate ($CaSO_4$), were found to be the most harmful salts of RO brine due to their easy precipitation and the main responsible of inorganic membrane fouling leading to a continuous decline of the permeate flux during DCMD operation. Due to salt crystals deposition, a final wetting of the membrane pores was observed, especially for the membrane TF450 having large pore size. Consequently, the DCMD process ended early limiting the possibility to concentrate the RO brine sufficiently to precipitate the sodium chloride (NaCl).

Five different chemical pretreatments (CPTs) were proposed and tested with two objectives: i) extend the membrane lifetime by reducing fouling phenomenon and ii) prevent pore wetting by removing $CaCO_3$ and $CaSO_4$. These CPT combined different chemicals like sodium hydroxide (NaOH), sodium carbonate (Na_2CO_3) and barium chloride ($BaCl_2$) in order to remove calcium and sulfate ions. These CPTs were applied before carrying out the DCMD process. In contrast to what it was observed with synthetic brine, the results showed that the membrane TF450 membrane was not appropriate for RO brine treatment. Its large pore size facilitated wetting even when $CaCO_3$ and $CaSO_4$ were previously precipitated outside the membrane module. On the contrary, the membrane TF200 membrane presented better results in terms of RO brine concentration and

separation factor, especially when the chemical treatments subjected to remove sulfates were considered (i.e. CPT-3: addition of $NaOH+Na_2CO_3$, CPT-4: addition of $NaOH+Na2CO_3$ at 348K and CPT-5: addition of $BaCl_2$). When applying these CPTs, RO brine was concentrated up to the saturation point of NaCl (i.e. 300 g/L) and the initial permeate flux was increased considerably compared to that of the DCMD carried out without any CPT while the permeate flux decline with time was smaller. In addition, a good permeate quality was achieved at the end of DCMD test, especially with the application of CPT-4 and CPT-5. However, CPT-5 could not be recommended when treating RO brine for water consumption due to the toxicity of the residual barium formed during the pretreatment process. It was found that CPT-4 was the most adequate pretreatment to apply before performing DCMD process for the treatment of RO brine.

After their use in MD (chapter 3), PTFE membranes were discarded due to the effects of fouling or wetting phenomena. These disposed membranes were proposed for their reuse in MF for wastewater treatment. Due to the membrane requirements and the operating conditions of the MF process (i.e. membrane pore size, membrane structure and the necessary transmembrane pressure, TMP) the discarded MD membranes could be reused in MF for the treatment of humic acid (HA) aqueous solutions (chapter 4). A previous compaction with distilled water was needed not only to reduce their pore sizes but also to improve the HA separation factor and also to clean the membrane surface from foulants and crystals deposited on the membrane surface and in the membrane pores.

Similar to MD, in MF the larger pores of the membrane TF450 was found to be more prone to be fouled and blocked either by RO brine and synthetic brine foulants and by HA particles than the smaller pores of the TF200 membrane. The membranes used for the treatment of RO brine showed lower initial MF permeate fluxes than those previously used in AGMD for the concentration of synthetic brine. In general, PTFE membranes discarded from MD demonstrated to be useful in MF process, offering an economic and environmental important possibility for the future of both MD and MF technologies.

Statistical design of experiments (DoE) and response surface methodology (RSM) were used to optimize a photovoltaic-powered FO pilot plant (chapter 5). The results showed an increment of the permeate flux (J_w) when both the feed flow rate and the temperature of the FO process were increased. An increase of the feed flow rate caused a reduction of the thickness of the feed boundary layer and also a reduction of the external polarization effect, leading to lower polarization effect on the permeate flux. Furthermore, an increase in the temperature resulted in an increase of both the solubility and diffusivity membrane parameters (i.e. permeability) and the permeate flux as consequence. In addition, an improvement of the permeate flux was achieved when the draw solution flow rate was increased due to the reduction of the external concentration polarization. However, this fact also led to an increase in the reverse solute diffusion (J_s). Therefore, higher solute flux selectivity (J_w/J_s) values were achieved when both the feed flow rate and the temperature

were increased due to the much higher J_w compared to that of J_s. Moreover, an increase in the specific FO performance index was achieved when these operational conditions were increased.

The optimal FO operating variables of the pilot plant, corresponding to the maximum specific FO performance index, were determined by Monte Carlo Simulation (MCS) method and subsequently confirmed experimentally. The obtained results were 0.83 L/min feed flow rate, 0.31 L/min draw solution flow rate and 305 K temperature. Nevertheless, except the specific FO performance index, the other responses of the FO pilot plant (i.e. J_w, J_s, J_w/J_s, the total energy consumption (E_c) and the specific water permeate flux ($J_{w,sp}$)) were reduced with the dilution of the draw solution with time (i.e. reduction of the FO driving force).

The option to couple the FO optimized plant with an RO plant in order to regenerate the draw solution (i.e. maintain constant the salt concentration of the draw solution and consequently the necessary FO driving force) was also proposed in chapter 5.

6.2. Future perspectives

Since MD proved to be a promising technology for the treatment of high saline aqueous solutions (i.e. both synthetic and pretreated RO brines) up to saturation point (chapter 3) with a high performance, an interesting research area can be focused on the study of the MD process to regenerate the draw solution of the FO while producing distilled water, forming a hybrid FO/MD membrane separation process. The integration of FO and MD processes is more advantageous provided that MD can be used to the treatment of high saline solutions, can be used for the production of distilled water, it exhibits low tendency to fouling and can be coupled to renewable energy sources among others. In this sense, the use of NaCl aqueous solutions as draw solutions has been considered in various research studies. However, the use of RO brines (i.e. pretreated RO brines) as draw solutions, preventing their discharge to the environment, has not been considered yet. A schema of a possible FO/MD hybrid system, object of futures studies, is shown in Fig. 6.1.

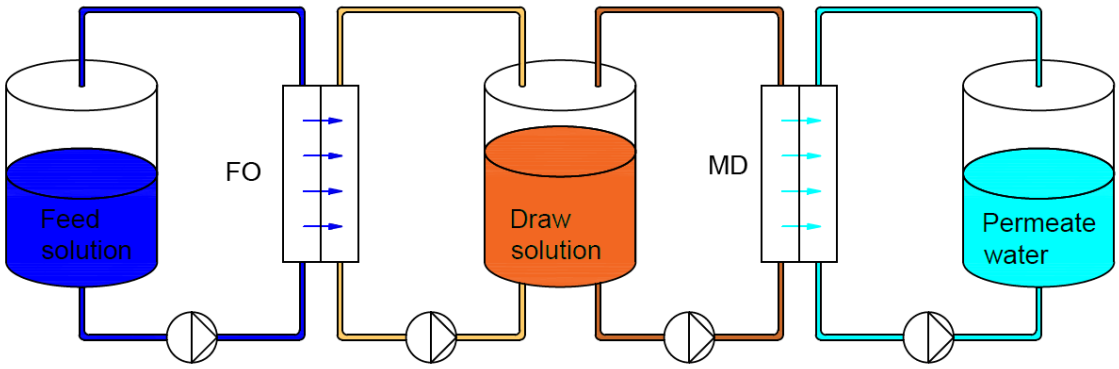

Figure 6.1. Schema of an FO/MD hybrid system.

This promising research area requires further studies before its industrial implementation. Among others, membranes and modules designed specifically for both MD and FO technologies, energy consumption analysis, coupling to renewable energy sources are needed.

After the interesting results obtained with the reused MD membranes in MF process and taking into consideration that RO is the worldwide used technology in desalination, another future research area that needs to be deeply explored is the reuse of RO membranes in FO or even in MD process. RO membranes are commonly discarded after detecting their low water production rate due to the irreversible fouling phenomenon. After a cleaning and or modification, these membranes can be used in FO due to some similarities of the RO and FO membranes. Membrane modification can be performed to form a hydrophobic layer

on the recycled RO membrane support for MD applications. Both options can be a great possibility to prevent the disposal of RO membrane modules.

Another interesting research study can be focused on a combined hybrid system for the concentration and purification of RO brines with the objective to approach the maximum possible to a zero-liquid discharge (ZLD). As it is schematized in the following figure (Fig. 6.2), a chemical pretreatment of the RO brine together with two or more steps of MD (i.e. DCMD and AGMD or TSGMD, for example) can be used to produce high quality water. First, RO brine can be chemically pretreated as it was performed in chapter 3. Subsequently, MD is employed for the concentration of the pretreated RO brine while producing high quality permeate. As the permeate quality decreases with time, once the permeate concentration exceeds an established permeate quality value, a second MD step can be considered for the treatment of the permeate in order to increase its quality. In addition, a membrane crystallizer (MCr) is recommended to recover the salts formed when the feed RO brine exceeds the limiting salt saturation concentration.

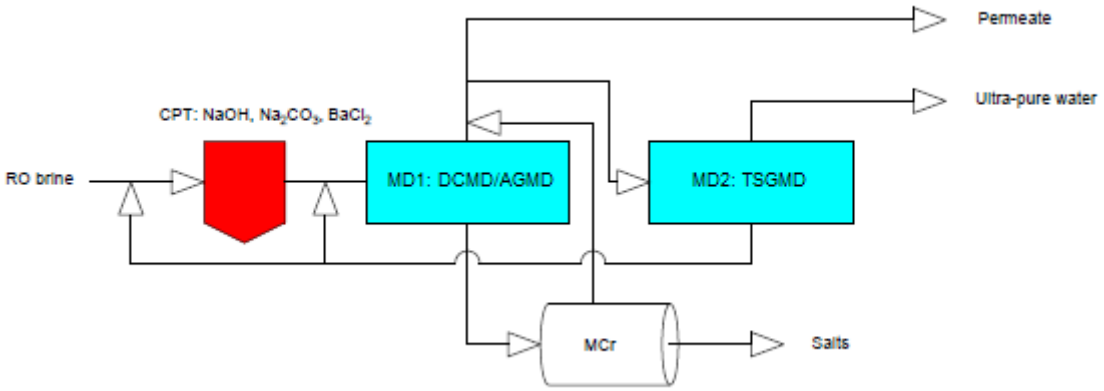

Figure 6.2. Schema of a ZLD hybrid system.

Appendix A

List of figures in order of appearance

Chapter 5

Appendix B

List of tables in order of appearance

Chapter 2

Chapter 3